USING SOUTH AFRICAN FLY ASH AS A COMPONENT OF ALKALI-ACTIVATED BINDER

JULIA SHEKHOVTSOVA

A thesis submitted in partial fulfilment of the requirements for the degree of

PHILOSOPHIAE DOCTOR (CIVIL)

In the

FACULTY OF ENGINEERING, BUILT ENVIRONMENT AND INFORMATION TECHNOLOGY

UNIVERSITY OF PRETORIA

January 2015

DECLARATION

I, the undersigned hereby declare that:

- I understand what plagiarism is and I am aware of the University's policy in this regard;
- The work contained in this thesis is my own original work;
- I did not refer to work of current or previous students, lecture notes, handbooks or any other study material without proper referencing;
- Where others people's work has been used this has been properly acknowledged and referenced;
- I have not allowed anyone to copy any part of my thesis;
- I have not previously in its entirely or in part submitted this thesis at any university for a degree.

Signature of student:

Name of student:	Julia Shekhovtsova
Student number:	04442165
Date:	January 2015

ACKNOWLEDGEMENT

I wish to express my gratitude to:

- The University of Pretoria for the financial support of this project, the provision and the use of laboratory facilities;
- My supervisor, Professor Elsabe Kearsley for opportunity to work on this project, her support, guidance, encouragement and help in improvement of this thesis
- Dr R Kruger and Ash Resources for providing a part of fly ash for this study;
- Mr Derek Mostert for helping me with experiment set up and valuable discussions of the results;
- Personnel of Civil Engineering Department (Jenny Callanan, Vanessa Doman, Johan Scholtz, Jaco Botha, Rikus Kock, Rita Peens and Petro Venter). One way or another they were helping me during my study;
- Staff of the Laboratory for Microscopy and Microanalysis at the University of Pretoria (André Botha, Alan Hall, Antoinette Buys) for assistance during SEM investigation;
- Wiebke Grote and Jeanette Dykstra for conducting XRD and XRF analyses during this study;
- Dr Liezel Van Der Merwe and Dr Linda Prinsloo for their helpful input;
- My husband, Maxim Kovtun for helping me on each stage of this study. For his encouragement, unconditional support, love and believing in me;
- My family and friends for being there for me.

SUMMARY

This thesis focuses on alkali-activation of South African fly ash with the aim to utilize high volumes of fly ash in construction material, such as concrete. This new type of binder does not contain Portland cement and could reduce carbon dioxide emission related to Portland cement production. At the same time fly ash utilization contributes to growth and economy of the country, conservation of natural resources and improvement of environmental aspects.

Although numerous studies have been devoted to alkali-activated materials and geopolymers, only a few studies were performed using South African fly ash. Rational technological parameters such as elevated temperature curing and mix composition of alkali-activated fly ash cements contained South African raw materials were determined in this thesis. Curing at 60 ºC for 16 hours gives the best trade between energy consumption and strength of the alkali-activated fly ash cements. Alkali content should not exceed 12 % Na_2O (preferably 9 %) which causes high standard deviation of the compressive strength and coefficient of variation between different batches of the concrete, as well as facilitates efflorescence formation. Produced alkali-activated fly ash cements were characterized by using different techniques (XRD, ATR-FTIR, SEM).

Alkali-activated fly ash cements are assumed to be low heat binders but the current study shows that significant amount of energy can be released during elevated temperature curing of these cements. Increased amount of alkali can cause temperatures up to 150 ºC which will negatively affect structure development of alkali-activated fly ash cement resulting in observed strength drop when alkali concentration exceeds 9 % Na_2O of fly ash mass. This finding is a valuable addition to the existing knowledge on alkali-activated materials which was not mentioned anywhere previously.

For the first time initial shrinkage of alkali-activated fly ash cured at elevated temperature during the first 24 hours was investigated in this thesis. Initial shrinkage of alkali-activated fly ash depends on alkali content and increases with an increase in amount of alkali. The initial shrinkage of alkali-activated fly ash concrete is significantly less, up to twofold, than the shrinkage of fly ash-OPC blended concrete even when the latter was cured at room temperature and 99 % relative humidity in comparison to curing of alkali-activated fly ash concrete at 60 ºC in dry oven.

Heat cured alkali-activated fly ash concrete has engineering properties similar to OPC concrete's properties. The alkali-activated fly ash concrete with 9 % Na_2O, containing 500 kg

of fly ash per cubic meter with dolomite aggregates provides adequate workability, and has the following characteristics:

- Slump of fresh concrete 50 mm
- Compressive strength at 28 days 45.5 MPa
- Elastic modulus at 28 days 30 GPa
- Poisson's ratio at 28 day 0.11
- Modulus of rupture at 28 days 5.7 MPa
- Split tensile strength at 28 days 3.2 MPa
- Initial shrinkage (during first 24 hours) 1400 microstrain
- Drying shrinkage after 1 year 300 microstrain
- Creep after 1 year 600 microstrain

The durability indices indicate that the alkali-activated fly ash concrete is comparable to the conventional concrete, and service life of structures made from the alkali-activated fly ash concrete should meet modern requirements. The alkali-activated fly ash concrete developed can thus be recommended for precast concrete units.

TABLE OF CONTENTS

LIST OF TABLES

LIST OF FIGURES

LIST OF ABBREVIATIONS

AAFA	Alkali Activated Fly Ash
AAM	Alkali Activated Material
AAR	Alkali Aggregate Reaction
AAS	Alkali Activated Slag
ATR FTIR	Attenuated Total Reflectance Fourier Transform Infrared spectroscopy
CS	Characteristic Strength
FA	Fly Ash
FAC	Fly Ash Cenosphere
HC	Heat Curing
GP	Geopolymer
GPC	Geopolymer Concrete
LOI	Loss on Ignition
MAS NMR	Magic Angle Spinning Nuclear Magnetic Resonance
M_s	Silica modulus
NBO	Non-bridging oxygen
NC	Concrete containing Portland Cement
OPC	Ordinary Portland Cement
SANS	South African National Standard
SEM	Scanning Electron Microscopy
XRD	X-ray Diffraction
XRF	X-ray Fluorescence

TERMINOLOGY

Amorphous phase	non-crystalline phase of material without a long-order structure characteristic to crystal
Autogenous shrinkage	shrinkage due to chemical reaction without any loss of moisture
Carbon dioxide equivalent (CO_2-e)	Carbon dioxide equivalent is a measure used to compare the emissions from various greenhouse gases based upon their global warming potential
Cenosphere	is a lightweight, hollow sphere made largely of silica and alumina and filled with air or inert gas
Heat curing	same as elevated temperature curing, heat treatment – curing of paste/concrete at temperatures higher than ambient
M_2O	alkali oxide, where M is Na or K
Paste	in this thesis refers to alkali-activated fly ash paste without any fine and coarse aggregates
Plerosphere	is a relatively big fly ash particle packed inside with fine fly ash particles
Silica modulus	weight ratio of silicon oxide to sodium oxide
Sodium silicate	same as $Na_2O{\cdot}nSiO_2$, liquid glass, water glass, soluble glass – a chemical alkaline compound containing sodium oxide and silicon dioxide used in this thesis in aqueous form

1 INTRODUCTION

1.1 BACKGROUND

It is known that concrete is one of the most widely used construction materials and Ordinary Portland Cement (OPC) usually has been used as a binder component in it. Production of OPC requires high energy efforts and has a significant impact on the global emissions of greenhouse gases. During the production of 1 tonne of Portland cement between 0.73 and 0.99 tonnes of CO_2 is released to the atmosphere (Hasanbeigi et al., 2012; Mahasenan et al., 2003; Flower and Sanjayan, 2007). One of the major cement manufacturers in South Africa, Pretoria Portland Cement (PPC) reported that in 2011 its carbon footprint for cement was 892 kg CO_2 per tonne of cement (PPC Integrated Annual report, 2011) which is an increase of 2.6 % compared to 2010. The biggest part of the CO_2 is emitted during clinker manufacture at 1400-1500 °C due calcination of limestone into lime at temperatures of 600-900 °C. Globally, the cement industry accounts for approximately 5 % of the current anthropogenic carbon dioxide emissions (Hasanbeigi et al., 2012).

Increased demand for construction materials and particularly concrete leads to increasing pollution and greenhouse gas emissions. The problem of greenhouse gas emission is discussed at international level. Treaties (such as the Kyoto protocol) that set binding obligations on industrialized countries to reduce emissions of greenhouse gases were signed between many countries including South Africa.

In the light of these events opportunities to reduce CO_2 emission by using alternative binders to OPC are investigated all over the world. Partial replacement of cement by fly ash or slag was found to reduce concrete CO_2 emissions by between 13 and 22 % (Flower and Sanjayan, 2007).

Alkali-activated binders and geopolymers are potential alternatives to OPC. Geopolymers are inorganic materials with three-dimensional silico-aluminate structures resulting from polycondensation. Davidovits called the reaction which takes place as a result of alkaline activation of aluminosilicates at low temperatures geopolymerization (Davidovits, 1988). According to data published in literature, carbon emissions of geopolymers can be 80 % less than that of traditional cements (van Deventer et al., 2010) and greenhouse gas emissions can be reduced by 44 to 64% (McLellan et al., 2011). Recent conclusions of Turner and Collins (2013) show the CO_2 footprint of geopolymer concrete to be only 9 % less than that of OPC concrete.

According to van Jaarsveld et al. (2002) the formation of geopolymer starts from the dissolution of aluminosilicates from the raw material in high pH alkaline solutions, with the formation of mobile precursors which orientate then condensate and harden with the formation of amorphous or semi-crystalline structure.

Rich sources of aluminosilicates, most widely used for alkali-activation, are fly ashes, metakaolin and blast furnace slag.

Benefits of producing alkali-activated materials include:

- Utilization of by-products of industry productions (fly ashes, slags, etc.)
- Material with good properties can be produced;
- Expanding the raw material base of the building industry without using natural mineral resources;
- Reduce greenhouse gas emission by cement replacement.

1.2 PROBLEM STATEMENT

In this particular work chemical activation of fly ashes will be investigated. Utilization of ash is a very important problem for South Africa as energy production mostly relies on coal. Sasol (petrochemical) and Eskom (power utility) are the largest coal processing companies in South Africa. More than 30 million tonnes of coal is consumed annually by Sasol and about 8 million tonnes of gasification ash is produced (Matjie et al., 2005). Eskom consumes more than 100 million tonnes of coal per annum (Eskom Holding Ltd, n.d) and more than 35 million tonnes of ash (fly + bottom) were produced in 2011 (Eskom Holding Ltd, 2011). Almost 90 % of the ash produced by Eskom is fly ash. The morphological features of fly ash results in improved workability of cement systems, while the pozzolanic activity makes fly ash suitable for use as cement extender (Kruger and Krueger, 2005). However, in South Africa only about 5 % of all fly ash produced by Eskom is beneficially used (Eskom Holding Ltd, n.d; Bada and Potgieter-Vermaak, 2008) and millions of tonnes of ash are being stored and disposed in ash dams and landfills annually, creating the risk of toxic elements present in fly ash being released, into soils and ground water (Carlson and Adriano, 1993). There is always a risk of failure of a fly ash disposal dam itself. The catastrophic dike failure at the Kingston Fossil Fuel Plant (Tennessee, USA) has been reported in 2008. Massive release of fly ash and mud sludge disrupted power and natural gas line, destroyed several homes, causing an enormous impact on the environment (United States Environmental Protection Agency, 2009).

This thesis is an attempt to *develop an alternative application for South African fly ash as a raw material for producing an environmentally friendly sustainable construction material*. The study contributes towards finding a solution for fly ash utilization and reducing the impact of greenhouse gas emission by potential cement replacement. Although a considerable amount of literature exists on alkali-activation of fly ashes, little is known about activation of South African coal fly ash in particular.

1.3 OBJECTIVES

Since alkali-activated/geopolymer binders are quite new for South Africa it is necessary to develop mix designs using local materials. The knowledge and understanding of the factors affecting properties of alkali-activated cements and geopolymers will make a valuable contribution to promoting fly ash utilization in these materials. In order to be able to produce environmentally friendly inorganic material the main objectives of this study are to:

- Develop and optimize the mix design of alkali-activated fly ash (AAFA) cement paste;
- Investigate and understand factors affecting AAFA material properties;
- Investigate possible reasons for loss in performance of AAFA cement pastes containing high amount of alkali;
- Evaluate properties of AAFA concrete;
- Estimate carbon footprint of AAFA material production.

1.4 HYPOTHESIS

South African fly ash is suitable for alkali-activation and can be used for production of Portland cement-free construction material.

1.5 METHODOLOGY

Initially it was decided to start working with AAFA cement pastes, to reduce experimental material costs and obtain main trends before investigating alkali-activated concrete. Figure 1.1 represents an outline of the organization of the study.

During the first stage of experimental work the compressive strength of AAFA cement paste was chosen as a main indicator of material properties. Experiments were performed in order to understand the effect of the following parameters on the strength and microstructure of AAFA cement pastes:

- Sodium oxide content and age;
- Temperature and duration of elevated temperature curing;

- Water to binder solids ratio;
- Mineralogy of initial fly ash;
- Type of activator;
- Soluble SiO_2 concentration;

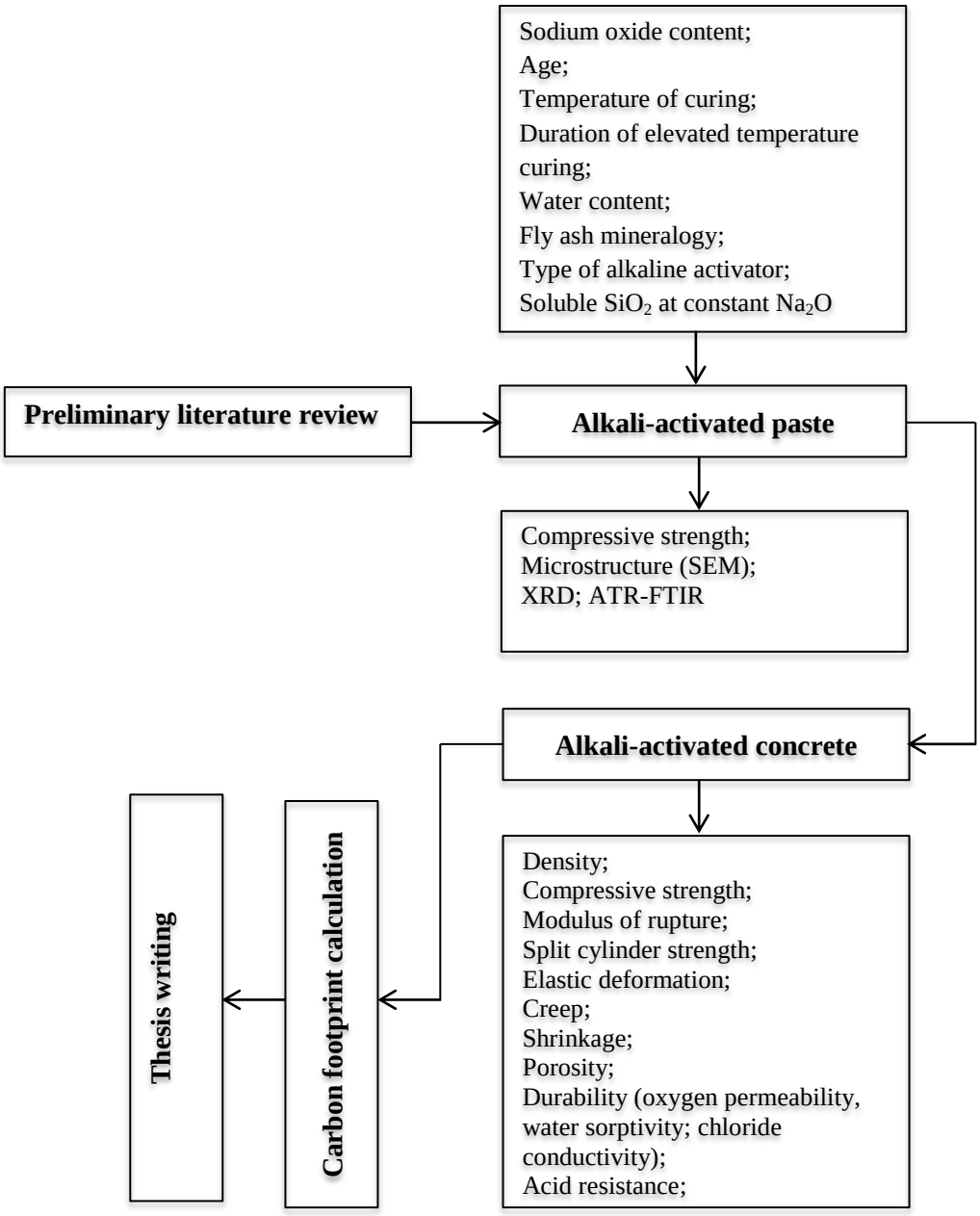

Figure 1.1: Outline of study organization

The microstructure, morphology and composition of the resulting products of alkali-activation were studied by scanning electron microscopy (SEM), X-ray diffraction (XRD) and Attenuated Total Reflectance Fourier Transform Infrared Spectroscopy (ATR-FTIR). For the

first time, in-situ evaluation of volume changes as well as heat evolution of AAFA cement paste samples were performed during elevated temperature curing.

Major parameters which may affect the strength and other properties of AAFA cement pastes were investigated and compared to results published previously in literature. Optimal values of these parameters were used to design AAFA concrete mixes and efficient conditions of curing.

The following properties of heat cured AAFA concrete were measured to evaluate and characterise material:

1) compressive strength;
2) density;
3) modulus of rupture;
4) split cylinder strength;
5) elastic deformations;
6) creep;
7) shrinkage during elevated temperature curing;
8) drying shrinkage;
9) porosity;
10) durability indices (oxygen permeability, water sorptivity and chloride conductivity);
11) acid resistance.

These properties were compared to previously published results on geopolymer concrete as well as to properties of OPC-fly ash blended concrete. A basic estimation of the carbon footprint of AAFA concrete raw materials was performed in order to estimate its compatibility.

1.6 SCOPE OF RESEARCH

One low calcium fly ash from Lethabo power station was used for the majority of the experimental work. In addition fly ash from Matla power stations was used to investigate the effect of mineralogical composition on compressive strength of AAFA cement paste. Fly ashes were activated by sodium hydroxide solution with concentrations from 3 to 15 % of fly ash mass (in terms of Na_2O). Water to binder solids ratio, temperature and duration of elevated temperature curing were kept constant. For further investigations only Lethabo fly ash was used. The Na_2O content that provided the highest compressive strength at 28 days was used to investigate the effect of temperature and duration of elevated temperature curing on the strength development of AAFA cement pastes. Four different temperatures (25 °C, 40 °C, 60 °C and 80 °C) and six durations of elevated temperature curing (ranging from 4 to

24 hours with 4 hour intervals) were studied in order to find efficient curing conditions. The effect of water to binder solids ratio (in the range of 0.18 to 0.29) on the strength development of the AAFA cement pastes was investigated for the Na_2O content that provided the highest 28-days compressive strength. The pastes were cured at 60 °C for 24 hours. The effect of different concentrations (3–12 % of fly ash mass) of KOH and the effect of combined activator consisting of NaOH and sodium silicate on the compressive strength of AAFA cement paste at constant water to binder solids, temperature and duration of elevated temperature curing were studied. The effect of soluble silicon oxide content on the strength development of paste was investigated at constant sodium oxide content. The combined effect of the variables on the compressive strength of AAFA cement pastes was not studied.

The Na_2O content and curing conditions that provided the highest compressive strength of AAFA cement paste was used to design AAFA concrete. The experimental work of this thesis is limited to laboratory scale.

1.7 ORGANIZATION OF THE THESIS

- Chapter 1 serves as introduction to the thesis.
- Chapter 2 presents a comprehensive literature review on alkali-activated binders and geopolymers. Synthesis process, properties of alkali-activated binders, different variables affecting them, materials used for the manufacture and curing condition are discussed as well as challenges faced during geopolymer production.
- Chapter 3 describes the composition of initial materials, techniques and methods used in experimental program.
- Chapter 4 presents the results of the study of AAFA paste. Factors affecting the compressive strength of alkali-activated paste are discussed. SEM, XRD and ATR-FTIR analysis of certain mixes are presented. This chapter also contains results of volume changes of AAFA cement pastes with different concentrations of Na_2O during elevated temperature curing, which was not previously published anywhere.
- Chapter 5 contains the results and discussion of the experimental study of AAFA concrete. Evaluation of properties of AAFA concrete are presented and compared to already published results on geopolymer concrete. An estimation of CO_2-e emission related to the materials used for alkali-activated concrete production was performed.
- Chapter 6 gives the conclusions and recommendations for future studies.
- Chapter 7 contains a list of References

2 LITERATURE REVIEW

2.1 INTRODUCTION

This chapter provides a comprehensive literature review of alkali-activated binders and/or geopolymers. Terminology, materials used for the manufacture, synthesis process, properties of alkali-activated binders, different variables affecting them as well as their production challenges is discussed. In South Africa it is a relatively new material which is not used in general and few local material studies have been performed. The information presented in this chapter gives basic principles of alkali activation and will be useful for future studies.

2.2 DEFINITION AND HISTORICAL BACKGROUND

Alkali-activated binders are the materials produced by the reaction between initial materials, consisting of silicon and aluminium oxides as well as alkaline solutions. As a result the glassy phase of aluminosilicates is partially or completely dissolved in the alkaline activator with the subsequent formation of a well compacted structure formed at low temperatures. The main reaction product is X-ray amorphous aluminosilicate gel (Palomo et al., 1999a). This gel has been found to be responsible for the cementitious properties of the final material (Criado et al., 2008) and its quantity affects the mechanical strength of the final product (Zhang et. al., 2013).

The term ‘geopolymer’ was first used in the end of the 1970s. French scientist Davidovits (2005) called inorganic material containing a three-dimensional silico-aluminate framework resulting from inorganic polycondensation reaction which takes place as a result of alkaline activation of aluminosilicates at low temperatures a ‘geopolymer’.

It is obvious that both types of materials are produced through alkali activation of aluminosilicates. The question arises:

Are alkali-activated materials geopolymers and vice versa?

All geopolymers are part of the bigger group of alkali-activated materials, as Davidovits said alkali activation or alkalination is the first step of geopolymerization. But not all alkali-activated materials are geopolymers, only those that have three-dimensional frameworks and where the aluminium in the product structure is presented in the IV-fold coordination. For investigating the molecular framework of geopolymers Davidovits suggested the use of Nuclear Magnetic Resonance (MAS-NMR) spectroscopy. For geopolymer cement ^{27}Al MAS-NMR displays a singular resonance at 55 ppm shown on Figure 2.1 which indicates that Al is

of the AlQ^4(4Si) unit and tetrahedral coordinated. The absence of any of other resonance and the extremely narrow peak at 55 ppm, excludes any residual singular building units of low molecular weight such as dimers and trimers. However, ^{27}Al MAS-NMR cannot differentiate between the various frameworks proposed for geopolymer materials (based on poly(sialate) (Si-O-Al-O-), poly(sialate-siloxo) (Si-O-Al-O-Si-O-) or poly(sialate-disiloxo) (Si-O-Al-O-Si-O-Si-O-)). This differentiation is carried out with ^{29}Si MAS-NMR spectroscopy where the chemical shift δ(^{29}Si) depends on the local environments of the ^{29}Si nucleus.

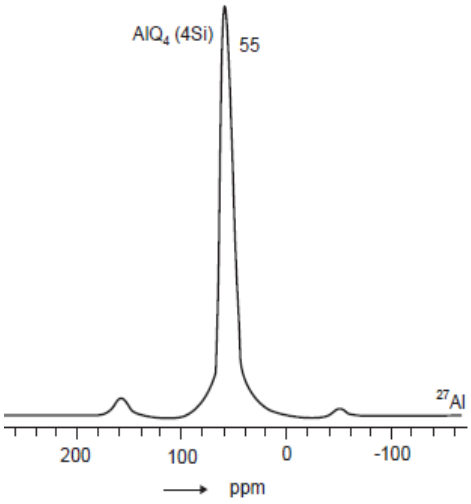

Figure 2.1: ^{27}Al MAS NMR of true geopolymer (Davidovits, 2008)

^{29}Si MAS NMR spectroscopy of fully cured geopolymers, as shown in Figure 2.2, reveals a broad resonance located around -85 to -95 ppm, depending on the Si/Al ratio, which can be linked to the resonance of tetrahedral silicon. The absence of sidebands indicates that specimens were fully cured and no free soluble silicon components are present in the pore solution (Duxson et al., 2005).

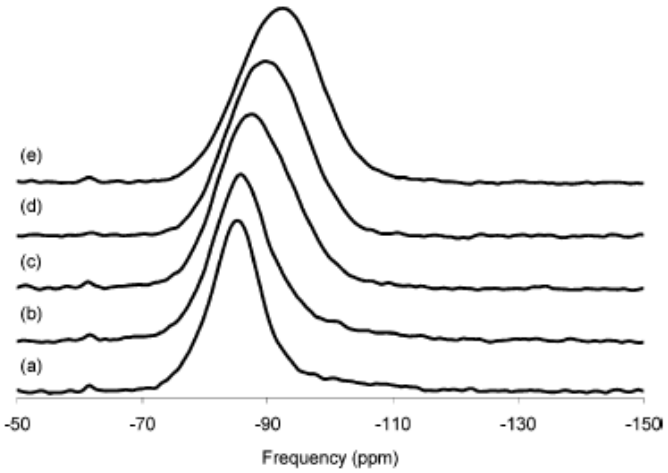

Figure 2.2: ^{29}Si MAS NMR spectra of Na-geopolymers with Si/Al of (a) 1.15, (b) 1.40, (c) 1.65, (d) 1.90, and (e) 2.15 (Duxson et al., 2005)

The hydraulic binders yielding hydrated calcium silicate C-S-H produces peaks on the NMR MAS ^{29}Si in the region -68 to -85 ppm attributable either to the monosilicate (Q^0) or the disilicates (Q^1)(Q^2), while the peaks, which characterize the geopolymer, occur in the region -85 to -100 ppm and correspond to the three-dimensional lattice (Davidovits, 2008).

One of the first attempts to manufacture alkali-activated concrete was undertaken by Purdon in 1940 (Purdon, 1940). Different types of activator solutions were introduced to the mixture of coarse aggregate, sand and granulated blast furnace slag. Relatively high compressive strengths of between 20 MPa and 45 MPa were obtained after 28 days of curing.

In 1959 a book by the Soviet scientist Glukhovsky on "Soil silicates" was published. He suggested using various friable soils and wastes of manufactures as fillers and soluble glass or alkaline solutions as binder (Glukhovsky, 1959). Later the same author developed the technology for alkali-activated slag cement production (Glukhovsky and Pakhomov, 1978). These books are not widely known in the international scientific community as they were published in Russian. The production of alkali-activated slags cement was however adopted on industrial scale in the former USSR.

In 1976 Davidovits patented the invention of a wood-fiber panel covered on one side with a layer of white hydrosodalite that had been obtained by reaction between kaolin and caustic soda (U.S. Patent No. 3940470, 1976).

In 1979 Davidovits introduced a new term – 'geopolymer' for inorganic material with three-dimensional silico-aluminate structures, formed as a result of polycondensation reaction or so-called geopolymerization (Davidovits, 2005). These silico-aluminate structures can be expressed using Equation 2.1:

$$M_n[-(SiO_2)_z-AlO_2]_n \cdot wH_2O \qquad (2.1)$$

where M is a cation (K, Na, Ca) and *n* is the degree of polycondensation, *z* is 1, 2, 3 or >> 3 and *w* has a value up to about 7.

Davidovits called these frameworks 'polysialates' (U.S. Patent No 4349386, 1982). Sialate is an abbreviation for silicon-oxo-aluminate building unit. Polysialates are chain and ring polymers that can be cross-linked together with Si^{4+} and Al^{3+} in IV-fold coordination with oxygen as indicated in Figure 2.3 (Davidovits, 2005).

Later it was discovered that the addition of ground blast furnace slag, which is a latent hydraulic cementitious product, to the polysialate type of geopolymer, accelerates the setting

time and significantly improves compressive and flexural strength (U.S. Patent No 4509985, 1985).

In 1987 Davidovits suggested the use of nuclear magnetic resonance for studying the structure of geopolymer. The works of Davidovits created interest in studying geopolymers and their properties all over the world.

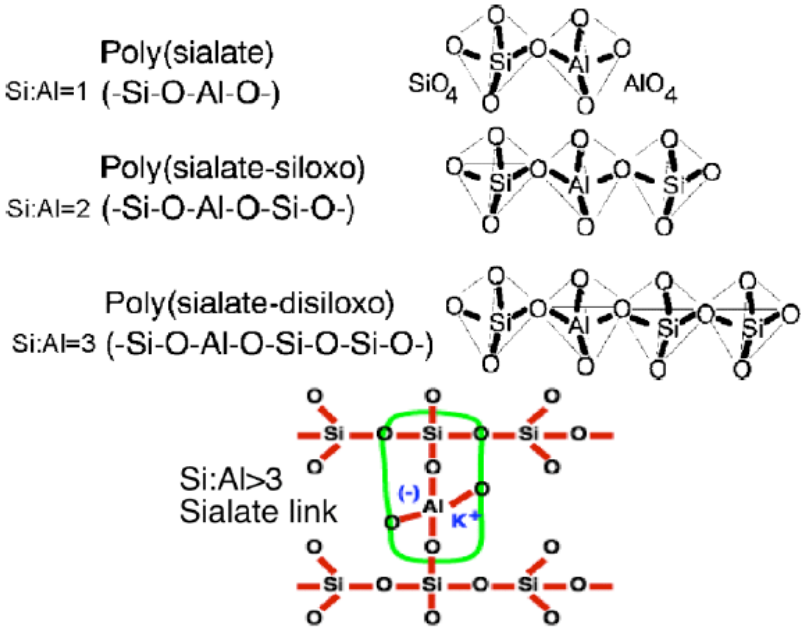

Figure 2.3: Geopolymer terminology according to Davidovits (2005)

2.3 RAW MATERIALS FOR ALKALI ACTIVATION

Theoretically any material containing silicon and aluminium oxides can be activated by alkalis (Pachego-Torgal et al., 2008b). A brief introduction to the main initial materials used for alkali activation will be given in this section. Fly ash will however be the focal point in this review as only this material fits the scope of the present research.

2.3.1 Fly ash

Fly ash, or pulverized fuel ash, is a residue derived from the combustion of pulverized coal in furnaces of thermal power plants. It consists essentially of microscopically small particles of aluminium silicate glass. The characteristics of fly ash vary according to the combustion operation system as well as the coal composition (Xu, 1996). Fly ash has pozzolanic properties, which means that it is able to develop strength when it reacts with lime (e.g. lime liberated by hydrating Portland cement) in the presence of moisture, which makes it a valuable cement extender.

Fly ash may be used as a cement extender, either by grinding it with Portland cement at a cement factory or mixing it on site with Portland cement for use in concrete, mortar or plaster. According to SANS 50197-1 (2000), the following types of Portland cement/fly ash blended cements can be produced in South Africa:

- Portland fly ash cement CEM II/A-V containing 6-20 % by mass of fly ash;
- Portland fly ash cement CEM II/B-V containing 21-35 % by mass of fly ash.

The addition of fly ash to cement has been investigated in numerous studies (Dhir et al., 1988; Fraay et al., 1989; Langan et al., 2002; Kearsley and Wainwright, 2003). Some of benefits of using fly ash in concrete can include:

- Improved workability of the cement systems due to the morphology of fly ash particles;
- Increased compressive strength as a result of the reduced water demand;
- Improved durability due to the pozzolanic reaction between fly ash and calcium hydroxide resulting in a greater amount of calcium silicate hydrate.

Fly ash is actively been used in alkali-activated cements and concretes (Görhan and Kürklü, 2014; Nuruddin et al., 2012; Mandal and Pal, 2012; Arioz et al., 2012; Al Bakri et al., 2011; Oh et al., 2012; Chindaprasirt et al., 2007; Hardjito and Rangan, 2005; van Jaarsveld et al., 2003; Palomo et al., 1999). The binder structure in low-calcium alkali-activated system is known to be disordered, highly cross-linked aluminosilicate gel (N-A-S-H type gels). Reaction of high-calcium fly ash-based geopolymer is more complex due to presence of soluble Ca (Li et al., 2013). Compared to low-calcium fly ash, activated high calcium exhibited a different composition of the hydrate assemblages. Ca species of oxides and silicate minerals from high-calcium fly ash could either (1) precipitate as $Ca(OH)_2$, (2) be bonded in geopolymeric gel by replacing cations within the geopolymer or (3) react with dissolved silicate and aluminate species to form C-S-H gel (Guo et al., (2010)). Yip et al. (2005) suggested that the coexistence of geopolymeric gel and C-S-H gel is possible and is responsible for the strength increase.

The activation mechanism of fly ash in a basic environment was studied by Katz (1998). He found that the degree of reactivity increases with increasing concentration of the activator solution and curing temperature. Fernandez-Jimenez and Palomo (2003) reported that the most important factors influencing alkali activation are: percentage of unburnt material, amount of reactive silica, particle size distribution and content of vitreous phase. They suggested using fly ashes with the following characteristics: the percentage of unburned

material should be lower than 5 %, the Fe_2O_3 content should not be higher than 10 %, the CaO content should be low, the content of reactive silica should be between 40-50 %, the percentage of particles with size lower than 45 μm should be between 80 and 90 % and the vitreous phase content should be high.

Winnefeld et al. (2010) have studied alkali-activated low and high calcium fly ashes. They concluded that high vitreous phase content and low calcium content are important factors determining the reactivity and the performance of fly ashes in alkali systems. Thus, the investigated low calcium fly ashes were much more reactive than the high calcium lignite coal fly ashes and using high calcium fly ash does not seem to be suitable for alkali activation according to them. However, high calcium fly ashes used in this study had high sulfate content and low amount of reactive phase and thus strength development high-calcium fly ashes was low.

In contrary to previous study, Diaz-Loya et al. (2011) obtained the highest compressive strength of geopolymer concretes produced from high-calcium fly ash. Diaz et al. (2010) concluded that the setting time of geopolymers increases exponentially as the CaO content decreases below 20 %, however the decrease in CaO is accompanied by decline in the compressive strength of resulting geopolymer. Thus, both low- and high-calcium fly ashes can be successfully used for alkali-activation.

2.3.2 Fly ash in South Africa

South Africa produces more that 40 million tonnes of ash annually. Sasol produces about 8 million tonnes of gasification ash per year (Matjie et al. 2005), while Eskom produced more than 35 million tonnes of ash (fly + bottom) in 2011 (Eskom Holdings Ltd, 2011). Figure 2.4 shows a statistical overview of ash produced and sold by Eskom.

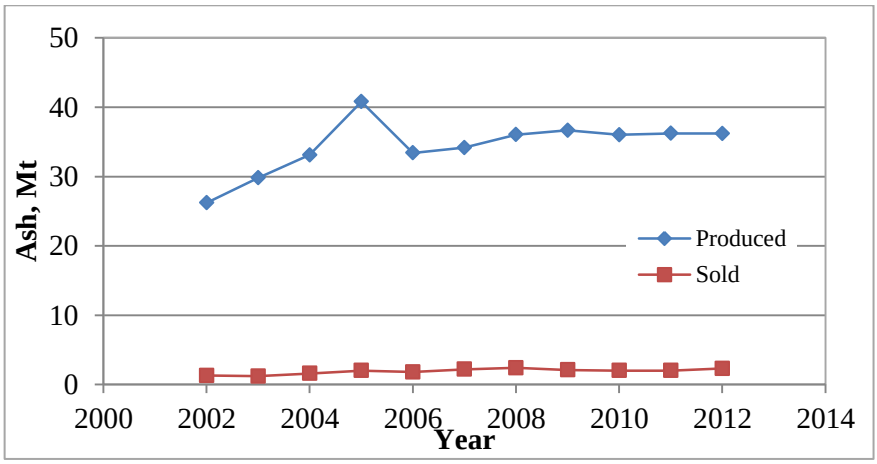

Figure 2.4: Statistical overview of ash produced and sold by Eskom (Eskom Holdings Ltd, 2012)

More than 90 % of Eskom ash is fly ash. However, in South Africa only about 5 % of all fly ash produced by Eskom is beneficially used (Eskom Holding Ltd, n.d.; Bada and Potgieter-Vermaak, 2008) and millions of tonnes of ash are being stored and disposed in ash dams and landfills annually, creating the risk of toxic elements present in fly ash being released, into soils and ground water (Carlson and Adriano, 1993) suggesting that utilization of ash is a very important problem for South Africa.

For South Africa siliceous fly ashes (SANS 50197-1:2000) are typical but their characteristics vary from plant to plant (Bosch and Willis, 1990). In some cases the chemical composition of fly ash from the same plant may vary significantly due to processing coal from different basins making the use of generated ashes in Portland cement concrete almost impossible. Utilizing a large amount of such fly ashes in alkali-activated materials and geopolymers will improve the ecological situation in the region, allow producing materials with good properties and also extend the raw-materials base of the building industry. It is thus necessary to comprehensively investigate and create a database of knowledge about alkali-activated South African fly ashes in general, using fly ash with a good consistency for better understanding of the newly formed material.

2.3.3 Blast furnace slag

Blast furnace slag is a by-product of iron making and results from fusion of limestone with minerals from the coke and siliceous and aluminous residue remaining after the reduction and separation of iron from the ore. This material has very high economic value when rapidly cooled which leads to vitrified reactive material that has hydraulic properties. The principal hydration products of slag are essentially similar to those found in Portland cement, making slag a valuable material for cement replacement. According to the European standard Portland slag cement may contain up to 30 % (mass) of granulated blast furnace slag, while in blast furnace cement this amount even is higher, up to 95 % (mass) (EN 197-1, 2000).

Slag has been extensively used for alkali activation in numerous studies (Wang et al., 1995; Barharev et al., 1999; Xu et al., 2008). The main difference of slag-based alkali-activated systems from low-calcium alkali-activated binders is the presence of high amount of calcium oxide. Assessment of reaction products formed by alkali activation of slag showed that the main reaction product is an aluminium-substituted calcium silicate hydrate (C-A-S-H type) gel, with disordered tobermorite-like C-S-H (I) type structure. More information on the reaction mechanism of alkali activation of slag is presented in the following section.

Slag is also the main component of alkali slag cement, which has been studied in detail in the USSR by the scientists Glukhovsky and Pakhomov (1978). Authors investigated alkali slag cements containing slags with various chemical compositions. Their results have shown that cements can be manufactured using both basic and acid slags with the correct choice of alkaline activator. A criterion of choice is the basicity index of slag. The setting time of the cements depend on the nature and quantities of the alkaline component, the basicity of the slag, its structure, fineness, type and additive condition. Setting time fluctuate: initial setting occurs from 30 minutes to 1 hour; with the final set from 2 to 5 hours. Strengths of cements with a specific surface area of 300-350 m^2/kg and 3 % Na_2O varied from 50 MPa to130 MPa for concretes and from 40 MPa to 100 MPa for mortars.

Douglas et al. (1991) investigated alkali slag concrete with different percentages of Na_2O. The compressive strength of alkali slag concrete samples varied from 45.4 MPa to 59.6 MPa at 28 days.

Wang et al. (1994) investigated type and fineness of slag and their influence on properties of alkali-activated mortars. Figure 2.5 shows the effect of slag type on the 28 day strength for different activators. It is clearly seen that the type of slag has a significant influence on the strength of mortars especially for systems where weak alkaline activators were used. The authors also noticed that slag with high alumina content (up to 16.1 %) gives high early strength, with a greater amount of slag reacting often leading to quick setting. Minor constituents in the slag, such as P, F, S, Mn and Ti, often affect slag quality. The optimum fineness is, 450-650 m^2/kg for acid and neutral slags, and 400-550 m^2/kg for basic slags.

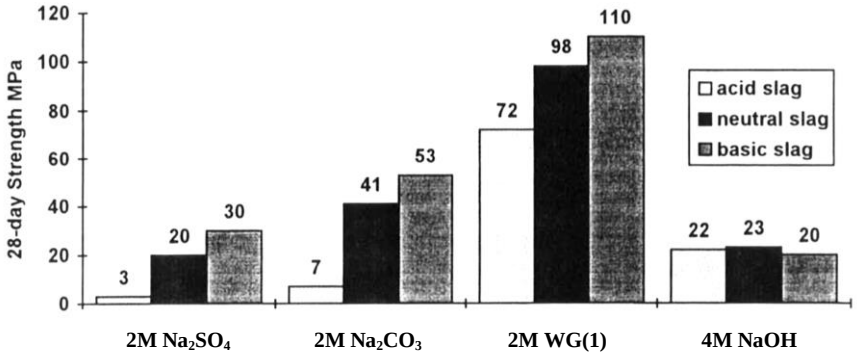

Figure 2.5: Type of activator versus 28-day strength for different types of slag (20 °C; fineness = 450 ± 30 m^2/kg; alkali solution/slag = 0.41; sand/ slag = 2) (Wang et al., 1994)

Fernandez-Jimenez et al. (1999) investigated the influence of specific surface of the basic slag on the development of mechanical strength in alkaline-activated slag cement mortars. They concluded that the effect of specific surface area is significant for flexural and compressive strength only at 3 days of curing and not significant at other ages. Generally, the increase in

slag specific surface area favours the reactivity, but they indicated that the mixes with higher specific surface area require higher mixing liquid content to obtain similar plasticity conditions, which produces a decrease in final strengths. The variation of mechanical strengths with specific surface area is highly influenced by the alkaline activator nature, indicating that this is the main binary interaction. When the slag was activated using NaOH and Na_2CO_3, an increase in the slag specific surface area from 450 to 900 m^2/kg, resulted in an increase in mechanical strengths. However, when the slag is activated with $Na_2SiO_3 \cdot nH_2O$ + NaOH, mechanical strengths do not increase, but decrease when the specific surface area increase.

2.3.4 Metakaolin

Metakaolin is formed from calcination of kaolin and provides an aluminium source with reasonably well-defined stoichiometry close to $2SiO_2 \cdot Al_2O_3$. Metakaolin is not cementitious by itself but having a high surface area of about 20000 m^2/kg, when mixed with Portland cement and hydrated, lime formed as a hydration product of cement is consumed by metakaolin, C-S-H is formed resulting in increased strength of the product. Metakaolin may also be activated by other materials such as alkali metal hydroxides, water glass, etc. (Ramachandran, 2002).

Alkali activation of metakaolin has been the subject of numerous investigations (Wang et al., 2012; Yip et al., 2008; Kong et al., 2007; Duxson et al., 2005; Duxson et al., 2007a, Duxson, 2006; Rowles, 2004). Davidovits (1994a) developed a new type of binder obtained from the alkali activation of metakaolin with NaOH solution. The aluminosilicate kaolinite reacts with NaOH at 100-150 °C and polycondenses into hydrated sodalite. Alonso and Palomo (2001a) have studied the activation of metakaolin by sodium hydroxide solution with different concentration. The results are shown on Figure 2.6.

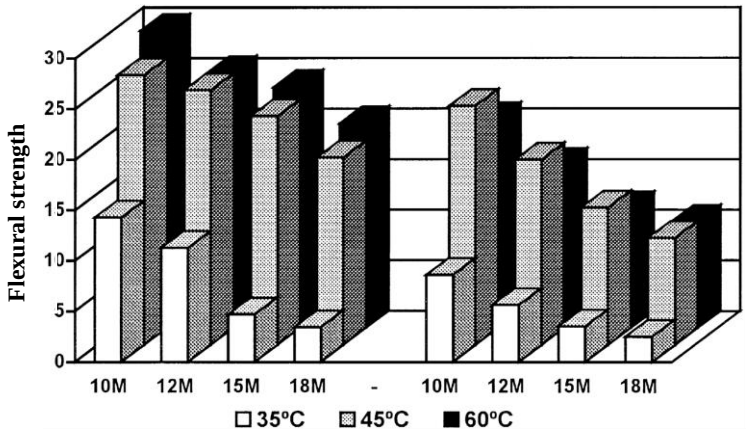

Figure 2.6: 24 Hour flexural strengths of specimens containing metakaolin with different solution concentrations (Alonso and Palomo, 2001a). On the left side metakaolin to $Ca(OH)_2$ ratio is 7:3, on the right 1:1

Zibouche et al. (2009) studied the influence of secondary minerals in metakaolin on the geopolymerization reaction. They compared two metakaolins, one from pure kaolinite and the other from Algerian kaolin containing illite and quartz. Sodium silicate was used as alkaline solution. They concluded that the secondary phases, at concentrations used in their work, do not prevent the geopolymerization reaction.

2.3.5 Other materials

The source of alkali activation does not have to be one material but a combination of different types of materials is possible too. Swanepoel and Strydom (2002) investigated the properties of geopolymeric material obtained from a mixture of South African fly ash and kaolinite activated by NaOH and sodium silicate solution. Specimens were cured for different times at different temperatures. Compressive strength samples cured at 60°C for 48 hours show a maximum strength of almost 8 MPa after 28 days.

Bernal et al. (2011) analysed sodium silicate-activated slag-metakaolin blends. Results showed that increasing metakaolin content in binders leads to a reduction of compressive strength and this effect was more significant when a higher silica modulus activator was used. All the mortars assessed show mechanical strengths of at least 40 MPa after 7 days of curing.

Zhao et al. (2007) used combinations of slag and fly ash in the presence of low alkalinity activator to manufacture alkali-activated binder. According to them fineness has a significant effect on the material strength, but the particle size distribution is more important. The mass ratio of fly ash to slag also has an influence on the mechanical strength. They noticed that the inclusion of fly ash can reduce the cost without negatively affecting the strength.

Fly ash cenosphere (FAC)/metakaolin-based geopolymeric composites with various FAC contents were studied by Wang et al. (2011). According to them compressive strength, thermal conductivities and bulk densities of the composites decreased with increasing FAC contents.

Zhihua et al. (2003) refer to a new kind of alkali-slag-red mud cementitious material. The blend of red mud and granulated blast furnace slag was activated by sodium silicate with modulus 1.2 and sodium aluminate clinker. Cement paste specimens were cured in a fog room at 20±3 °C for 24 h followed by curing in water at 20±2 °C. Compressive strength after 1 day curing was 20.2 MPa, after 7 days – 36.5 MPa and after 28 days – 56.0 MPa. Geopolymers synthesized at 23 °C and 40-50 % relative humidity from red mud and class F fly ash was investigated by Zhang et al. (2014). 28-day compressive strength ranging from 11.3 to 21.3 MPa was obtained.

Binders based on a natural pumice-type pozzolan are known (Kani et al., 2011). Xu and van Deventer (2000) studied the alkaline activation of some natural aluminosilicate minerals and they reported that all of them have some reactivity and can be source materials for geopolymers. The highest compressive strength of 18 MPa was obtained from the mineral stilbite in a KOH solution.

A wide range of raw materials can be used for alkali activation. This study is focused only on utilizing fly ash, as energy production in South Africa mostly relies on coal and big amounts of fly ash are being generated annually, suggesting that the use of large volumes of fly ash in alkali-activated binders is topical for South Africa.

2.4 ALKALINE ACTIVATORS

The most widely used alkali solutions in geopolymer synthesis are silicates, hydroxides and mixtures thereof discussed in this section.

Sodium hydroxide is commonly used for synthesis of geopolymers due to its low price and wide availability. However the use of it requires high caution due to the highly corrosive nature of this activator. It is also necessary to keep in mind that NaOH flakes or pearls easily absorb moisture from the air producing highly concentrated liquids that may provoke severe burns. It is essential to restrict contact of the NaOH with air and keep it in sealed containers. The solubility of NaOH at 25 °C is 53.3 % by mass (Provis, 2009). During dissolution of NaOH in water heat is released which can cause vaporisation of the solution.

Katz (1998) in his study of alkali-activated fly ash tested four sodium hydroxide concentrations. The effect of the concentration of the solution on compressive strength at 7 days is shown on Figure 2.7 below. He concluded that the concentration of the alkaline solution plays a significant role on compressive strength development. After 7 days, the compressive strength of the mixture with the lowest concentration was only 0.2 MPa. He supposed that this was due to weak Van Der Waals's forces between the small fly ash particles and not to the formation of hydration products. The 4 M mixture produced a compressive strength of 6.1 MPa after 7 days. Hence, the degree of reactivity increases with the NaOH concentration.

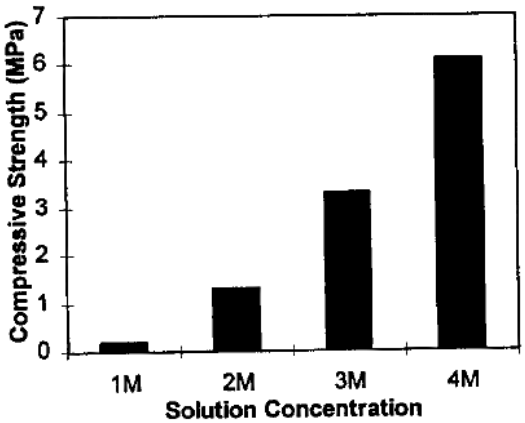

Figure 2.7: Effect of solution concentration on the compressive strength of alkali-activated fly ash paste at 7 days (Katz, 1998)

The use of potassium hydroxide solution is not common for geopolymer synthesis. However Palomo, Grutzeck and Blanko (1999a) investigated the mechanism of activation of a fly ash with highly alkaline solutions made with NaOH and KOH. They noticed that 12 M NaOH solution gives faster activation and higher strength than 18 M KOH solution.

Van Jaarsveld and van Deventer (1999a) affirmed the significance of alkali metal cation effect on every stage of the geopolymerization of fly ash. They claimed that the type of alkali metal present influence the speed of condensation reaction and final structure formation. They also mention that mixtures containing K^+ had higher compressive strength but this may only be true for systems activated using silicate solutions.

Sodium silicate is another widely used activator solution. Due to its lower pH it is often preferred to alkali hydroxide solutions. The viscosity of silicate solutions is much higher than that of alkali hydroxide solutions and the viscosity is a function of composition and temperature. High viscosity of silicate solutions may be problematic as fresh geopolymer mixtures may stick to mixing equipment.

Hardjito and Rangan (2005) have noticed that higher concentration (in terms of molar) of sodium hydroxide solution results in higher compressive strength. An increase in the ratio of sodium silicate solution to sodium hydroxide solution (by mass) leads to higher compressive strength of geopolymer concrete.

The use of alkali-carbonate solution is not common for geopolymerization of fly ash but it is used for the alkali activation of high calcium materials. Wang et al. (1994) studied alkali activation of slag with different types and concentration of activators. They concluded that the anionic component of the activator solution has an effect on the strength and other properties. The optimum dosage, taking all factors such as slag type, activator and curing condition, into account is in the range between 3.0-5.5 % Na_2O by slag weight. The authors suggested using sodium silicate solution with a modulus of 0.75-1.25 for acid slag, 0.9-1.3 for neutral slag and 1.0-1.5 for basic slag.

Fernandez-Jimenez and Palomo (2005a) studied the influence of type and concentration of alkaline activator on the properties of activated ash. They investigated three different alkaline compounds: NaOH, sodium silicate and anhydrous sodium carbonate. Their results indicate that the Na_2O content plays an important role in the development of mechanical strength. Increasing the concentration of the Na_2O leads to increased mechanical strength as shown in Figure 2.8. They also reported that the presence of soluble silica has a beneficial effect on strength development while the presence of CO_3 anion in the activator corresponds to material with relatively low mechanical strength; even high contents of Na_2O are available in the samples.

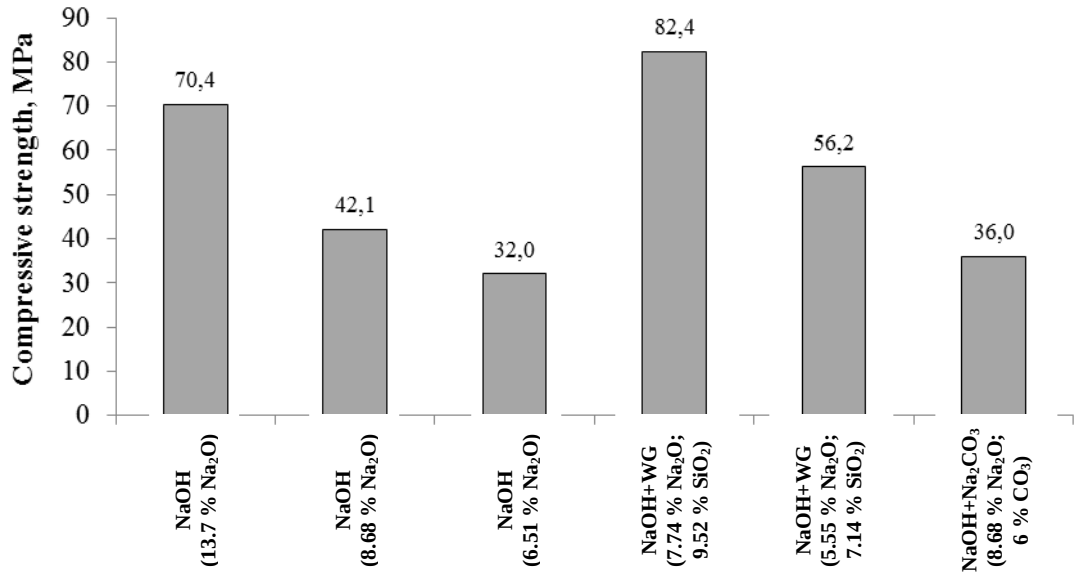

Figure 2.8: Compressive strength of alkali activated fly ash binder with different activators (Fernandez-Jimenez and Palomo, 2005a)

Bakharev et al. (1999) investigated alkali activation of Australian slag with sodium silicate, sodium hydroxide, sodium carbonate, sodium phosphate, and combinations of these activators. Figure 2.9 shows the compressive strength of alkali-activated slag pastes. The compressive strength obtained for sodium silicate-activated slag cements was in the range from 20 MPa to 40 MPa and depended on the modulus of the solution and concentration of alkalis. They mentioned that at a high modulus early strength decreased, and the setting time was significantly shortened. At high concentrations of alkalis the slag activated with the sodium silicate solution was found to have a high shrinkage and behaved like fast-setting cement.

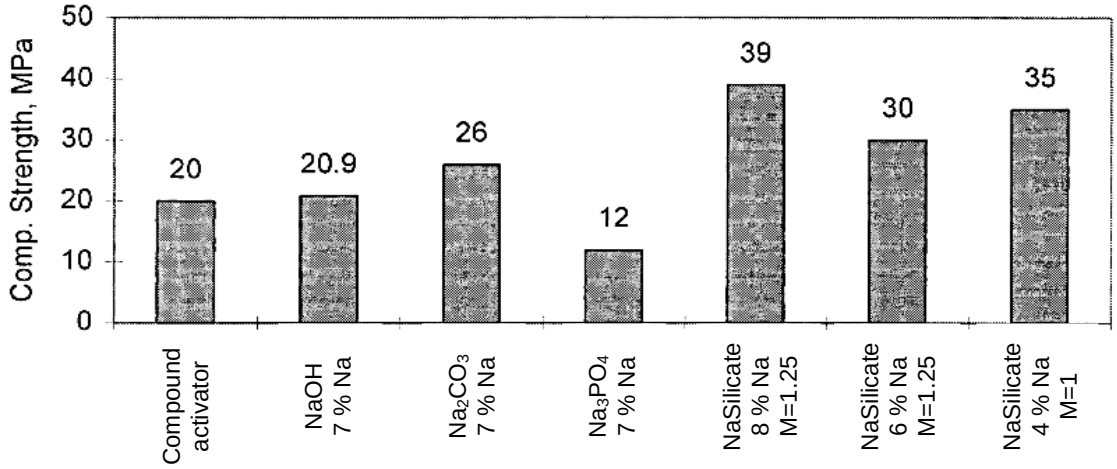

Figure 2.9: The 28-day compressive strength of alkali-activated slag pastes (Bakharev et al., 1999)

NaOH, KOH, sodium or potassium silicates, Na_2CO_3 and Na_2SO_4 are commonly used as activators. According to the majority of investigations the most effective ones for alkali activation of fly ash are solutions of caustic alkalis and low modulus liquid glass, or combinations of these. High level of caution has to be maintained during working with concentrated alkali with obligatory use of protective clothing, gloves and eyewear. All pieces of equipment have to be properly cleaned after each usage.

2.5 MECHANISMS AND KINETIC OF REACTION, REACTION PRODUCTS

There are two different models of alkali activation (Li et al., 2010). The first is alkali activation of metakaolin or fly ash as example (Si + Al) by medium and high alkaline solutions with the formation of poorly ordered structure but with good mechanical properties. The second model is of blast furnace slag (Si + Ca) by mild alkaline solution with C-S-H gel as the main reaction product. The exact mechanism of reaction which can explain the hardening of alkali-activated binder is not yet fully understood (Pachego-Torgal et al., 2008a).

2.5.1 Reaction mechanism of alkali activation of metakaolin and fly ash

Duxson et al. (2007b) proposed the mechanism for geopolymerization of aluminosilicate sources shown in Figure 2.10. According to them geopolymerization goes through the following steps:

- Dissolution of solid aluminosilicate source in alkaline solution with liberation of aluminate and silicate monomers.
- The species released by dissolution are incorporated into the aqueous phase. Dissolution of amorphous aluminosilicates is rapid at high pH, and this quickly creates a supersaturated aluminosilicate solution.
- In concentrated solutions this results in the formation of a gel, as the oligomers in the aqueous phase form large networks by condensation. This process releases the water that was nominally consumed during dissolution. Water plays the role of a reaction medium and resides within pores in the gel. The time for the supersaturated aluminosilicates solution to form a continuous gel varies considerably with raw material processing conditions and solution composition and synthesis conditions.
- After gelation the system continues to rearrange and reorganize, as the connectivity of the gel network increases, resulting in the three-dimensional aluminosilicate network commonly attributed to geopolymers.

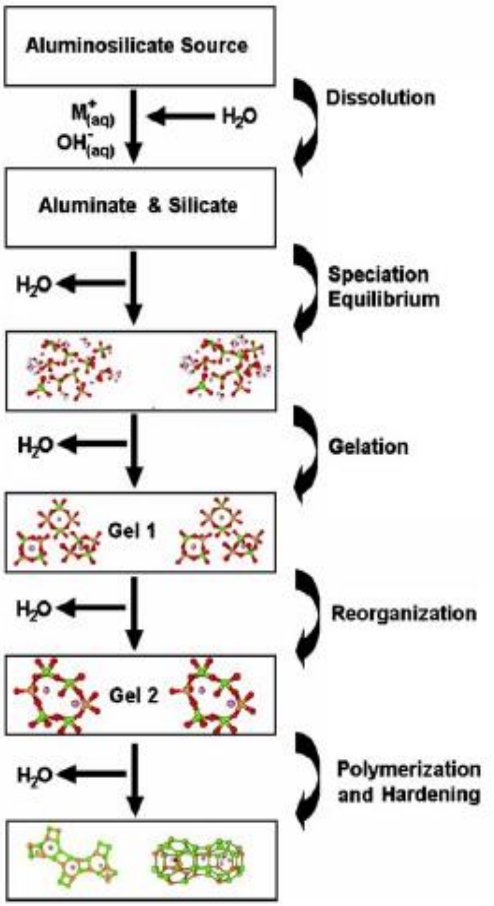

Figure 2.10: Conceptual model for geopolymerization (Duxson et al., 2007b)

Provis and van Deventer (2007) proposed the geopolymerization reaction sequence shown in Figure 2.11. They conclude that the products of geopolymerisation reaction should include both gel and zeolitic phases.

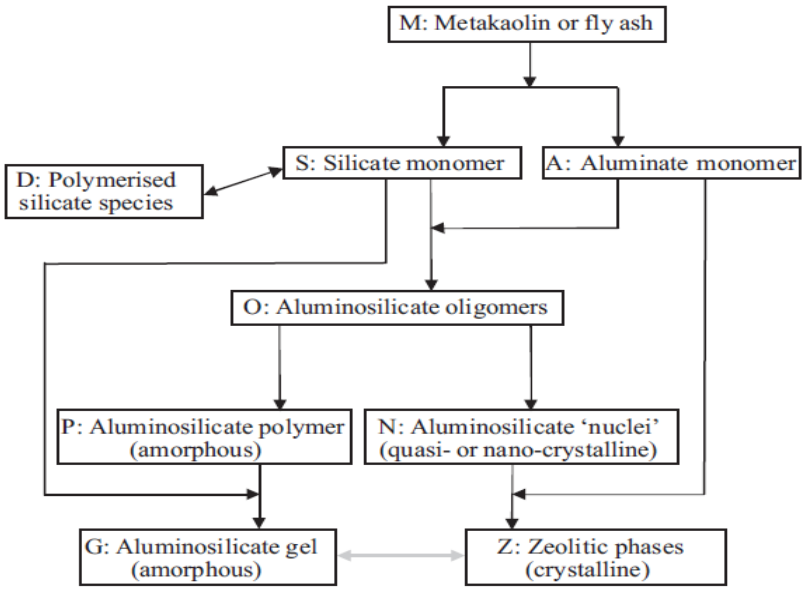

Figure 2.11: Reaction sequence of geopolymerization (Provis and van Deventer, 2007)

Fernandez-Jimenez et al. (2006b) described the activation model of fly ash as follows. Firstly the vitreous component of fly ash is dissolved and no strength development is observed during this process. Secondly (induction period) an unstable aluminium rich gel precipitates. The beginning of this stage is associated with the initial setting of the paste. During the third stage Al-rich gel is transformed into Si-rich gel, considerably increasing the mechanical strength. A schematic description of the evolution of mechanical properties is shown in Figure 2.12.

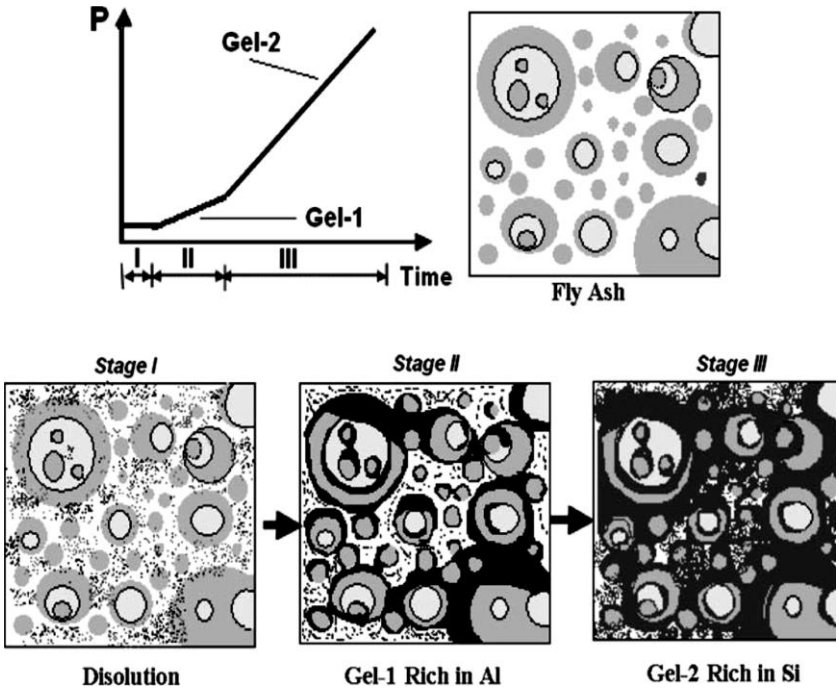

Figure 2.12: The schematic description of mechanical properties evolution (Fernandez-Jimenez et al., 2006b)

The dissolution process starts with an attack on the fly ash particles by the alkaline solution (Fernandez-Jimenez et al., 2005c). As a result the reaction product is generated both inside and outside the shell of the sphere until the ash particle is completely or almost completely consumed (Figure 2.13 a-c). At the same time, precipitation of reaction products occur as the alkaline solution penetrates the larger sphere and fills up the interior space with reaction product, forming a dense matrix (Figure 2.13 b). Due to the massive precipitation of reaction products, some portions of smaller particles are covered with the products providing a crust which prevents contact with the alkaline solution (Figure 2.13 e) thus resulting in unreacted fly ash particles. As a consequence, several morphologies may co-exist in a single paste.

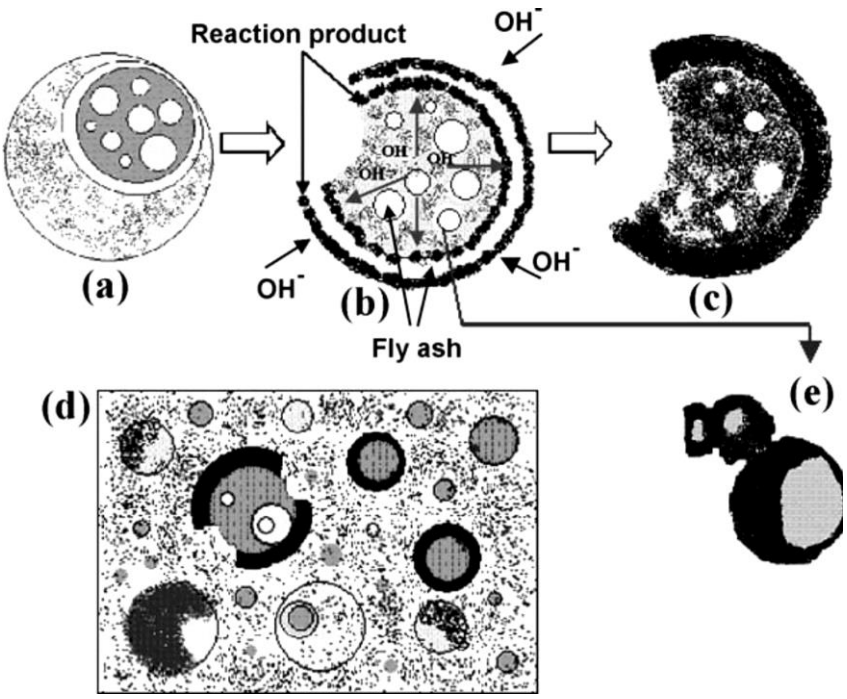

Figure 2.13: Descriptive model of the alkali activation of fly ash (Fernandez-Jimenez, 2005c)

Palomo, Grutzeck and Blanco (1999a) concluded that the alkali activation reaction of fly ashes is an exothermic process during which covalent Si-O-Si and Al-O-Al bonds break down and ions migrate to the activation solution. The products of the fly ash destruction accumulate during the induction period when heat release barely exists. Thereafter condensation of the structure occurs accompanied by a strong exothermal step. As a result a material with poorly ordered structure but high strength is formed. The authors mention that all the reaction steps occur at almost the same time.

The kinetics of hydration of alkali-activated materials was investigated in several studies. Ma et al. (2012) investigated the kinetics of hydration of fly ash activated with different sodium silicate solutions at 40 °C as shown in Figure 2.14. They concluded that the heat released by alkali-activated fly ash is considerably lower that for OPC and the addition of SiO_2 retarded the reaction, while Na_2O was favorable to the reaction.

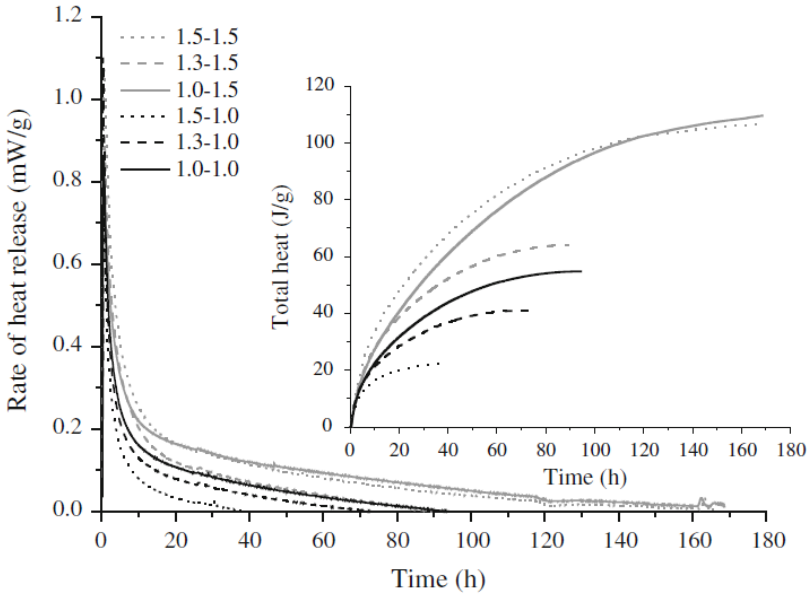

Figure 2.14: Heat evolution and cumulative heat of alkali-activated fly ash with different sodium silicate solutions (Ma et al., 2012). The legend shows proportions of SiO_2 (first number) to Na_2O (second number) in sodium silicate solution

Recent results of Zhang et al. (2014) on the effect of fly ash on geopolymerization characterized by isothermal calorimetry are shown in Figure 2.15. They found that the magnitude of the first exothermic peak, attributed to the dissolution stage of the solid precursors decreased and delayed when metakaolin was partially replaced with fly ash.

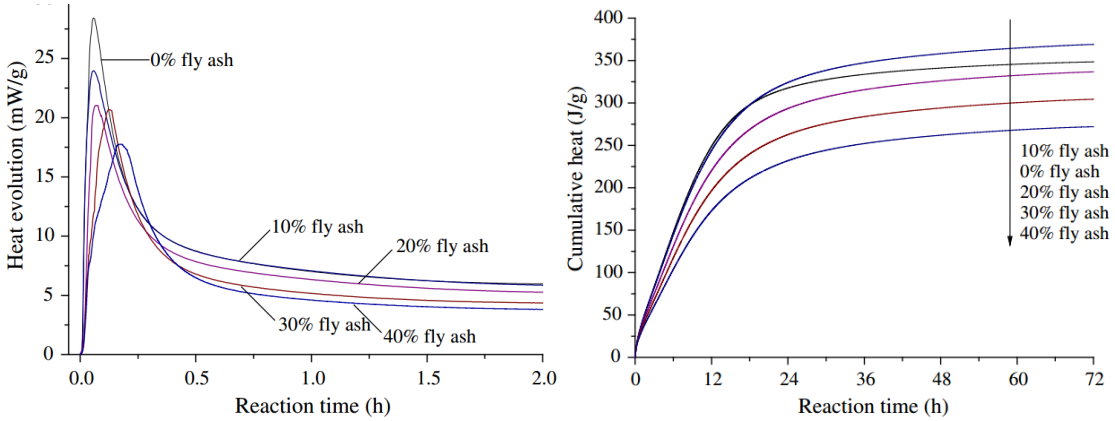

Figure 2.15: Heat evolution (left) **and cumulative heat** (right) **of alkali-activated metakaolin with partial replacement by fly ash (Zhang et al., 2014)**

2.5.2 Reaction mechanism of alkali activation of slag

Fernandez-Jimenez and Puertas (1997) investigated the kinetics of hydration of alkali-activated slag at different temperatures. A mixture of water glass and NaOH solution was used as activator. The degree of reaction was determined by means of the heat of hydration after the induction period. They associated the first step of hydration with the first step on the curves in Figure 2.16, beginning with the slag dissolution reaction. The second step was

called the induction period or period of low reactivity. The third and fourth steps the authors associated with the second peak on the curve. In these steps, a massive precipitation of reaction products took place. The final and fifth step corresponds to a low reactivity period and the end of reaction. They concluded that alkaline activation of slag is a fast process as the second peak appears on the curve after less than 10 hours.

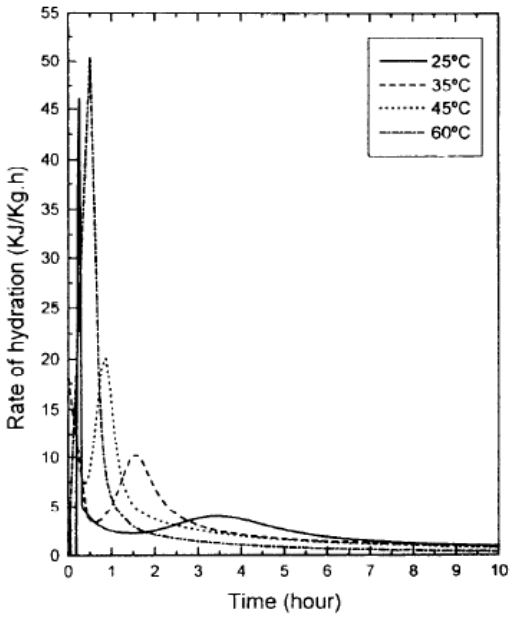

Figure 2.16: Slag rate of hydration vs. time (Fernandez-Jimenez and Puertas, 1997)

Krizan and Zivanovic (2002) analysed the heat release in alkali-activated GGBFS, and have noticed that the higher Na_2O and silica modulus were related to higher hydration levels. Meanwhile, the process begins with the destruction of the Ca–O, Mg–O, Si–O–Si, Al–O–Al and Al–O–Si bonds of the slag grain. Since the Ca–O and Mg–O bonds are much weaker, more Ca and Mg enter into water than Al and Si, and the Si/Al-enriched layer forms quickly on the surface of slag. The initial peak corresponds to the wetting and dissolution of slag grains and adsorption of some ions onto the surface of slag grains, and the second peak to the formation of precipitate layer at the slag particle surface. They mentioned that the precipitation of C-S-H gel results in a very long induction effect, varying from about 5 to 14 h, observed before the appearance of the accelerated hydration peak. The higher the activator dosage, the shorter is the induction period. When the slag grains were coated by a hydrate layer, the hydration kinetics was controlled by a diffusion process until the completion of the reaction with the diffusion process being affected by the degree of structural defectiveness.

The study of Wang and Scrivener (1995) mentioned that during the hydration of alkali-activated slag, the products form by a dissolution and precipitation mechanism during the

early stages of reaction, but at later stages the reaction may continue by a solid state mechanism.

Li et al. (2010) concluded that the reaction mechanism of alkali activation of GGBFS is more complicated than geopolymers due to the significant content of calcium.

2.5.3 Hydration products

Results of different investigations show that the reaction products of alkali activation depend on the type of raw materials used. However, it is commonly acknowledged that C-S-H is the major reaction product in alkali-activated GGBFS and three-dimensional zeolite like polymer is a binding phase in geopolymers (Li et al., 2010). In Table 2.1 typical reaction products found by different researchers are shown.

Table 2.1: Reaction products in different alkali-activated materials

Reaction products	Type of raw material	Type of activator	Authors
Low calcium silicate hydrate; hydrotalcite	Slag	NaOH, sodium silicate	Wang and Scrivener, (1995)
C-S-H phase; hydrotalcite; hydrogarnet; tetracalcium aluminate hydrate; stratlingite; ettringite	Slag	Sodium silicate + KOH	Chen and Brouwers, (2007)
Amorphous phase; faujasite (after 90 days)	Metakaolin	NaOH	Palomo et. al (1999b)
Amourpous phase; crystalline phases presented in initial fly ash; C-S-H phase in case of slag	Fly ash + Slag	Sodium silicate + NaOH	Škvára et. al, (2003)
Amorphous alkali aluminosilicate gel; + chabazite, Linde type A, Na-Pl (gismondine) zeolites, hydroxysodalite in case of only NaOH	Fly Ash	Sodium silicate + NaOH	Bakharev, (2005b)
Aluminosilicates gel with low-ordered crystalline structure; + hydroxysodalite, herschelite in case of NaOH; + hydroxysodalite, Trona, Nahcolite in case of Na_2CO_3	Fly ash	NaOH, NaOH+sodium silicate, NaOH+Na_2CO_3	Fernandez-Jimenez and Palomo, (2005a)

2.6 FACTORS AFFECTING ALKALI ACTIVATION AND FINAL MATERIAL PROPERTIES

Different factors affecting alkali-activated material properties will be discussed in this section. The focus will be on alkali-activated materials based on fly ash due to the scope of this thesis.

2.6.1 Chemical and mineralogical composition of initial materials

According to Xu and van Deventer (2000) factors such as the percentage CaO, K_2O, the molar Si–Al ratio in the original mineral and the type of alkali had a significant effect on compressive strength. Arjunan, Silsbee and Roy (2001) concluded that the chemical and mineralogical composition of the low calcium fly ashes do not influence the alkali activation.

It was already previously mentioned that Fernandez-Jimenez and Palomo (2003) suggested that the CaO content should be low in alkali-activated fly ashes. However Diaz et al. (2003) only partially agreed with these fly ash requirements. They consider 5 to 15 % of CaO in fly ash desirable for many applications.

The geopolymerization process is highly dependent on the individual fly ash source (Duxson, 2009). Knowledge of the chemical and mineralogical composition is critical as not all aluminium and silica takes part in the geopolymerization process (Van Jaarsveld et al., 1997). Hence a detailed analysis of the mineralogical composition of each batch of fly ash has to be performed.

2.6.2 Type, concentration and modulus of activator

Komljenović et al. (2010) establish that the nature and concentration of the activator is the most dominant parameter in the alkali activation process. KOH and NaOH+Na_2CO_3, showed a very low activation potential compared to NaOH. $Ca(OH)_2$ showed a considerable activation potential, in most cases higher than NaOH. However, it must be taken into account that the concentration of CaO was higher compared to that of the other activators. Concentration of activator can also considerably influence the mechanical characteristics of alkali-activated fly ash mortars. The increase in activator concentration led to increased compressive strength.

Guo et al. (2010) obtained a high compressive strength when the molar ratio of SiO_2/Na_2O for the activator was 1.5 and Na_2O content was 10 % of the fly ash mass.

Higher concentration of Na_2O in the system does not always result in higher compressive strength. The results of a number of studies prove this statement (Palomo et al., 1999a; Van Jaarsveld and van Deventer, 1999a; Steveson and Sagoe-Crentsil, 2005b; Somna et al., 2011).

Although the Na_2O content may have improved the solubility of the aluminosilicate source, the recent results of Heah et al. (2013) showed that excess Na_2O content in the system could seriously weaken the formed structure. Some researchers observed in geopolymers the formation of zeolite (Provis et al., 2005; Bakharev, 2005b) or hydroxysodalite (Palomo et al., 1999a; Fernandez-Jimenez and Palomo, 2005a). Correlation between zeolite formation and decreased strength was observed in certain systems (Provis, 2009), but it is still unclear whether zeolite formation leads to performance loss or high concentrations of alkali itself is the problem or the decreased strength could even be caused by a combination of factors.

Panias et al. (2007) reported that the amount of sodium silicate solution in the synthesis of geopolymers substantially affects the obtained compressive strength. Sodium silicate solution controls the soluble silicate concentration and the predominant silicate species in the geopolymeric system, improving the mechanical strength of the produced materials. A maximum compressive strength of 41.3 MPa was achieved when the concentration of the soluble Si in the aqueous phase of the geopolymeric system was equal to 2.3 M.

The results of Pacheco-Torgal et al. (2011) show that flexural and compressive strength of metakaolin activated by sodium hydroxide solution increased with an increase in sodium hydroxide. Alonso and Palomo (2001a) found that flexural strength values of metakaolin activated by calcium hydroxide solution cured for 24 hours decrease as activator concentration increase.

The different researchers refered to used different alkali concentrations for different raw materials. Calcium free materials demand higher alkali concentrations. Mixtures of waterglass and sodium hydroxide solution as activator gives better strength results for low calcium fly ash. However, higher alkali contents does not necessary result in higher strength. Thus for each particular fly ash there has to be an optimum and this topic will be studied in detail in the following chapter. Special attention will be paid to the question of strength decreasing in samples with raised alkali content if such be the case. The explanation of this phenomenon will fill a gap in knowledge and will result in better understanding of the geopolymerization process.

2.6.3 Fineness of raw materials

Wang et al. (1994) claimed that optimum fineness depends on slag basicity coefficient, activator and curing conditions. The higher fineness the higher strength. However, a certain workability is nessesary for shaping of products: if the workability and alkali amount are kept constant the optimum range of fineness is: 450-650 m^2/kg for acid and neutral slags, 400-550

m^2/kg for basic slags. The authors noticed that the strength increase with increased fineness was more pronounced at early ages. This statement was shared by Somna et al. (2011). Strength development of original fly ash with a median particle size of 41 µm was lower than that of ground fly ash with a median particle size of 10.5 µm. They therefore concluded that an increase in fineness of fly ash resulted in a significant increase in strength development of paste especially at the early age of 7-14 days.

Based on the results of investigations into the reactivity of fly ashes Fernandez-Jimenez and Palomo (2003) concluded that the fineness of the fly ashes plays an essential role in the development of the mechanical strength of materials obtained after activation. When the particle fraction sized higher than 45 µm was removed, the mechanical strength of alkali-activated fly ash remarkably increase, reaching 70 MPa after 1 day.

Kumar and Kumar (2011) investigated the effect of mechanical activation of fly ash on reaction and properties of resulting geopolymer. They concluded that reactivity of fly ash increases rapidly when particle size is reduced to less that 5-7 µm. The 28-days compressive strength of ambient-cured fly ash geopolymer increased from about 3 MPa when raw fly ash was used, to more than 35 MPa for fly ash milled during 90 minutes. Measured heat evolution shown that the maximum rate of heat evolution increased and time at which maximum peak occurred shifted to lower time with increase in milling time.

Rahier et al. (2003) concluded that the reaction rate increases for alkali-activated metakaolinite with decreasing metakaolinite particle size. They mentioned that for the largest particles hindered mass transport occurs during the polymerization.

Fineness affects the compressive strength of geopolymers especially at early age for both high and low calcium raw materials.

2.6.4 Temperature, duration and type of curing

Temperature of curing is a significant factor affecting the final properties of alkali-activated fly ash cements. A wide temperatures range from ambient to 90 °C was used for producing alkali-activated binders and concretes (Fernandez-Jimenez and Puertas, 1997; Van Jaarsveld et al., 2002; Khale and Chaudhary, 2007; Chi, 2012; Ariffin et al., 2011; Muñiz-Villarreal et al., 2011). Almost all researchers noticed the importance of heat treatment for fly ash-based alkali-activated material with good mechanical properties (Bakharev, 2005b; Winnenfeld et al., 2010; Criado et al., 2010; Kovalchuk et al., 2007). It was stated by Hardjito and Rangan (2005) that heat curing temperatures can be as low as 30 °C, which would be attainable in tropical climate conditions. Katz (1998) reported that no reaction took place at room

temperature and higher temperatures are needed for activating fly ash. However, the results of Somna et al. (2011) disproved his assumption. Compressive strength values of 20-23 MPa at 28 days were obtained with NaOH concentrations of 9.5-14.0 M for samples cured at ambient temperature. In this case they were however using ground fly ash with a median particle size of 10.5 µm. Curing fly ash geopolymer at ambient temperature is possible although the reaction in this condition is very slow (Hole, 2009).

Bakharev (2005b) reported that long pre-curing at room temperature was beneficial for strength development of fly ash geopolymers. This statement is shared by Hardjito and Rangan (2005). They also confirmed that higher curing temperature resulted in higher compressive strength, although an increase in the curing temperature beyond 60 °C did not increase the compressive strength substantially. Longer curing time improved the polymerization process resulting in higher strength.

Palomo et al. (1999a) affirmed that the activation reaction is notably influenced by the temperature. Temperature is especially important for 2 and 5 hours of curing. The mechanical strength of prisms cured at 85 °C is much higher than those cured at 65 °C. The longer the duration of curing, the higher the average strength becomes.

Bakharev et al. (1999) reported that heat curing produced considerable acceleration in strength development of alkali-activated slag, while Fernandez-Jimenez et al. (1999) mentioned that the increase of curing temperature does not favour the increase of mechanical strengths of slag mortars at later ages, but has a positive effect at early ages when the activator is $Na_2SiO_3 \cdot nH_2O$ + NaOH or Na_2CO_3.

Wang et al. (1994) mentioned the effect of different types of curing regimes on compressive strength. For example, phosphorous slag (neutral or acid in nature) activated by water glass had a strength of 30 MPa under normal curing, 62 MPa after steam curing and 71-76 MPa after autoclaving, while basic granular blast furnace slag activated by the same solution had a strength of 80 MPa under normal curing and 85-95 MPa after steam and autoclaving.

Van Jaarsveld et al. (2002) supposed that mild curing improve physical properties while curing under higher humidity is not usually beneficial. Rapid curing and/or curing at too high temperatures will result in cracking and thus have a negative effect on physical properties.

Different curing conditions are used for different raw materials and activators. Almost all authors admitted the importance of heat treatment for alkali-activated low calcium fly ash with preferable pre-curing at ambient temperature.

2.6.5 Water content

It is known that water plays an important role in hydration process of Portland cement. Generally, with the given concrete materials and testing conditions, the quantity of used mixing water determines the strength of the concrete, so long as the mix is of a workable plasticity. This basic principle has been brought out by Duff Abrams (1919) and known as Abram's law.

Fernandez-Jimenez and Palomo (2005a) mentioned the importance the 'water to binder ratio' for alkali-activated fly ash binder. Hardjito and Rangan (2005) reported that as the ratio of water to geopolymer solids by mass increases, the compressive strength of fly ash-based geopolymer concrete decreases. They admitted that water released during the chemical reaction that occurs in the formation of geopolymers leaving behind discontinuous pores in the matrix. The water in a geopolymer mixture plays no role in the chemical reaction, but it provides workability during handling.

In contrast, Duxson et al. (2007) stated that water consumed during dissolution of aluminosilicates released during condensation, plays the role of a reaction medium, resideing within pores in the gel. Such gel structure is commonly referred to as bi-phasic, with the aluminosilicate binder and water forming two phases.

Zuhua et al. (2009) reported that water is indispensable during geopolymerization, especially for the destruction of solid particles and the hydrolysis of dissolved Al^{3+} and Si^{4+} ions. The results of their work also indicated that 7.4 % of structural water is necessary to keep stable strength of calcined kaolin-based geopolymer.

Provis and van Deventer (2007) believed that water affects the geopolymerization in each stage. The stated that the rate of aluminosilicate dissolution decreases in the presence of additional water. While the rate of condensation or polymerisation reaction is hypothesised to increase in the presence of additional water under the very water-poor conditions prevalent during geopolymerization.

Panias et al. (2007) agreed that water content is a crucial parameter in the synthesis of fly ash-based geopolymers for the development of mechanical strengths. A reduction of water content in the synthesis of fly ash geopolymers improved their compressive strength.

The results of Van Jaarsveld et al. (2002) show that the water content, curing as well as calcining conditions affect the final properties of a geopolymer. Steveson and Sagoe-Centsil (2005a) studied relationships between composition, structure and strength of metakaolin-

derived inorganic polymers and they reported that the compressive strength showed a clear correlation with the water content and microstructure. Low water content samples had lower porosity and higher compressive strength, while high water content samples were very porous and weak as a result.

Wang et al. (1994) advised researchers to consider liquid to slag (l/s) ratio when alkali is used in liquid form. Increasing l/s ratio results in increased alkaline activation due to the introduction of more alkali and a simultaneous increase of pore volume in hardened concrete due to introducing more water. The effect of l/s ratio on the compressive strength is positive at lower l/s ratios.

2.6.6 Age

De Vargas et al. (2011) reported that temperature and age only affected the strength gain of alkali-activated fly ash samples with Na_2O/SiO_2 molar ratios of 0.3 and 0.4. For the Na_2O/SiO_2 0.20 samples, mechanical results changed very little with time.

Stability of amorphous geopolymer gels was studied by Lloyd (2009) through the use of accelerated ageing tests. The strength development of metakaolin-based geopolymers, cured and aged at 23 °C was very rapid in the first 3 days, achieving almost 70 MPa. But after 28 days a clear, statistically significant, decline in strength development was observed. Accelerated ageing of geopolymers were done in the following order: sealed samples were cured for 28 days in water baths, after the initial 24 hours in moulds. Samples were then cured in water baths at 95 °C. After one day of ageing at 95 °C the compressive strength increased. Between one and three days at 95 °C a dramatic reduction in compressive strength was evident and the strength then remained relatively stable for the next 25 days of ageing at 95 °C. The strength loss observed was approximately 60 % of the cured value and the author concluded that it could lead to failure of concrete produced with this type of binder. Unlike metakaolin-based geopolymers, fly ash-based geopolymers were found to be resistant to strength regression during accelerated ageing, in fact the strength of those samples were even higher after 28 days of ageing at 95 °C than before ageing suggesting that fly ash can provide the basis for long-lasting materials.

The author also reported that fly ash-containing geopolymer mortars increased in strength over a six-month period as shown in Figure 2.17, while the strength of alkali-activated slag remained constant over the test period, indicating that slag reacts in a short period of time.

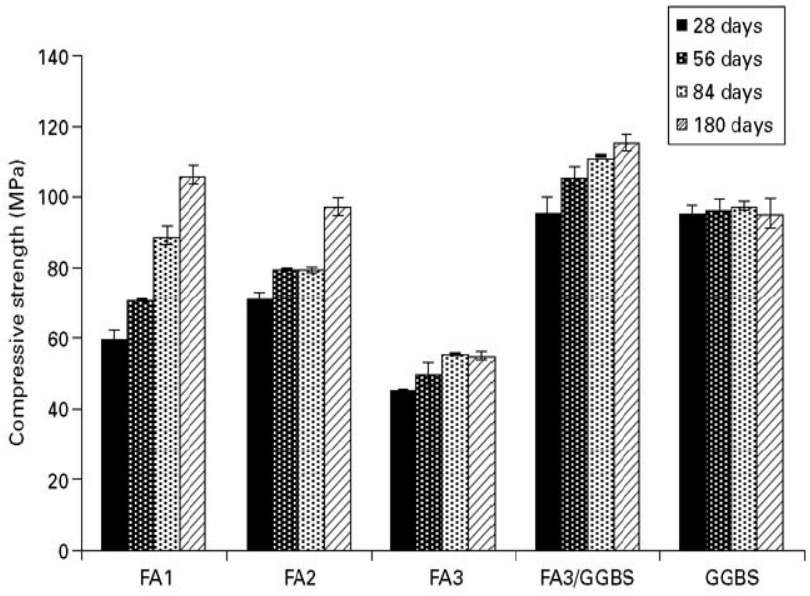

Figure 2.17: Strength development profiles of geopolymer mortars synthesized from fly ash (FA1, FA2, FA3), ground granulated blast-furnace slag (GGBS) and a blend of fly ash and slag (FA3+GGBS) (Lloyd, 2009)

2.7 OTHER PROPERTIES OF GEOPOLYMER BINDERS IN COMPARISON TO ORDINARY PORTLAND CEMENT (OPC)

This section provides a review of engineering properties of geopolymers.

2.7.1 Environmental aspects of geopolymer production

Production of cement requires high energy efforts and has a significant impact on the global emissions of Greenhouse Gases. During the production of 1 tonne of cement between 0.73 and 0.99 tonnes of CO_2 is released to the atmosphere (Hasanbeigi et al., 2012; McLellan et al., 2011; Flower and Sanjayan, 2007). One of the major cement manufacturers in South Africa Pretoria Portland Cement (PPC) reported that in 2011 its carbon footprint for cement was 892 kg CO_2 per tonne of cement which is an increase of 2.6 % compared to 2010 ('PPC Integrated Annual Report', 2011). Globally, the cement industry accounts for approximately 5 % of the current anthropogenic carbon dioxide emissions (Hasanbeigi et al., 2012).

Geopolymer manufacture consumes less energy and results in reducing greenhouse emission with Portland cement replacement. According to data published in literature carbon emissions of geopolymers can be 80 % less than traditional cements (van Deventer et al., 2010) or reduce greenhouse gas emissions by 44-64% (McLellan et al., 2011). Recent conclusions of Turner and Collins (2013) show the CO_2 footprint of geopolymer concrete is only 9 % less than that of OPC concrete. The CO_2 footprint of alkali-activated concretes is highly dependent

on the type, concentration and dosage of the alkali activators (as production process of alkali have relatively high CO_2 emissions) as well as curing conditions for the concrete and the mix proportions of the ingredients (Yang et al., 2013). Heath et al. (2014) believe that using multiple initial aluminosilicate sources, activators and curing temperatures for geopolymer manufacture lead to a complex mix design and has potential to reduce global warming potential of geopolymers compared to Portland cement.

In light of the latest tendencies: the distribution of carbon credits under the Kyoto agreement and the possibility of applying carbon taxes in South Africa, the advantage of geopolymer binders over OPC binders is obvious. At the same time giving an economic value to industrial by-products and utilizing it in large amounts will lead to improvement of the environment, economic and social life.

2.7.2 Compressive strength

The compressive strength of geopolymers will not be discussed here in detail as previously it was already mentioned that many factors, such as raw material composition, type and concentration of activator, etc. affect strength. Wallah and Rangan (2006) reported that low calcium fly ash-based geopolymer concrete with consistent reproducible quality and long-term stability can be produced. The behaviour and failure mode of fly ash-based geopolymer concrete in compression is similar to that of Portland cement concrete (Rangan, 2009).

2.7.3 Shrinkage, creep, elastic constants

Li et al. (2005) measured the drying shrinkage of cement and geopolymer mortar prisms. The drying shrinkage of three geopolymer mortars with different water to cementitious material ratios (0.34-0.42) was 0.084 %, 0.065 % and 0.048% at 150 days, while the drying shrinkage of Portland cement mortar was 0.091 % at the same age at 0.34 water-cementitious materials ratio. The shrinkage of geopolymers was lower than Portland cement materials and it seemed to be affected by water content in the system.

Results of Atiş et al. (2009) show that the shrinkage of slag mortar activated by liquid sodium silicate and sodium hydroxide was 3 and 6 times more than the shrinkage of Portland cement and Portland cement mortar, respectively. The shrinkage of sodium carbonate activated slag mortar was lower or similar to Portland cement mortar. So it can be concluded that shrinkage of alkali-activated slags are highly affected by the type of activator.

Rangan (2009) reported that low calcium fly ash geopolymer concrete undergoes very little drying shrinkage, about 100 micro strains after one year. This value is significantly smaller

than that usually observed in Portland cement concrete. He also noticed that the values of basic creep coefficients are about 50 % of that recommended for Portland cement concrete, between 0.6 and 0.7 for 40 MPa, 47 MPa and 57 MPa geopolymer concrete and between 0.4 and 0.5 for geopolymer concrete with compressive strength of 67 MPa.

Recent work of Sagoe-Crentsil et al. (2013) investigated the creep behaviour and drying shrinkage performance of fly ash geopolymer concrete and compared them to equivalent grade of OPC concrete. It was reported that drying shrinkage values fell below the standard 700 μstrain limit, with geopolymer typical values less than 400 μstrain. Values of creep coefficients were found to be 45 % lower in geopolymer concrete than corresponding OPC concrete.

Works of scientists from Australia (Rangan et al., 2005) show that the values of Young's modulus of fly ash-based geopolymer concrete are similar to those of Portland cement concrete using the same coarse aggregate type. The Poisson's ratio falls between 0.12 and 0.16, that is within the range observed for Portland cement concrete. The stress-strain relation in compression of fly ash-based geopolymer concrete is also similar to Portland cement concrete.

2.7.4 Acid and sulphate resistance, sea water resistance

First of all it is necessary to take into account that the main reaction product of geopolymers is aluminosilicate gel with a three-dimensional structure which is different from products of hydration of OPC and thus the behaviour of geopolymers in different aggressive environments will differ from OPC binders.

Gourley and Johnson (2005) affirmed that appropriately formulated and cured geopolymer concrete (GPC) is virtually acid resistant compared to OPC concrete. They reported that sewer pipe concrete made of 60 MPa OPC concrete and repeatedly immersed in pH=1 sulphuric acid had more that 10 % mass loss after 30 cycles while GPC had less than 2 % mass loss.

Bakharev (2005c) also investigated durability of geopolymers exposed to 5 % solutions of sulphuric and acetic acids. The best performance with the least weight loss was recorded for samples activated by sodium hydroxide solution. However the samples activated by combination of sodium and potassium hydroxide solution performed well with 4.5 % strength loss in the first month (compared to the initial compressive strength determined after pre-curing – heat – cooling periods) and about 10 % strength decline in the second month of exposure, which continued over the next 4 months, reaching 38.3 % after 6 months of testing.

Samples activated by sodium hydroxide solution had a rapid strength loss of about 45 % after 2 months of exposure, recovered slightly and had about 40 % strength reduction after 6 months of testing. OPC and OPC + FA paste samples had 91 % and 69 % strength loss, respectively, after 2 months, and about 91 % and 84 %, respectively, after 6 months of exposure.

Bakharev et al. (2003) also found that alkali-activated slag (AAS) concrete exposed to acetic acid solution had a superior durability to OPC concrete in the same conditions. If compared to specimens stored in water, OPC samples had about 47 % and AAS about 33 % strength reduction when stored in the acid solution for 12 months. After 12 months of exposure, OPC had a pH decreased to below 9 to a depth of 22 mm, while AAS concrete had a pH reduction to below 9 to a depth of 16 mm.

It was found by Song (2007) that geopolymer resistance against sulphuric acid attack in terms of the surface appearance, mass loss and residual compressive strength was superior to Portland cement paste. Geopolymer concrete samples retained their shapes without softening and peeling after immersion in a 10 % sulphuric acid solution for 56 days or in 1 % acid for one and a half years. In the same acidic situation, the paste in the outer layer of Portland cement concrete was completely dissolved and destroyed, exposing aggregates after only 28 days.

Palomo et al. (1999b) studied metakaolin mixtures activated with NaOH and waterglass when submitted to sulphuric acid (pH=3), sea water (pH=7) and sodium sulphate (pH=6) for 90 days. They reported a minor flexural strength decrease from 7 to 28 days immersion, between 28 and 56 days flexural strength rises, decreasing again from 56 to 90 days and rising from that day onward. The behaviour was similar for all solutions. According to these authors, unreacted sodium particles are not in the structure of the hardened material, remaining in a soluble condition thus when in contact with a solution they are leached increasing the binder porosity and lowering mechanical strength. On the other hand, the strength increase after 3 months indicates that the reaction process is still evolving, with the formation of zeolitic precipitates (faujasite) thus lowering porosity and increasing strength.

Bakharev (2005a) found that geopolymer material produced using class F fly ash exposed to sulphate solutions showed no visual signs of deterioration. After 5 month of immersion in different solutions weight gain was observed for all samples, except those that were activated by mixture of NaOH and KOH and were immersed in Mg_2SO_4 solution. The OPC and OPC + fly ash samples were covered with a 1-mm thick white cover when exposed to the magnesium sulphate solution and the part which was immersed in sodium sulphate was cracking. OPC

and OPC + fly ash samples immersed in the solution of sodium and magnesium sulphate had the most significant deterioration and gained in weight 9.1 % and 7.3 % respectively. The authors concluded that the best performance in different sulphate solutions was observed in geopolymer activated by sodium hydroxide solution.

At the same time Lloyd et al. (2012) affirmed that mass loss as measure of corrosion is not an accurate method of measure for the penetration of acid into material due to the details of the degradation mechanism, which involves the formation of a degraded product layer on the sample surface. They suggested that corroded depth should be measured as it was found to be more sensitive to mechanisms of degradation than mass loss.

Li et al. (2005) showed that geopolymer mortar prisms immersed in sodium sulphate solution did not undergo any dangerous expansion, and formation of gypsum and/or ettringite was not observed.

The resistance of fly ash-based geopolymer concrete in 5 % sodium sulphate solution and in 2 %, 1 % and 0.5 % sulphuric acid solutions was investigated by Wallah et al. (2005). The changes in compressive strength, mass and length of samples were measured for various exposure periods. The results showed excellent resistance to sulphate solution of fly ash-based geopolymer concrete. Acid attack did however reduce the compressive strength of geopolymer concrete more than 2.5 times after 1 year of exposure in 2 % sulphuric acid solution. The reduction of compressive strength was much lower in the case of 1 % and 0.5 % concentration.

Recent results of Bernal and Provis (2014) show that exposure of alkali-activated materials (AAM) to sulphate salts can negatively affect the structure of these materials, depending on the cation accompanying the salt. Immersing AAM to the Na_2SO_4 favours the structural evolution, while immersing to the Mg_2SO_4 promotes the destruction of the main reaction products via cation-exchange mechanism.

In general it can be concluded that the performance of geopolymers in acid environment is better than that of OPC binders. The mechanism of sulphate attack accepted for OPC binders cannot be applied to geopolymers as no $Ca(OH)_2$ is formed during geopolymerization and no gypsum and ettringite will be generated.

2.7.5 Corrosion of reinforcement, resistance to carbonation, chloride ingress

The main reason for failure of reinforced concrete structures is the corrosion of reinforcement (Bertolini et al., 2004). In OPC binders, steel bars are protected by a passivity layer, due to the

high alkalinity of calcium hydroxide. Corrosion of steel bars may happen if the pH decreases thus destroying the passivity layer, due to carbonation or chloride ingress.

Work of Morris and Hodges (2005) showed that steel, copper and type 316 stainless steel can be successfully embedded in fly ash-based geopolymers. Aluminium and zinc cannot be used due to severe corrosion in contact with the fresh binder.

Roy et al. (2000) compared chloride diffusion of OPC and alkali-activated binders and reported that the alkali-activated binders had almost half of the diffusion values of the OPC binders. Bakharev et al. (2001b) investigated the resistance of alkali-activated slag concrete to carbonation by examining the performance of AAS concrete in two carbonation tests. It was found that AAS concrete of Grade 40 had lower resistance to carbonation than that of OPC concrete.

At the same time Miranda et al. (2005) confirmed that activated fly ash mortars passivate reinforcing steel as rapidly and effectively as Portland cement mortars.

The results of the rapid chloride penetration test for alkali-activated granulated blast furnace slag/metakaolin blends, are dominated by pore solution chemistry, and show almost no change from 28 to 90 days of curing, contrasting other measures of the pore system (Bernal et al., 2011). Some studies about chloride diffusion clearly show that alkali-activated binders are able to prevent the ingress of harmful elements that could start steel corrosion.

Accelerated carbonation testing shows rapid carbonation accompanied by a loss in strength, and this occurs faster at higher metakaolin content. Recent conclusions made by Bernal et al. (2012) state that accelerated testing is very aggressive towards alkali-activated binders. The pore solution pH under this test is significantly lower than at natural CO_2 concentrations, leading to a falsely short predicted service life.

Little information was found in literature about the resistance of geopolymers to carbonation, chloride ingress and corrosion of steel reinforcement.

2.7.6 Alkali-silica reaction

Alkali-silica reaction is a chemical reaction of alkali cations and hydroxyl ions from concrete pore solution and reactive silica which occurs in aggregates. The reaction causes expansion, cracking, loss of strength and may lead to complete destruction of the concrete (Diamond, 1975).

Although alkali-activated fly ashes and metakaolin contain a high level of alkali elements, they do not appear to be associated with the occurrence of alkali-silica reaction because of the lack of calcium. That problem must be taken into consideration when calcium based binders are used Pacheco-Torgal et al. emphasized (2012). This statement is proved partially by results of Bakharev et al. (2001a). They investigated the durability of AAS concrete exposed to alkali-aggregate reaction (AAR) and reported that expansion of AAS concrete prisms was 0.04 % after 50 days and 0.1 % after 22 months. The expansion in OPC concrete was about 0.03 % after 22 months of experiment. It was found that AAS concrete had lower resistance to alkali-aggregate attack than that of OPC concrete of similar grade.

Li et al. (2005) have been using crushed quartz glass with amorphous silica content above 90 % as reactive fine aggregate to investigate the presence of alkali-silica reaction in geopolymer mixtures compared to normal cement mixtures. Geopolymer mortar samples were prepared from metakaolin, silica fume and alkaline activators and cured at 60 °C for 3 hours, then at 20 °C for 21 hours. Cement mortar samples were cured at 20°C for 24 hours. The largest expansion, 0.72 % at 90 days, was observed for mortar with high alkali cement with 0.94 % alkali content. Mortars with low alkali cement (0.59 % and 0.47 % alkali content) generated 0.53 % and 0.46 % expansions at 90 days. Geopolymer mortar with 12 % alkali content exhibited only 0.01 % expansion at 14 days. At 90 days the rate of expansion even decreased to -0.03 %. The authors concluded that geopolymers do not generate any dangerous alkali-silica reaction.

Fernandez-Jimenez et al. (2007) reported that the expansion recorded in alkali-activated fly ash mortar after 16 days did not exceed the limit established in the accelerated method. However, after 180 days of accelerated testing, expansion in the prisms exceeded that ceiling (regardless of the type of activating solution used). Such expansion was nonetheless less intense than in OPC mortars under similar conditions.

2.7.7 Fire resistance

Some literature shows that alkali-activated fly ash (AAFA) is more resistant to elevated temperatures than traditional Portland cement (Rashad and Zeedan, 2011). The relative residual strengths, for all AAFA pastes activated with liquid sodium silicate were superior to that of traditional Portland cement systems after exposure to 200 °C, 400 °C, 600 °C, 800 °C and 1000 °C. AAFA system appears more useful than OPC as a fire resistant binder. The initial strength for the higher activator concentration was 47.3 MPa while the residual strength after exposure to 1000 °C was 33.4 MPa (see Figure 2.18). In Figure 2.18 M2 contains lower concentration of activator, M3 – moderate, M4 – higher concentration of activator. The initial

strength at lower activator concentration and moderate activator concentration were 5.5 MPa and 15.6 MPa respectively while their residual strengths were 36.3 MPa and 40.3 MPa respectively after exposure to 1000 °C. Consequentially, it could be better to use lower concentrations of sodium silicate to activate fly ash required for fire resistant bonding materials. Unfortunately, authors did not provide information on the dimensional stability of the material produced.

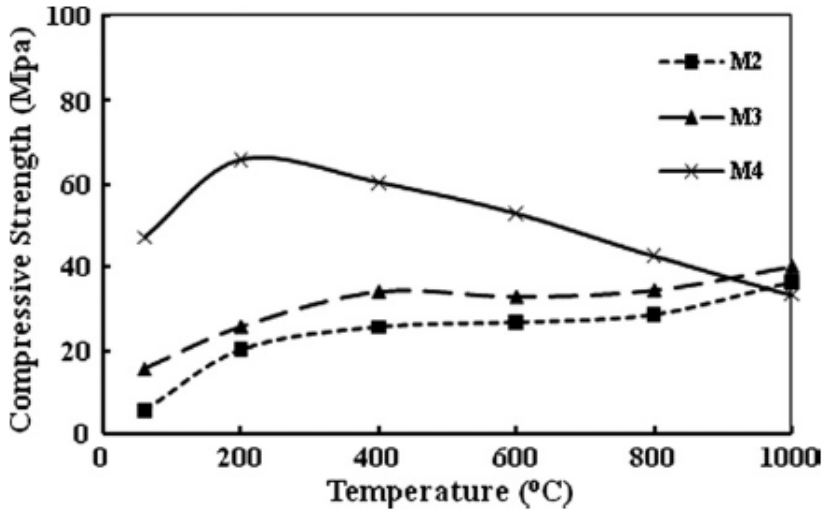

Figure 2.18: Residual compressive strength of AAFA after thermal loading (Rasad and Zeedan, 2011)

Kong and Sanjayan (2010) found that elevated temperature strength is dependent on the aggregate size of the geopolymer concrete. Concrete containing smaller sized aggregates (<10 mm) explodes at temperatures much lower than 800 °C, while geopolymer concretes containing larger aggregates (>10 mm) are more stable in elevated temperatures with a consistent strength loss of 61.8 % due to differing thermal expansion between geopolymer matrix and aggregate.

Bakharev (2006) studied thermal stability of geopolymers prepared using low calcium fly ash and sodium and potassium alkaline activators. It was found that samples with sodium containing activators had rapid deterioration of strength at 800 °C which the author connected to an increase in average pore size. The compressive strength of fly ash activated with potassium silicate was significantly increased with heating and deterioration of strength started only at 1000 °C. Even though the thermal properties of geopolymer materials were found to be superior to Portland cement concretes when exposed to 800-1000 °C, due to high shrinkage as well as large changes in compressive strength and microstructure with increasing temperature in the range of 800-1200 °C these materials were found unsuitable for refractory insulation applications.

Lemougna et al. (2011) found that geopolymer products from volcanic ash were relatively stable to heat, retaining about 60 % of their initial compressive strength and shrinking slowly up to 900 °C. The compressive strengths of the heated materials and their thermal behaviour were suitable to use this material for low-grade refractories as well as in potential building applications.

2.8 GEOPOLYMER ISSUES

Even though geopolymers seem to be materials with a big potential the question naturally arises: w*hy it is still not widely used?*

In general, even if there are assumptions that alkali-activated materials were used thousands of years ago during the construction of the Egyptian pyramids, for modern science it is a rather new material known for the last 30 years. It is much safer to use Portland cement which is well known already for more than one and a half century. The absence of any regulatory documentation and standards, unified requirements to raw materials, testing techniques and methods on this particular binder do not simplify the evolution of geopolymers. The durability question of these binders still remains open. Even though widely accepted accelerated durability tests which are used for OPC concrete give an indication of the expected performance, it is not a definite proof. Therefore, the process of adoption of new materials to industrial scale application is very slow and requires verification over time in the real-world (Duxson and van Deventer, 2009).

Some problems during material synthesis could arise. Using concentrated alkaline solutions for activation can cause some problems induced by the highly corrosive nature of alkalis and sufficient safety precautions need to be in place during the synthesis process. In case of using by-products as a raw material for alkali activation, inconsistency of chemical composition can be a serious issue. Fast settings may occur when calcium containing raw materials are used (Lee and van Deventer, 2002). Efflorescence on alkali-activated/geopolymer materials is another possible problem, (Škvára et al., 2009; Pachego-Torgal, 2012 et al.; Temuujin and Van Riessen, 2009), but efflorescence can be reduced either by the addition of alumina-rich admixtures, such as calcium aluminate cements, or by hydrothermal curing at elevated temperatures (Kani et al., 2011).

Van Deventer et al. (2012) mentioned that it was important to control the rheology of alkali-activated concrete without adversely affecting the final properties of hardened concrete by the use of chemical admixtures as superplasticisers. The results of Puertas et al. (2003) have demonstrated that the nature of superplasticisers had a very marked effect upon the activation process and the behavior of cements containing activated slag. However, this effect was not

so strong in case of alkali-activated fly ash cements. Thus, there is a need to develop whole set of new admixtures for alkali-activated fly ash cements (Van Deventer et al., 2012).

Alkali activators (sodium and potassium silicates, sodium and potassium hydroxides, sodium carbonate) are freely available on the South African market; however, their prices are rather high and will significantly affect commercial profitability of production of alkali-activated materials.

2.9 APPLICATION EXPERIENCE OF ALKALI-ACTIVATED/GEOPOLYMER BINDERS AND CONCRETES

Few successful examples of using alkali-activated binders and concretes on industrial scale can be found in literature.

In the former USSR a few plants produced AAS binder. A wide range of products and structures were made for industrial, civil, agricultural, hydraulic and road construction. It was established during maintenance that alkali slag concrete strength increased by 1.5-2.5 times after 6-12 years compared to the designed strength. The strength of concrete piles was 70 MPa while design strength was only 30 MPa. Concrete in the stressed trays in the Tatarbynarsk irrigation system increased in strength from 25 MPa to 50 MPa. The freeze-thaw resistance of the concrete from those trays after 9 years maintenance was 700 cycles without visible defects. Water impermeability increased from 1 to 2 MPa (Glukhovsky and Pakhomov, 1978). Multistory residential buildings in Lipetsk town, Russia that were built in the late seventies using AAS concrete are still operating to this day.

Australian researchers in collaboration with the Ukrainian scientist Krivenko (Xu et al., 2008) investigated the properties of alkali-activated concrete manufactured in 1964 and 1982 after more than 20 years of maintenance. Samples were taken from pre-stressed irrigation chutes, drainage systems, residential 15-storey buildings and slabs. All samples had good appearance without visible cracks and no evidence of alkali-aggregate reaction. All samples had strength significantly higher than designed strength and excellent durability over service life of up to 35 years in aggressive conditions.

Rocla adapted a conventional pipe making process to make steel reinforced geopolymer concrete pipes in an existing plant (Gourley and Johnson, 2005). The authors mentioned those pipes pass all Australian Standard requirements. Sleeper trial specimens made from 60-80 MPa geopolymer concrete have been interspersed in mainline tracks since 2002 without any problem arising. In 2011 Rocla reported on the successful use of geopolymer materials in

commercial scale production. 3000 components have been produced for a customer's patented crypt. The project required 2500 tonnes of geopolymer material (Rocla Pty Ltd, 2011).

Geopolymer concrete is currently actively promoted in Australia. The E-Crete™ R&D Batch plant of "The Zeobond Group" was used to develop mix designs and supply concrete for precast wall panels at "Antonello Precast". Precast concrete was successfully used for implementation in several projects (Zeobond Pty Ltd, n.d.).

Wagners Concrete Pty Ltd (Australia) produce environmentally advanced concrete under the brand name Earth Friendly Concrete. A geopolymer binder is made from the chemical activation of two industrial wastes – blast furnace slag and fly ash. This geopolymer has been used on a number of different projects in Australia and a total volume of over 3000 m^3 has been poured already. They also won a contract to supply 33 large floor beams that will form three suspended floor plates of the new Global Change Institute building at the University of Queensland (Aldred and Day, 2012; Wagners Concrete Pty Ltd, 2012).

2.10 ALKALI-ACTIVATED MATERIALS IN SOUTH AFRICA

Not a lot of works on alkali activation of South African fly ash have been done until now and even less has been published.

Van Jaarsveld et al. started working on stabilisation and solidification of waste materials through geopolymerization. After their work it has become apparent that these materials could be used for immobilisation of heavy metals and the fabrication of structural products (Van Jaarsveld et al., 1997; Van Jaarsveld et al., 1999b).

Shuttleworth (1995) investigated factors influencing the reactivity of fly ash in the synthesis of mineral polymers. It was found that Sasol, Matla and Lethabo fly ashes are the most reactive, while Thuthuka, Matimba and Duvha fly ashes had lowest strength development due to high Fe_2O_3 content. Na_2O and CaO content of fly ash glass are important for early strength development. Even though only three mix formulations were used in the study, it was found that reaction kinetics was strongly influenced by the initial mix proportions.

The research of Swanepoel and Strydom (2002), (Swanepoel, 2001) on geopolymerization of fly ash and kaolinite mixtures yielded conflicting results. They reported the potential suitability of South African fly ash for geopolymerization despite achieving quite low strength (8 MPa) at high energy efforts (60 °C for 48 hours).

Gokhale (2001) investigated immobilisation of organic substances into a geopolymeric matrix. It was found that the addition of 5 % of chlorophenol almost destroyed the fly ash-based matrix.

The possibility of using industrial wastes and fly ash in particular as a raw material for manufacturing geopolymeric insulating refractory material were performed by Jonker (2006) at Tshwane University of Technology. Acceptable geopolymeric porous insulating refractory material with low shrinkage, relatively high (13.8 MPa) strength and service temperature at 1220 °C were developed.

Muntingh (2006) analysed the diffusive properties of fly ash-based geopolymers by two independent methods. It was found that the Chloride Diffusion Coefficient for all geopolymeric formulations used in this study was significantly lower than for OPC or any other concrete mixture, suggesting that geopolymers are durable materials.

2.11 CONCLUSIONS AND STUDY MOTIVATION

From the review of existing literature it can clearly be seen that the interest in geopolymer binders increased in the last decade, suggesting that it has a big potential and can be an alternative binder to well-known Portland cement in the not so distant future. South African companies, such as Eskom and Sasol produce huge amounts of ash and only about 5 % of it is beneficially used indicating that the utilization of ash is a very important problem for South Africa. Giving an economic value to this industrial by-product and utilizing it in large amounts in alkali-activated material production will lead to improvement of the environment; allowing production of materials with good properties and also extending the raw-materials base of the building industry.

Basic principles of geopolymerization were presented in this chapter. Alkali activation of fly ash was a subject of numerous studies; however it was found that the properties of the final material varied significantly. One of the reasons for that is the quality of the initial source of aluminosilicates for geopolymer production (chemical composition, reactivity, particle size distribution, etc.). Thus, each particular fly ash has to be tested for suitability in geopolymer production that will also expand the already existent database of geopolymer knowledge.

The knowledge and understanding of the factors affecting the nature and properties of alkali-activated cements and geopolymers is very important for producing material with a good performance. Thus, a “variable parameter – property” relationship will be investigated in this study using local materials. Special attention will be paid to the question of strength decreasing in samples with raised alkali content, as the explanation of this phenomenon is not

clear (Provis, 2009). This will fill a gap in knowledge and enable a better understanding of the alkali activation process.

The evaluation of strength, permeability, shrinkage and creep behaviour of AAFA concretes will give an idea of the durability of these materials. Calculation of carbon footprint related to mixture components give an indication of environmental effectiveness of these materials and will make a valuable contribution to promoting the use of these materials in South Africa.

3 MATERIALS AND METHODS

3.1 INTRODUCTION

This chapter starts from the characterization of initial materials used for the preparation of alkali-activated fly ash (AAFA) pastes and concretes. A brief overview of evaluation techniques and methods used in this thesis along with procedures of sample preparation is provided here in order to obtain and understand relationships between strength, microstructure and composition of the AAFA cement pastes. Standard methods and techniques described in literature are discussed in this chapter and applied in experiments.

The experimental part of this thesis developed in two stages: 1) investigation of AAFA pastes; 2) investigation of AAFA concrete. Each part consists of material synthesis and their chemical and physical characterization.

The methodology of this thesis is to obtain the maximum, within the bounds of scope, information about alkali-activation of local fly ashes, parameters affecting their properties as well as characterization of the final material with the aim of promoting AAFA binders as a material for greater fly ash utilization or even as a potential alternative to Portland cement.

3.2 CHARACTERIZATION TECHNIQUES

3.2.1 X-Ray Diffraction (XRD)

The samples for XRD analysis were prepared using a back loading preparation method. Small samples prepared for phase determination test were pre-ground in a mill. After addition of 20 % internal standard of Si (Aldrich 99 % pure) for determination of crystalline and amorphous content, milling in a McCrone micronizing mill with alcohol was conducted. They were analysed using a PANalytical X'Pert Pro powder diffractometer with X'Celerator detector and variable divergence and receiving slits with Fe filtered Co-Kα radiation. The data was collected in the angular range $5° \leq 2\theta \leq 90°$ with a step size 0.008° 2θ and a 13 s scan step time. The phases were identified using X'Pert Highscore plus software. The relative phase amount (weight %) was estimated by the Rietveld method using Autoquan/BGMN software employing Fundamental Parameter Approach. In the Rietveld method an observed data pattern is compared to a calculated pattern. By variation of all parameters the difference between the calculated and observed pattern is then minimized by a least square procedure, until the best possible fit is obtained.

The background was fitted by the polynomial order which was determined automatically depending on the angular range. Amorphous compounds are invisible for the Rietveld method. Only crystalline phases are taken into account and their sum is normalized to 100%. The amount of the crystalline phases is overestimated should amorphous material be present. To overcome the problem an internal standard is added (a known amount of pure crystalline phase) and the overestimation of this phase and of all the other phases can be corrected. From the overestimation of the standard phase a correction factor is calculated, which is in turn applied to all crystalline phases.

The recalculated weight percentage is the amount of phases taking into account the true weight of the internal standard added. It represents the sample after the addition of an internal standard phase. The amorphous content is calculated, based on the actual sample.

3.2.2 Attenuated Total Reflectance Fourier Transform Infrared spectroscopy (ATR-FTIR)

There are two most common forms of solid sample preparation for IR spectra collection; both involve grinding material to fine powder and then dispersing it in a matrix. Ground material can be dispersed in a liquid, for example in mineral oil, or pressed with potassium bromide (KBr) re-crystallization which results in a clear glassy disk ready to be analysed. Attenuated total reflectance (ATR) FTIR allows transmission spectra without using any matrix but it is essential to provide good optical contact between the sample and ATR crystal.

An attenuated total reflection accessory operates by measuring the changes that occur in a totally internally reflected infrared beam when the beam comes into contact with a sample as it shown in Figure 3.1. An infrared beam is directed onto an optically dense crystal with a high refractive index at a certain angle. This internal reflectance creates an evanescent wave that extends beyond the surface of the crystal into the sample held in contact with the crystal. This evanescent wave protrudes only a few microns (0.5-5 μ) beyond the crystal surface and into the sample. In regions of the infrared spectrum where the sample absorbs energy, the evanescent wave will be attenuated or altered. The attenuated energy from each evanescent wave is passed back to the IR beam, which then exits the opposite end of the crystal and is passed to the detector in the IR spectrometer. The system then generates an infrared spectrum (www.perkinelmer.com, 2014).

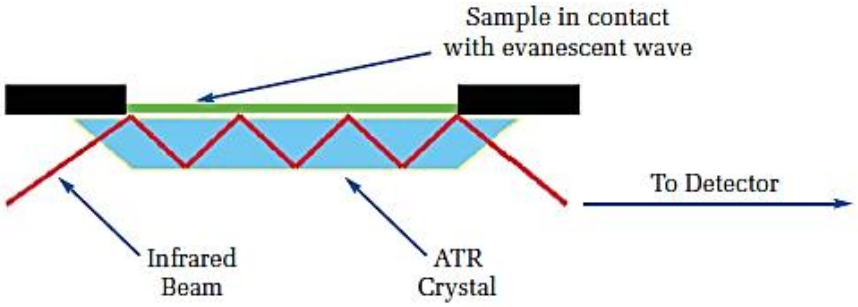

Figure 3.1: A multiple reflection in ATR crystal (www.perkinelmer.com, 2014)

The most frequently used small crystal ATR material is diamond because it has the best durability and chemical inertness. The small area ATR crystal top-plates generally provide only a single reflection but this is sufficient, given the very low noise levels.

In this thesis FTIR was performed using a Golden Gate diamond ATR cell (Bruker), which fits in the macro sample compartment of a Vertex 70v (Bruker Optics) spectrometer. The contact area between the sample and the diamond ATR crystal was 2 mm diameter. After the crystal area has been cleaned and the background collected, the powdered alkali-activated cement paste was placed onto the small crystal area. The sample height was not more than a few millimetres. Once the solid has been placed on the crystal area, the pressure arm was positioned over the sample area. Then the pressure arm locked into a precise position above the diamond crystal and force is applied to the sample, pushing it onto the diamond surface. Spectra were recorded with 32 acquisitions at 4 cm^{-1} resolution over a spectral range of 4000-600 cm^{-1} for hardened samples with different sodium oxide content at comparison testing age in transmittance mode.

3.2.3 Scanning Electron Microscopy (SEM)

Samples of AAFA cement paste were crushed for SEM investigation. Fractured surfaces of activated fly ashes, coated with carbon or gold, were investigated by scanning electron microscopes JEOL JSM 5800 (Japan) at 20 kV and Zeiss Ultra Plus scanning electron microscope (Carl Zeiss, Germany) at 3 kV. SEM analysis was performed at different ages.

3.3 MATERIALS

3.3.1 Fly ash

Although there are a number of raw materials used for alkali-activation, fly ash is of particular interest in South Africa due to its accessibility around Gauteng, Mpumalanga and Limpopo provinces. There are few major producers of fly ash in South Africa: Ash Resources (Ltd) Pty and their Durapozz, Durapozz Pro, SuperPozz, Pozzfill ashes and Pozzsand (Lethabo and

Matla power stations); Ulula Ash (Kriel power station) and Sephaku Smartash and Hardash (Kendal power station). Fly ashes from other power stations are not widely used due to their inconsistent composition.

A few batches of fly ash obtained from Lethabo power station were used as only source of aluminosilicates for the majority of the experimental work presented in this thesis. In addition, fly ash from Matla power station was used for comparison. These particular fly ashes were chosen because they have consistent quality and comply with the chemical and physical requirements of SANS 50450-1:2014. Using other South African fly ashes (except of fly ashes from Kriel and Kendal power stations) is possible at this stage as deviations in initial material composition can only be taken into account once the factors affecting alkali-activation are quantified. Fly ashes used in this study are siliceous fly ashes (SANS 50197-1:2000), which means the proportions of reactive calcium oxide is less than 10 % by mass. The chemical composition of each fly ash batch was monitored by X-Ray fluorescence spectrometry (XRF) at the Geology Department of the University of Pretoria and is shown in Table 3.1.

Table 3.1: Chemical composition of fly ashes, % by mass

	Lethabo I	Lethabo II	Lethabo III	Lethabo IV	Matla	Uncertainty	Limit of detection
SiO_2	55.14	55.22	53.86	55.83	53.44	0.4	0.02
TiO_2	1.50	1.57	1.56	1.56	1.74	0.03	0.0032
Al_2O_3	32.17	31.93	30.78	30.25	30.21	0.3	0.01
Fe_2O_3	3.61	3.36	3.30	3.92	2.92	0.3	0.0097
MnO	0.03	0.02	0.03	0.03	0.03	0.0065	0.0013
MgO	0.81	0.73	1.14	1.13	1.85	0.1	0.0118
CaO	4.50	4.57	4.34	4.05	6.38	0.07	0.01
Na_2O	<0.01	<0.01	0.23	0.16	0.39	0.11	0.0265
K_2O	0.76	0.87	0.82	0.75	0.85	0.06	0.005
P_2O_5	0.27	0.42	0.52	0.43	0.93	0.08	0.01
Cr_2O_3	0.04	0.06	0.04	0.04	0.02	0.0053	0.0006
NiO	0.01	0.02	0.02	0.02	0.01	0.01	0.0013
V_2O_5	0.03	0.02	0.03	0.03	0.03	0.0018	0.0008
ZrO_2	0.04	0.03	0.05	0.05	0.04	0.005	0.0009
SO_3	0.13	0.23	-	-	-		
SrO	0.13	0.12	-	-	-		
LOI	0.67	0.80	2.51	0.86	1.01		

The chemical composition of fly ashes used is consistent and fits in the range of typical values declared by the producer.

The particle size distribution of all used fly ashes was measured using the Malvern Mastersizer laser diffraction instrument in the Civil Engineering Laboratory of the University of Pretoria and shown in Figure 3.2.

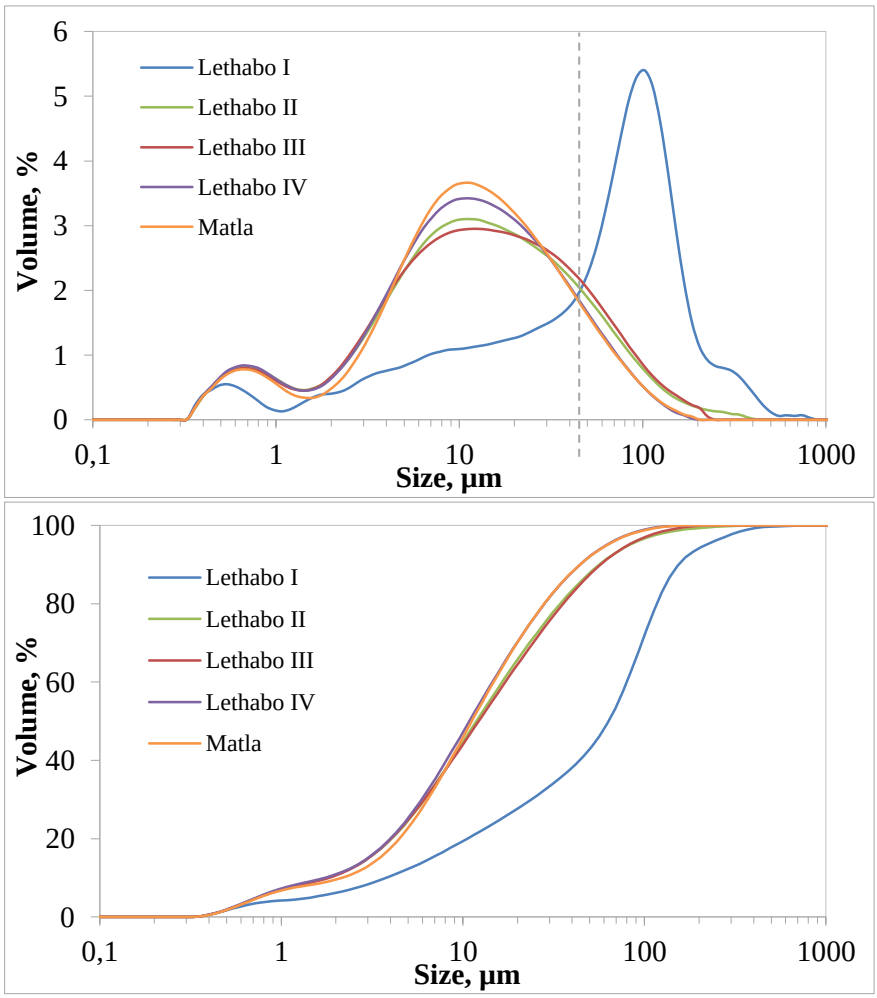

Figure 3.2: Particle size distribution of used fly ashes

From the Figure 3.2 it is clearly seen that all fly ashes except of Lethabo I have almost the same particle size distribution. The principal difference between these ashes that Lethabo I is unclassified fly ash with the median size of 102.5 µm, known under the trade name Pozzfill. The other samples were significantly improved by particle size distribution classification with finer particles grade (median size in range 10.5 – 11.6 µm) and more than 80 % of particles are finer than 45 µm. Unclassified Lethabo I fly ash was used only for trial mixes but not for the majority of experiments. Fly ash has microscopically small particles consisting of aluminium-silicate glass (Krüger, 2003) mostly spherical shape and hollow (cenospheres) or packed by small microspheres inside of bigger ones (plerosphere). The morphology of typical classified fly ash is shown in Figure 3.3.

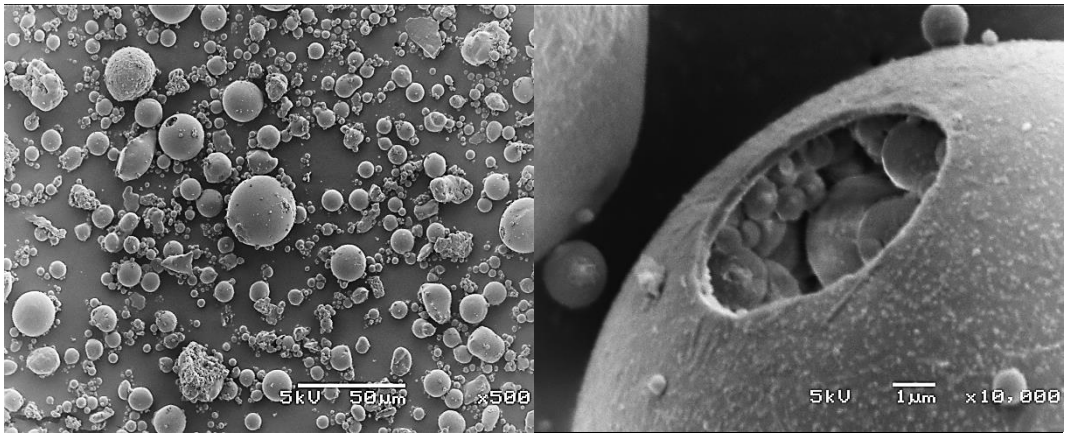

Figure 3.3: SEM images of classified Lethabo fly ash

The crystalline phases of fly ashes were analysed by X-ray powder diffraction method (XRD) at the Geology Department of the University of Pretoria. The XRD patterns of all used fly ashes are shown in Figure 3.4. 20 % silicon was added to the fly ash as internal standard for determination of amorphous (glass) content. Size of the fly ash was reduced before XRD analysis by milling fly ash with ethanol in the McCrone micronizing mill for 5 minutes. The relative phase amounts were estimated using the Rietveld method. Fly ashes consist mainly of amorphous phase with crystalline inclusion of mullite and quartz. Phase composition of fly ashes is shown in Table 3.2.

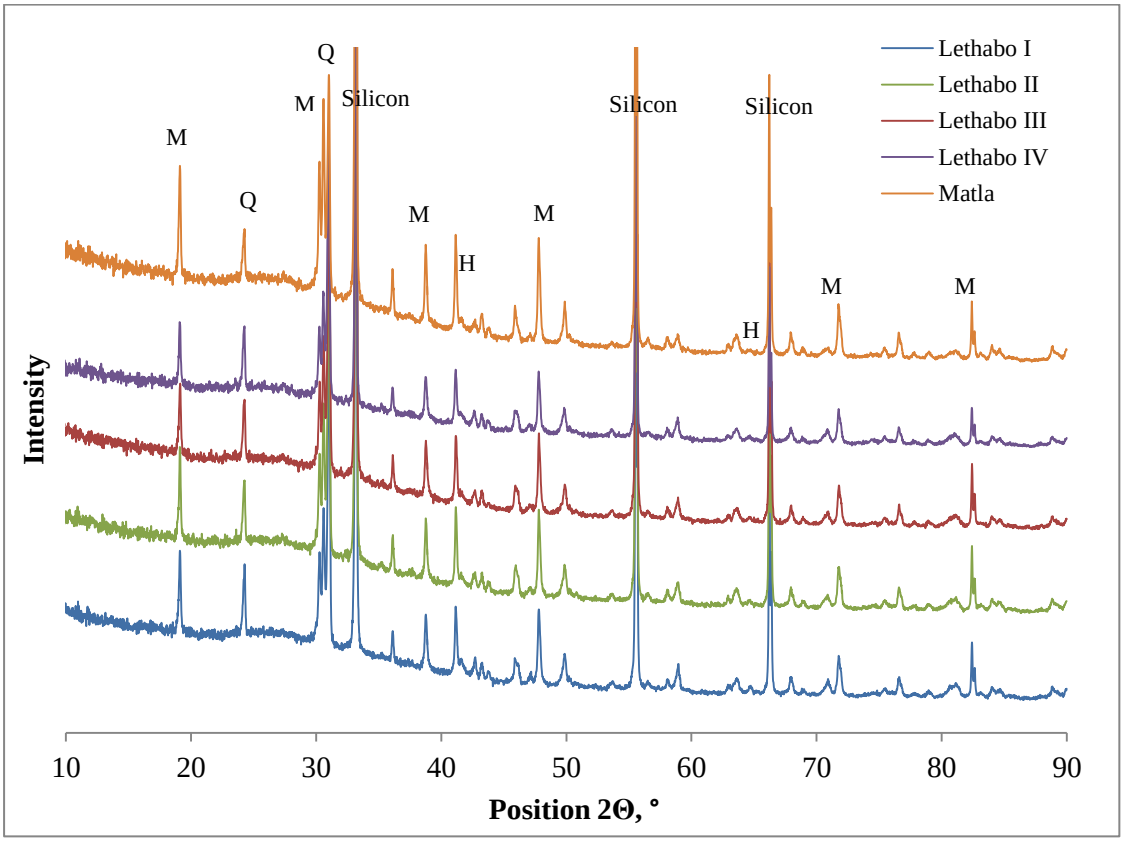

Figure 3.4: X-ray diffraction pattern of fly ashes M – mullite, Q – quartz, H – hematite

Table 3.2: Phase composition of fly ashes, weight %

	Lethabo I	Lethabo II	Lethabo III	Lethabo IV	Matla
Amorphous	61.7	59.9	59.4	56.0	57.5
Mullite	25.8	29.9	27.1	30.0	35.2
Quartz	11.6	10.2	12.6	13.1	7.3
Hematite	0.9	-	0.8	0.9	-

The ATR-FTIR spectra of original fly ashes are shown on Figure 3.5. All spectra exhibit the broad band with several peaks at around 1055-1020 cm^{-1} attributed to T-O-Si (where T= Si or Al) asymmetric stretching vibration of TO_4 tetrahedral molecules and typical for silicates and aluminosilicate glasses and minerals (Lee and Van Deventer, 2002). Broad weak peaks at around 902-904 cm^{-1} and at 821 cm^{-1} can be assigned to mullite (Voll et al., 2002). A weak double band at 790-775 cm^{-1} and a shoulder at 692 cm^{-1} assigned to quartz (Ghosh, 1978; Zhang et al., 2012a). The results of IR analysis are in agreement with XRD results.

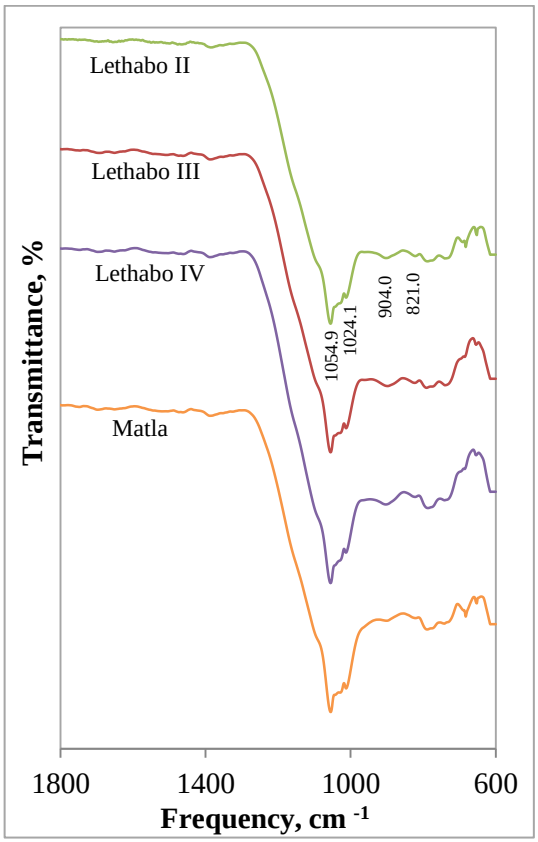

Figure 3.5: ATR-FTIR spectra of fly ashes

3.3.2 Activating solutions

Sodium hydroxide flakes (98.5 % purity) obtained from Protea Chemicals were dissolved in distilled water in order to obtain activating solution. Activator solutions were prepared and

cooled down to room temperature before mixing. The Na_2O content in the mixture has been calculated as percentage of fly ash mass.

Activating solutions with different Na_2O and SiO_2 contents were prepared as well to investigate the effect of soluble silicates at constant sodium oxide contents. Concentration of SiO_2 was varied from 3 to 12 % of fly ash mass with 3 % intervals. Commercially available sodium silicate solution (Silchem 2008 from Protea Chemicals) containing 14.17 % Na_2O and 29.05 % SiO_2, with silica modulus (M_s) of 2 and density of 1530 kg/m^3 was used.

Caustic potash (91 % purity) was used for making an activator solution and compared to mixture with caustic soda solution to investigate the effect of alkali metal cation on the strength of paste. The purity of sodium and potassium hydroxide was not taken into account during mixture design and it was assumed to be 100 % final amount of total alkali to fly ash mass. The actual alkali content was slightly lower and the water to binder solids ratio increased when potassium hydroxide was used as activator as 8 % of the impurities in caustic potash were water.

3.3.3 Aggregates

Dolomite sand with a fineness modulus of 3.86 and 9 % passing the 75 µm sieve was used to produce AAFA concrete. Crushed dolomite stone (9.5 mm) was used as the coarse aggregate for concrete. Dolomite aggregates were chosen due to their abundance in South Africa as well as their popularity in the construction industry. Dolomite sand and stone was obtained from Lyttelton Dolomite (Pty) Ltd, Pretoria, South Africa.

3.3.4 Mix proportions and synthesis of AAFA

AAFA pastes were prepared in three series: 1) Na-series, where sodium hydroxide solution was used as an activator; 2) Na-Si series, where combinations of sodium hydroxide and sodium silicate were used; 3) K-series where the activator was potassium hydroxide. Detailed mix composition and curing conditions for different series are shown in Table 3.3. The mixture ID indicates tested variable and its value. For example, the sample Na3 contained 3 % of Na_2O in respect of fly ash mass. For T65D4 temperature and duration of heat treatment were variables at 65 °C and 4 hours respectively.

Table 3.3: Mix composition and curing condition of AAFA pastes

Mixture ID	Actual content of alkali, % of fly ash mass		w/s	Temperature of curing (°C)	Duration of curing (h)	Material content (kg/m^3)			
	M_2O	SiO_2				Fly ash	MOH	Sodium silicate (M_s=2)	Water
Na3	2.96	-	0.20	60	24	1544	59.8	-	304.6
Na6	5.91	-	0.20	60	24	1527	118.2	-	297.0
Na9	8.86	-	0.20	60	24	1499	174.2	-	287.7
Na12	11.93	-	0.20	60	24	1469	227.5	-	277.9
Na15	14.78	-	0.20	60	24	1438	278.3	-	268.1
T65D4	8.86	-	0.20	65	4	1499	174.2	-	287.8
T70D4	8.86	-	0.20	70	4	1499	174.2	-	287.8
T75D4	8.86	-	0.20	75	4	1499	174.2	-	287.8
T25D24	8.86	-	0.20	25	24	1499	174.2	-	287.8
T40D24	8.86	-	0.20	40	24	1499	174.2	-	287.8
T60D4	8.86	-	0.20	60	4	1499	174.2	-	287.8
T60D8	8.86	-	0.20	60	8	1499	174.2	-	287.8
T60D12	8.86	-	0.20	60	12	1499	174.2	-	287.8
T60D16	8.86	-	0.20	60	16	1499	174.2	-	287.8
T60D20	8.86	-	0.20	60	20	1499	174.2	-	287.8
T60D24	8.86	-	0.20	60	24	1499	174.2	-	287.8
T80D4	8.86	-	0.20	80	4	1499	174.2	-	287.8
T80D8	8.86	-	0.20	80	8	1499	174.2	-	287.8
T80D12	8.86	-	0.20	80	12	1499	174.2	-	287.8
T80D16	8.86	-	0.20	80	16	1499	174.2	-	287.8
T80D20	8.86	-	0.20	80	20	1499	174.2	-	287.8
T80D24	8.86	-	0.20	80	24	1499	174.2	-	287.8
WS0.18	8.86	-	0.18	60	24	1545	179.4	-	262.7
WS0.22	8.86	-	0.22	60	24	1466	170.2	-	306.3
WS0.24	8.86	-	0.24	60	24	1420	164.9	-	331.1
WS0.26	8.86	-	0.26	60	24	1370	159.1	-	357.9
WS0.29	8.86	-	0.29	60	24	1326	154.0	-	381.0
K3	2.88	-	0.20	60	24	1525	57.5	-	305.5
K6	5.46	-	0.21	60	24	1501	107.3	-	301.0
K8	8.19	-	0.21	60	24	1474	158.0	-	296.0
K11	10.92	-	0.21	60	24	1445	206.6	-	290.6
Na3Si3	2.97	3.00	0.20	60	24	1504	29.8	155.2	224.0
Na3Si6	3.00	6.00	0.20	60	24	1462	1.5	301.8	147.6
Na6Si3	6.00	2.92	0.20	60	24	1491	90.2	150.1	218.8
Na6Si6	6.00	5.85	0.20	60	24	1451	59.8	292.1	149.1
Na6Si9	5.94	8.77	0.20	60	24	1414	30.8	427.0	82.5
Na6Si12	5.89	12.1	0.20	60	24	1388	-	577.5	-
Na9Si3	8.89	3.00	0.20	60	24	1474	143.5	152.1	212.2
Na9Si6	8.91	6.00	0.20	60	24	1398	109.7	288.7	132.9
Na9Si9	8.91	8.96	0.20	60	24	1379	82.1	425.4	64.9
Na9Si12	8.95	12.0	0.20	60	24	1356	55.1	560.1	-
Na5.7Si6.5	5.70	6.45	0.20	60	24	1438	48.0	319.6	137.9
MatlaNa9	8.86	-	0.24	60	24	1419.62	164.9	-	331.1

The samples of AAFA pastes were prepared by mixing fly ash with the activating solution in a pan mixer for 4 minutes. The mixture was transferred into moulds, vibrated for an appropriate time to remove air and then cured at mentioned conditions. The amount of alkali and SiO_2 introduced with the activator solution was calculated as percentages of fly ash mass. To regulate the amount of water in pastes, water to binder solids ratio was used as a variable (Rangan, 2008). Total amount of water was calculated as the sum of water necessary to produce MOH (solid) from M_2O and distilled water added to produce alkaline solution, where M is Na or K. Binder solids were calculated as a sum of fly ash mass, M_2O and SiO_2 if any. Water to binder solids ratio was chosen as low as possible and was kept constant at 0.2 for all experiments unless otherwise mentioned. An example of mix design is presented in Appendix A. AAFA materials were characterized on paste samples to eliminate any possible effect on the result by minerals in the aggregates.

The concrete mix design was made based on results presented in Chapter 4. Consumption of materials per cubic meter of concrete along with curing condition details is provided in Chapter 5. Fly ash, sand and coarse aggregate were premixed for 1-1.5 min and then an activator solution was added. All components were mixed together for another 3 to 4 minutes. Fresh concrete was cast into different sized moulds, vibrated to remove air and then placed into oven for heat treatment. In this work, all paste/concrete samples were not sealed during heat curing. After elevated temperature curing, all samples were demoulded and tested after one-hour. The remaining samples were kept in a room with constant temperature and humidity (25±2 °C; 55±5 % respectively) until testing age.

3.4 TEST METHODS

3.4.1 Strength of hardened paste and concrete

Flexural strength of AAFA paste was determined using 40×40×160 mm prisms. Samples were tested immediately after elevated temperature curing, at 28, 91, 182 and 364 days. Paste compressive strength was determined on halves of 40×40×160 mm prisms, broken during flexural testing. Specimens were tested at rate of 2400±200 N/s until fracture (SANS 50196-1:2006). The test results are expressed as a mean of the six compressive strength determinations made on a set of three prisms. If one result within the six determinations varied by more than ± 10 % from the mean of the six, this result was discarded and the mean of remaining five results was calculated. If further result within these five determinations varied by more than ± 10 % from their mean, the set of results should be discarded. However, some of the obtained results contain more than one outlier, these values were clearly marked

but were not discarded as strength deviation of AAFA pastes seem to be higher than that of Portland cement.

Compressive strength of AAFA concrete was determined using 100 mm cubes crushed at a rate of 0.3±0.1 MPa/s until the specimen fails (SANS 5863:2006). At least three cubes were used for strength determination.

Flexural strength (modulus of rupture) of hardened 100×100×500 mm concrete beams at 28 day was determined by the two-point loading method that produces a constant bending moment along the central part of the test specimen (SANS 5864:2006).

Splitting tensile strength was recorded for 28 days cylindrical 150×300 mm AAFA concrete specimens at 0.03±0.01 MPa/s until failure. Tests were conducted according to SANS 6253:2006.

3.4.2 Deformations in pastes and concrete

Modulus of elasticity and Poisson's ratio were obtained for heat cured AAFA concrete cylinder specimens with dimensions 150×300 mm at the age of 28 days in compression. Strain-measuring device was attached to the specimen by embedded gage points. Then specimen with the device was subject to stress in the range of 0 to 40 % of ultimate strength and readings responding to longitudinal and transverse deformations were taken. Tests are conducted according to ASTM C 469-02.

Creep of heat cured (60 °C for 24 hours) AAFA concrete was studied for a period of one year using 150×300 mm cylinders. The creep test was conducted on two series of AAFA concrete, all of them after elevated temperature curing. For the first sample series, creep testing was started immediately after elevated temperature curing period, while for the second series it was begun at the age of 28 days. Samples were loaded at sustained stress of 40 % of the compressive strength on the day of loading in a spring-loaded system while a third cylinder was kept unloaded. An external strain-measuring device was used to measure strain on two gage lines on the perimeter of each specimens. Creep load was checked and adjusted if it was necessary at every measurement. Change in length was measured before and after loading, then daily for a week, then weekly for a first month and monthly until 1 year. Creep was calculated in microstrains.

Drying shrinkage behavior of heat cured AAFA concrete was studied for a one year on a set of three beams with dimensions of 100×100×300 mm. Metal anvils were embedded in concrete, 15 mm from sample ends, during casting. All AAFA concrete samples were subject

to elevated temperature curing and it is expected that the measurements do not represent the full pattern of volumetric changes AAFA paste experienced. Dimensional measurements were taken on hemispherical surfaces of anvils using a micrometer equipped with invar steel reference bar against which the measuring equipment was checked before each use. Measurements were recorded at regular time intervals and length change was calculated in microstrain.

In this research, all samples were not sealed during elevated temperature curing but only covered with film. In-situ evaluation of volume changes of paste during heat treatment gives valuable information about strains in the sample. The shrinkage cone method for measuring the shrinkage from work of Eppers and Müller (2010) was revised and adapted to measure length changes of AAFA cement paste and concrete during elevated temperature curing at 60 °C for the first 24 hours. A laser was pointed vertically at the surface of a cone-shaped sample in a cylindrical jar, shown in Figure 3.6. The cone geometry of the sample ensures that the change in height corresponds to the linear length change of the material. The shrinkage-measuring device in this thesis consists of a Micro Epsilon optoNCDT1700 laser-optical sensor with a measuring range of 2 mm on a stand, which allows displacement measurement. The distance is linearized and then issued via an analogue interface.

Figure 3.6: Shrinkage cone method for measuring shrinkage

The AAFA cement pastes were prepared in a Hobart mixer according to SANS 50196-1:2006. Fly ash was placed in the mixer bowl, the alkaline solution was added and paste was mixed by

hand for a minute. The hand mixing was used at the initial stage of the mixing to prevent spill of fly ash in case if mechanical mixing would be applied from the beginning. After hand mixing, the pastes were mechanically mixed for additional one and a half minute. The AAFA cement concrete was prepared in a pan mixer by one minute mixing of dry components, adding the alkaline solution and additional one and a half minute mixing. AAFA paste/concrete was cast into the pre-heated cone-shaped mould (covered with a removable plastic cone to prevent direct contact with metallic surface) and then was compacted. A reflector made out of light white plastic was embedded into paste surface and the specimen was weighed. The reflector was made from plastic to prevent its sinking into fresh sample under gravity action, which would significantly influence the readings. The sample's effective height was calculated as difference between cone mould height, the distance from the mould's top and to reflector measured with vernier calliper and the reflector thickness and was used as the reference length for calculating the shrinkage. Cone geometry of the sample ensures that volume change in the sample corresponds to the sample height change. More information on this topic can be seen in Appendix E. The specimen was placed into an oven underneath the pre-heated measuring device so that the laser beam was reflected by reflector disc. The laser was adjusted to have a maximum range, and the measurements were started as soon as the oven was closed. The process from the beginning of mixing fly ash with an activator to the first displacement measurement took about 5 minutes. The relative displacement was recorded by data logger (Graphitech, Japan) with a ten seconds interval during 24 hours. After this period of time specimen was weighed and the total mass loss was calculated as a percentage as in Equation 3.1.

$$M_{loss} = (m_1-m_2)/(m_1-m_m)\cdot 100\% \quad (3.1)$$

Where m_1 – mass of the mould with paste/concrete before elevated temperature curing, g; m_2 – mass of the mould with sample after elevated temperature curing, g; m_m – mass of the empty mould, g.

Length change of sample was calculated according to Equation 3.2:

$$\Delta L = (L_i-L_0)/L \quad (3.2)$$

Where L_i – laser reading at i-time, µm; L_0 – initial laser reading, µm; L – samples effective height, m.

As the measurements were taken during elevated temperature oven curing, the effect of thermal expansion of the cone and measuring device itself were eliminated by pre-heating them before the experiment for at least 24 hours at the temperature of experiment. The raw

materials (fly ash, sodium hydroxide solution, aggregates) were kept in a room with controlled environment (25±2 ºC and 65±5 % relative humidity) for at least 24 hours before the test.

AAFA pastes with varying concentrations of sodium oxide and concrete were studied in-situ for volume changes during elevated temperature curing in oven.

3.4.3 Durability of concrete

To evaluate the transport properties and durability of produced concrete a few techniques, known in South Africa as durability indices, were applied to AAFA concrete samples (Alexander et al.,1999; Beushausen and Alexander, 2008). Samples for durability index tests were dried in the oven at 50 °C for 7 days.

Oxygen permeability testing was conducted on 30 mm thick, 68 mm diameter heat cured AAFA concrete samples. These samples were dried in an oven at 50 °C for 7 days, measured by calliper and placed in a compressive collar with a rigid sleeve. The sample with collar and rigid sleeve was placed into the permeability test chamber and oxygen under gauge pressure (100±5 kPa) was allowed to flow though the permeability cell. Pressure readings with time were automatically taken until the pressure dropped to 50±2.5 kPa, or for 6 h±15 min, whichever comes first. The coefficient of permeability is determined from the slope of the line produced when the natural log of the ratio of initial pressure to pressure at any time is plotted against time (SANS 516-2:2009). Test result was calculated from the mean of four test determination of the same material.

Water sorptivity testing consists of measuring the mass of water absorbed with time from the bottom of a concrete sample, of which the sides had been sealed. The sorptivity was determinated from the slope of the straight line produced when the mass of absorbed water is plotted against the square root of time and calculated according to Equations 3.3 and 3.4.

$$M_{wt} = F\sqrt{t} \tag{3.3}$$

Where F is the slope of the best fit line from plotting M_{wt} against $\sqrt{t}$; M_{wt} is the mass of absorbed water at each weighing period, g.

$$S = \frac{Fd}{M_{sv} - M_{s0}} \tag{3.4}$$

Where S is the water sorptivity, mm/hr$^{0.5}$; F is the slope of the best fit line, g/hr$^{0.5}$; M_{sv} is the vacuum saturated mass of the specimen, g; M_{s0} is the mass of the sample, g.

The test result was calculated as the mean of four determinations. Tests were conducted according to SANS 516-3:2009.

Chloride conductivity testing consists of measuring the electrical current passed through a 30 mm thick slice of 68 mm diameter core. The specimens are saturated with 5 M NaCl solution before the test. A potential difference of 2, 5 or 10 V was applied cross the ends of the specimen, which was immersed in a sodium chloride solution. The conductivity was determined from the specimen dimension and the specimen electrical resistance ((thickness/area) × (current/potential difference). Test result was calculated as the mean of four determinations. Tests were conducted according to SANS 516-4:2009.

Basic acid immersion tests were conducted on two series of heat cured AAFA concrete 100 mm cubes. Firstly, samples were immersed in sulphuric acid immediately after elevated temperature curing, while the second set of samples were immersed after 28 days of curing. The compressive strength of samples immersed in acid was compared to strength of samples cured at constant room temperature and humidity. Change in mass and appearance of samples was also evaluated. Concentration of sulphuric acid was that to achieve a pH of solution 2-3. The pH of the solution was checked monthly by indicator strips and acid was added to maintain a pH of 2-3.

3.4.4 Heat evolution during elevated temperature curing

The heat evolution of AAFA cement pastes during elevated temperature curing was investigated during the first 24 hours in order to obtain information, which might correlate with some physical properties. During the first part of the temperature development test AAFA pastes with different sodium oxide contents were cast into a plastic mould of three 40×40×160 mm prisms. For each mix, six moulds were cast with a total paste volume of 4.6 l. The pastes with different alkali content were cured separately. Moulds were placed into an oven at 60 °C immediately after casting. Grounded thermocouples were embedded into the cores of moulds during casting. Two thermocouples were measuring temperature in the oven. Temperature development in the sample cores was recorded at one minute intervals for the 24 hours of elevated temperature curing using a data logger (Graphitech, Japan).

During the second part of the test, moulds of different sizes, made of metal and plastic were used. AAFA pastes with 9, 12 and 15 % Na_2O were studied. Temperature development of the pastes with 3 and 6 % Na_2O was not investigated due to results obtained during the first part of the test. Each of the three pastes was cast into a set of plastic and metal moulds (one of each): 100 mm and 150 mm cubes, 40×40×160 mm prisms. The total volume of each mix was

10.2 l. Grounded thermocouples were placed in the core of each mould. All six moulds were put into the oven at 60 °C and the temperature development in sample cores was recorded for the 24 hours of elevated temperature curing. Properties of moulds material are presented in Table 3.4.

Table 3.4: Mould material properties

Material	Density, kg/m^3	Specific heat capacity, J/(kg·K)	Thermal conductivity, W/(m·K)	Thermal diffusivity, 10^{-6} m^2/s
Steel	7850	452	40	11.27
Nylon 6	1160	1700	0.28	0.14

The oven used in this work was not equipped with a refrigerator. The net volume of the oven was 202.5 l. The ratio between paste and the oven volume was constant at 0.0228 and 0.0504 for the first and second part of the experiment respectively.

3.5 CONCLUSIONS

This chapter describes the initial materials, experimental procedures, and brief theory of used equipment. Various types and concentrations of activator solutions as well as synthesis conditions were employed to produce the AAFA cement paste with the aim to better understand and predict final material properties. The methodology was divided into two main parts: the synthesis of AAFA materials and their characterization. Several analytical techniques have been proposed to characterize hardened material, while the others have been performed in-situ during elevated temperature curing of AAFA cement pastes/concrete in order to obtain more information about reaction kinetics and deformations.

4 EXPERIMENTAL STUDY ON ALKALI-ACTIVATED FLY ASH CEMENT PASTES

4.1 INTRODUCTION

Different variables affecting the compressive strength of alkali-activated fly ash pastes will be discussed in this chapter. Numerous works have been done on this theme; however the literature review shows that the properties of alkali-activated fly ash products are highly affected by the initial material composition, their proportions and curing conditions. Not many published results on factors affecting alkali activation of South African fly ash were found. Thus it is necessary to establish a "variable parameter-property" relationship to better understand the activation of local fly ash and find the most suitable mixture proportions and curing conditions. Compressive strength was chosen as the main indicator of material properties and structure development due to the ease and affordability of this testing technique. Determination of compressive strength for the majority of samples in this chapter was performed on halves of 40×40×160 mm prismatic specimens broken during flexural strength testing. All samples were prepared without using any fine aggregate to eliminate the influence of aggregate mineralogy on the characterization of paste composition. The microstructure and composition of the resulting products of alkali activation were studied by scanning electron microscopy (SEM) and X-ray diffraction (XRD). Attenuated Total Reflectance Fourier Transform Infrared Spectroscopy (ATR-FTIR) spectra of AAFA pastes are discussed in detail. The shrinkage cone method was adopted and used for the first time to measure length changes of AAFA cement pastes during elevated temperature curing immediately after casting.

4.2 TRIAL EXPERIMENT OF AAFA CEMENT PASTES PRODUCING

Samples in this section were prepared using unclassified Lethabo fly ash and different concentrations of sodium oxide, calculated as percentage of fly ash mass. Water to binder solids ratio was kept constant at 0.2. Samples were cured in an oven at 60 °C for 24 hours. Compressive strength of AAFA cement pastes is shown on Figure 4.1. The error bars on all figures in this chapter represent the deviation of the compressive strength of six samples tested from the mean. Table F.1 in Appendix F contains the results of compressive strength tests.

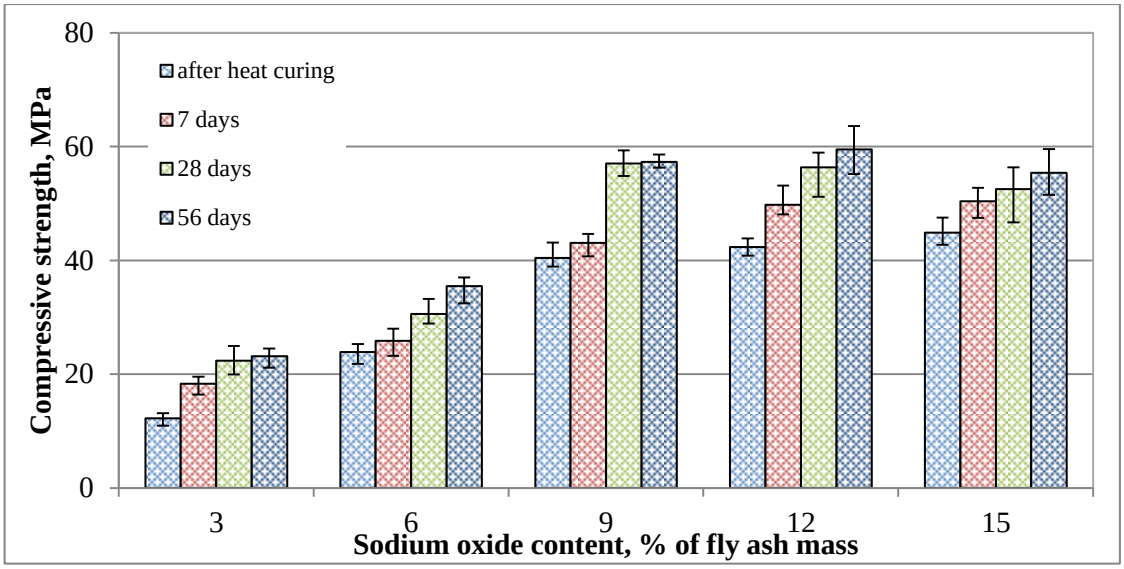

Figure 4.1: Effect of Na_2O content on the compressive strength development of alkali-activated unclassified Lethabo fly ash

The results show that the compressive strength of alkali-activated unclassified fly ash strongly depends on sodium oxide concentration. Increasing of sodium oxide content from 3 % to 6 % and 9 % result in significantly increased compressive strength at all testing ages. Further increasing of sodium oxide concentration to 12 % and 15 % affected only early compressive strength (immediately after heat curing and 7-days). 28-days compressive strength of Na12 and Na15 was lower compared to Na9 (56.3 MPa, 52.6 MPa and 57.0 MPa respectively). However, it is interesting to notice that the difference between Na9 and Na12 in compressive strength is minimal, but the compressive strength of Na15 dropped compared to Na9 and Na12 after 28 days of curing. This observation indicates the presence of an optimal concentration of sodium oxide. In the next section results obtained for classified fly ash will be discussed in detail and compared to published literature.

4.3 FACTORS AFFECTING STRENGTH OF ALKALI-ACTIVATED FLY ASH (AAFA) CEMENT PASTE

4.3.1 Effect of sodium oxide content and age

All samples for this test were prepared using one batch of classified Lethabo fly ash at constant water to binder solids ratio of 0.2 and cured at 60 °C for 24 hours. The Na_2O content has been calculated as percentage of fly ash mass. The influence of the Na_2O content on the flexural and compressive strength of AAFA paste is shown in Figure 4.2 and 4.3 respectively. Flexural and compressive strength and standard deviation values are shown in Table F.2 and F.3 respectively in Appendix F.

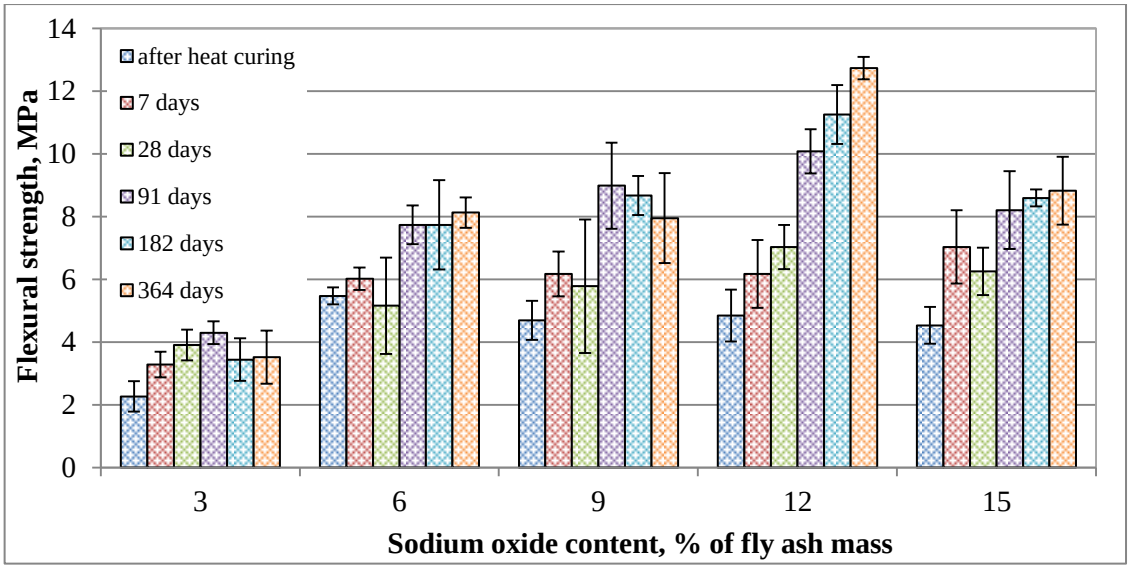

Figure 4.2: Effect of Na_2O content on the flexural strength development of alkali-activated classified Lethabo fly ash

Despite the fact that the water to binder solids ratio was constant of 0.2 for all mixes in this section, consistency of mixes was different from each other. Mix Na3 was dry and lumpy while mix Na15 had a viscous flow. Na_2O from solid NaOH was considered as a part of solids because it was assumed that sodium would be bond in the paste matrix. Different researchers use different parameters to regulate water content in alkali-activated mixes (Katz, 1998; Barbosa et al., 2000; Fernandez-Jimenez and Palomo, 2003; Rangan, 2008; Bernal et al., 2013; Puertas and Torres-Carrasco, 2014) which leads to a confusion of terms and makes it impossible to compare results of different research groups. Thus, for future studies it is recommended to use consistency as a constant parameter for investigation of effect of sodium oxide content on the compressive strength.

Flexural strength of Na6 AAFA paste, shown in Figure 4.2, is higher than that of Na3, however there is no clear trend between further increasing in sodium oxide and flexural strength.

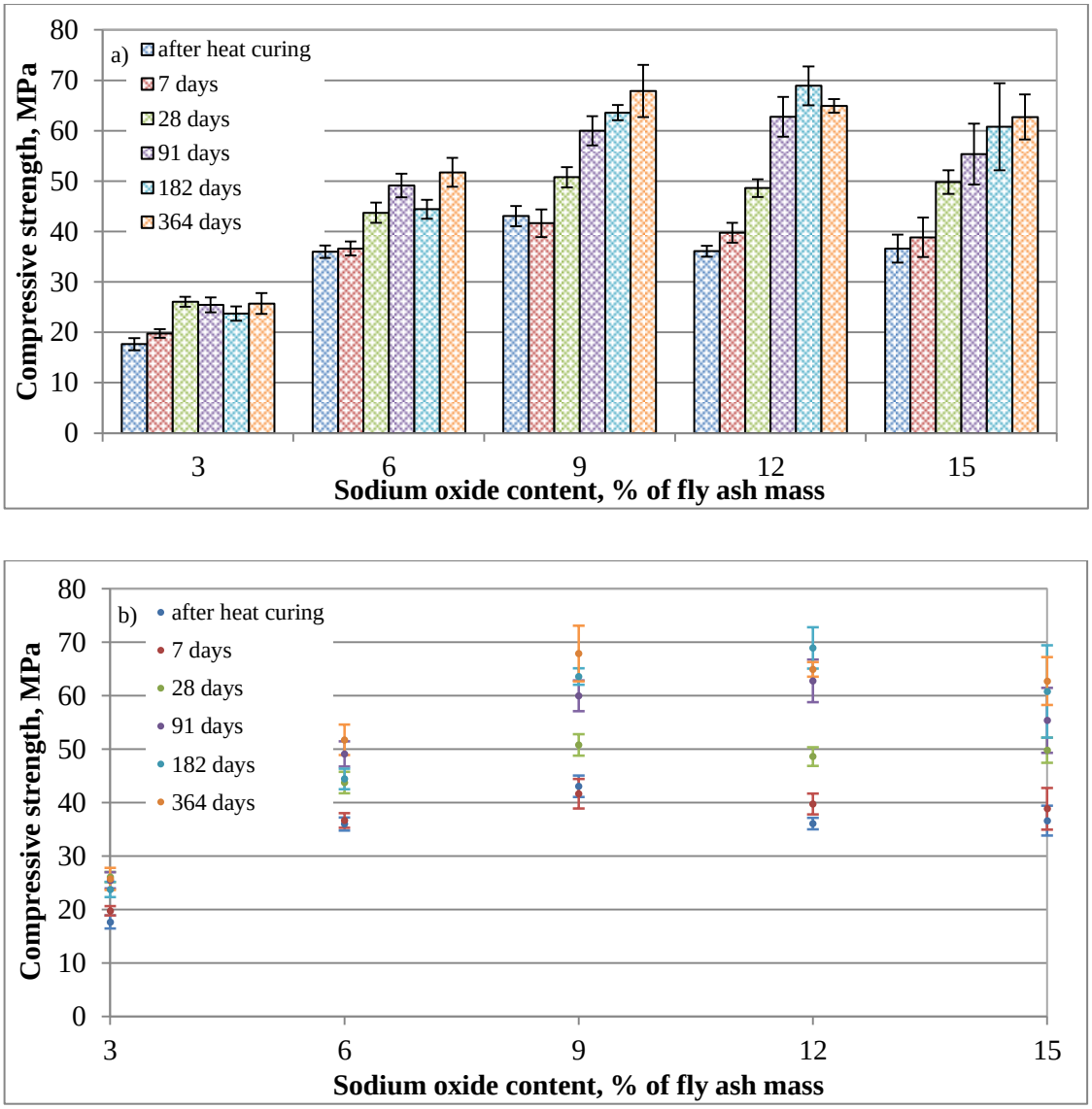

Figure 4.3: Effect of Na_2O content on the compressive strength development of alkali-activated classified Lethabo fly ash

The process of alkali activation starts from the dissolution of fly ash vitreous phase with the subsequent formation of aluminosilicate gel and requires the presence of strong alkalis (Palomo et al., 1999a). The higher the amount of aluminosilicates gel, the higher the mechanical strength (Criado et al., 2007a). The dissolution rate of the vitreous phase of aluminosilicates and the resulting compressive strength of the final material is strongly affected by the concentration of the alkaline solution (Fernandez-Jimenez and Palomo, 2005a; Fernandez-Jimenez et al., 2005c) and this is confirmed by the present study. An increase in Na_2O from 3 to 9 % by fly ash mass resulted in a significant increase in the compressive strength of paste at all ages. Figure 4.3 b shows that the optimum of sodium oxide lies between 9 and 12 % of fly ash mass. Calculated, using fitted functions, maximum compressive strength corresponds to sodium oxide content of 10.6 to 11.9 % of fly ash at different age. A further increase in alkaline content above 12 % however did not result in an

increase in compressive strength but decreased strength. This is in good agreement with the results published by Steveson and Sagoe-Crentsil (2005b) and Gou et al. (2010) who noticed an increase in compressive strength with increased alkali content up to 10 % but a decrease in strength at 12 % and 15 %. A question of strength reduction at higher alkali concentration was repeatedly raised in publications. Somna et al. (2011) reported a decrease in compressive strength for a sodium hydroxide concentration of 16.5 M compare to 9.5-14 M, due to early precipitation of aluminosilicate products. Rattanasak and Chindaprasirt (2009) found that higher concentrations of Si^{4+} and Al^{3+} were obtained with a 10 M NaOH solution compared to a 15 M NaOH solution. Concentration of OH^- beyond some point resulted in a decrease in Al and Si which were able to participate in the geopolymerization. Palomo et al. (1999a) indicated that the strength decrease of the alkali cement is caused by an excess of OH^- concentration in the system. Some correlation between zeolite formation and decreases strength has been observed in certain systems (Provis, 2009; Criado et al., 2007a). However it is still unclear whether the concentration of alkalis itself or other factors caused by high alkali concentration is the reason for the strength decrease in some cases. To explain the phenomenon, detailed characterization of AAFA cement pastes with different concentrations of alkali will be performed and discussed later in this chapter in order to find a correlation between composition, microstructure and the compressive strength.

In this study, a gain in strength of up to 30 % and more was observed after 28 days of curing for all samples (see Table F.3, Appendix F). A noticeable change in compressive strength with time was observed by other researchers (De Vargas et al., 2011; Somna et al., 2011). This confirms that age has a significant effect on the strength of AAFA cement pastes, and the structural development does not stop with the discontinuation of elevated temperature curing. The strength increase probably relates to the transformation of aluminosilicate gel to more stable structures (Škvara et al., 2009; Ravikumar et al., 2010). At the age of 28 days the highest compressive strength value was again obtained for the 9 % Na_2O paste. The paste with 12 % Na_2O yielded a higher compressive strength value after 91 and 182 days but after one year of curing the strength of Na12 was lower than Na9. The difference in compressive strength values between 9 and 12 % at later ages is negligible and therefore using lower alkali content is more economical, as the alkali is the most expensive component in the AAFA cement paste composition. Therefore, 9 % Na_2O can be considered as the most suitable alkali concentration to produce AAFA cement paste containing the South African fly ash studied in this research.

It should be mentioned that the greatest gain in strength was observed for AAFA cement pastes with high alkali content. Similar findings were reported by De Vargas et al. (2011).

The authors explained that the gain in strength with time was caused by additional reaction products generated during the reaction between alkali activator and fly ash microspheres, which packed inside plerospheres. The alkaline solution first partially dissolved the external layer of the plerosphere and only then attacked the microspheres.

As can be seen from the standard deviation values in Table F.3 (Appendix F), the observed compressive strength of the 15 % Na_2O paste samples varied significantly. It can be assumed that the high concentration of alkali in the pastes results in inconsistent compressive strength. Additional tests were performed on larger sample populations for Na9, Na12 and Na15 pastes to establish the distribution of the compressive strength and results are shown in Table 4.1. Curing conditions were the same as in the first test. Samples Na3 and Na6 were not studied in this test due to their relatively low compressive strength compared to samples with higher alkali content and satisfactory standard deviation. At least 36 compressive strength determinations at the age of 28 days were performed for each of these pastes. For the paste with 9 % Na_2O, 6 results within 36 determination of the compression strength varied by more than ± 10 % from the mean, which was 16.7 % of the total sample population. For the paste with 12 % Na_2O, 7 strength values out of 42 varied by more than ± 10 % from the mean, which was also 16.7 %. The paste with 15 % Na_2O had 18 strength values out of 36 varied by more than ± 10 % from the mean, which represented 50 % of the total sample population. The strength deviation was thus greater for AAFA cement pastes containing 15 % Na_2O.

Table 4.1: Compressive strength, standard deviation and coefficient of variation at 28 days of alkali-activated classified Lethabo fly ash cement paste (larger sample population)

Na_2O, % fly ash mass	Average strength, MPa	Standard deviation, MPa	Coefficient of variation, %
9	51.4	4.52	8.8
12	41.4	3.33	8.1
15	35.6	5.79	16.3

Results show that the coefficient of strength variation within the large batch of Na15 paste was much higher than that of Na9 and Na12 pastes (16.3 %, 8.8 % and 8.1 % respectively). It is interesting to note that high alkali content affects not only the deviation of compressive strength within a batch but also between two batches of the same composition. The average 28-days strength of the Na9 paste for the second (large) batch was almost the same as for the first batch (51.4 MPa and 50.8 MPa respectively) while the average 28-days strength of Na15 paste for the second batch was much lower than for the first batch (35.6 MPa and 49.8 MPa respectively). The same trend could be observed for Na12 paste where the average 28-days strength for the first batch was 48.6 MPa while it reached only 41.4 MPa for the second batch.

Limited strength deviation should be expected because of variability of fly ash composition due to variations in coal composition and burning conditions. Nevertheless, the strength deviation between batches was much greater with higher alkali concentrations.

Another important observation was the formation of efflorescence on surfaces of Na12 and Na15 paste samples after 28 days of hardening (See Figure 4.4). Qualitative XRD analysis of efflorescence showed the presence of thermonatrite, which is sodium carbonate. The formation of efflorescence is an indirect indicator of excess Na_2O in the AAFA cement pastes with 12 and 15 % Na_2O. The excess alkali migrates with moisture to the surface of the samples and produces salts, which appear as white efflorescence. The presence of excess alkali could be one of the causes of the lower strength, high standard deviation, and variations in the strength between the batches of AAFA cement pastes.

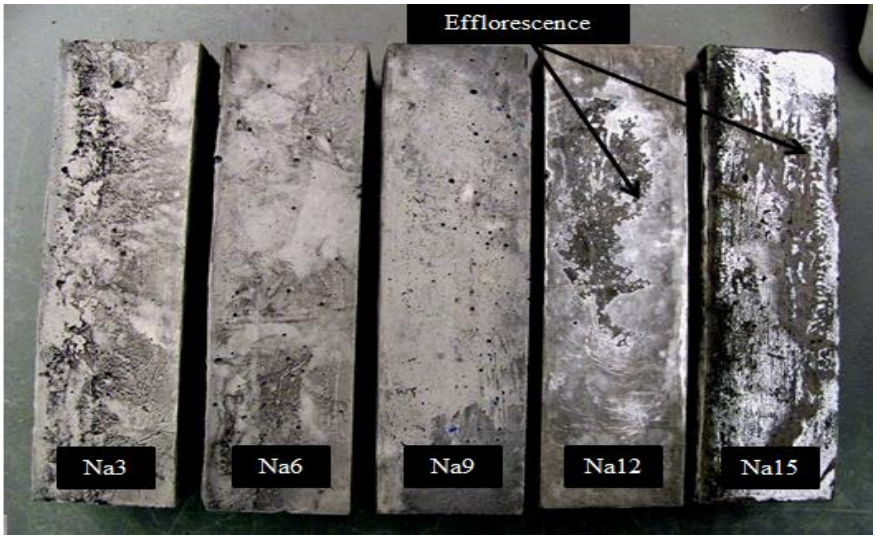

Figure 4.4: The surface of AAFA paste samples after 28 days of curing

Efflorescence formation is not only an aesthetical problem but also a technical one. As efflorescence formation require some time to develop, plaster or paint applied on surfaces of such materials immediately after their production can come off with time. Thus, careful selection of alkali dosage should be implemented.

4.3.2 Effect of temperature and duration of elevated temperature curing on the compressive strength

It is expected that an elevation of curing temperature would accelerate the dissolution of the amorphous phase of fly ash and, as a result, the strength development of the AAFA cement paste. Previous research showed that temperature accelerated the alkali activation of metakaolin (Alonso and Palomo, 2001a) as well as slag pastes (Bakharev et al., 1999). The accelerating effect of elevated temperature also applies to fly ash pastes (Katz, 1998). Results

presented in this thesis confirm the trend. Some researchers (Swanepoel and Strydom, 2002; Chindaprasirt et al., 2007) reported 48 hours as optimal heat curing duration. In order to obtain the values of curing temperature and duration which provide the maximum compressive strength, mixtures containing 9 % Na_2O at constant water to binder solids ratio were subjected to different temperatures and periods of heat treatment. Table F.4, Appendix F presents the compressive strength and standard deviation values of samples from this test.

The importance of elevated temperature curing can be clearly seen in Figure 4.5a. Samples cured at 25 °C did not set after 24 hours and could be hardly demoulded after 7 days, when the compressive strength was 1.1 MPa. Even such low strength was an indicator of chemical reaction between the fly ash and the activator solution. The strength of the paste cured at 60 °C for 24 hours and tested immediately after the elevated temperature curing exceeded the strength of the paste cured at 25 °C for 91 days. Curing of the AAFA cement paste at 25 °C is not practical due to slow strength development, intensive efflorescence formation, relatively low strength and high standard deviation (see Table F.4, Appendix F). Thus, elevated temperature curing is necessary to provide faster strength development and lower standard deviation of the strength. An increase in temperature from 25 to 60 °C produced significant acceleration in the strength development. Immediately after elevated temperature curing, the paste cured at 40, 60 and 80 °C for 24 hours had a compressive strength of 1.6 MPa, 49.4 MPa and 53.0 MPa, respectively. The increase in the compressive strength of the paste was a result of an increase in the degree of polymerization caused by the elevation of curing temperature (Rovnaník, 2010). It is important to note that when the paste was cured at elevated temperature for 24 hours, an increase in the temperature to above 60 °C did not result in a considerable gain in compressive strength. The use of 60 °C instead of 80 °C for prolonged elevated temperature curing of AAFA cement pastes will require less energy and, thus, will be more economical.

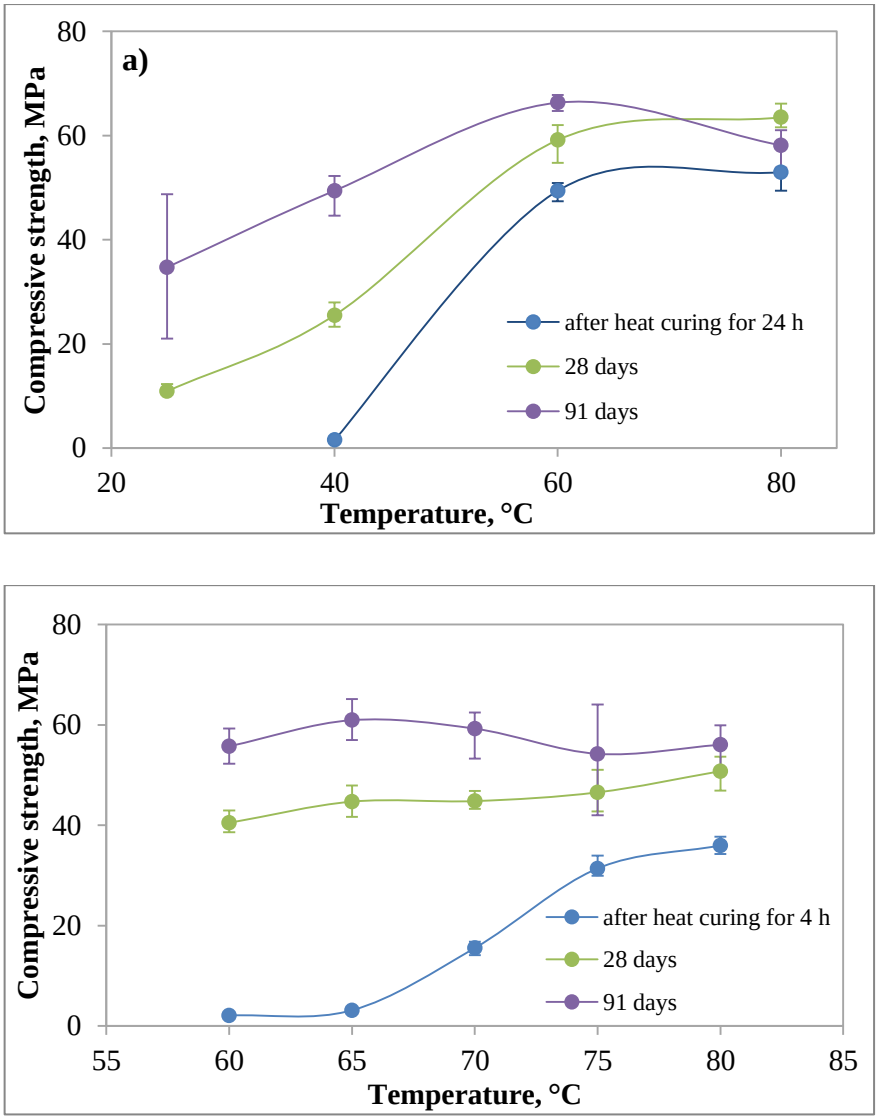

Figure 4.5: Effect of curing temperature on the compressive strength of AAFA cement pastes

After 28 days of curing the compressive strength of sample T40D24, T60D24 and T80D24 increased from 1.6, 49.4 and 53.0 MPa to 25.5, 59.1 and 63.5 MPa, respectively. Sample T25D24 could not be demoulded at 1 day but it still gained 10.9 MPa after 28 days of hardening. Compressive strength of the AAFA cement pastes increased with the reaction time and the gain was greater in case of the pastes cured at low temperatures (25 and 40 °C). At the age of 91 days, the paste cured at 80 °C had lower compressive strength in comparison to the paste cured at 60 °C. This strength decrease was probably caused by the contraction of aluminosilicate gel due to dehydration and excessive shrinkage occurring during the curing at high temperatures for 24 hours (Van Jaarsveld et al., 2002). Chindaprasirt et al. (2007) drew conclusions on the effect of elevated temperature curing on strength considering 7-days strength results, but the results of this study and other studies (De Vargas et al., 2011; Arioz et al., 2012) show that the difference in strength of AAFA cement pastes cured at low and high

temperatures decreases with age and even more, lower temperatures could lead to higher strength in the long term.

Another important observation is the long-term gain in compressive strength of the AAFA cement pastes cured at elevated temperatures for different period of time. After 28 days of hardening, the compressive strength of sample T60D4 raised by 20 times from 2.1 MPa to 41.5 MPa, while the compressive strength of sample T80D4 increased only by 1.4 times from 36.0 to 50.8 MPa (see Table F.4 Appendix F). For samples T60D24 and T80D24, the compressive strength increased from 49.4 to 59.1 MPa and from 53.0 to 63.5 MPa, respectively showing the 1.2 times gain for the both samples. These results show that the aging of the AAFA cement pastes has a greater effect on the strength development of the pastes cured at the lower temperature for a short period of time.

Palomo et al. (1999a) showed that the speed of reaction between alkali and fly ash depend on curing temperature, especially in the first few hours. A relatively small increase in temperature of elevated temperature curing resulted in a significant gain in the compressive strength of the pastes cured for a short period of time (Figure 4.5b). Increasing the temperature from 65 to 70 °C produced a significant increase in the strength from 3.2 to 15.5 MPa. A further increase (by 5 °C) doubled the strength from 15.5 to 30.5 MPa. Subsequently, increasing the temperature to 80 °C did not lead to a significant increase in the strength in comparison to 75 °C. After 28 and 91 days of hardening, the difference in the strength of the AAFA cement pastes, cured at elevated temperatures in the range of 60 to 80 °C, was not significant. Thus, despite the significant effect the increase in the curing temperature (in the range from 60 to 80 °C) has on the early compressive strength of the pastes, the difference in the curing temperature has a limited effect on the long-term strength of the pastes when elevated temperature curing was applied for a short period of time (4 hours).

Figure 4.6 shows the effect of duration of elevated temperature curing on the compressive strength of the AAFA cement pastes cured at 60 and 80 °C.

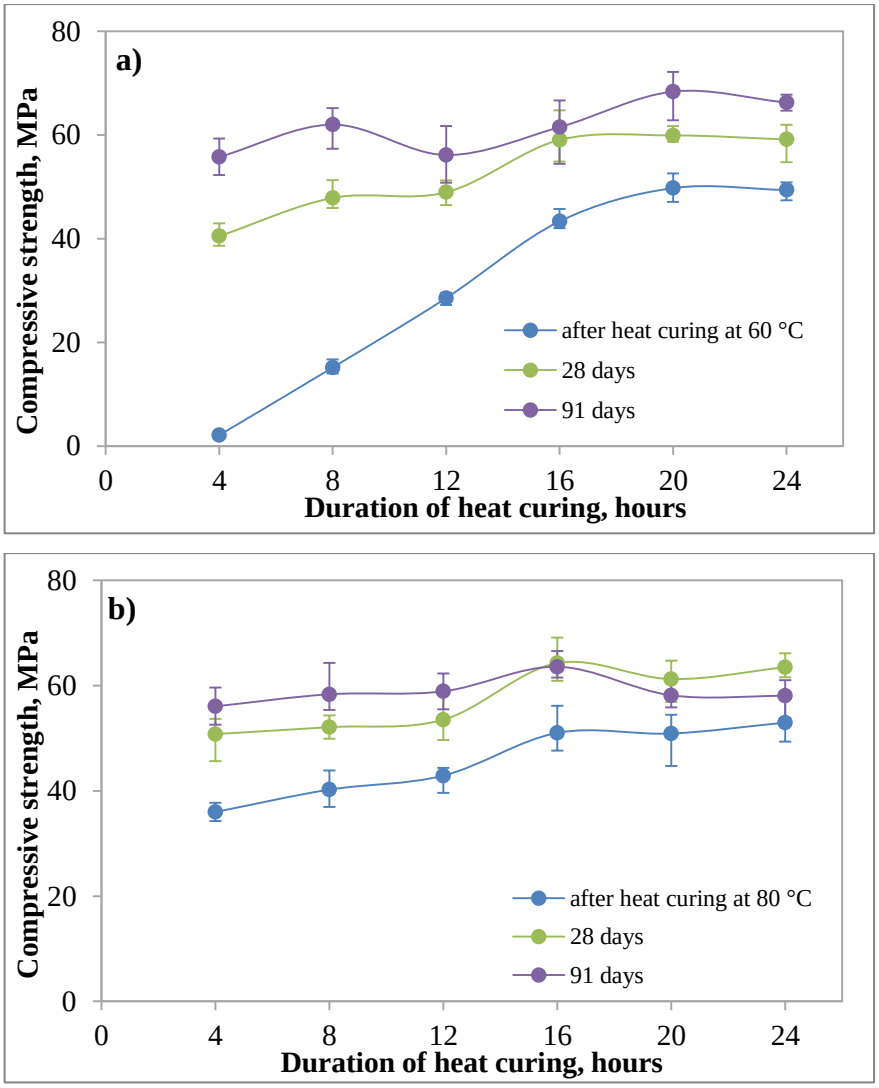

Figure 4.6: Effect of duration of elevated temperature curing on the compressive strength of AAFA cement pastes cured at: a) 60 and b) 80 ºC

After 4 hours of elevated temperature curing at 60 °C (see Figure 4.6a), the compressive strength of the paste tested immediately after the curing was 2.1 MPa. With other parameters being equal, the compressive strength of the paste cured at 80 °C was 36 MPa (see Figure 4.6b). This once again confirms that temperature during the initial curing plays a key role in the strength development of AAFA cement pastes. For longer durations of elevated temperature curing, the difference in the strength of the pastes cured at 60 and 80 °C becomes less prominent. The compressive strength of sample T60D24 was 49.4 MPa while T80D24 was 53.0 MPa. It is important to note that a significant increase in the compressive strength, tested immediately after heat curing, of the paste cured at 60 °C was observed only when the duration of the curing was increased to 16 hours (see Figure 4.6a). Subsequent increase in the duration of heat curing did not result in a substantial increase in strength. A similar trend was observed when the paste was cured at 80 °C (see Figure 4.6b). Insignificant strength gain took place when the duration of heat curing exceeded 16 hours. In the long term, curing at 80 °C

for more than 16 hours negatively affected the compressive strength. At 28 and 91 days, the pastes cured in an oven for 20 and 24 hours had lower strength in comparison to the paste cured for 16 hours. Van Jaarsveld et al. (2002) reported that curing for longer periods of time at elevated temperature appeared to weaken the microstructure suggesting that small amounts of structural water needed to be retained in order to reduce cracking and maintain structural integrity. Despite the fact that few researchers (Swanepoel and Strydom, 2002; Chindaprasirt et al., 2007) reported 48 hours as an optimal duration of elevated temperature curing, results of this study confirmed the findings made by Van Jaarsveld et al. (2002) and indicated that the duration of elevated temperature curing should be limited to 16 hours.

4.3.3 Effect of water to binder solids ratio

To establish the effect of water to binder solid ratio on the compressive strength of paste, mixtures containing 9 % Na_2O and cured at 60 °C for 24 hours was used. For this experiment fly ash to sodium hydroxide ratio were kept constant but the amount of water added varied. In Table F.5 (Appendix F) compressive and flexural strength of pastes with different water to binder solids ratios are shown. Figure 4.7 shows compressive strength – water to binder solids ratio relationship.

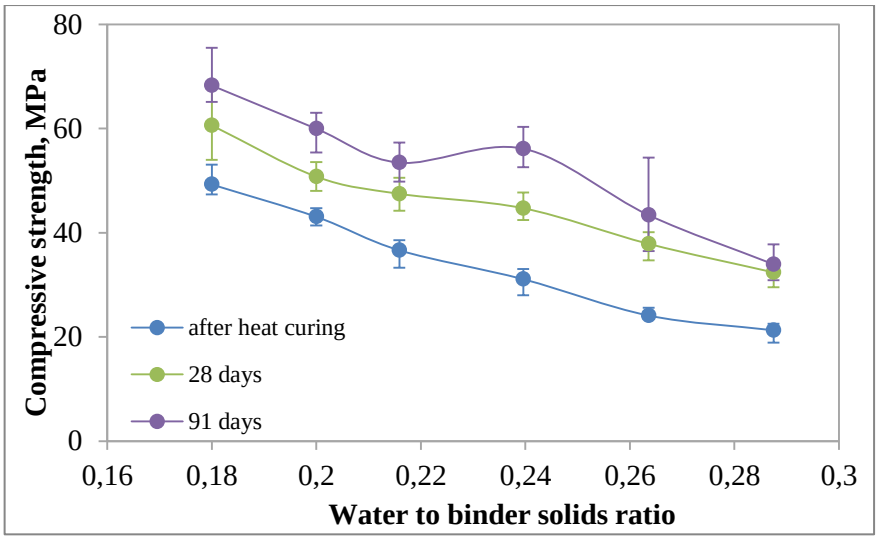

Figure 4.7: Effect of water to binder solids ratio on the compressive strength

Increasing in the water to binder solids ratio of the pastes from 0.18 to 0.29 resulted in a decrease in the compressive strength from 49.3 to 21.3 MPa but the consistency of the pastes improved. From the same mixtures different independent variables reflecting the amount of water (liquid to solid ratio, water to fly ash ratio, etc.) were recalculated and plotted against compressive strength in Appendix B. Fernandez-Jimenez and Palomo (2005a) admitted the importance of water to binder ratio. According to Davidovits (1988), no water combined

within the geopolymer. Water acts as carrier of alkalis (Škvára et al., 2009) and provides consistency to the fresh geopolymer mixture (Hardjito and Rangan, 2005). Škvara et al. (2009) reported that about 65 % of all water in geopolymers was in "free" condition as it was evoporable at 180 °C, with 30 % persumed to come from nano-pores in the geoplymer gel.

The water introduced to the paste could evaporate from unsealed samples during elevated temperature curing, thus negatively affecting the final structure of material. Samples should therefore preferably be sealed to prevent extensive moisture evaporation. During the design of AAFA cement concretes a required workability should be achieved at the lowest possible water to binder solids ratio.

4.3.4 Effect of mineralogical composition of initial fly ash

Fly ash from Matla power station was used for sample preparation in this test. A mix composition with 9 % Na_2O of fly ash mass, water to binder solids ratio of 0.24 cured at 60 °C for 24 hours was used. The compressive strength and standard deviation values are shown in Table F.6 (Appendix F) and compared with Lethabo fly ash paste in Figure 4.8.

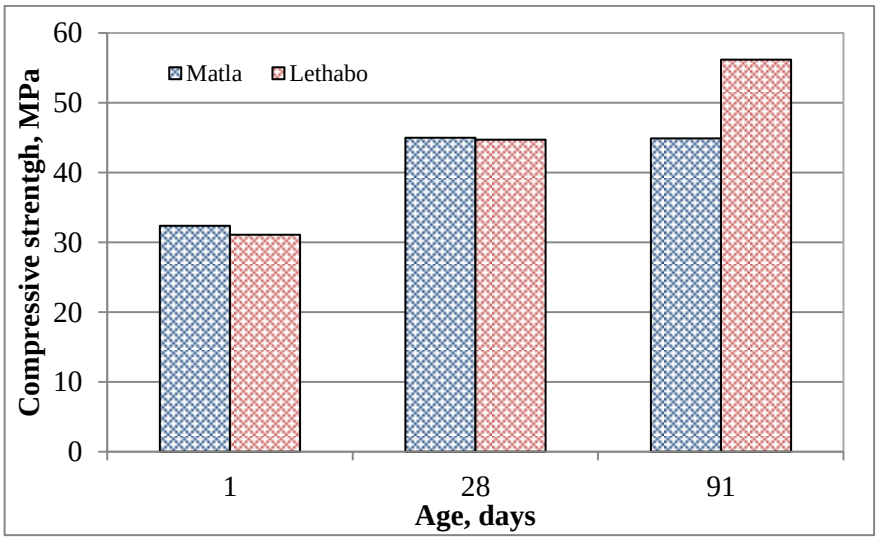

Figure 4.8: Compressive strength comparison of Matla and Lethabo AAFA pastes at different age

Samples of Matla and Lethabo fly ash tested immediately after oven curing and at 28 days had almost the same compressive strength values. The compressive strength values of samples of Matla fly ash at 91 days were much lower compare to Lethabo fly ash, 44.9 MPa and 56.2 MPa respectively.

A significant difference in 91 days strength values between samples of the two different fly ashes is evident. Particle size of two fly ashes is almost the same as it can be seen in Figure

3.1. There is a slight difference in CaO content (see Table 3.1 Lethabo II and Matla); however this difference is small to affect compressive strength. Significant differences can be observed in the mineralogical composition of the fly ashes. The quantity of crystalline mullite is higher in Matla fly ash than in Lethabo (see Table 3.2, Lethabo II and Matla), affecting the amorphous alumina oxide content. The elemental composition of the amorphous phase shown in Table 4.2 was calculated by subtracting the contribution of the crystalline phases from XRF data (Rickard et al., 2011).

Table 4.2: Chemical composition of amorphous phase of fly ashes, %

Fly ash name	Main oxides			
	SiO_2	Al_2O_3	CaO	SiO_2/Al_2O_3
Matla	36.2	4.9	6.4	7.3
Lethabo	36.6	10.5	4.3	3.5

It can be seen from Table 4.2 that the SiO_2/Al_2O_3 ratio of Matla fly ash is higher compare to Lethabo fly ash. The concentration of reactive aluminium is lower in Matla fly ash at almost the same SiO_2 content so the total amount of reactive phases is less and might result in the formation of a smaller amount of the gel responsible for final strength of the paste. This could be the reason the lower compressive strength value of samples containing Matla fly ash.

4.3.5 Effect of activator type

In this paragraph the effect of activator type on the compressive strength will be shown for three examples. According to literature reviewed the caustic alkalis and alkali silicates were found to be the most suitable for alkali activation of low calcium fly ash. Thus, it was decided not to use alkaline salts of weak acid, such as carbonates or sulfates for alkali activation of South African fly ash.

In this experiment the effect of potassium hydroxide (KOH) and sodium silicate solution ($Na_2O{\cdot}nSiO_2$) as activators was investigated and compared to mixtures where sodium hydroxide (NaOH) was used as activator. Water to binder solids ratio and curing conditions were the same for all mixtures. As the purity of potassium hydroxide was lower than that of sodium hydroxide, the actual percentage of potassium oxide in the mixture was lower. However, even if it is not possible to directly compare the strength of pastes with different concentrations the trend is still clear. A sodium silicate solution with a silica modulus of two was used with a 10 M sodium hydroxide solution in proportion 2:1 by mass. The silica modulus of produced silicate activator solution was 1.14. Additional water was added to produce water to binder solid ratio of 0.2. A percentage of sodium oxide per fly ash mass was introduced with sodium silicate and sodium hydroxide solutions calculated by taking the

chemical composition of both liquids into account. Compressive strength results and standard deviation values for this test are presented in Table F.7 (Appendix F). Compressive strength development of samples activated by different alkaline solution showed on Figure 4.9.

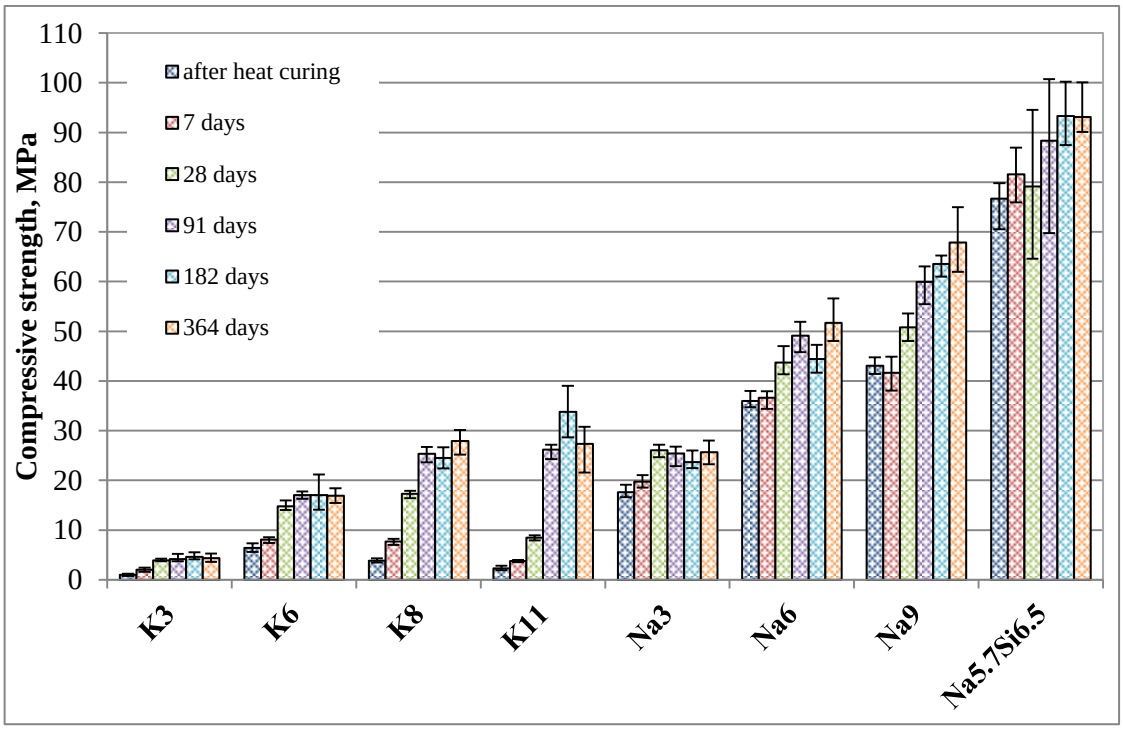

Figure 4.9: Compressive strength development of samples activated by different alkaline solutions

It seems that the alkali metal cation significantly affects the compressive strength development. Smaller ionic size of Na^+ compare to K^+ results in better dissolution of raw materials (Abdul Rahim et al., 2015). Previous studies found that more of the fly ash dissolves in the sodium-based system than in the potassium equivalent, and similar results were found for metakaolin (Steveson and Sagoe-Crentsil, 2005a, b). The compressive strength of samples activated with potassium hydroxide is significantly lower than that activated with sodium hydroxide not only for comparable samples, but even if the amount of alkali present is higher in mixtures containing potassium. These results differ from results presented by Van Jaarsveld et al. (1999a), who reported that potassium-containing matrixes are stronger than those containing sodium. The authors however used a combination of sodium and potassium hydroxide with Na, K silicate solution, which is a much more complex system, where along with Na-K the joint effect of soluble silicates were working as well. The results of this study support the outcome of Steveson and Sagoe-Crentsil (2005b) who also noticed that the sodium-based inorganic polymer is stronger than its potassium-based equivalent. Nevertheless, the compressive strength of metakaolin activated by potassium hydroxide solution was found to be higher than fly ash based materials (Steveson and Sagoe-Crentsil,

2005a,b). That again confirms the importance of availability of reactive aluminosilicates, in other words the chemical and even more the mineralogical composition of the initial source of aluminosilicates.

From Figure 4.9, it can clearly be seen that the addition of soluble silicates to the activator mixture dramatically affects the compressive strength. Even if the total amount of the alkali for the mixture with combined activator was 5.7 % of fly ash mass compare to 6 % for sodium hydroxide solution mixture, the compressive strength values immediately after heat curing were 76.7 MPa and 36.0 MPa respectively. These results are in good agreement with results of Fernandez-Jimenez and Palomo (2005a) who obtained more than 55 MPa in compression for a total amount of Na_2O of 5.55 % and 7.74 % for SiO_2 with respect to fly ash mass for NaOH – sodium silicate combined activator.

For both NaOH-activated and NaOH + sodium silicate-activated fly ash mixtures, the alkali content in the present study was almost the same and at the other parameters being equal, the only difference was the presence of additional 6.5 % soluble SiO_2 (per fly ash mass), which contribute to strength performance and doubled the compressive strength. Soluble silica added with alkaline silicate solution participates in the alkali activation process, increasing the amount of total reactive phase and as a result the quantity of final aluminosilicate gel responsible for the performance of hardened material. In the case of alkali hydroxide solutions, silicate species leach out from the vitreous phase of fly ash, while the alkali silicate solution is a more complex system and soluble silicate are already present in the aqueous phase along with the silicates gradually leached from the vitreous phase of fly ash. An increase in the concentration of silicate leads to an increased degree of polymerization of silicates (Korneev and Danilov, 1996). Thus, the higher strength of sodium silicate-activated samples is conditional not only on the increased amount of aluminosilicates gel, but also probably on the degree of polymerization. A more detailed study of different concentrations of soluble silicates at different amounts of alkali was conducted.

4.3.6 Effect of SiO_2 concentration

To study the effect of soluble SiO_2 (introduced with alkaline activator) on the compressive strength of AAFA paste, mixtures of sodium silicate with silicate modulus of two and sodium hydroxide at different proportions were used as activator to produce the pastes at fixed Na_2O concentrations of 3, 6 and 9 % of fly ash mass. Concentration of SiO_2 was varied from 3 to 12 % of fly ash mass with 3 % intervals. Water to binder solids ratio of all mixtures was kept constant at 0.2. Samples were cured at 60 °C for 24 hours and then tested in compression at different ages. Samples containing 3 % Na_2O were not produced with 9 and 12 % SiO_2 due to

the relatively low silicate modulus of the sodium silicate used. Table F.8 (Appendix F) presents the compressive strength and standard deviation values for the Na-Si series of AAFA cement pastes. Figures 4.10-4.12 show the effect of soluble silicate concentration on strength development of the pastes at different fixed sodium oxide concentrations.

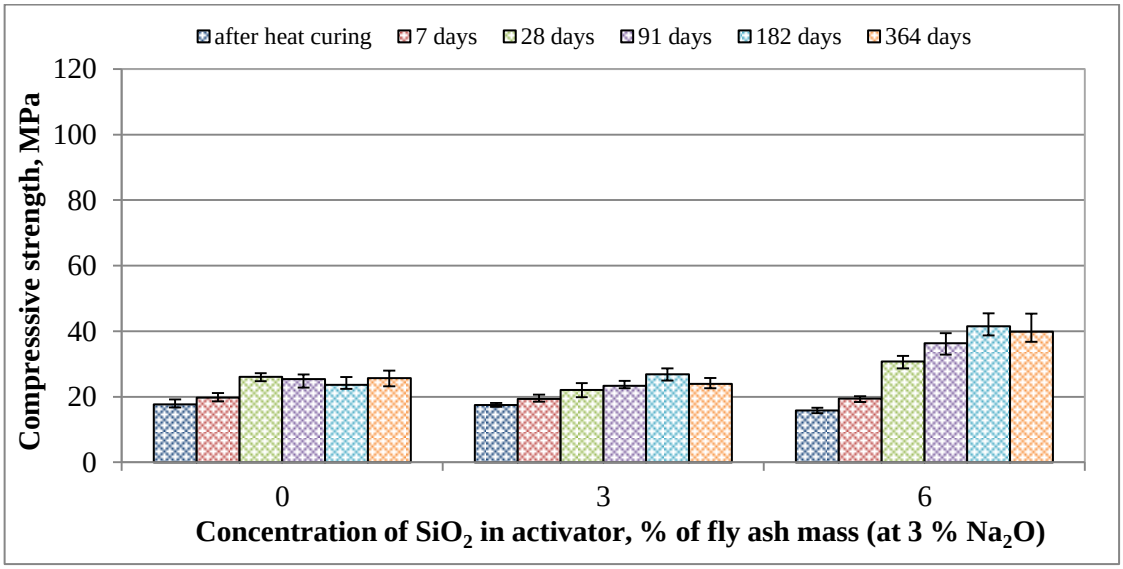

Figure 4.10: Effect of SiO_2 concentration on the compressive strength of AAFA paste with constant Na_2O of 3 % of fly ash mass

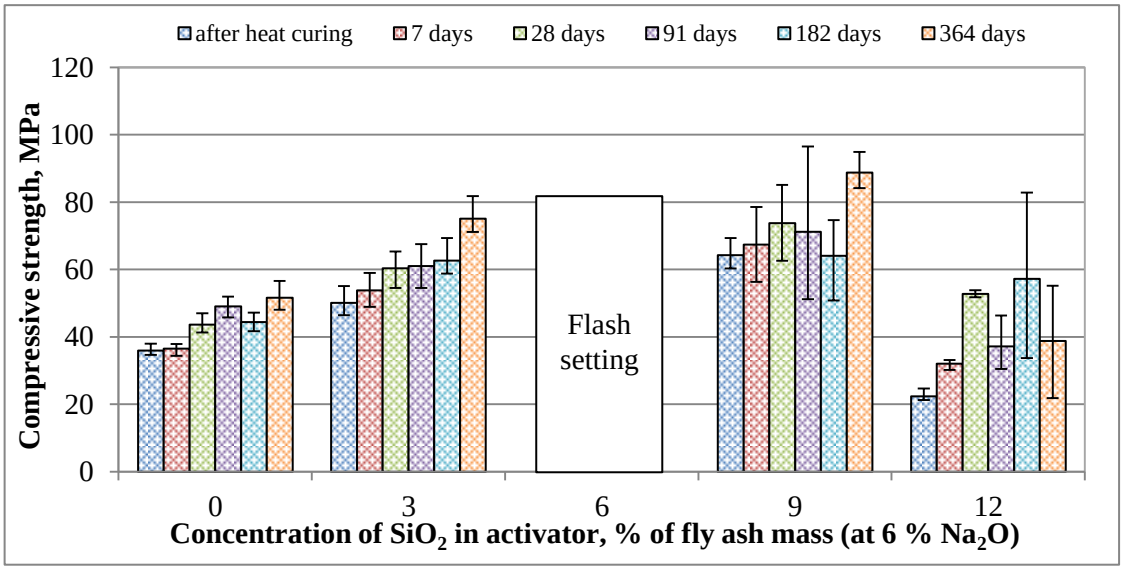

Figure 4.11: Effect of SiO_2 concentration on the compressive strength of AAFA paste with constant Na_2O of 6 % of fly ash mass

The compressive strength of pastes presented in Figure 4.10 is a function of SiO_2 content used with a fixed Na_2O concentration of 3 % of fly ash mass. It can be clearly seen that addition of 3 % soluble SiO_2 did not affect the compressive strength of pastes at any investigated age in comparison to sample without addition of soluble SiO_2. Addition of 6 % SiO_2 did not affect the strength of samples tested immediately after heat curing or after 7 days. However, the

strength of samples with 6 % SiO_2 tested after 28 days was 30.8 MPa compared to 26.1 MPa of sample without any addition of silicate but with the same Na_2O content. With age this difference becomes even more pronounced. It is also clearly visible that the strength development of samples activated only by sodium hydroxide solution was completed by 28 days, while samples containing Na-Si activator continue to gain strength up to 182 days.

When the concentration of sodium oxide was constant at 6 %, the concentration of SiO_2 introduced with sodium silicate becomes a very important parameter affecting the performance of the paste (see Figure 4.11). The presence of as little as 3 % of SiO_2 increases the compressive strength significantly. Increasing concentration of SiO_2 to 9 % of fly ash mass results in increased average compressive strength but also scatters compressive strength values. This scattering effect is more significant at higher SiO_2 contents of 12 %. The compressive strength of Na6Si12 was much lower than that of Na6Si9 suggesting that the concentration of SiO_2 increase the compressive strength only up to a certain point, but a further increase in SiO_2 content lead to decreased compressive strength.

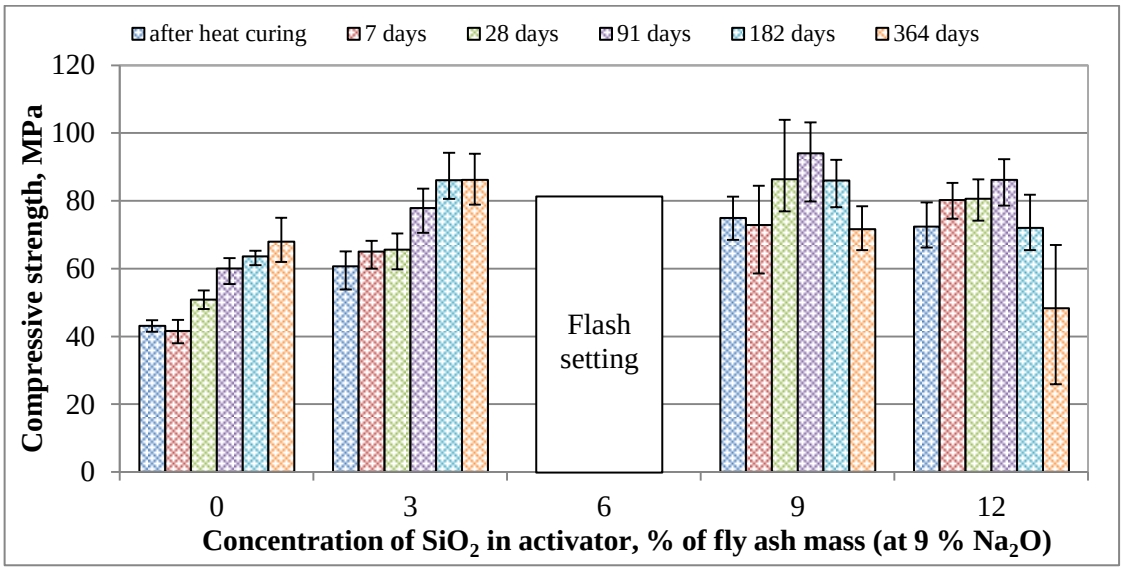

Figure 4.12: Effect of SiO_2 concentration on the compressive strength of AAFA paste with constant Na_2O of 9 % of fly ash mass

The same trend was observed in Figure 4.12 where the addition of only 3 % SiO_2 to the activator solution (at 9 % Na_2O per fly ash mass) increases the compressive strength by 30 to 40 % at different ages compared to mixtures where only sodium hydroxide was used. Increase in SiO_2 to 9 % of the fly ash mass leads not only to higher strength, but higher strength deviation as well. Compressive strength results of Na9Si12 was lower than that of Na9Si9.

In this study mixtures with 6 % SiO_2 and 6 or 9 % Na_2O provoked flash setting of the AAFA paste in the mixer, before paste was cast into moulds. The mixture with 9 % Na_2O and 9 %

SiO_2 was cast into moulds but set about 10 minutes after mixing. It is interesting to note that this mixture becomes fluid after an hour in the oven. These solutions were not stable and precipitation was formed. In general the presence of soluble SiO_2 in the activator solution is preferable for the compressive strength compared to activator where only alkali hydroxides used. The highest compressive strength at 28 days was obtained for paste with 9 % Na_2O and 9 % SiO_2 of fly ash mass. Similar findings were reported by Ma et al. (2012). However, regardless of Na_2O content, high SiO_2 content (9 and 12 % of fly ash mass) resulted in higher deviation of compressive strength. Thus the optimal silica content for activator solution in this study with respect to 6 and 9 % Na_2O is 3 % of fly ash mass.

4.4 CHARACTERIZATION OF AAFA CEMENT PASTES

Detailed characterization of AAFA cement pastes with different concentrations of sodium hydroxide is the main aim of this section in order to obtain information about the structure and composition of the secondary products of alkali activation which might be helpful in explaining the variation of strength and strength drop for samples with high alkali dosages.

4.4.1 Porosity

To see whether there is any difference in porosity of hardened mixtures with all five levels of sodium oxide content, a basic porosity test was performed. Three slices of AAFA paste cut from prismatic specimen were weight in dry and water saturated condition. Apparent porosity was calculated as the difference between saturated and dry specimen mass divided by sample volume (measured by hydrostatic weighing). Figure 4.13 shows the relationship between porosity and sodium oxide content in AAFA paste.

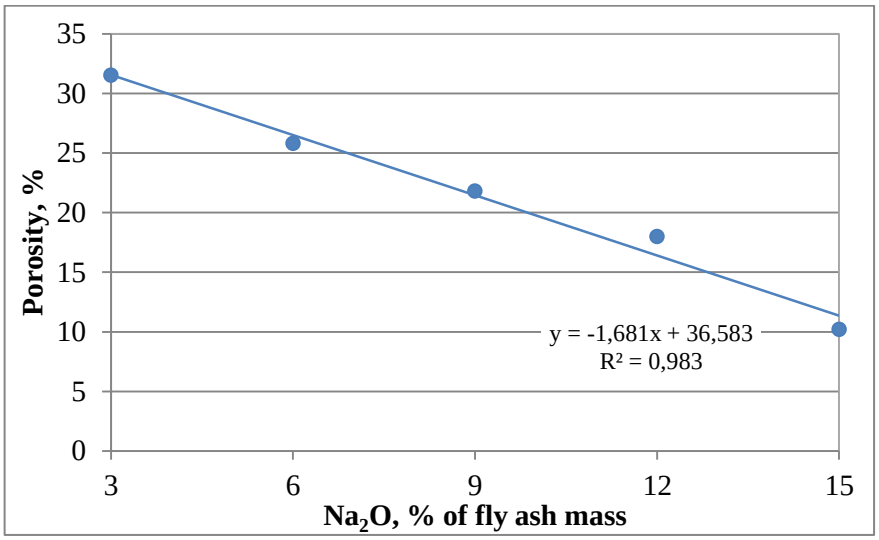

Figure 4.13: Effect of sodium oxide content in AAFA paste on the porosity of specimens

It can clearly be seen that there is linear relationship between sodium oxide content and porosity. Pore volume decreased with increasing sodium oxide content in the system, thus samples with 15 % Na_2O denser than samples with lower alkali content and supposed to be stronger, but results shows the drop in strength. To see if there was any change in composition of hardened AAFA paste with increasing alkali content, XRD and ATR-FTIR analysis were performed.

4.4.2 XRD study

Two independent series of AAFA pastes produced at different times from different batches of Lethabo fly was analyzed at different ages using XRD techniques and their patterns are shown in Figures 4.14 and 4.15.

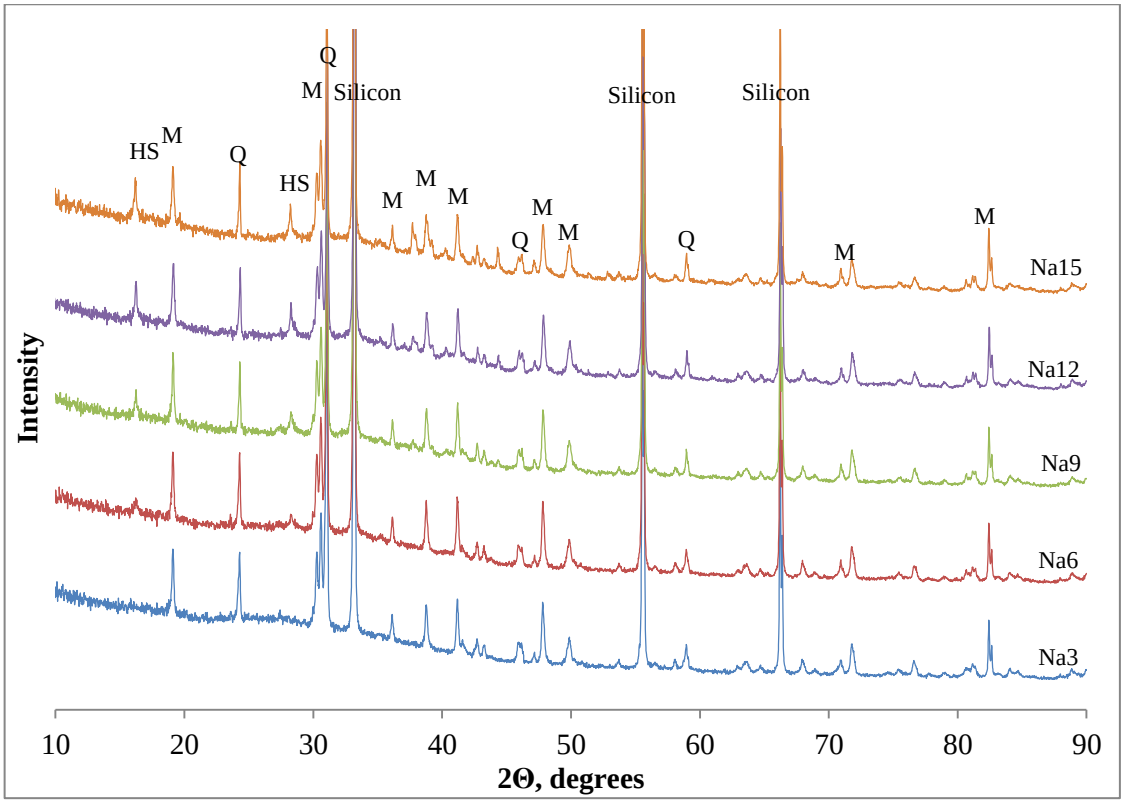

Figure 4.14: XRD pattern of AAFA cement pastes containing unclassified Lethabo fly ash with different sodium oxide content after 45 days of curing, where Silicon is chemically pure silicon, added to determinate amount of amorphous phase, M – mullite, Q – quartz, HS – hydroxysodalite

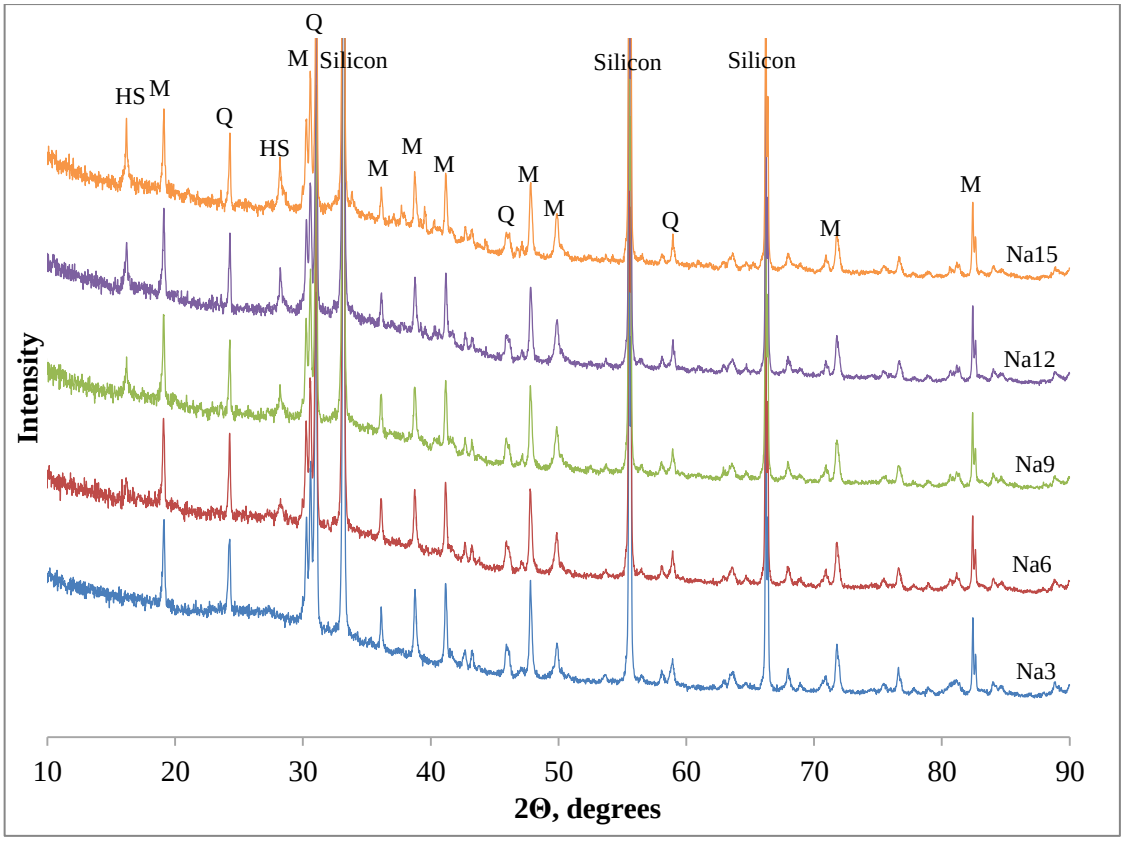

Figure 4.15: XRD pattern of AAFA cement pastes containing classified Lethabo fly ash with different sodium oxide content after 72 days curing, where Silicon is chemically pure silicon, added to determinate amount of amorphous phase, M – mullite, Q – quartz, HS – hydroxysodalite

The major minerals observed in AAFA samples are quartz (SiO_2) and mullite ($Al(Al_{1.272}Si_{0.728}O_{4.864})$ and they were revealed in initial fly ash. Those phases seems to be unaffected by alkali activation, as the intensity of peaks is almost the same in all samples irrespective of batch of fly ash and analysis date.

The most distinct change in both XRD patterns is the appearance of new peaks at around 16.19° 2Θ and 28.21° 2Θ in Na6, Na9, Na12 and Na15 samples that were assigned to the formation of sodalite ($Na_8Al_6Si_6O_{24}Cl_2$). However, the crystal structure of hydro- or hydroxy-sodalite is almost similar to that of sodalite, but contains water molecules or NaOH in the cavities of crystal lattice. By heating or under reduced pressure, all or a part of this water can be easily removed from the crystal lattice without being associated with any structural deformation and destruction (Henmi, 1987). Therefore, sodalite is regarded as hydroxysodalite in this thesis. The relative intensity of hydroxysodalite peaks, shown in Figures 4.16 and 4.17, was found to be a linear function of sodium oxide content, suggesting that the amount of hydroxysodalite formed increased with increasing sodium hydroxide content irrespective of batch of fly ash. The presence of sodalite in alkali-activated materials was stated in previous studies (De Silva et al., 2009; Fernandez-Jimenez et al., 2006a). The

authors also noticed that the amount of sodalite depends on alkali concentration. Some investigations are ongoing into whether observation of zeolites in geopolymers is linked to change in material performance. Correlation between zeolite formation and decreased strength was observed in certain systems, however it is still unclear if zeolite formation leading to loss of material performance or any other factor (Provis, 2009). It seems that the newly formed phase of hydroxysodalite is not responsible for the strength drop observed in this research for Na15 samples as the phase was found not only in Na15 samples but in samples with different concentration of sodium oxide as well.

The distinct peak at around 16.19º 2Θ was not found in Na6 samples, however a visible hump could be observed. The peak at around 28.21º 2Θ is more sensitive to sodium oxide content change as can be seen from Figures 4.16 and 4.17. For each additional 3 % of sodium oxide the intensity of the peak at 28.21º 2Θ almost doubled.

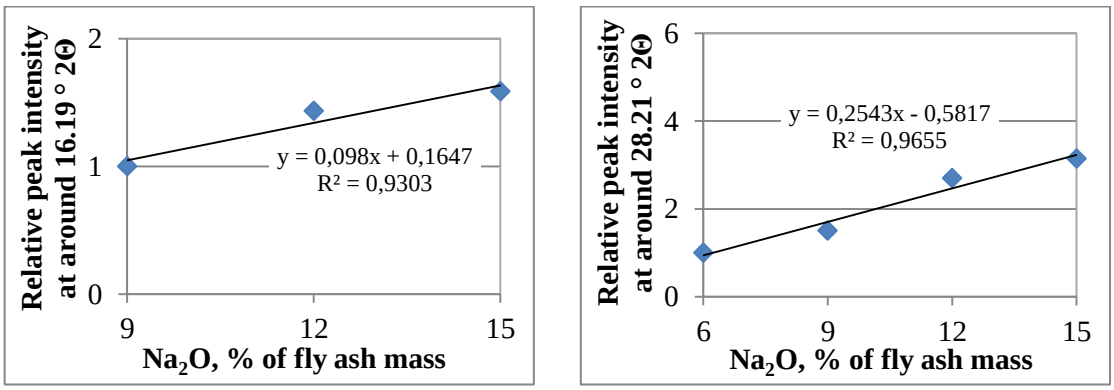

Figure 4.16: Relative intensities of hydroxysodalite peaks at different sodium oxide contents in AAFA cement pastes containing unclassified Lethabo fly ash

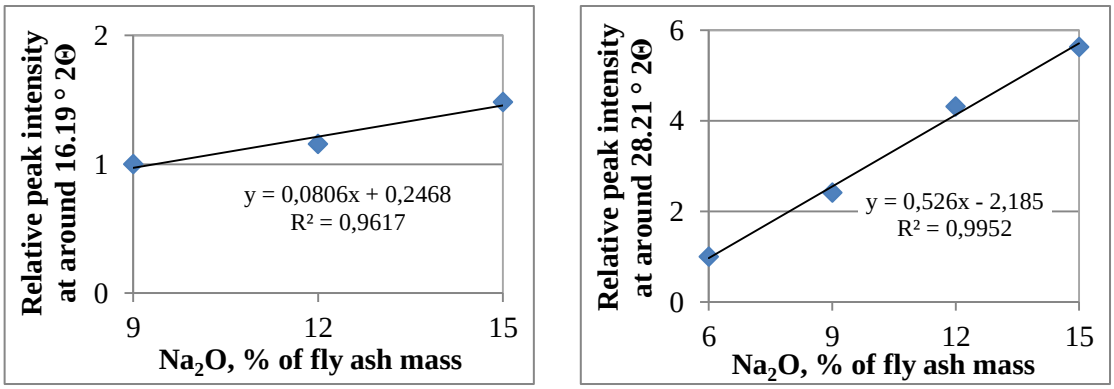

Figure 4.17: Relative intensities of hydroxysodalite peaks at different sodium oxide contents in AAFA cement pastes containing classified Lethabo fly ash

The presence of small but distinct double peaks at 37.69º 2Θ, 37.92º 2Θ and a peak at 44.29º 2Θ in Na12 and Na15 samples is attributed to the presence of thermonatrite (hydrated sodium carbonate), suggesting excessive sodium hydroxide in those samples which react with carbon dioxide in the air.

It is known that fly ash usually contains amorphous phase, which does not contribute to diffraction peaks but appears in the diffraction pattern as a halo around 20-35° 2Θ and can be seen in Figure 4.14 and 4.15. A known weight of Aldrich 99 % pure silicon was added to the sample prior to phase analysis for determination and quantification of amorphous content. Quantitative analysis of alkali-activated pastes presented in Table 4.3 shows that the quantity of amorphous phase slightly increased with increasing of sodium oxide content.

Table 4.3 Quantitative XRD analysis of AAFA pastes amorphous phase, weight %

	Na3	Na6	Na9	Na12	Na15
AAFA cement paste containing unclassified Lethabo fly ash	65.08	64.72	66.70	66.70	70.25
AAFA cement paste containing classified Lethabo fly ash	66.42	67.57	68.03	70.37	70.24

4.4.3 ATR-FTIR characterization

4.4.3.1 Effect of sodium oxide content and age

Fourier transform infrared (FTIR) spectra of hardened samples at different ages with different sodium oxide contents were analysed and the results are shown in Figure 4.18, 4.19 and 4.20.

At frequencies higher than 1800 cm^{-1}, no significant difference in spectra between samples was observed. The spectra only display the bands of water adsorbed by the solid samples, at around 3700 cm^{-1}. A few bands at ~ 2360 cm^{-1} have been assigned to carbon dioxide trapped in cavities of solid samples (Farmer, 1974). Thus only the IR spectra from 1800 cm^{-1} to 600 cm^{-1} are illustrated in this section.

Bands at 1600-1700 cm^{-1} can be assigned to bending vibrations of H-O-H in water molecules (Bakharev, 2005a). The band at about 1440-1460 cm^{-1} is related to the formation of carbonate by reaction of alkali metal hydroxide with atmospheric CO_2 (Farmer, 1974). The high intensity of the carbonate peak in Na12 and Na15 samples indicate excessive amount of alkali which was not consumed during geopolymerization and reacted with carbon dioxide in the air with the formation of efflorescence on sample surfaces. The presence of alkali carbonate is confirmed by XRD results.

The strongest band in the initial fly ash is centred at ~1055 cm^{-1} and can be attributed to T-O-Si (where T= Si or Al) asymmetric stretching vibration of TO_4 tetrahedral molecules and typical for silicate and aluminosilicate glasses and minerals (Lee and van Deventer, 2002; Zhang et al., 2013). The frequency of this band depends on the state of hydration, non-bridging oxygen (NBO) concentration and Al content (Zhang et al., 2013).

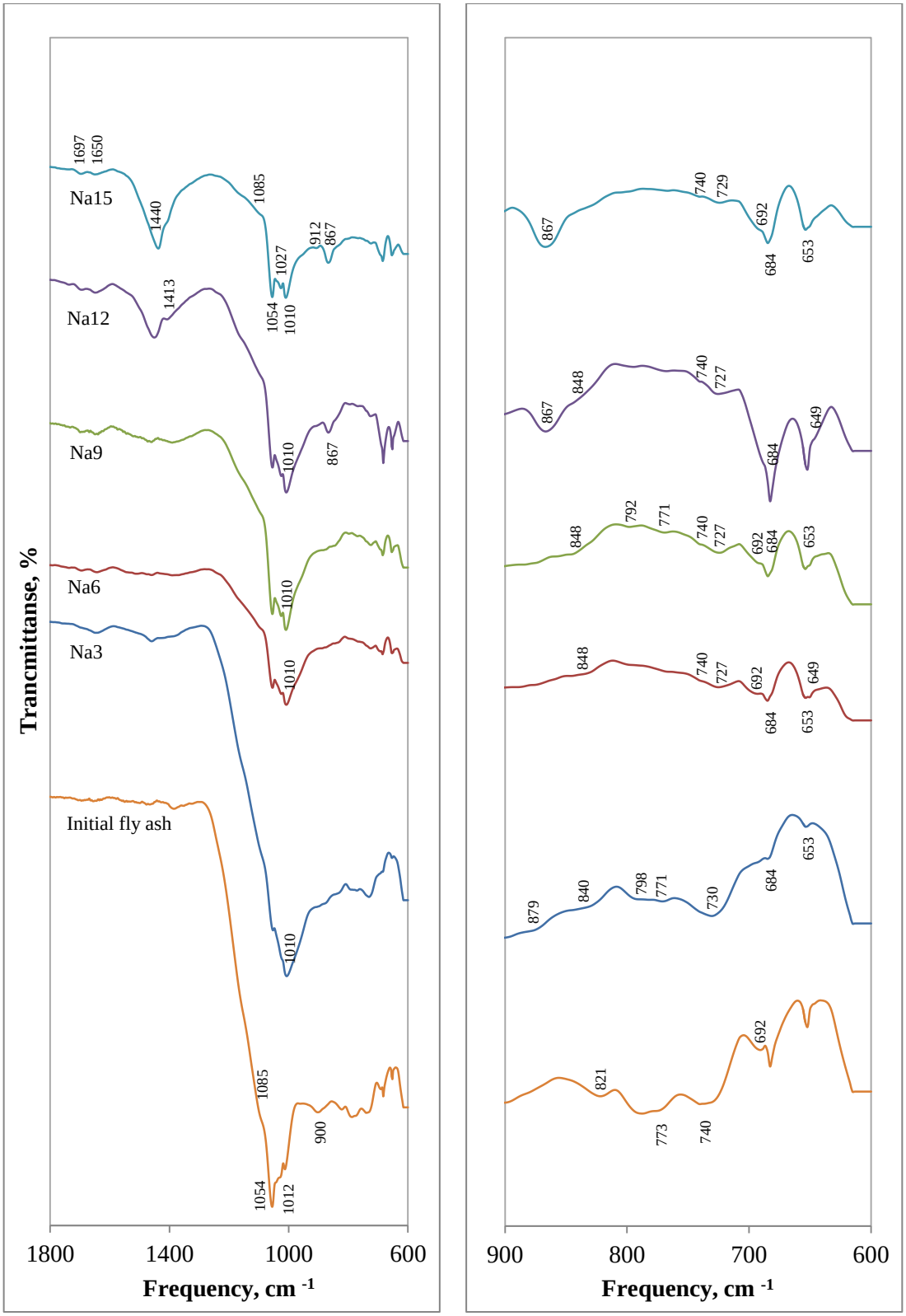

Figure 4.18: ATR-FTIR spectra of AAFA pastes with different sodium oxide content at 1 day (after heat curing)

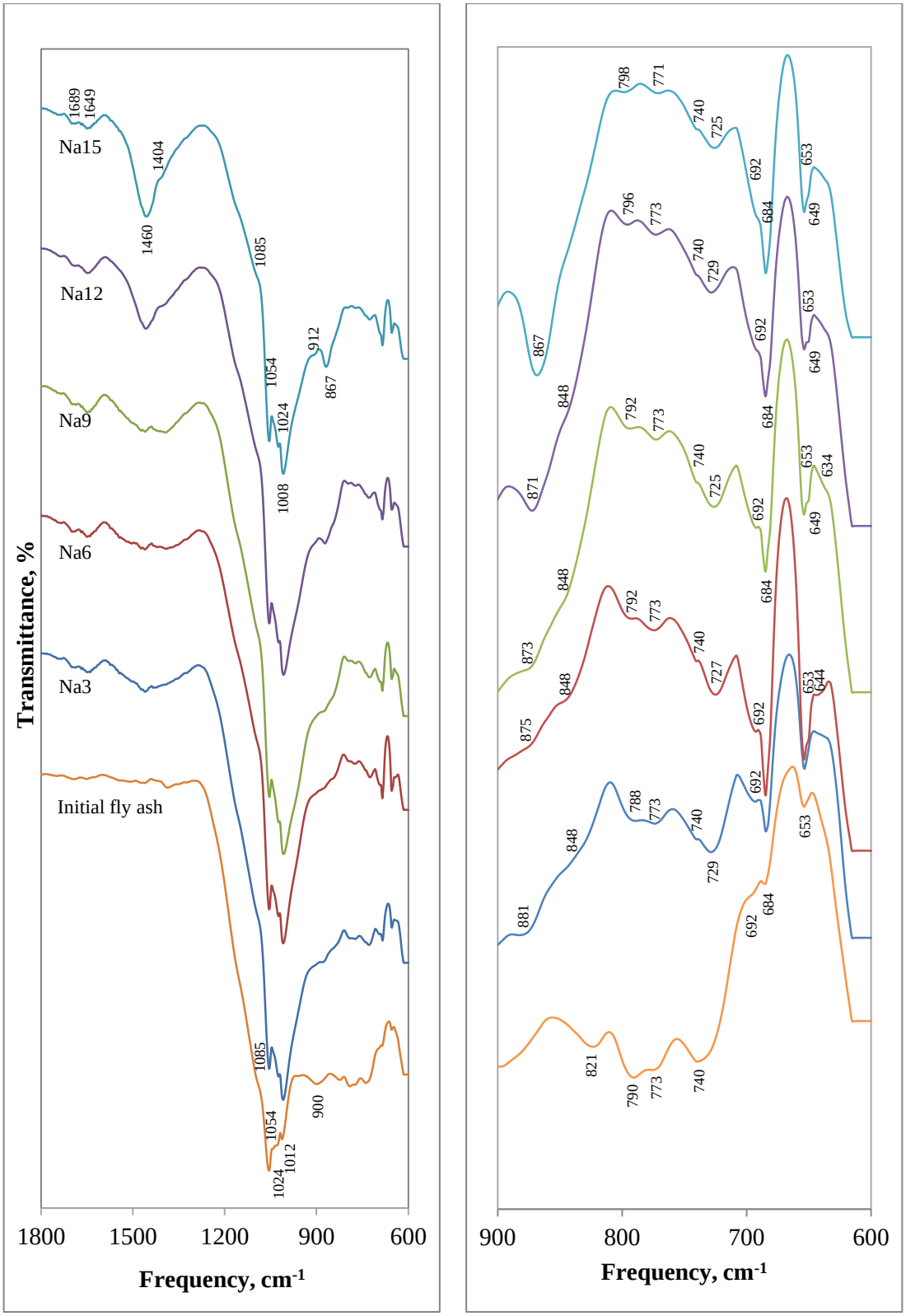

Figure 4.19: ATR-FTIR spectra of AAFA pastes with different sodium oxide content at 28 days

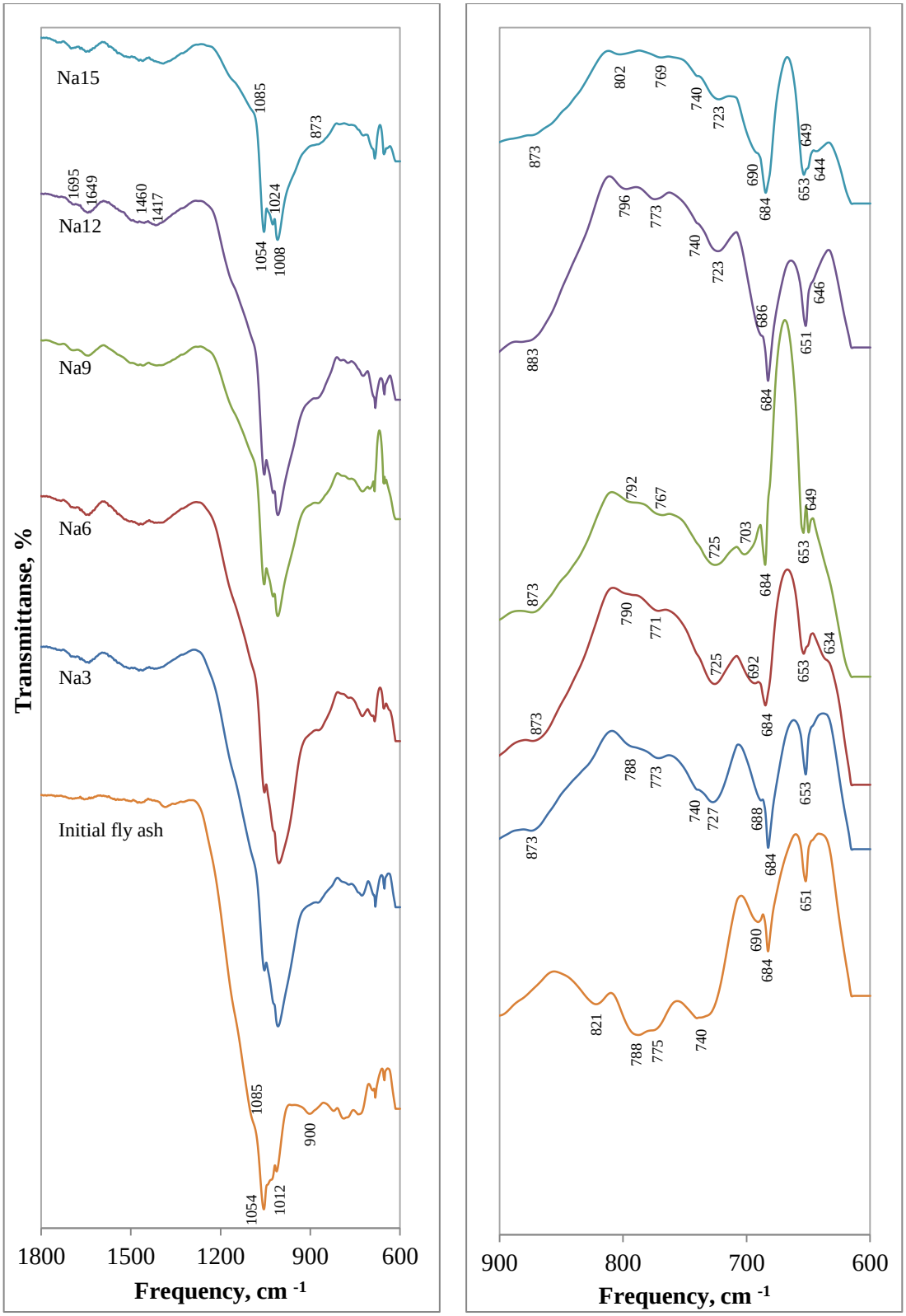

Figure 4.20: ATR-FTIR spectra of AAFA pastes with different sodium oxide content at one year

The strongest band in alkali-activated pastes was observed at lower frequencies (1010-1008 cm^{-1}) compared to spectra of fly ash. Such a big shift (45-47 cm^{-1}) suggests that the reorganization of TO_4 species and formation of new product with different microstructure compare to initial fly ash has taken place. This shift can be attributed to the partial replacement of SiO_4 specie by AlO_4, resulting in a change in the local chemical environment of Si-O bonds (Davidovits, 2008) and is an indicator of geopolymer formation.

A broad hump at 900 cm^{-1} and at 821 cm^{-1} in the initial fly ash vanished as a result of alkali activation and it is not found in AAFA pastes. However a new small shoulder appeared at ~868 cm^{-1} for Na12 and Na15 after 1 day curing, for 28 days-samples at ~ 881 cm^{-1} (Na3), in Na6 at 875 cm^{-1} and Na9 at 873 cm^{-1}. For Na12 and Na15 a clear band appeared and there is a slight shift towards lower frequencies, 871 and 867 cm^{-1} respectively. For one year samples a shoulder around 873 cm^{-1} was observed in all AAFA paste samples, except Na12, where the shoulder appeared at 883cm^{-1}, however such a low intensity of this band may relate to an inhomogeneous distribution of mineral matter in the sample. This band was not revealed in the initial fly ash and its intensity seems to be sensitive to sodium oxide concentration. Andini et al. (2008) linked this band to Al-O symmetric stretching vibrations in tetrahedral and attributed this peak to geopolymer formation, while Gervais et al. (1987) and Rahier (1997) linked this peak to the presence of non-bridging oxygen. Uchino et al. (1989) suggested that the band around 870 cm^{-1} is due to an overlap of Si-OH bending vibrations and a Si-O stretching vibration of Si-OH which can be caused by some bond breakage sites in the network structure of geopolymeric cement products. Despite the conclusions made by other researchers the band at around 868 cm^{-1} was assigned in this thesis to out-of-plane bending vibration in carbonates as the intensity of this band seems to be in strong correlation with the intensity of the band at around 1440-1460 cm^{-1} which is undoubtedly caused by carbonate species. A detailed study of published IR spectra of different carbonate minerals (Farmer, 1974) shows that band at ~868 cm^{-1} can be assigned to sodium carbonate hydrate (thermonatrite) which was also found on the XRD pattern of AAFA cement pastes. Alonso and Palomo (2001b) also assigned bands between 865 and 875 cm^{-1} to the presence of carbonates.

There is a very small but clear peak at 912 cm^{-1} in the Na15 sample and a shoulder in Na12 after 1 day curing at elevated temperature. A noticeable shoulder can be observed in Na15 after 28 days of curing. Zhang et al. (2012a) assigned this band to stretching of Si-O^- (M, Me, Fe) where M is an alkali metal or Me is alkali-earth metal, or Si-OH. Lancellotti et al. (2013) assigned this band to stretching vibrations of Al(VI)-OH. The authors also noticed that the presence of Al(VI) could be related to less geopolymerization. Thus, the presence of a band at

around 912 cm^{-1} in elevated cured samples could be an indicator of less polymerized or depolymerized structure and lower compressive strength as a result. This conclusion is in good correlation with the compressive strength of AAFA cement pastes results presented earlier in this chapter.

Comparison of the vibrational spectra of crystalline quartz (Ghosh, 1978; Saikia et al., 2008) with that of initial fly ash made it possible to detect a shoulder around 1085 $cm^{-1}$and a very weak double band at 790-775 cm^{-1} assigned to quartz. A shoulder at 692 cm^{-1} in the initial fly ash and AAFA paste can also be attributed to quartz (Ghosh, 1978; Zhang et al., 2012a). The presence of quartz has been confirmed by XRD results.

The peak at 740 cm^{-1} present in the initial fly ash was observed in AAFA as a shoulder is due to the stretching motion of elongated AlO_6 octahedra (Schroeder and Lyons, 1966) and can be attributed to mullite (Zhang et al., 2012a). The other bands of mullite were not detectible by FTIR probably due to the overlapping of bands by Si-O stretching vibration in quartz or secondary aluminosilicate gel (Fernandez-Jimenez and Palomo, 2005b). A new broad peak at 725-729 cm^{-1} is observed in AAFA cement pastes. These external bands are associated with the presence of rings with a variable number of units, which may in turn bond to form three-dimensional structures (Fernandez-Jimenez and Palomo, 2005b). Increases in the number of members of a ring cause the bands to shift towards lower frequencies. Specifically, the band appearing at around 720-730 cm^{-1}, according to aluminosilicate theory may be associated with the T–O bonds in the interconnected tetrahedral that form single four rings (S4R) or double four ring (D4R) units. Criado et al. (2007b), Fernandez-Jimenez and Palomo (2005b) said the band appearing between 730-720 cm^{-1} might be associated with Al-rich structures having a Si/Al ratio close to one, such as hydroxysodalite. The presence of hydroxysodalite was confirmed by XRD analysis in this study.

Peaks at 684 and 653 cm^{-1} observed in the initial fly ash as well as in all AAFA cement pastes suggest that the phase assigned to those peaks was not altered during alkali activation. A new shoulder at 649 cm^{-1} that was not present in the initial fly ash was observed in all age samples, starting from Na6. Fernandez-Jimenez et al. (2005b) associated this band with single six rings or double six ring units. However, no other phases except hydroxysodalite were found in alkali-activated pastes using XRD. Ilia et al. (2009) assigned this band to vibrations in Si-O-Al^{IV} (Al in octahedral coordination).

4.4.3.2 Effect of temperature

Infrared spectra of AAFA cement pastes at the age of one year cured at different temperatures is shown in Figure 4.21. There is a noticeable difference in intensity of peaks at around

1460 cm^{-1} which is assigned to carbonate species. This peak is higher for samples cured at 25 °C and 40 °C compared to 60 °C. Actually, samples with 9 % sodium oxide cured at 25 and 40 °C had white efflorescence on the surface a few days after curing in oven, suggesting that not all alkali was consumed by the geopolymerization process. A new peak was observed at around 849 cm^{-1} in the sample cured at 25 °C. Bakharev (2005c) assigned this band to T-OH stretching modes, where T is Si or Al. Zhang et al. (2009) admitted that the existence of Si-OH may be a result of decreased degree of condensation, thus a reduction in mechanical strength. The compressive strength obtained in this research for samples cured at 25 °C was lower than that of other samples cured at elevated temperatures, which is in good correlation with the assumption of Zhang et al. (2009).

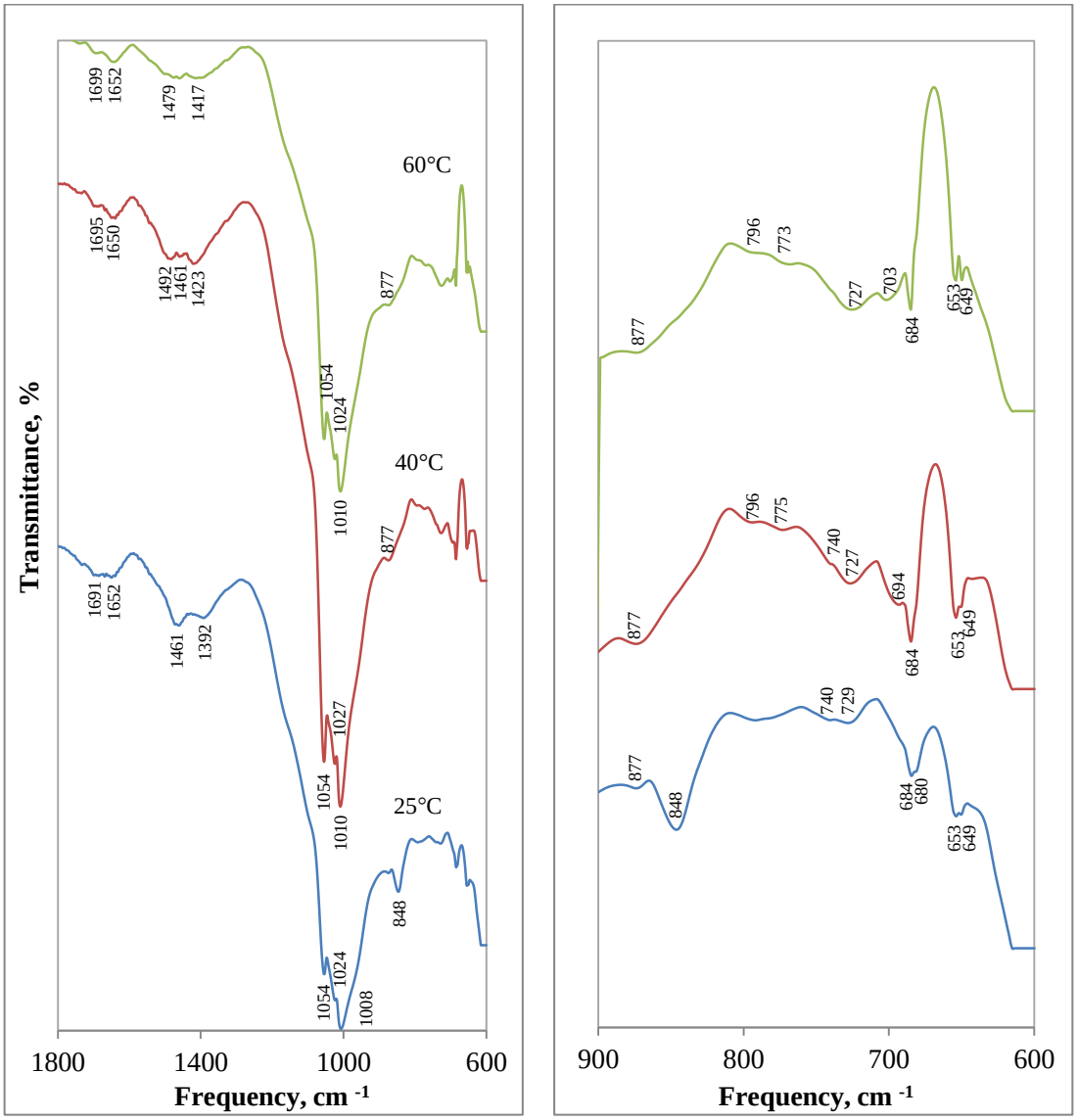

Figure 4.21: ATR-FTIR spectra of AAFA paste with 9 % sodium oxide cured at different temperatures at the age of one year

4.4.3.3 Effect of different activators

Figure 4.22 shows the effect of soluble silica on the ATR-FTIR spectra of pastes. It seems that soluble silica does not have a noticeable effect on the overall structure of pastes compared to samples where only sodium hydroxide as activator was used, as no new bands were observed.

Figure 4.23 shows the effect of different concentrations of potassium oxide on the FTIR spectra of pastes at the age of one year. The intensity of peaks at 1633, 1400, 831 and 700 cm^{-1} seems to be related to potassium oxide concentration. Those peaks are clearly defined and have strong intensity in the K11 sample. Farmer (1974), Miller and Wilkins (1952) assigned the peaks to the presence of potassium bicarbonate, which can be formed when excessive amounts of alkali, not consumed during the polymerization process, reacts with the carbon dioxide in the air.

The presence of a peak in potassium hydroxide activated cement pastes at around 900 cm^{-1}, found in the initial fly ash, suggest that the phase assigned to this band is not noticeably affected by medium concentrations of potassium hydroxide activator compared to sodium hydroxide, which vanished the peak already at a concentration of 3 %. Zhang et al. (2012a) assigned a band between 915 and 900 cm^{-1} to stretching vibrations of $Si\text{-}O^{-}$. These bands are usually found in fly ashes with a high reactivity. This means that the potassium hydroxide solution is less effective in dissolution of fly ash compare to the sodium hydroxide solution. However, the intensity of the band at 900 cm^{-1} is lower compare to its intensity in the initial fly ash suggesting some alteration has taken place.

The presence of a peak at 868 cm^{-1}, which was assigned to sodium carbonates in samples activated by sodium hydroxide solution, is possible in samples activated by potassium hydroxide solutions as sodium hydroxide was present in potassium hydroxide flakes as impurity (amount of 0.5 %). The intensity of this peak in K8 and K11 samples is very low compared to samples Na12 and Na15, which indicate insignificant amounts of sodium carbonates.

Other distinct differences were observed at frequencies of 735-733 cm^{-1}. A broad band was observed at these frequencies in the initial fly ash, while for sodium hydroxide activated samples of the same age this band is shifted towards lower frequencies, 727-723 cm^{-1}, suggesting the formation of Al-rich structures. Appearance of the band at the same frequencies as in the initial fly ash indicates that this phase was not affected much by the potassium hydroxide solution.

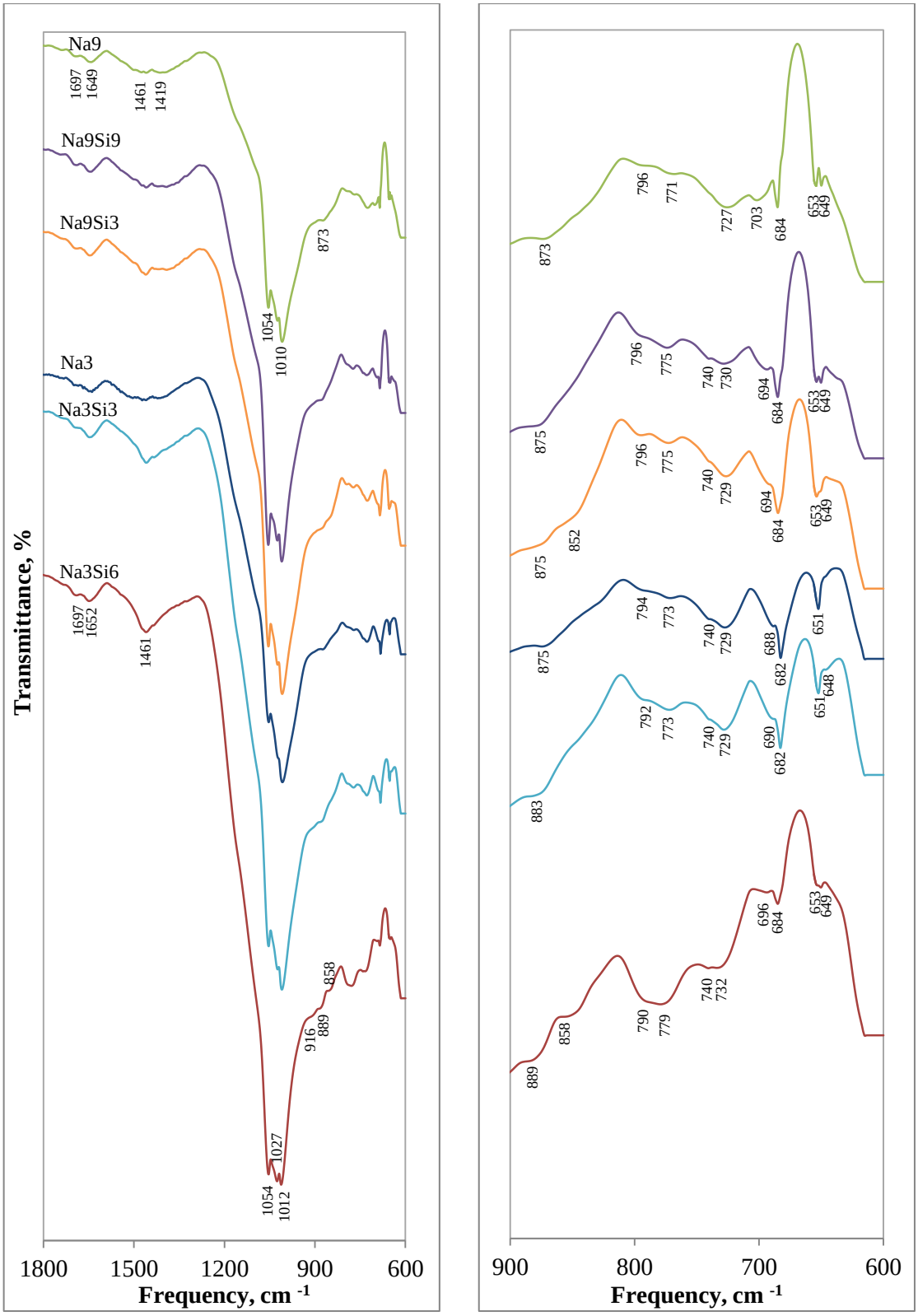

Figure 4.22: ATR-FTIR spectra of AAFA pastes contained different levels of soluble silica at the age of one year

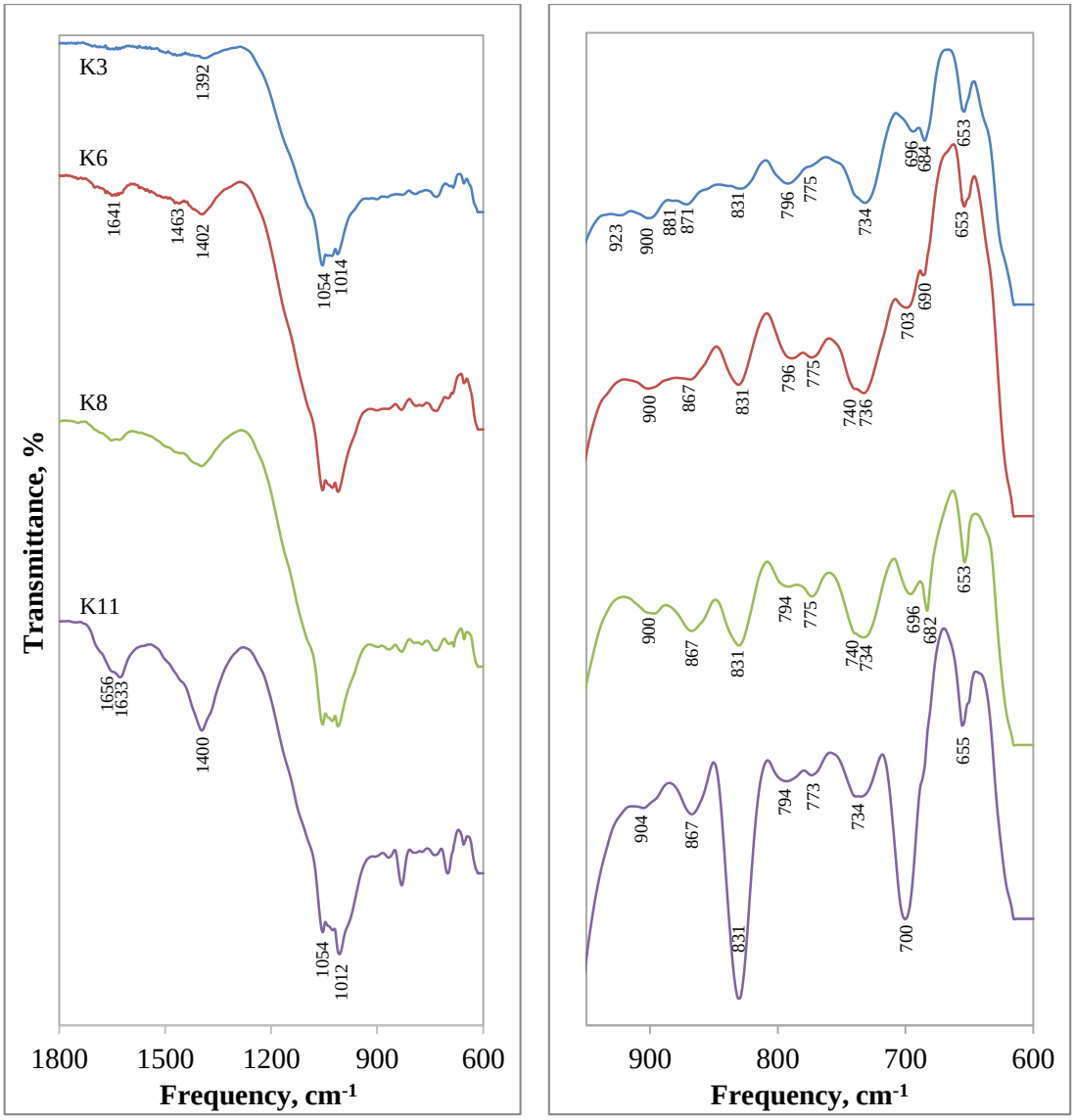

Figure 4.23: ATR-FTIR spectra of AAFA pastes activated by different concentrations of potassium hydroxide at the age of one year

In general the results of ATR-FTIR are in agreement with the results of XRD. There is a definite transformation of the glassy phase of the initial fly ash during alkali activation. The presence of alkali carbonates in mixtures with high alkali content confirmed by both, XRD and ATR-FTIR techniques, suggesting that not all alkali was consumed during the activation process but it is unlikely that their presence would affect the compressive strength significantly. The presence of Al-rich structures is confirmed by ATR-FTIR, while XRD showed the prominent peak of hydroxysodalite. However the presence of hydroxysodalite would not explain the strength drop as hydroxysodalite is observed not only in Na15 but in Na9 and Na12 as well, with a negligible difference in its amount. Thus in the next section microstructural characterization of AAFA pastes with different concentrations of sodium oxide will be presented.

4.4.4 SEM observation

Scanning electron microscopy observations were performed on samples of AAFA cement pastes containing unclassified Lethabo fly ash with different sodium oxide levels. The aim was to see if there is any difference in structure of these mixtures which can possibly explain observed trends in the strength development. SEM images of AAFA cement pastes with different Na_2O contents at the age of 40 days are presented in Figure 4.24 – 4.28.

Figures 4.24 – 4.26 show the microstructure of AAFA cement paste with 3, 6 and 9 % Na_2O. The surface of individual particles on these pictures is covered by shell shaped reaction products (point 1, Figures 4.24 and 4.25) with smooth fly ash particles under it. It was found in previous research that the reaction product of the alkaline solution and fly ash is disordered aluminosilicates gel, also known as geopolymeric gel (Palomo et al., 1999a; Duxson et al., 2007b). It can be seen that fly ash particles are glued to each other by reaction products. Voids can be observed between fly ash particles indicating that not enough gel phase was formed to fill it, resulted in friable appearance of the microstructure. The amount of unreacted fly ash particles (point 2, Figures 2.26-2.28) decreased with increased concentration of sodium oxide, and the matrix appears more continuous, which is evidence of increased gel formation (see Figure 4.27 and 4.28). As it is assumed that the amount of aluminosilicates gel is responsible for the mechanical properties of the final product (Zhang et al., 2013), it is expected that the more continuous appearance of the matrix is related to the greater amount of gel resulting in the higher compressive strength. This is in good correlation with the compressive strength results with the exception of sample Na15. The matrix of sample Na15 appears continuous and the structure looks more solid, but the compressive strength tends to be less than that of Na9 and Na12.

Small cracks can be observed in these images (see point 3, Figure 4.27 and 4.28). The nature of these cracks is not yet clear. De Vargas et al. (2011) discovered similar cracks in AAFA based geopolymers. They reported that microfissures could be found easier in the samples with higher amounts of alkali (Na_2O/SiO_2=0.4 compared to Na_2O/SiO_2=0.2) but they did not observe a reduction in compressive strength. At the same time Fernandez-Jimenez and Palomo (2005a) linked cracks with thermal treatment during the activation process or mechanical damage during sample preparation for SEM observation. However all the samples presented in the micrographs in this study had the same regime of heat treatment and were prepared in the same way, but cracks were only observed in samples Na12 and Na15, where a more continuous matrix is present.

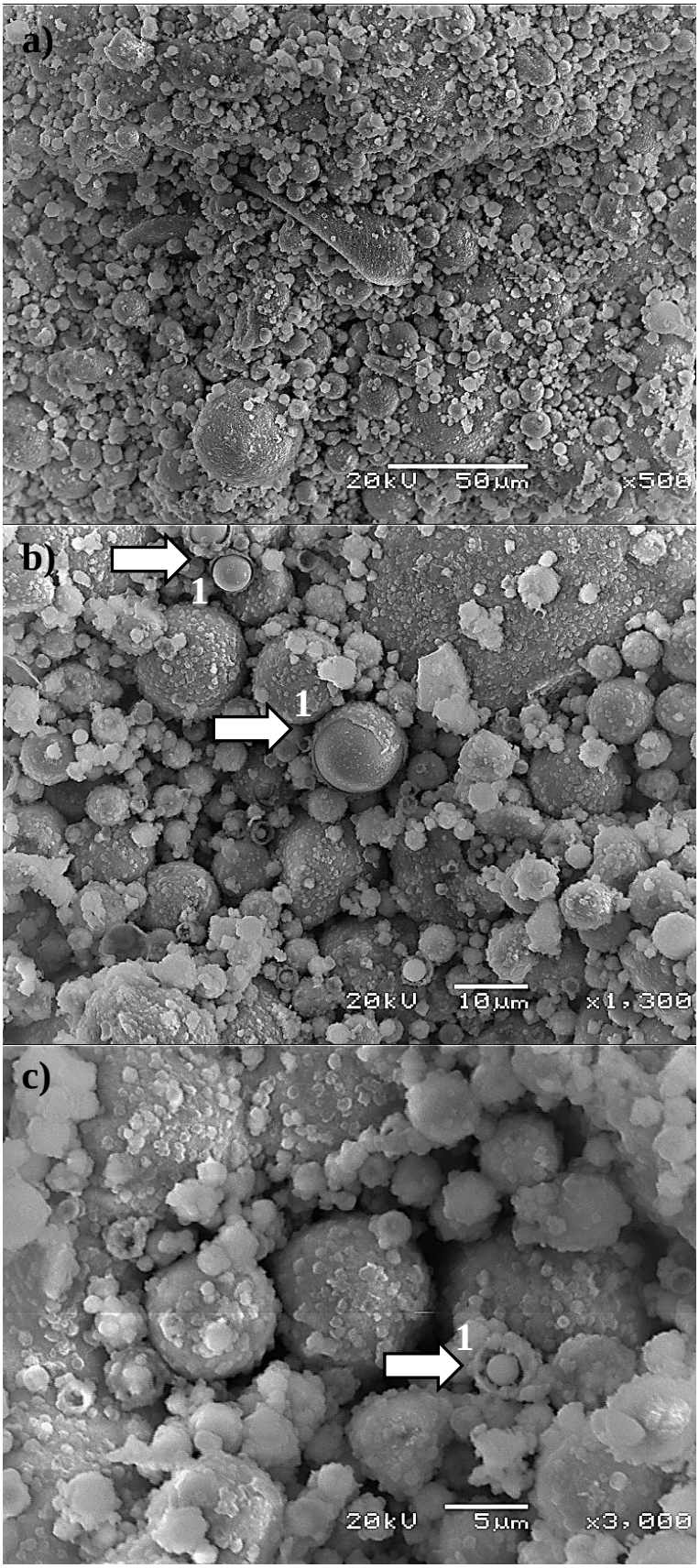

Figure 4.24: Microstructure of unclassified Lethabo AAFA cement paste with 3 % sodium oxide a) × 500; b) × 1300; c) × 3000

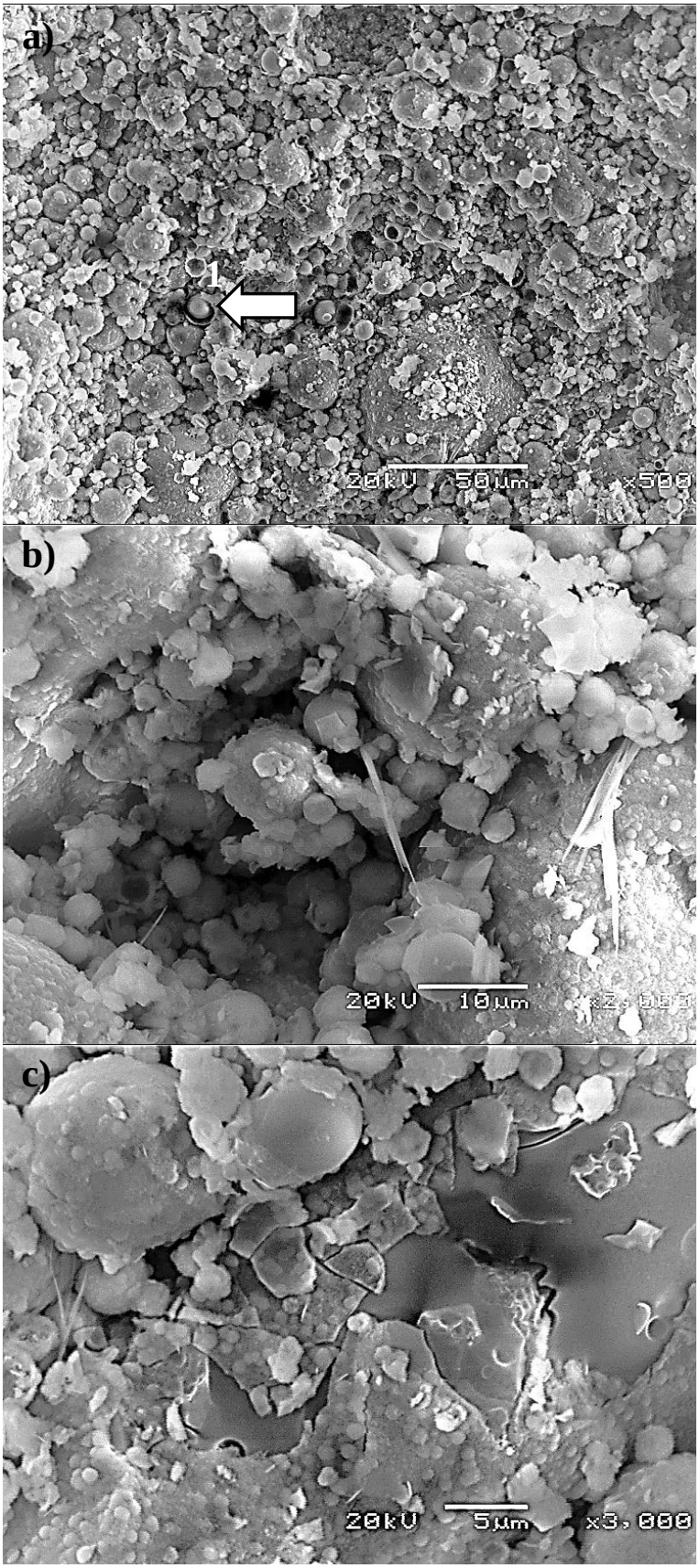

Figure 4.25: Microstructure of unclassified Lethabo AAFA cement paste with 6 % sodium oxide a) × 500; b) × 2000; c) × 3000

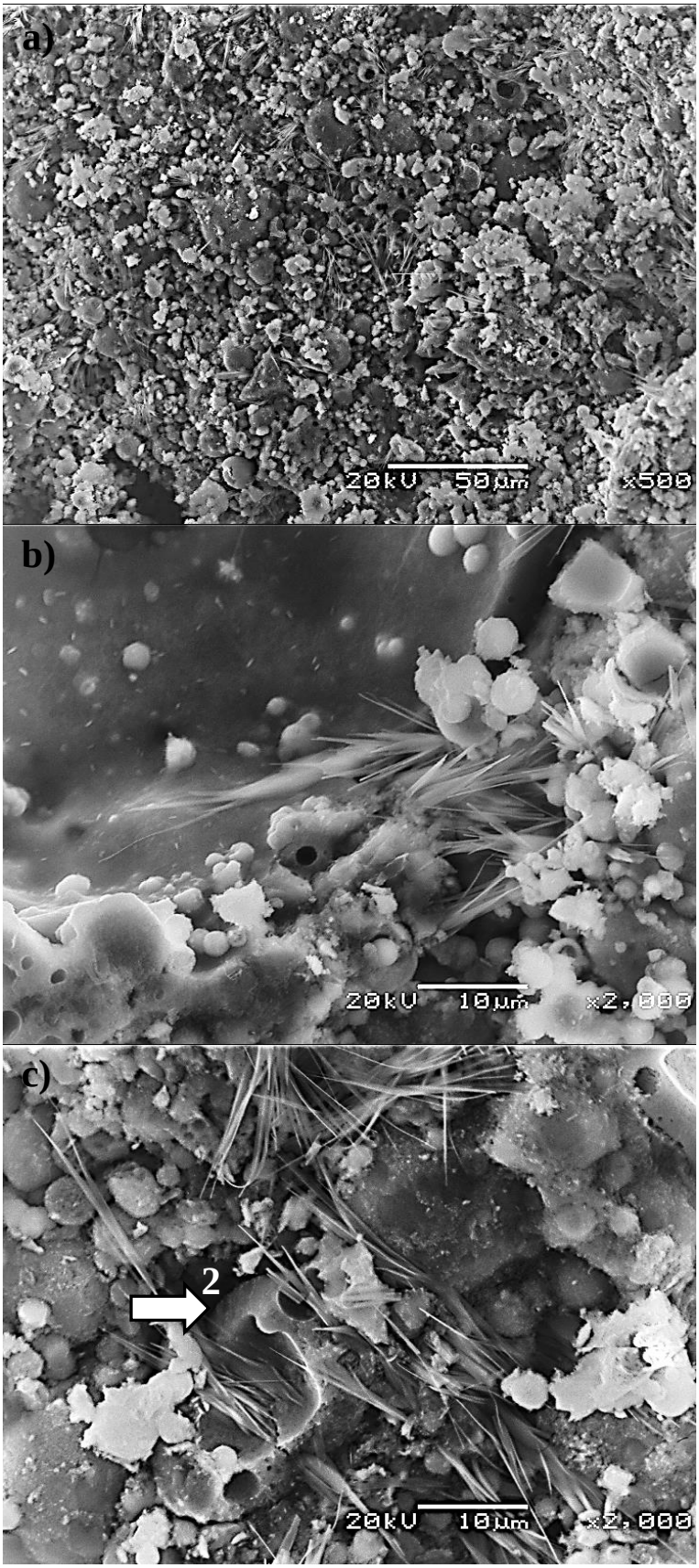

Figure 4.26: Microstructure of unclassified Lethabo AAFA cement paste with 9 % sodium oxide a) × 500; b) × 2000; c) × 2000

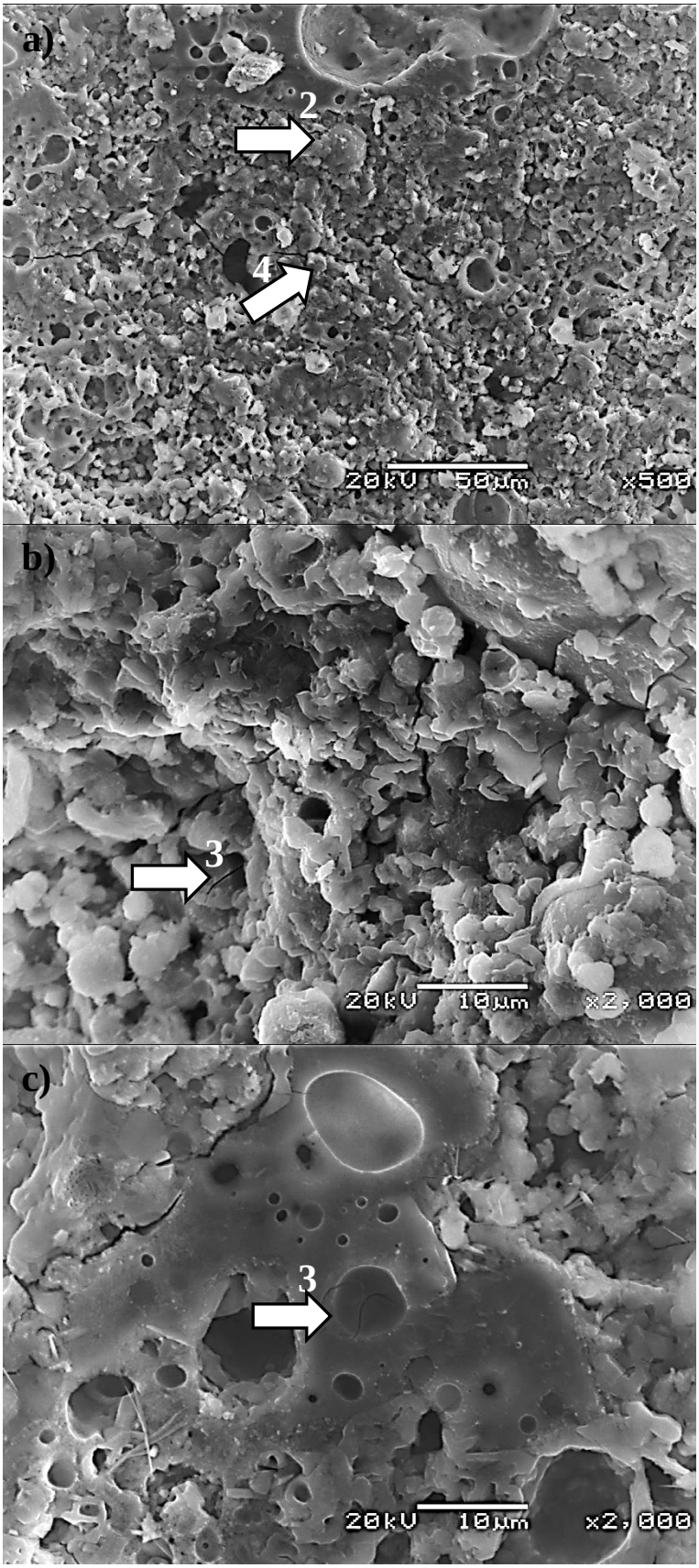

Figure 4.27: Microstructure of unclassified Lethabo AAFA cement paste with 12 % sodium oxide a) × 500; b) × 2000; c) × 2000

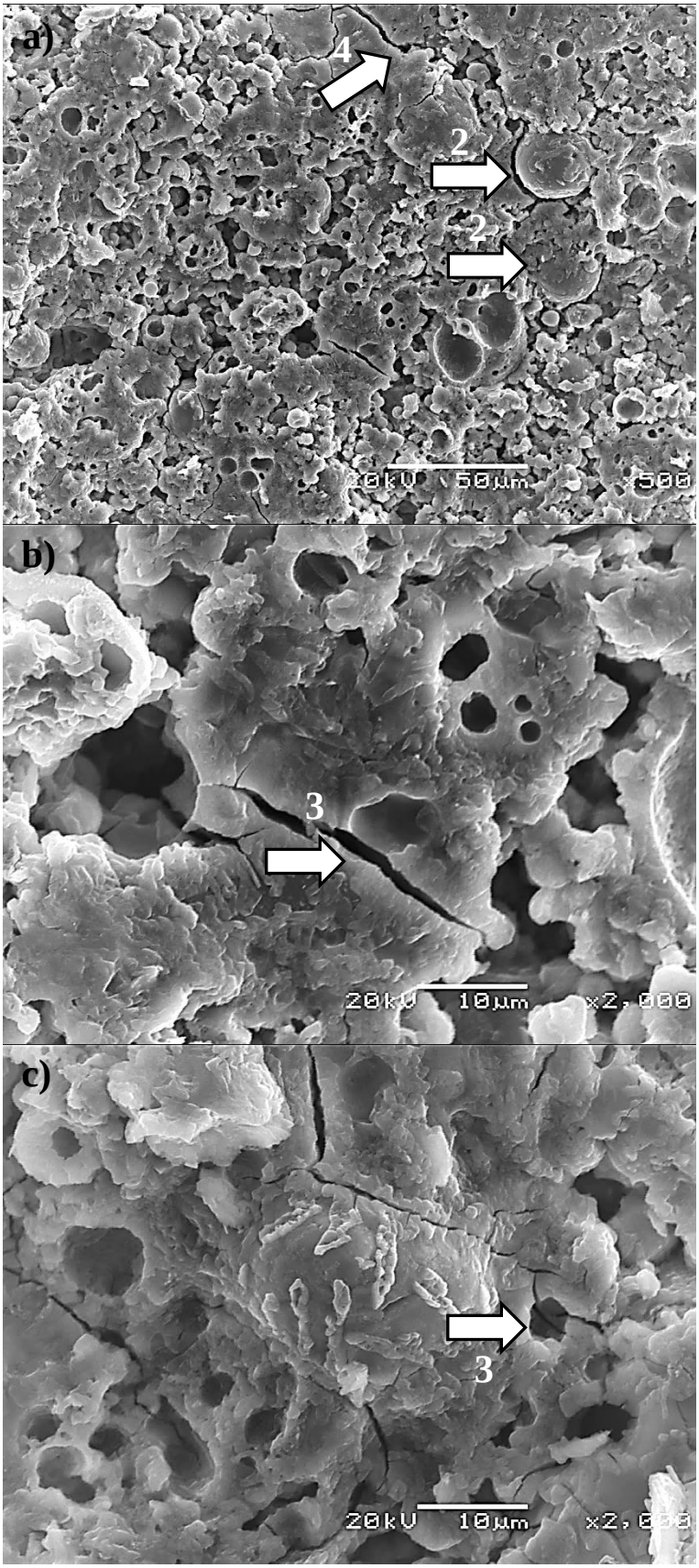

Figure 4.28: Microstructure of unclassified Lethabo AAFA cement paste with 15 % sodium oxide a) × 500; b) × 2000; c) × 2000

The appearance of microcracks differs from long, wider cracks which most probably result from sample preparation (point 4, Figures 4.24 and 4.28). Microcracks appear within the continuous matrix and do not go out beyond its bounds. It was assumed that these microcracks could be the cause of the strength drop and strength deviation at high Na_2O.

SEM observations AAFA cement pastes containing classified Lethabo fly ash were conducted on higher resolution scanning electron microscope at the age of 72 days. Figures 4.29 – 4.33 show the microstructure of classified Lethabo AAFA cement pastes with different concentrations of sodium oxide.

At close inspection the major product of alkali activation reaction (aluminosilicates gel) appeared to have a granular microstructure, which is clearly seen on higher resolution images (point 5, Figures 4.29 – 4.33). These grains consolidate and formed a visually more solid microstructure in samples with high alkali content. Again the denser microstructure contained some cracks, which can explain the strength drop at samples with higher alkali content, are observed. Ragged edges of these microcracks (point 3, Figure 4.32 and 4.33) suggest that cracks were formed when material was not completely hardened yet. In fact, a strength decrease was observed immediately after elevated temperature curing in some cases, thus it was assumed that processes in AAFA cement pastes during heat curing might be the reasons for compressive strength reduction in mixtures with high alkali content. Therefore, in-situ evaluation of temperature development in sample cores and volume changes during elevated temperature curing was conducted and the results are discussed in next sections.

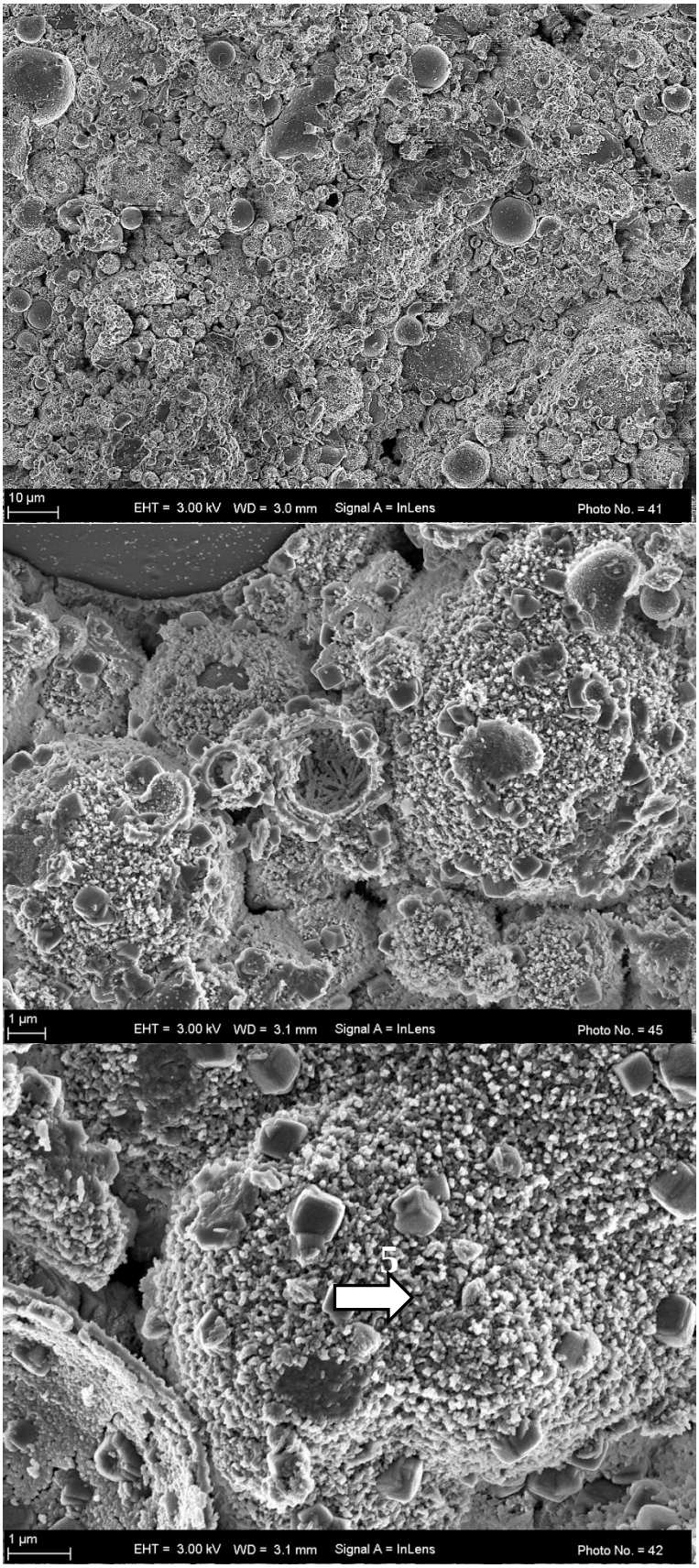

Figure 4.29: Microstructure of classified Lethabo AAFA cement paste with 3 % sodium oxide

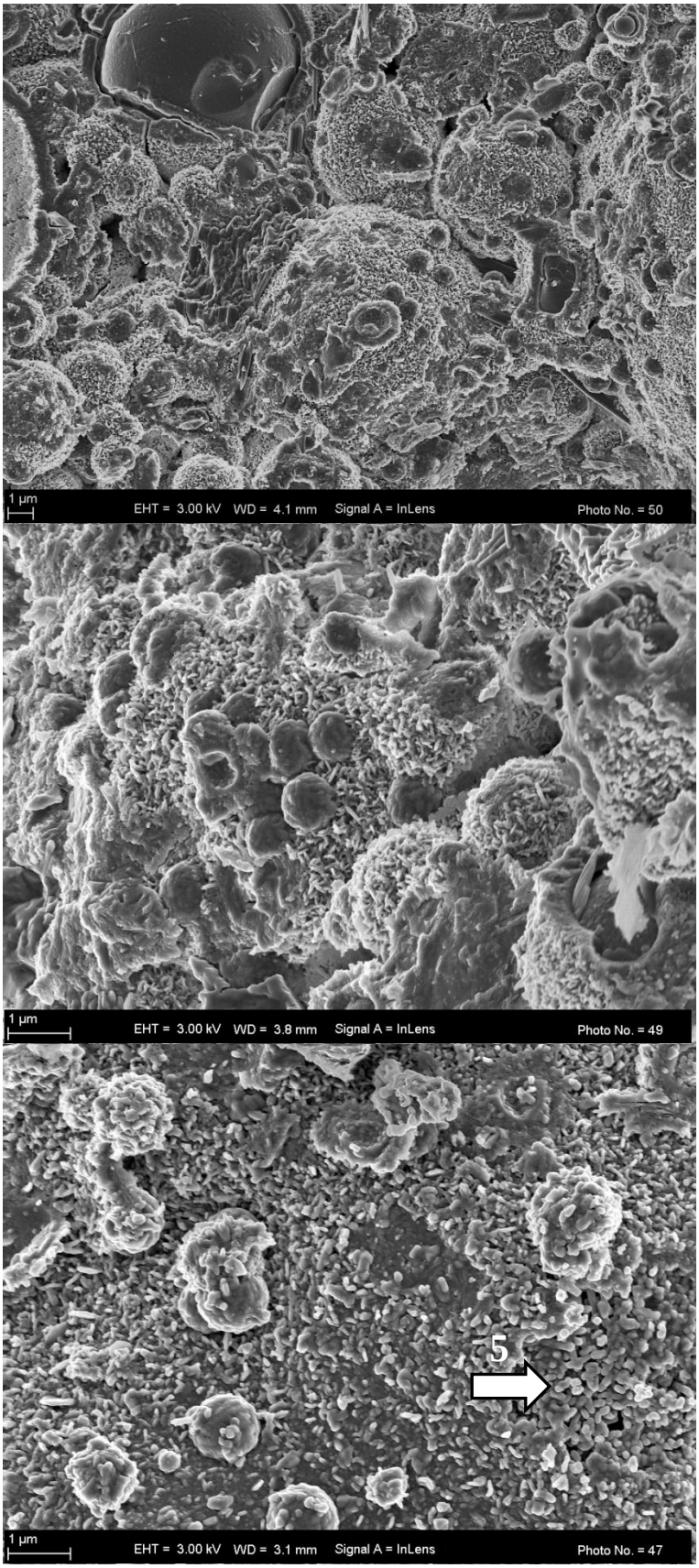

Figure 4.30: Microstructure of classified Lethabo AAFA cement paste with 6 % sodium oxide

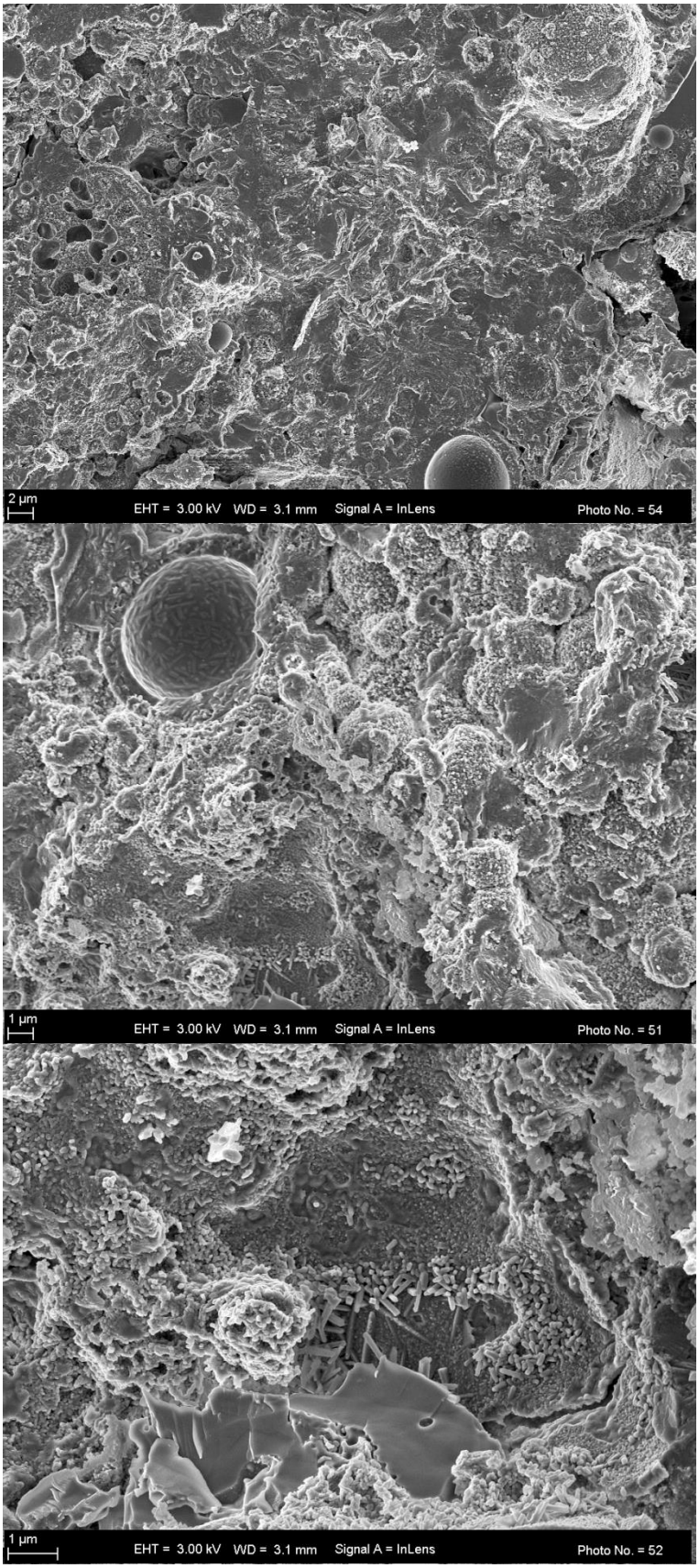

Figure 4.31: Microstructure of classified Lethabo AAFA cement paste with 9 % sodium oxide

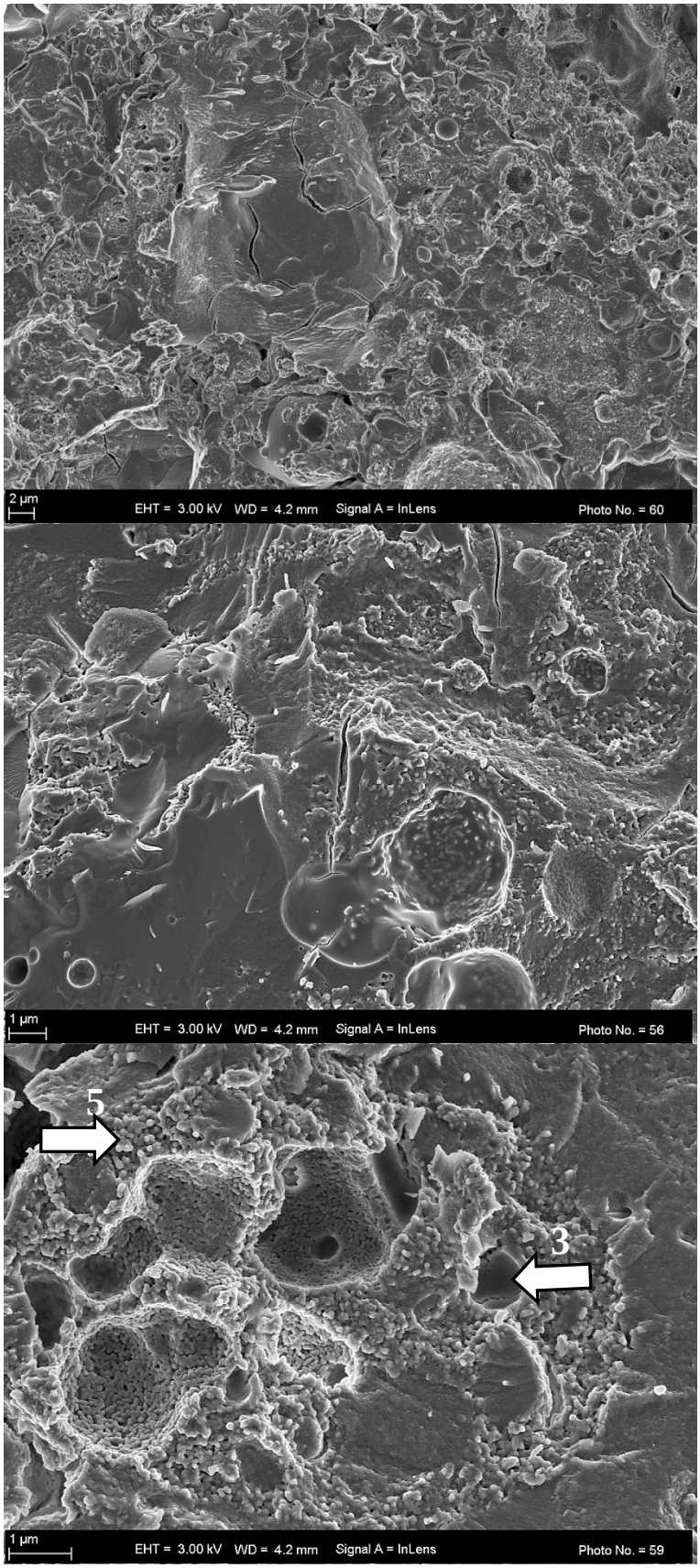

Figure 4.32: Microstructure of classified Lethabo AAFA cement paste with 12 % sodium oxide

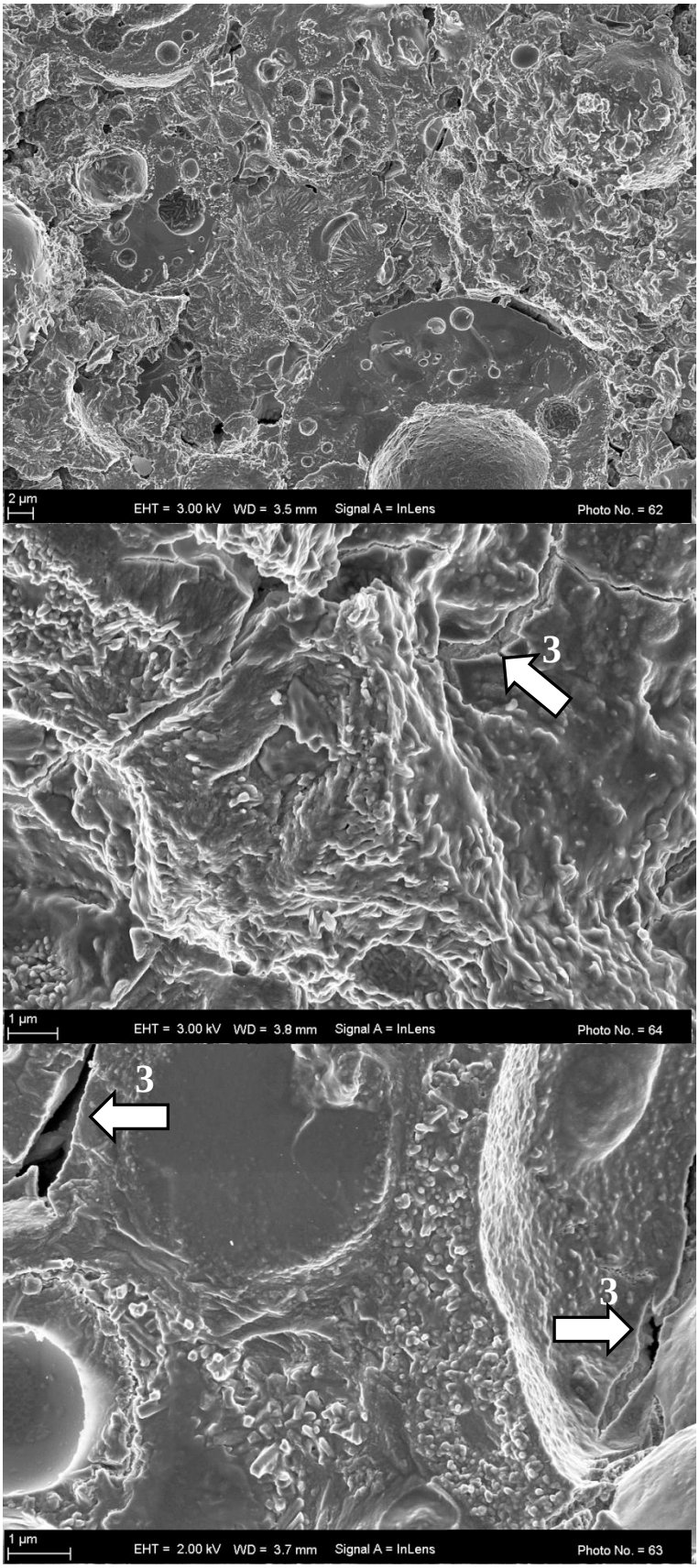

Figure 4.33: Microstructure of classified Lethabo AAFA cement paste with 15 % sodium oxide

4.5 TEMPERATURE DEVELOPMENT IN AAFA CEMENT PASTES DURING ELEVATED TEMPERATURE CURING

A few calorimetric studies have been performed in order to follow the reaction of alkali activation (Alonso and Palomo, 2001a; Krizan and Zivanovic, 2002; Brough and Atkinson, 2002; Deir, et al., 2014). In these studies, two main peaks were normally observed on the heat evolution graphs. The first peak corresponded to the dissolution of the aluminosilicate source in alkaline solutions; and the second peak indicated the formation of the reaction products (Alonso and Palomo, 2001b). Zhang et al (2014) reported that the heat release rate of metakaolin geopolymers increased monotonically with increasing NaOH concentration. An increase of alkali content resulted in a higher total heat release of AAFA (Ma et al., 2012). However, even if amount of heat, released during alkali activation, is known, it might dissipate into surrounding environment or increase the temperature of a sample during elevated temperature curing. Obviously, high rise of the sample's temperature can damage the microstructure of alkali-activated material, influencing compressive strength and other properties of the material. Temperatures widely used for alkali activation, are as high as 60 to 80 °C, which probably would not cause damage of the microstructure of AAFA. The cumulative heat from an oven and the alkali activation process might lead to substantial rise of sample's temperature, and affect the newly formed material microstructure. No studies were found on how the heat released during the alkali activation process, affects the temperature development inside of AAFA samples during elevated temperature curing. This work provides data on the temperature development of NaOH-activated fly ash pastes during elevated temperature curing at 60 °C. The test was conducted in two parts.

During the first part of the temperature development test AAFA pastes with different sodium oxide contents were cast into a plastic mould of three 40×40×160 mm prisms. For each mix, six moulds were cast with a total paste volume of 4.6 l (18 prisms). The pastes with different alkali content were cured separately. Moulds were placed into an oven at 60 °C immediately after casting. Grounded thermocouples were embedded into the cores of moulds during casting. Two thermocouples were measuring temperature in the oven. Temperature development in sample cores was recorded at one minute intervals for the 24 hours of elevated temperature curing. The temperature profile for each mixture was obtained as an average of four measurements and shown in Figure 4.34.

From Figure 4.34 it can be clearly seen that temperature inside of sample core increases with increasing sodium oxide content. Temperature inside the Na3 sample did not differ from the oven's temperature and was about 60 °C all the time. The maximum temperature in Na6 was

62.8 °C and the peak temperature was observed after 8.7 h in oven. The maximum temperature of 68.3 °C for Na9 was observed after 8.9 h. The peak temperatures of 71.3 and 68.2 °C were observed after 12.2 h and 15.0 h for Na12 and Na15 respectively. Temperature inside of the oven remained constant at 60 °C for all mixes.

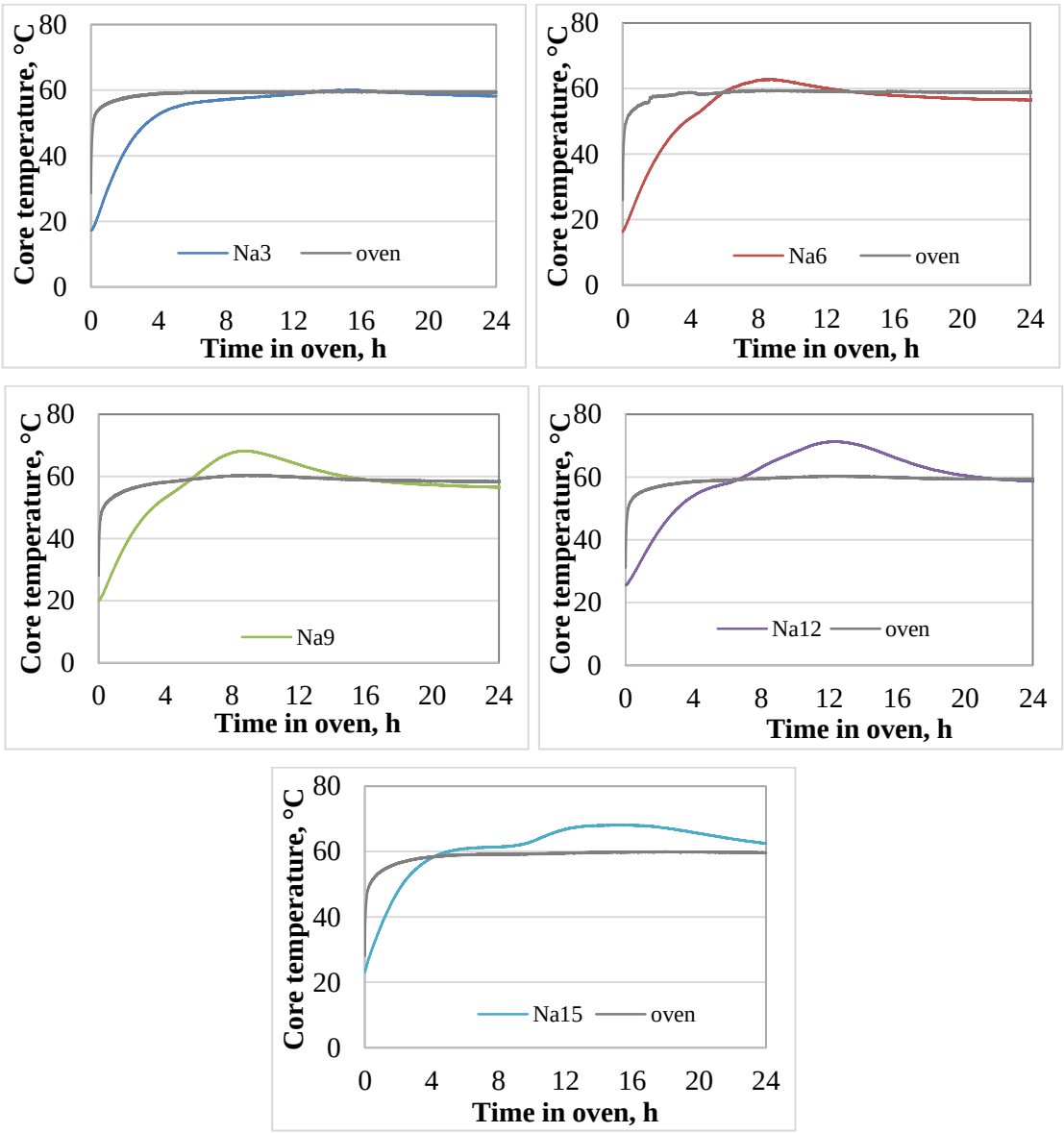

Figure 4.34: Temperature development in AAFA cement pastes with different sodium oxide content during elevated temperature curing (18 prisms)

The time of maximum temperature appearance also depends on sodium oxide content. The peak temperature of Na15 occurred the latest compared to other mixes. However, temperature in Na15 mixture is also the first to exceed the oven temperature, which suggests a high early heat release. Alonso and Palomo (2001a) reported a lower rate of polymer formation when activator concentration increases. It has been mentioned that high activator concentrations produced high pH in the liquid phase and anionic forms of silicate are more favoured,

delaying polymerization. It is interesting to note that the pastes with lower alkali content had narrower temperature humps. The hump is wider for Na12 and Na15, thus these pastes were exposed to temperatures higher that 60 °C for longer times, which might affected microstructure of AAFA cement pastes.

During the second part of the test, moulds of different sizes made out of metal and plastic were used. Three AAFA cement paste mixtures with 9, 12 and 15 % Na_2O were cast on different days. Temperature development of pastes with 3 and 6 % Na_2O was not investigated due to the results obtained during the first part of the test. Each of the three pastes was cast into a set of plastic and metal moulds (one of each): 100 mm and 150 mm cubes, 40×40×160 mm prisms. The total volume of each mix was 10.2 l. Grounded thermocouples were placed in the core of each mould. All six moulds were put into the oven at 60 °C and the temperature development in sample cores was recorded for the 24 hours of elevated temperature curing.

Results of temperature development of AAFA cement pastes with 9, 12 and 15 % of Na_2O are shown in Figures 4.35 – 4.37. Table 4.4 gives values for maximum temperature peak and time of its appearance after beginning of heat treatment.

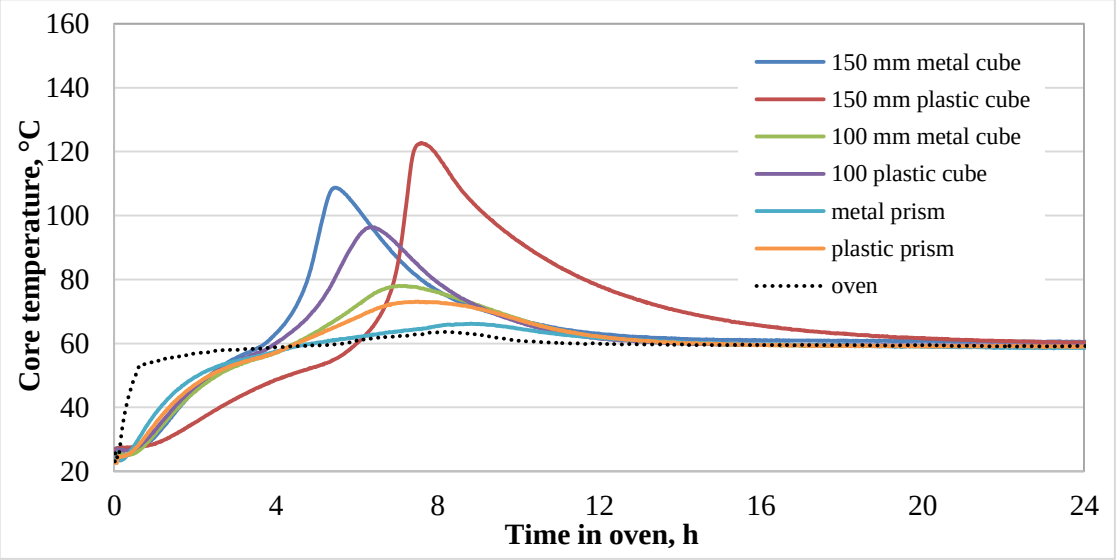

Figure 4.35: Influence of sample size and mould's material on the temperature profiles of AAFA cement paste with 9 % Na_2O during heat curing

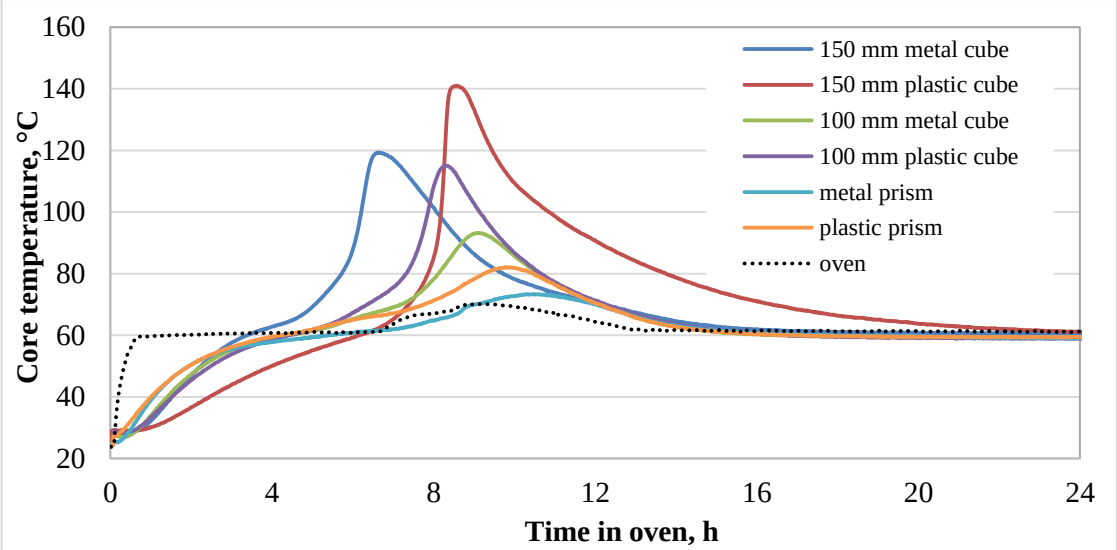

Figure 4.36: Influence of sample size and mould's material on the temperature profiles of AAFA cement paste with 12 % Na_2O during heat curing

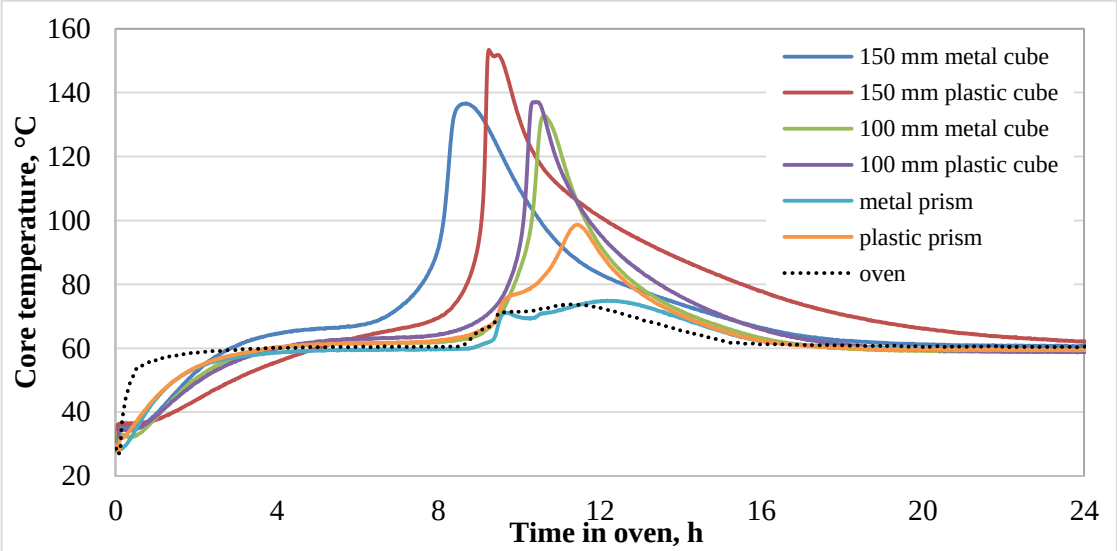

Figure 4.37: Influence of sample size and mould's material on the temperature profiles of AAFA cement paste with 15 % Na_2O during heat curing

Table 4.4: Values of maximum temperature peak and the time of its appearance

Thermocouple was embedded in:	Na9		Na12		Na15	
	Peak temperature, °C	Time of appearance of peak temperature, min	Peak temperature, °C	Time of appearance of peak temperature, min	Peak temperature, °C	Time of appearance of peak temperature, min
150 mm metal cube	108.7	327	119.3	397	136.7	521
150 mm plastic cube	122.7	455	141.0	515	153.4	555
100 mm metal cube	78.0	422	93.2	543	132.9	637
100 mm plastic cube	96.3	378	115.0	496	137.1	621
40×40×160 mm metal prism	66.2	528	73.4	620	74.9	731
40×40×160 mm plastic prism	73.1	447	82.1	587	98.7	686
oven	63.6	487	70.2	546	73.7	671

Several trends can be observed in the results. All trends were true for all alkali concentrations used in the study. The first trend is that the maximum temperature in the samples was higher when the pastes were cured in the plastic moulds in comparison to metal ones. The difference in the maximum temperature became more prominent with increase in the mould (sample) size. The trend can be explained by difference in thermal conductivity properties of the materials moulds were made of. Plastic moulds are less conductive, providing more insulation thus preserving the heat emitted during the alkali activation process more effectively than metal moulds. Hence, peak temperatures are higher in plastic moulds. This effect must be taken into account because the excessive heat can damage the paste microstructure or it can be effectively used for self-curing of AAFA cement concretes thus decreasing temperature/energy consumption during elevated temperature curing.

The second trend is the time of appearance of the peak temperature. For prisms and 100 mm cube moulds, the peak appears earlier in case of plastic moulds compared to metal moulds. The reverse can be seen in case of 150 mm cube moulds. The difference in the trend between different mould sizes is again governed by thermal conductivity of the materials moulds are made of. In case of prisms and 100 mm moulds, plastic preserves the heat emitted during the alkali activation process which accelerates the process, and the temperature inside of the samples reaches its maximum earlier in comparison to metal moulds. For 150 mm moulds, the reverse pattern can be seen. Before intensive alkali activation process takes place, a certain amount of energy must be transferred to activate the system. The amount of energy increases with increase in the sample size. At the initial stage, plastic moulds decrease energy flux transferred from the oven environment to the paste sample in comparison to metal moulds. This factor does not play a crucial role in the case of prisms and 100 mm cube moulds because the ratio of open area (top side of the moulds) to total volume is much higher in comparison to 150 mm moulds. Therefore, the trend is influenced by mould size and material. It is very important to note that the time of appearance of the peak temperature is affected by alkali concentration. The time of maximum temperature peak appearance, shown on Figure 4.38, increases with increase in alkali concentration from 9 to 15 % Na_2O, which is in good correlation with the results of Alonso and Palomo (2001a). This is true for all types of moulds regardless their size and material. Therefore, increased amount of alkali delays the alkali activation process, which is proven by the results of compressive strength obtained for samples cured in oven at the same condition for 4, 8 and 12 hours. Sample Na9 had compressive strength of 2.1 MPa after 4 hours of curing at 60 °C, while sample Na15 did not set yet by that time. The compressive strength of Na9 after 8 hours of curing was 15.2 MPa, while Na15 – 1.5 MPa. Rate of strength development can be an indirect indicator of reaction rate, it is eight times faster in Na9 than in Na15 (Strength development rate of

Na9=δR/δt=(15.2-2.1)/4=3.28 MPa/h; Na15=(1.5-0)/4 =0.38 MPa/h; relative strength development rate 3.28/0.38=8.6). With time the difference in reaction rate becomes less prominent as the compressive strength of Na9 after 12 hours in oven was 28.5 MPa, and for Na15 – 8.3 MPa. As the strength development rate of Na15 accelerates relative strength development of Na9 was only twice faster than Na15. (Strength development rate of Na9=(28.5-15.2)/4=3.33 MPa/h; Na15=(8.3-1.5)/4=1.7 MPa/h; relative strength development rate 3.33/1.7=1.95).

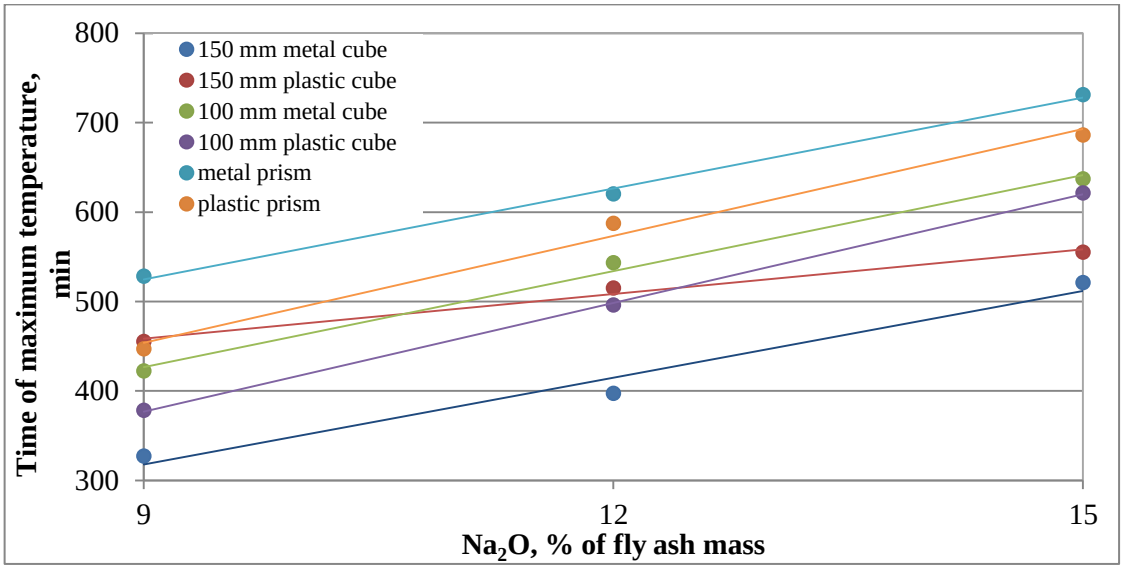

Figure 4.38: Relationship between time of appearance of maximum temperature and sodium oxide content for moulds of different sizes

The third trend indicates that the maximum core temperature inside the paste samples increases with increase in the sample size and alkali concentration. The lowest temperature corresponds to metal prism moulds and was 66.2 °C, 73.4 °C and 74.9 °C for Na9, Na12 and Na15 pastes respectively. In case of 150 mm plastic cube moulds, the temperatures for the Na9, Na12 and Na15 AAFA pastes reached 122.7 °C, 141.0 °C and 153.4 ºC respectively. These temperatures are the highest among all temperatures. The high temperatures cause internal stresses in the pastes due to thermal gradient and make all free water to boil. The boiling water produces vapour resulting in build-up of pressure inside the materials microstructure causing local microcracks and thus loss in the mechanical performance of the AAFA pastes. The alkali concentration higher than 9 % Na_2O significantly increases the amount of heat released during the alkali activation process which can be seen not only by the maximum temperatures reached in the paste samples but also by the temperature developed in the oven during elevated temperature curing. The ratio between paste and oven volume was higher than in the first part of the temperature development test and the oven was not equipped with a refrigerator resulting in the heat emitted by the AAFA pastes Na9, Na12 and Na15, increasing the oven temperature up to 63.7 °C, 69.3 °C and 72.7 °C respectively.

All pastes in this chapter (except of pastes from section 4.5) were prepared in plastic moulds and their volume was more than 9 l. According to the temperature profiles of Na9, Na12 and Na15 the peak temperatures for these pastes were about 73.1 °C, 82.1 °C and 98.7°C respectively. It is clearly seen that the temperature inside Na15 samples is very high. Pretoria, where all experiments were conducted, lies at high altitude and thus the boiling point temperature of water is about 95 °C, which means that all free water was boiling in Na15 samples and extensive vapour pressure built up inside the sample. Samples with 15 % sodium oxide has a continuous solid microstructure, so the internal pressure could not be released but induced internal strains in newly formed paste microstructure. As the vapour pressure reaches its maximum, internal strains break the newly formed microstructure and local microcracks with a width of a few hundred nanometres are observed (see Figure 4.33, bottom picture, right lower corner). For samples Na9 and Na12 vapour pressure should be much lower as the temperature inside of these samples was considerably less. The presence of a more friable microstructure compared to Na15 in this case would be convenient as the vapour could escape through it.

The temperature development test showed that the AAFA pastes might experience significant core temperature rise, dependent on the ratio of paste to oven volume, size, alkali concentration and mould material. Thus, future research has to take into account possible temperature rise in sample cores and in curing ovens as the excessive temperatures can affect the material performance.

In-situ evaluation of volume changes during elevated temperature curing was performed for the AAFA pastes with different sodium oxide concentrations as shrinkage strains might also lead to crack formation.

4.6 SHRINKAGE OF AAFA CEMENT PASTES DURING ELEVATED TEMPERATURE CURING

Early age shrinkage values for this test not necessary represent the amount of evaporated water during elevated temperature curing as along with a volume changes due to water evaporation, the chemical shrinkage and the thermal movement are also present. Shrinkage results of the AAFA cement pastes during heat curing are shown in Figure 4.39. Each line is an average of two measurements.

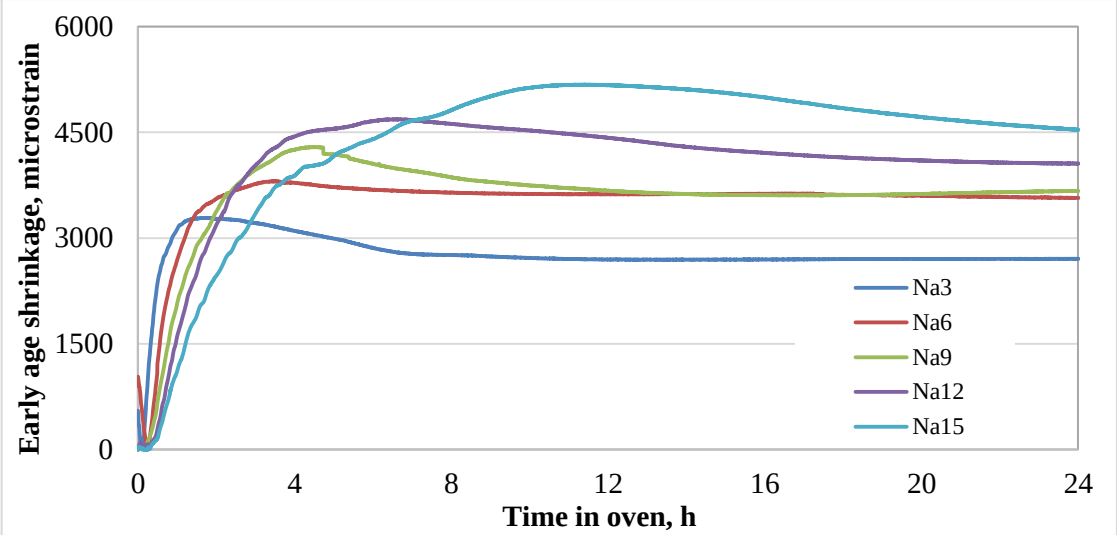

Figure 4.39: Early age shrinkage of AAFA cement pastes with different sodium oxide concentration during elevated temperature curing at 60 °C for 24 hours

It can be seen that the shrinkage value in the first 24 hours of elevated temperature curing strongly depends on alkali concentration. The maximum value of early age shrinkage of Na3 AAFA cement paste was almost 3300 microstrain. For Na6, Na 9, Na12 and Na15 these values were 3800, 4300, 4700 and 5200 microstrain respectively. There is a linear relationship between sodium oxide content and maximum early shrinkage value, shown in Figure 4.40. Maximum shrinkage rate is also a function of sodium oxide content as shown in Figure 4.40. Increase in sodium oxide content from 3 % to 15 % resulting in reduced maximum shrinkage rate.

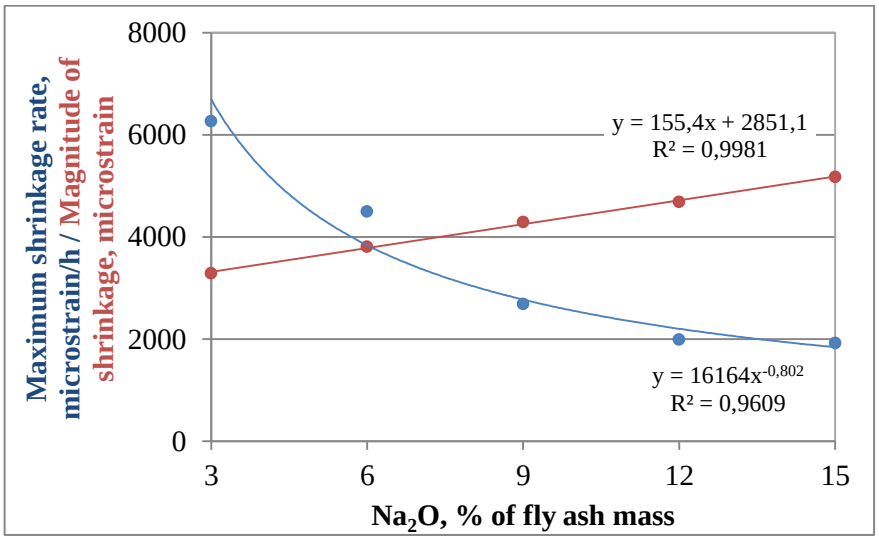

Figure 4.40: 'Maximum shrinkage rate and shrinkage magnitude vs. Na_2O content' relationship of AAFA cement pastes

In case of Na15 paste, the presence of the second phase of shrinkage (second slope – after 4 hours) could indicate that intensive shrinkage took place when early microstructural bonds

had been developed. This would cause significant damage of the microstructure resulted in formation of microcracks.

It is important to note that absolute values of the early age shrinkage of the AAFA cement pastes during elevated temperature curing are not critical even though they are relatively high. For comparative purposes, shrinkage of OPC paste with water to cement ratio of 0.28 was measured during elevated temperature curing (conditions were kept the same) and shown on Figure 4.41. It can be seen that the shrinkage of the OPC paste exceeded 11000 microstrain in less than an hour. This shrinkage value is more than twice as high as the highest shrinkage of the AAFA cement pastes. The total shrinkage of the OPC paste would be even greater but could not be measured because it readily exceeded the laser measurement limits.

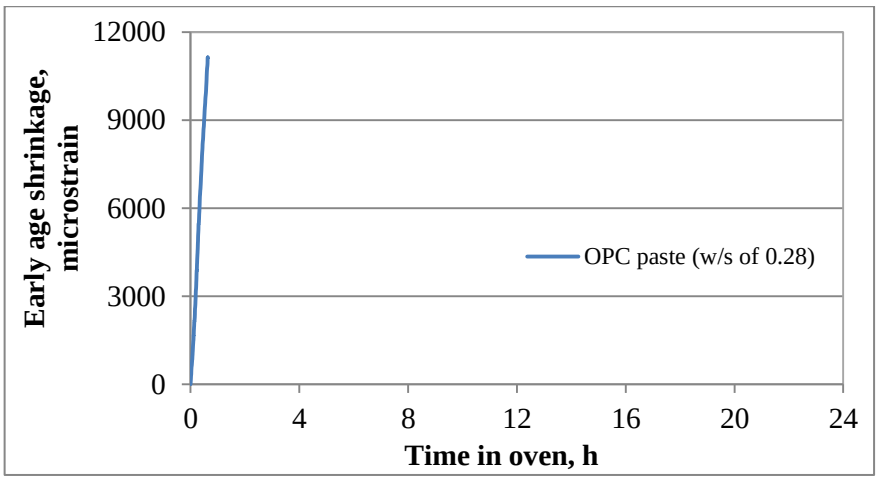

Figure 4.41: Early age shrinkage of OPC paste with w/c of 0.28 during elevated temperature curing at 60 °C for 24 hours

Average mass losses during elevated temperature curing for mixtures with different sodium oxide concentrations are shown in Figure 4.42.

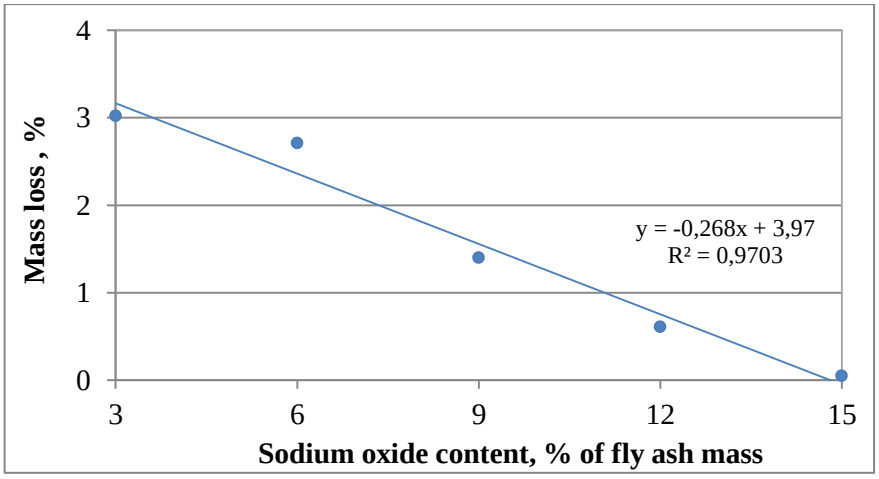

Figure 4.42: Average mass losses of AAFA cement pastes with different sodium oxide concentration after elevated temperature curing at 60 °C for 24 hours

The observed trend shows that mass losses decreases with increase in alkali concentration. In general mass losses were expected to be much higher than obtained results due to water evaporation. There are few possible reasons for such results. The first one is carbonation. Mass loss due to water evaporation could be compensated by a gain in mass caused by carbonation of the paste sample surfaces. The mass gain due to carbonation might increase with increase in alkali concentration because more alkali was available to react with CO_2 in the air. The pastes with 12 and 15 % Na_2O had considerably lower mass loss during elevated temperature curing in comparison to the rest of the pastes studied. As it was observed during strength tests in section 4.3.1, these pastes had excessive amounts of alkali, which was not bound in microstructure and was freely available for carbonation. However, no extensive efflorescence formation was observed immediately after elevated temperature curing in this test. Efflorescence formation was observed but only a few days after elevated temperature curing.

The second possible reason of the low mass loss is a sealing effect that might take place during the first minutes of elevated temperature curing. The sealing effect is the formation of a hard and vapour-impermeable crust of alkali activation products on the surface of samples. The sealing effect could be less prominent when lower alkali concentration was used, because the microstructure of Na3 and Na6 pastes, studied during SEM investigations, appeared friable and more porous due to the smaller amount of products formed during alkali activation reaction (see Figure 4.24 and 4.25). That fact that mass losses are higher in pastes with lower alkali content is reconciled with the arguments given in the previous section. For pastes with lower alkali content water evaporates through the loose microstructure, while more solid microstructure of samples with high alkali content prevent extensive evaporation, but might be affected by vapour pressure.

In Figure 4.43 the ‘mass loss-shrinkage’ relationship is shown. It can be seen that samples that had more mass loss, shrank less. It seems that the dominating factor, affecting early age shrinkage has a chemical nature. For example, the Na3 sample had not much of reaction products and major part of early age shrinkage can be related to the evaporated water.

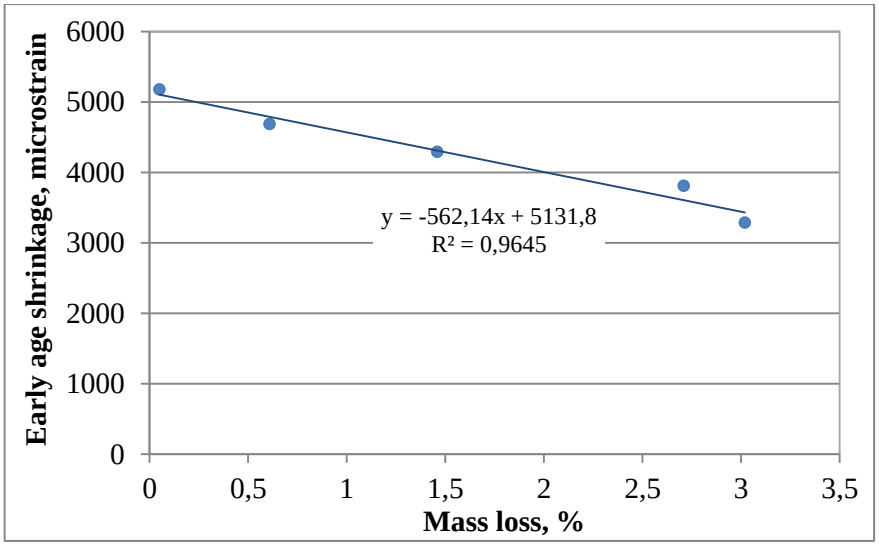

Figure 4.43: Mass loss - early age shrinkage relationship of AAFA cement pastes after elevated temperature curing at 60 °C for 24 hours

In contrast the Na15 sample did not lose any mass during the heat curing, however it had the highest shrinkage value, because more fly ash particles were dissolved in high alkaline solution, causing chemical contraction. In this thesis, unsealed cone samples were used to monitor shrinkage during heat curing, thus early age shrinkage value represent shrinkage due to chemical reaction as well as water evaporation, which cannot be separated.

4.7 CONCLUSIONS

In this chapter different factors affecting the compressive strength of AAFA pastes as well as their characterization were presented. The main conclusions of this chapter are summarized as follows:

- The alkali content plays an important role in the development of the compressive strength of the AAFA cement pastes and their microstructure. The recommended alkali concentration is 9 % Na_2O of fly ash mass which provides the highest compressive strength and low standard deviation at 28 days. Excessive alkali content (> 9 % Na_2O) results in a decrease in strength, high standard deviation and high coefficient of strength variation between different batches. Alkali content higher than 9 % Na_2O also causes efflorescence formation and the formation of microcracks in the microstructure of the pastes. Therefore, the amount of alkali must be strictly controlled during the production of AAFA cement.

- Temperature and duration of curing of the AAFA cement pastes affect the compressive strength significantly. Curing at 25 °C is possible, but it is not practical due to delayed setting, intensive efflorescence formation, very slow strength development, relatively low

strength at 28 days and large strength deviation. Therefore, it is important to provide elevated temperature curing thus accelerating the strength development of the AAFA cement pastes.

- Elevated curing temperature has a greater effect on the early strength than the long-term strength, especially of the pastes cured for a short period of time. An increase in temperature over 60 °C did not noticeably affect 28- and 91-days compressive strength of the AAFA cement pastes cured for 4 and 24 hours. A decrease in 91-days compressive strength of the paste cured at 80 °C for 24 hours was observed in comparison to the paste cured at 60 °C for the same period of time. The duration of elevated temperature curing has a more prominent effect on the early strength. The 28- and 91-days compressive strength is less affected by the duration of elevated temperature curing. There is no significant increase in the early compressive strength when the duration of elevated temperature curing exceeds 16 hours. Elevated temperature curing at 60 °C for 16 hours is recommended for curing of the AAFA cement pastes.

- The compressive strength of the AAFA cement pastes is significantly affected by the water to binder solids ratio. The compressive strength decreases with an increase in water to binder solids ratio. Therefore, AAFA cement concretes should be designed to achieve a required workability at the lowest possible water to binder solids ratio.

- Matla fly ash is suitable for alkali activation along with Lethabo fly ash, however the long-term compressive strength of AAFA pastes on the base of Matla fly ash is slightly lower compared to that of Lethabo. The reason for this difference is the mineralogical composition of fly ashes. The more amorphous phase is present the higher the compressive strength is.

- Using potassium hydroxide as activator solution results in the lowest compressive strength among all activator solutions, which makes it unfeasible to use. The presence of soluble silicates in activator solution favours alkali activation and compressive strength development as a result. Soluble silica added with alkaline silicate solution participates in the alkali activation process, increasing the amount of total reactive phase and as a result the quantity of final aluminosilicate gel responsible for the performance of hardened material.

- Increasing soluble SiO_2 in activator solution at constant Na_2O content lead to increase in compressive strength only to a certain point, afterwards a strength decrease was observed. However, regardless of Na_2O content, high SiO_2 content (9 and 12 % of fly ash mass)

resulted in higher deviation of compressive strength. The optimal silica oxide content for activator solution in this study with respect to Na_2O of 6 and 9 % of fly ash mass is 3 %.

- X-ray diffraction analysis of AAFA pastes with different concentrations of sodium oxide revealed the presence of a new phase – hydroxysodalite that was not observed in the initial fly ash. However, the presence of hydroxysodalite is not related to the strength decrease in pastes with higher alkali content, as hydroxysodalite was observed in paste with 9 % Na_2O as well.

- ATR-FTIR analysis showed a shift of a main peak in alkali-activated paste compare to the initial fly ash. This shift can be assigned to transformation of glassy phase of the initial fly ash and is an indicator of alkali activation reaction. ATR-FTIR revealed the presence of Al-rich structures and carbonates in AAFA pastes with 12 and 15 % Na_2O, which can be supported by the results of XRD analysis. The presence of alkali carbonates suggest that alkali was not only consumed during alkali activation reaction, and pastes with 12 and 15 % Na_2O had an excess of alkali that led to the efflorescence formation.

- Microstructure is known to be closely related to the mechanical strength of material. It was observed in this chapter that with an increase in sodium oxide content microstructure of AAFA pastes appeared to be more solid and less porous. However, mickocracks with ragged edges were observed in pastes with 15 % Na_2O as well. It was assumed that these microcracks were formed during elevated temperature curing of AAFA pastes and might be the reason for strength decrease and high strength deviation of AAFA pastes with 15 % Na_2O.

- It was found that the temperature inside AAFA paste samples depends on many parameters, such as sodium oxide content, size of samples, mould material. Core temperature of AAFA pastes increase slightly compare to oven's temperature with increasing NaOH concentration when the ratio of paste to oven volume ratio was 0.0228 and only plastic prism moulds were used. Temperature inside the oven was not affected by heat released during alkali activation process, when paste to oven volume ratio was 0.0228 and only plastic prism moulds were used.

- Core temperature of the AAFA pastes increase significantly compares to oven's temperature with increasing NaOH concentration and mould size. Temperature was also affected by material moulds were made of when the ratio of paste to oven volume ratio was 0.0504 and different sized and material moulds were cured together. Temperature inside the oven can be affected by heat released during alkali activation process if the

oven not equipped with refrigerator. Temperatures inside of samples rose up to 100 °C and promoted extensive water evaporation. Vapours built up a pressure inside the samples, affecting newly formed microstructure and promoting microcrack formation.

- For the first time early age shrinkage of AAFA pastes during elevated temperature curing was investigated. It was found that early age shrinkage during elevated temperature curing in oven is another possible reason for microcrack formation resulting reduced compressive strength for 15 % Na_2O pastes. Early age shrinkage value of AAFA pastes was found to be dependent on sodium oxide content. Early shrinkage value of 5000 microstrain were recorded for AAFA paste with 15 % Na_2O when paste had a low compressive strength of 1.5 MPa and the flexural strength could not be detected. Thus tensile stresses due to shrinkage were higher than developed strength to withstand internal stresses and microcracks were formed.

- It was substantiated in this chapter that higher sodium oxide contents in AAFA pastes promote higher temperatures and shrinkage values during elevated temperature curing, which induced internal stresses and lead to violation of microstructure continuity as a result of microcrack formation and might affect mechanical strength of AAFA cement paste.

5 EXPERIMENTAL STUDY ON ALKALI-ACTIVATED FLY ASH CONCRETE

5.1 INTRODUCTION

This chapter contains the results of testing alkali-activated fly ash concretes. Curing conditions for all AAFA concretes was elevated temperature curing in a dry oven at 60 °C for 24 hours unless otherwise mentioned. The trial experiments were conducted to confirm the main trends obtained for AAFA cement pastes. For further characterization of material, a big batch of AAFA concrete with the most suitable design was cast to investigate the main short- and long-term properties of concrete and compare results with literature. Along with the results on AAFA concrete, properties of fly ash-OPC blended concrete with the same binder content are presented for comparative purposes.

5.2 TRIAL EXPERIMENTS OF AAFA CONCRETE PRODUCING

The effect of alkali concentration on the compressive strength development was studied on a concrete mix with 400 kg/m^3 of fly ash and water to binder solids ratio of 0.3 as shown in Figure 5.1. Design of AAFA concrete mixes from this chapter presented in Appendix G.

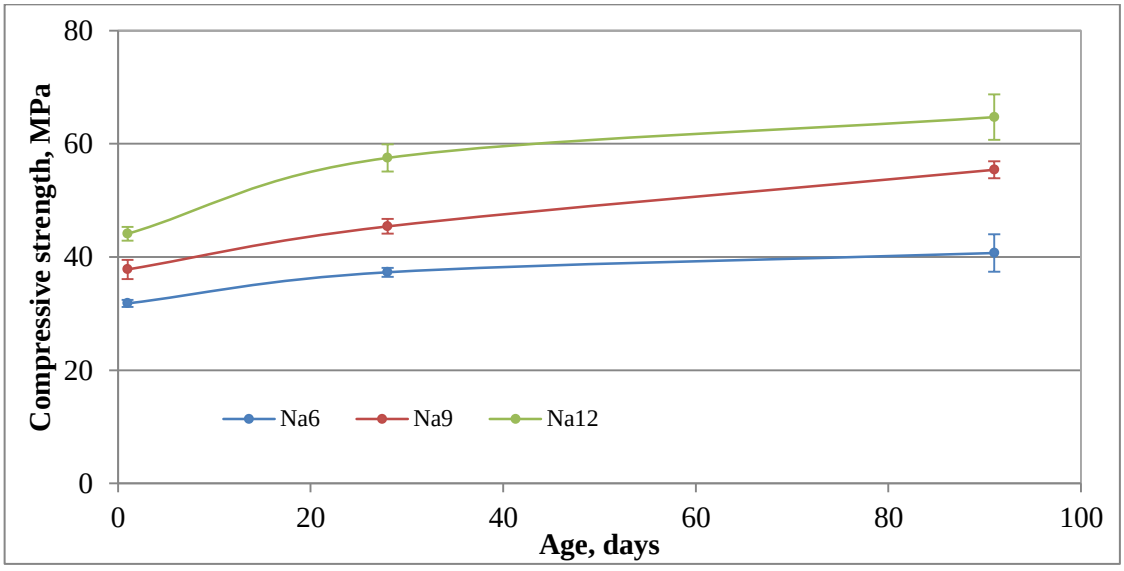

Figure 5.1: Strength development of AAFA concrete with different concentrations of sodium oxide

A mixture with 3 % sodium oxide was not used for preparation of AAFA concrete due to the low compressive strength obtained for corresponding AAFA paste. A mixture with 15 % sodium oxide was not used either as paste with such alkali content was found to have strength lower than that of the 12 % Na_2O mix. From Figure 5.1 it can be seen that with increasing sodium oxide content the compressive strength of AAFA concrete increases. However, it should be mentioned that the workability of all mixes was very low making the process of

concrete casting and finishing very difficult. Thus, it was decided to vary the amount of fly ash in the mixture, rich mixtures are usually more workable. Water to binder solids ratio was also varied. The effects of variation of fly ash content and water to binder solids ratio are shown in Figure 5.2.

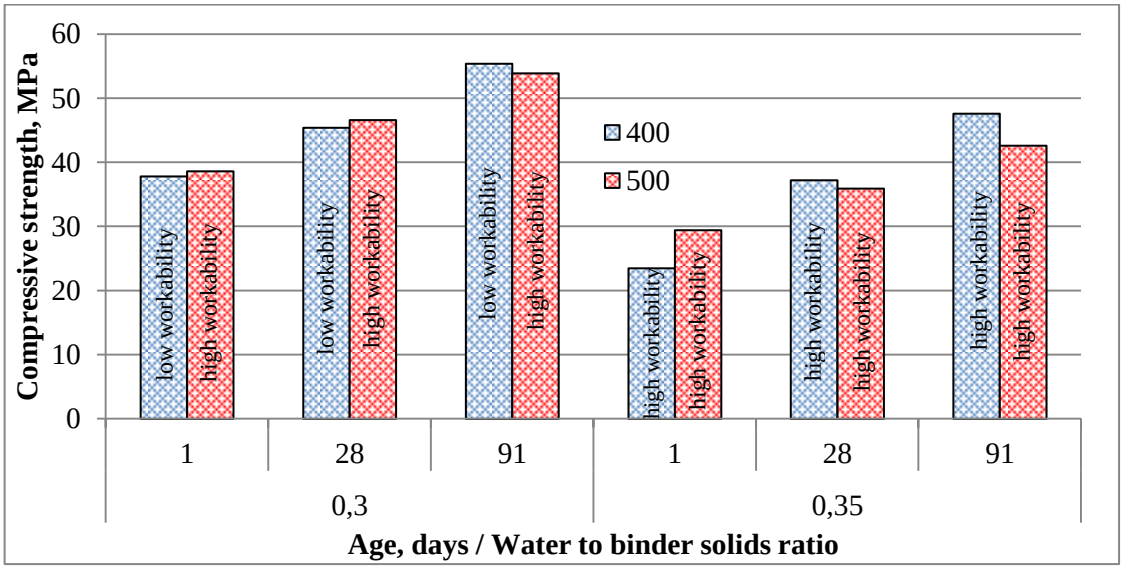

Figure 5.2: Effect of variation of fly ash content and water to binder solids ratio on the compressive strength and workability of AAFA concrete at different age (low workability - 0 mm slump; high workability - about 50 mm slump)

From Figure 5.2 it is clearly seen that an increase in amount of fly ash from 400 to 500 kg per cubic meter improved the workability of AAFA concrete without decreasing the compressive strength. Increasing water to binder solids ratio improved workability of AAFA concrete regardless of amount of fly ash used per cubic meter of concrete, but drastically decreased the compressive strength of concrete. Fly ash content per cubic meter of concrete of 500 kg was chosen for further testing.

The effect of water to binder solids ratio on the compressive strength was investigated on concrete mixes containing 500 kg of fly ash per cubic meter at constant sodium oxide content of 9 % of fly ash mass as shown in Figure 5.3. There is a linear relationship between water to binder solids ratio and the compressive strength. Compressive strength of AAFA concretes decreases with increasing water to binder solids ratio. The same trend was observed and discussed for AAFA pastes in the previous chapter. The consistency of AAFA concrete improved significantly with increasing of water to binder solids ratio. Water to binder solids ratio of 0.2 as used for AAFA paste preparation, could not be used for making concrete as the amount of dry components increased. A mix with water to binder solids ratio of 0.25 was very dry with a slump of 0 mm, while water to binder solids ratio of 0.3 provided good workability mix with 50 mm slump. Water to binder solids ratio of 0.35 was found to give the most

workable mixture with a slump of 70 mm, however the compressive strength of this mixture was 35-40 % lower than that of mixture with water to binder solids ratio of 0.25. Thus, water to binder solids ratio of 0.3 was chosen for preparation of a big batch of AAFA concrete, as this ratio provided good workability with a strength reduction of 15-20 % in comparison with the mix with the ratio of 0.25.

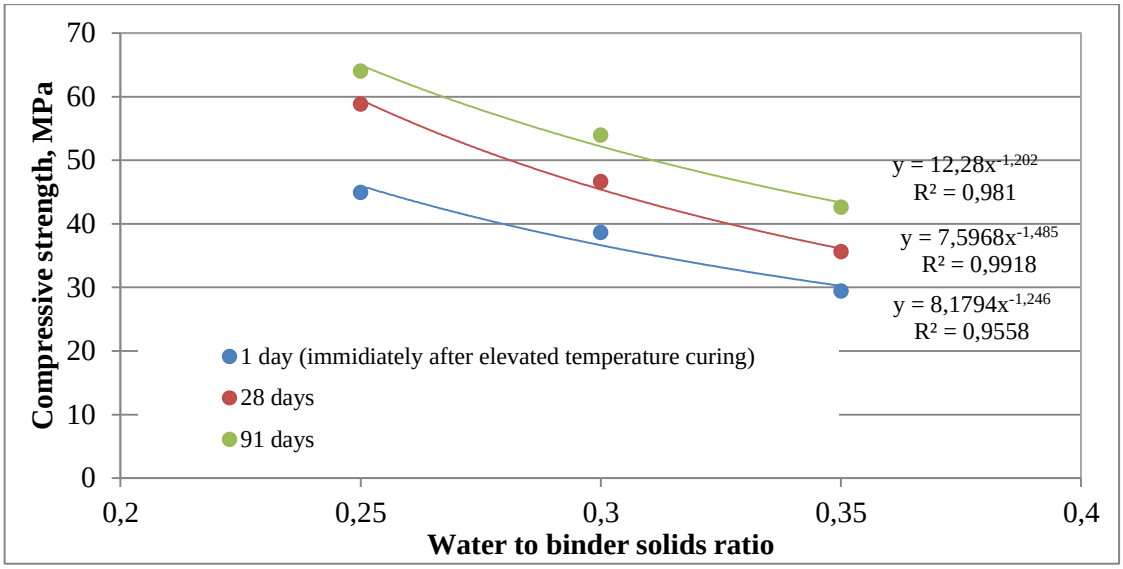

Figure 5.3: Effect of water to binder solids ratio on the compressive strength of AAFA concrete

The strength development of mixes with 9 and 12 % of sodium oxide at water to binder solids ratio of 0.3 and fly ash consumption per cubic meter of 500 kg is shown on Figure 5.4.

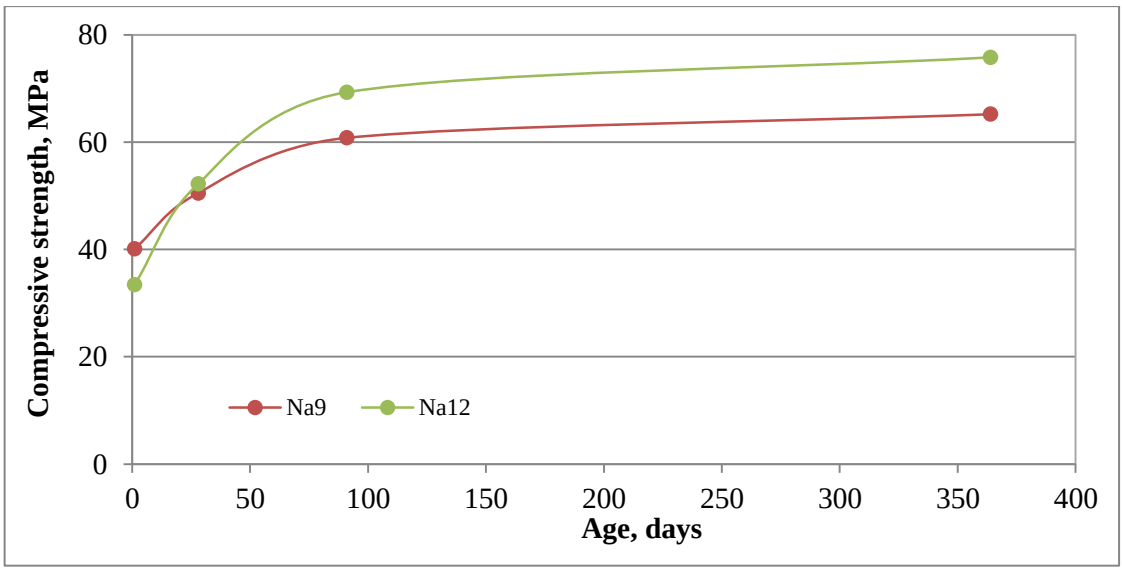

Figure 5.4: Strength development of AAFA concretes with 9 % and 12 % Na_2O

It is clearly seen from Figure 5.4 that compressive strength of Na12 is higher at all ages, suggesting that this amount should be used for producing big batch of concrete. However, the results of strength variation of mixtures with 9 % and 12 % sodium oxide at 28 days shown in

Figure 5.5 indicate, that using higher amount of alkali (12 % Na_2O of fly ash mass) results not only in higher average compressive strength of 54.0 MPa but at the same time in increased standard deviation of 4.6 MPa in comparison to 51.7 MPa and 2.6 MPa respectively for mix with 9 % sodium oxide. Characteristic strength of Na9 paste was 47.5 MPa compare to 46.4 MPa. Concrete with 9 % sodium oxide was chosen for making a big batch of concrete to study properties of AAFA concrete.

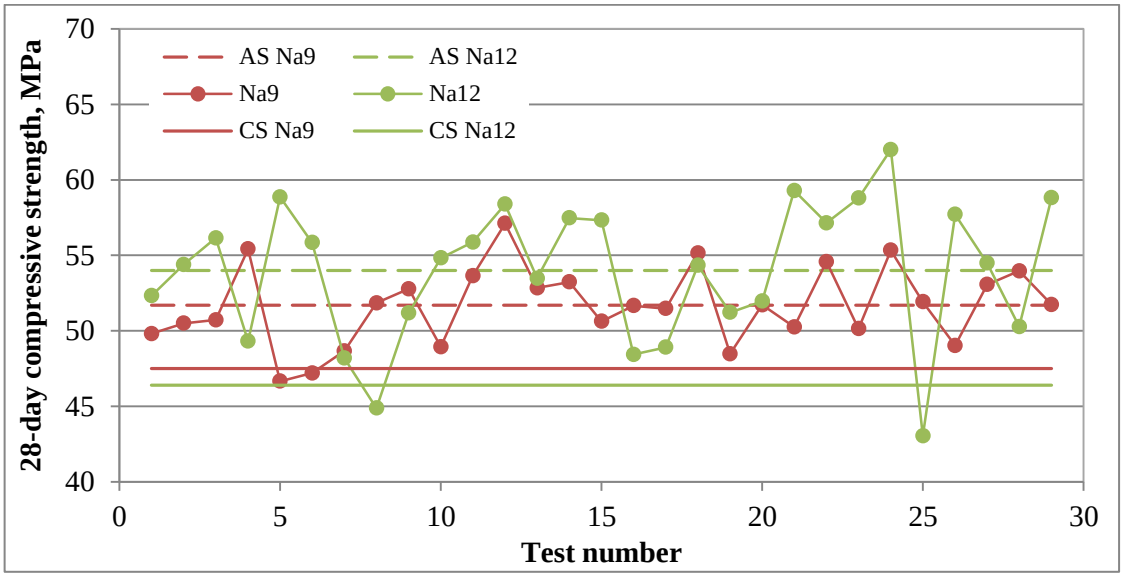

Figure 5.5: Individual strength results for mixtures with 9 % and 12 % sodium oxide, their average (AS) and characteristic (CS) strength

Five batches of concrete with 9 % sodium oxide at water to binder solids ratio of 0.3 and consumption of fly ash per cubic meter of 500 kg were cast at different days to confirm that 9 % Na_2O gives consistent strength results. The results of average compressive strength of each batch as well as average compressive strength between these batches at different testing times are shown in Figure 5.6. The average compressive strength of AAFA concrete between five batches immediately after elevated temperature curing (1-day strength) was 36.1 MPa, after 28 days – 46.6 MPa and after 91 days – 58.8 MPa. The calculated standard deviation of average compressive strength between different batches was 3.2 MPa for 1-day strength, 2.9 MPa for 28-day strength and 3.4 MPa for 91-day strength. Thus, the coefficient of strength variation between batches was 8.8 % for 1-day samples, 6.2 % for 28-day samples and 5.8 % for 91-day samples. Strength deviation of the AAFA concrete containing 9 % sodium oxide within the batch approximates with strength deviation between batches, which is a good indicator of stability of AAFA concrete compressive strength with 9 % sodium oxide.

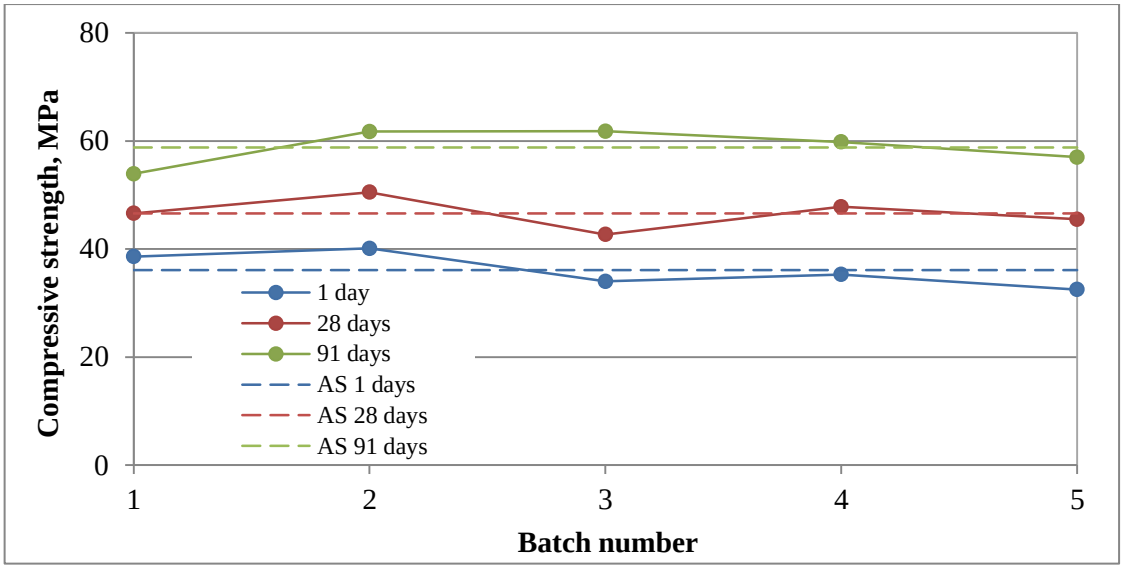

Figure 5.6: Strength variation of five bathes of AAFA concrete with 9 % sodium oxide at different age and their average strength

The trials on AAFA concretes confirm the general trends obtained for AAFA paste study:

- With increase in sodium oxide content the compressive strength of AAFA concrete increases;
- Higher amount of sodium oxide (12 %) results in higher strength variation of AAFA concrete;
- Increasing water to binder solids ratio increases the workability of AAFA concrete but decrease its compressive strength;
- Sodium oxide content of 9 % of fly ash mass provides sufficient repeatability of the compressive strength at all ages.

5.3 EVALUATION OF SHORT AND LONG PROPERTIES OF AAFA CONCRETE

A big batch of AAFA concrete containing 9 % sodium oxide, water to binder solids ratio of 0.3 and fly ash consumption per cubic meter of 500 kg (tagged as GP) was produced for detailed material characterization. Fly ash–OPC blended cement concrete with 500 kg of binder (fly ash + OPC cement) per cubic meter, water to cement ratio of 0.4 (tagged as NC) was cast, not for direct comparison of the strength and deformation properties of both concretes, but rather for comparison in durability properties. Water to cement ratio of NC was chosen so its consistency was similar to GP. Fine to coarse aggregate percentage ratio was kept constant at 35:65 for both GP and NC concretes. Mix design of both concretes are shown in Table 5.1.

Table 5.1: Material consumption for concrete producing, kg/m^3

Material name	GP	NC
Fly ash	500	150
CEM 52.5 N	-	350
9-mm dolomite stone	1113.2	1157.5
Dolomite sand	603.1	623.3
NaOH	58.1	-
Water	150.4	200
Theoretical density	2424.8	2480.8

All GP samples were cured at 60 °C in a dry oven for the first 24 hours. Further curing was done in two ways, to see how water curing influences properties of AAFA concrete. The first set of samples was placed in a room with constant conditions (25±2 °C temperature and 55 % relative humidity) until testing (tagged as GP (curing room)). To see how saturation in water influences properties of AAFA concrete, a series of samples cured in the curing room was placed into water for 24 hours before testing (tagged as GP (curing room + 24 h in water)). Another set was cured in water (tagged as GP (water)). The first set of fly ash–OPC blended concrete was cured at 25 °C and relative humidity of 99 % while the second set was steamed at 60 °C for the first 24 hours. Both sets of NC samples were then placed into water until testing age. Three samples were tested for each data point.

5.3.1 Strength of concrete

5.3.1.1 Compressive strength development

Compressive strength development of AAFA and fly ash-OPC concretes is shown in Figure 5.7. Compressive strength determination was conducted on sets of three cubes. Compressive strength of GP after elevated temperature curing was 32.5 MPa which is comparable to the strength of NC after steam curing (35.8 MPa). Further strength development of steamed NC is similar to NC cured under normal conditions, thus, all GP results will be compared to NC (normal). Table 5.2 contains the average compressive strength values and standard deviation of GP and NC concretes at different ages.

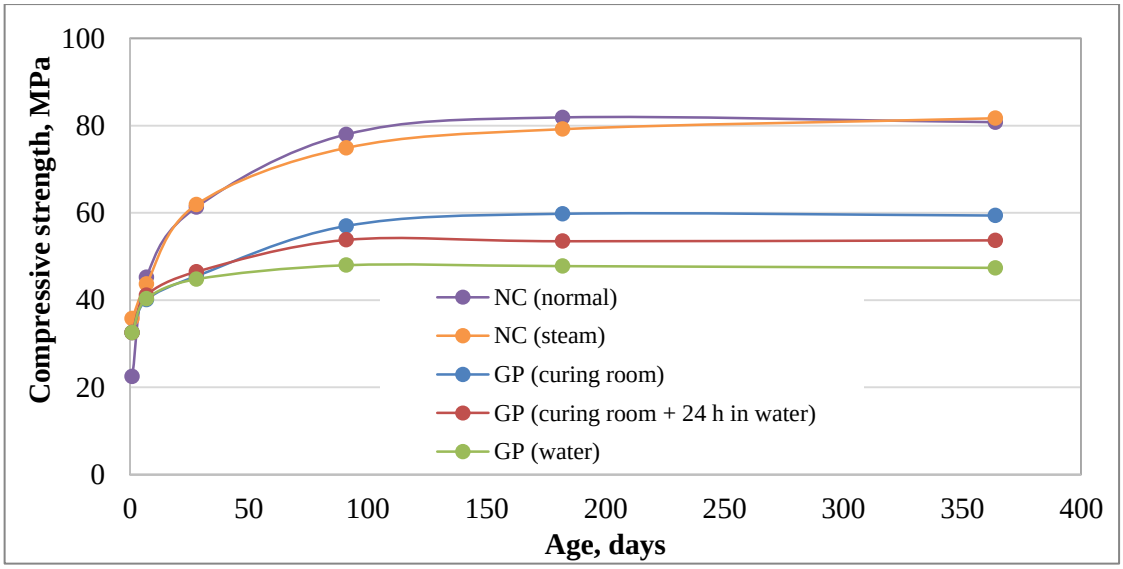

Figure 5.7: Strength development of AAFA concrete and fly ash–OPC blended concrete

Table 5.2: Average compressive strength and standard deviation values of AAFA concrete and fly ash–OPC blended concrete

	Compressive strength and standard deviation (in brackets), MPa at different age, days					
	1	**7**	**28**	**91**	**182**	**364**
NC (normal)	22.5 (0.4)	45.2 (1.6)	61.3 (2.1)	78.0 (2.5)	81.9 (3.2)	80.8 (1.4)
NC (steam)	35.8 (2.5)	45.3 (2.2)	61.9 (2.1)	74.5 (5.7)	79.2 (2.4)	82.4 (1.1)
GP (curing room)	32.5 (2.1)	40.1 (3.9)	45.5 (2.8)	57.0 (3.6)	59.8 (2.8)	59.4 (0.8)
GP (curing room + water 24 h before)	32.5 (2.1)	41.1 (4.5)	46.5 (1.5)	53.8 (2.0)	53.5 (2.3)	53.7 (0.3)
GP (water)	32.5 (2.1)	40.3 (3.6)	44.8 (1.8)	48.4 (0.3)	47.8 (2.0)	47.4 (1.6)

All series of GP had continuous strength gain until 91 days. After that, no significant strength gain was observed. 28-day strength of GP cured in curing room was 45.5 MPa, while for samples cured in water 28-day strength was 44.8 MPa. It seems that curing in dry condition is preferable for compressive strength of AAFA concrete and this is become more prominent in later age. 91-day compressive strength of GP (curing room) samples was 57.0 MPa, while the same of GP (water) was only 48.4 MPa, which is 15 % lower than GP (curing room). Compressive strength of samples submerged into water for 24 hours before testing was only 5 % lower than that of cured in dry conditions at the age of 91 days. In general, GP is stable in water as concrete samples placed into water did not lose strength over the testing period.

5.3.1.2 Tensile strength

Three specimens of each series of GP and NC were cast. Beam samples with dimensions of 100×100×500 mm were subject of two-point loading for determination of modulus of rupture. For splitting tensile strength, concrete cylinders with diameter of 150 mm and height of 300

mm were cast and subjected to compressive forces applied along two diametrically opposed lines. Table 5.3 contains the results of modulus of rupture and split tensile strength of GP and NC at 28 days.

Usually concrete is not expected to resist direct tension; however, the values of tensile strength of concretes give an idea of the load at which concretes may crack, as cracking is a form of tension failure.

GP concretes showed split cylinder strength in the same range than that of NC concrete despite the great difference in the 28-days compressive strengths. Water curing and soaking of GP concrete have a negative influence on the tensile strength, which correlates with compressive strength results.

The tensile strength of concrete is usually ignored in the design of concrete structures; however the design of concrete roads and pavements is based on flexural strength of concrete. According to the Portland Cement Association, as cited in Addis (1994), flexural strength may be taken as it shown in Equation 5.1

$$f_f = K f_c^{1/2} \tag{5.1}$$

Where, f_f is the flexural strength, MPa; f_c is the cube compressive strength, MPa and K has a value of 0.68.

The Joint CEB-FIB Committee, as cited in Addis (1994), used the following relationship between compressive and tensile strength (Equation 5.2).

$$f_t = 0.24 f_c^{2/3} \tag{5.2}$$

Where f_t is the split cylinder strength and f_c is the cube strength, MPa.

Table 5.3: Modulus of rupture and split tensile strength of GP and NC concrete at 28 day and standard deviations

	Measured tensile strength and standard deviation (in brackets), MPa		Calculated tensile strength , MPa	
	Flexural	Split	Flexural (Equation 5.1)	Split (Equation 5.2)
GP (curing room)	5.8 (0.12)	3.7 (0.26)	4.6	3.1
GP (curing room + water 24 h before)	4.5 (0.32)	3.8 (0.31)	4.6	3.0
GP (water)	5.5 (0.46)	2.5 (0.03)	4.6	3.1
NC (normal)	7.1 (0.33)	4.1 (0.28)	5.3	3.7

Table 5.3 shows the results of calculated values of tensile strength. The results show that the measured flexural and split tensile strength of GP concretes is higher than the predicted though calculations values. Similar trends were observed by Rangan (2009).

5.3.2 Deformations of concrete

5.3.2.1 E-value and Poisson's ratio

It is known that the stiffness of aggregate and its volume contribute the most to the elastic modulus of concrete in which it is used (Addis, 1994). Dolomite stone was used though out the study for making both GP and NC concretes. In Table 5.4 the static modulus of elasticity and Poisson's ratio of concretes at 28 days are shown.

Table 5.4: E-values and Poisson's ratios of GP and NC concrete at 28 day and its standard deviation

	E-value (GPa)	Poisson's ratio
GP (curing room)	32.9 (1.38)	0.11
GP (curing room + water 24 h before)	32.2 (1.18)	0.12
GP (water)	30.7 (1.00)	0.12
NC (normal)	43.5 (0.03)	0.12

The E-value of AAFA concrete is insignificantly higher for samples cured in dry conditions, which correlates with the compressive strength at the same age. The values of elastic modulus for GP are significantly lower compare to NC. However, comparison of these two values is unfair due to the different concrete grades to which GP and NC can be assigned. In general, elasticity modulus of GP concrete is lower than that of OPC concrete of similar grade with the same type of aggregate. Alexander (1994) reported static elastic modulus of 37 GPa for 30 MPa OPC concrete and 44 GPa for 40 MPa concrete at 28 days. The lower elastic modulus for AAFA concrete can be explained by weaker transition zones between aggregate and paste for GP concretes due to higher porosity for example or elastic properties of aluminosilicate gel is different compare to CSH gel.

Alexander and Davis (1992) suggested the relationship between compressive strength and elasticity modulus of concrete made with South African aggregates, shown in Equation 5.3 that could be used for prediction of elastic modulus:

$$E = K_0' + \alpha f_{cu} \tag{5.3}$$

Where E is the static modulus of elasticity at 28 days for a particular age being considered, GPa; f_{cu} – characteristic cube strength, MPa, corresponding to the age considered; K_0' - a

constant related to the stiffness of the aggregate, GPa; α - a strength factor, also related to the aggregate characteristics, GPa/MPa.

Assuming that characteristic strength of GP for different curing conditions is 30 MPa. Coefficients of K_0' and α for different types of aggregates are presented in Appendix D. Calculated according Equation 5.3 the elastic modulus of GP at 28 days is 37.5 GPa. The measured E-values are about 20 % lower than the calculated E-values. If the same degree of quality control is assumed for NC concrete as for GP, the characteristic strength of NC concrete at 28 day will be 45 MPa. In this case, the calculated elastic modulus will be 44.2 GPa which is close to the measured value. The nature and elastic properties of AAFA binder differ from that of OPC binder and lead to substantial difference between calculated and measured E-value, indicating that Equation 5.3 cannot be used for predicting E-value of AAFA concrete. The values of static Poisson's ratio of AAFA concrete are in the range of typical values for OPC mortars and concretes (between 0.1 and 0.2 (Addis, 1994)).

5.3.2.2 Shrinkage during first 24 hours

The results of shrinkage during the first 24 hours will be presented in this section. The Schleibinger shrinkage cone method for measuring autogeneous shrinkage of concrete was adopted and used (Eppers and Müller, 2010). Shrinkage of GP was recorded in situ during elevated temperature curing in oven at 60 °C. Shrinkage of NC during steam curing could not be recorded due to inappropriate laser working conditions when condensate could affect measurements and even disable measuring device. Thus, only shrinkage of normal cured NC during first 24 hours was recorded. As blended cement concrete was cured in high humidity room (about 99 % relative humidity) shrinkage of NC in this section can be considered as autogeneous (chemical), while volume changes of GP concrete during heat curing could be caused by drying shrinkage, chemical and even carbonation shrinkage which cannot be separated. Thermal expansion can be expected during elevated temperature curing of AAFA concrete. Figure 5.8 presents shrinkage of NC and GP concretes during the first 24 hours after casting.

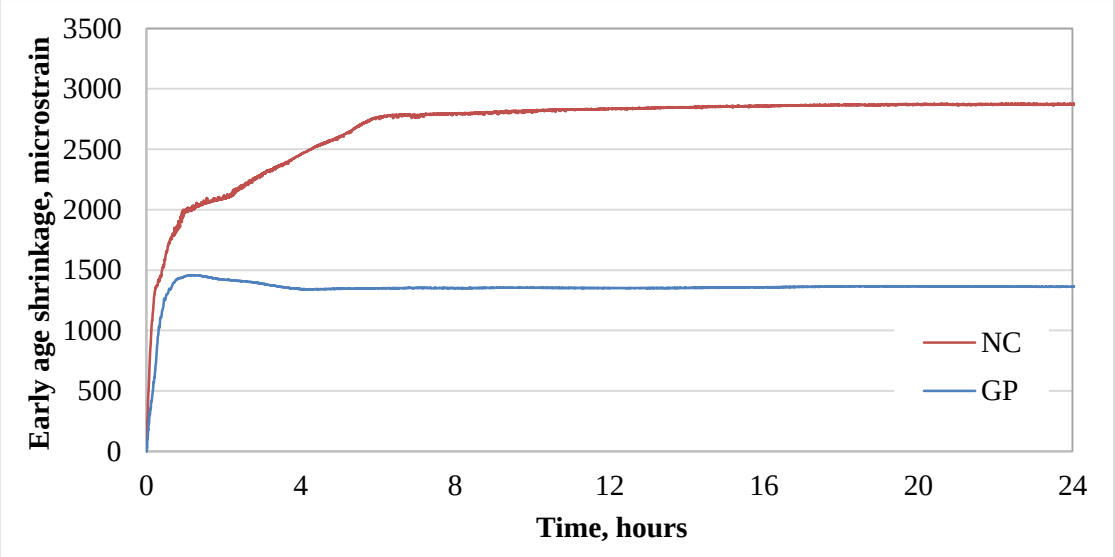

Figure 5.8: In situ early age shrinkage of NC and GP concretes during first 24 hours

Shrinkage of AAFA concrete (GP) in first 24 hours is significantly lower at 1460 microstains, compare to 2800 microstrains in blended cement concrete (NC). The result was unexpected as GP was cured at higher temperature thus water evaporation accompanied by volume changes is supposed to be more intensive at this temperature. The different nature of the reaction in AAFA binder compared to fly ash-OPC blended concrete results in such a substantial difference in the shrinkage value. The shrinkage of AAFA paste with 9 % Na_2O (Chapter 4) is predictably higher than that of AAFA concrete, despite lower water to binder solids ratio, 4000 microstain in comparison to 1400 microstrain for concrete. The lower shrinkage value for concrete is obvious as the paste volume in the concrete sample is about 38 % of total sample volume while the residual volume is occupied by aggregates, which does not participate in shrinkage and provide rigid skeleton.

The two-slope curve for the NC sample can probably be indicative of initial and final setting of concrete binder, suggesting the possible use of the shrinkage cone method for determination of concrete setting times.

5.3.2.3 Drying shrinkage

Drying shrinkage measurements for both GP and NC concretes were conducted on 100×100×300 mm beams. The drying shrinkage measurements of GP were started right after elevated temperature curing (60°C for 24 hour) and cooling of samples. NC samples were cured in water baths for 6 days and the first drying shrinkage measurements were taken on the 7^{th} day. The samples of both concretes were then stored in a room with constant temperature and relative humidity (25±2 °C and 55 % respectively) and measurements were taken at regular time intervals for one year. Drying shrinkage of the concretes is shown in Figure 5.9.

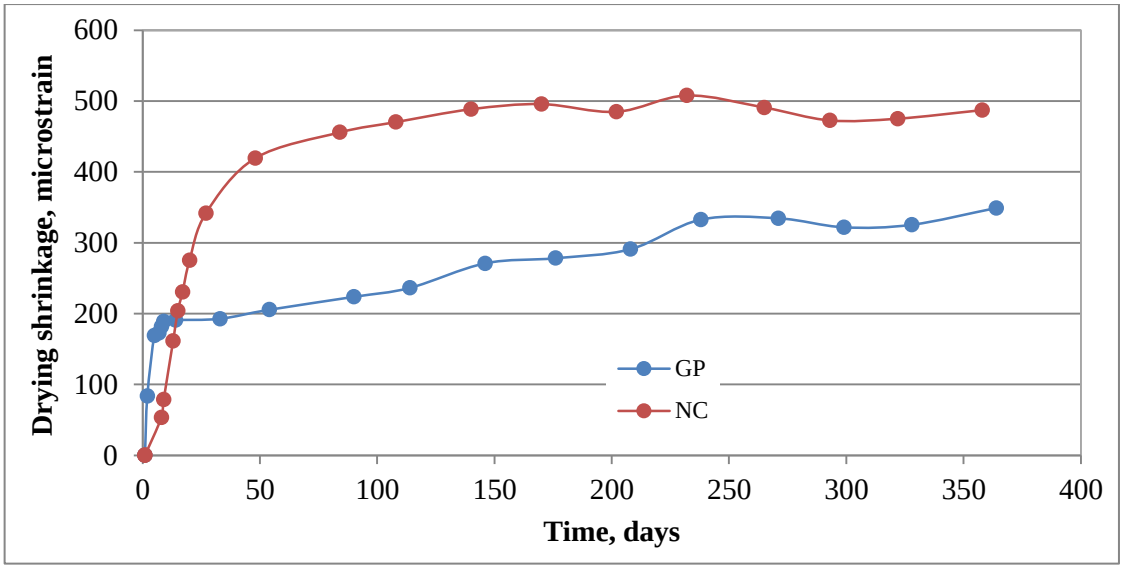

Figure 5.9: Drying shrinkage of NC and GP concretes

It can be seen from Figure 5.9 that drying shrinkage of NC is about 500 microstrain, while the drying shrinkage of GP is about 360 microstrain after one year curing. The drying shrinkage of GP concrete was expected to be lower compared to NC as the major part of shrinkage occurred during elevated temperature curing. Sagoe-Crentsil et al. (2013) reported values of drying shrinkage for 40 MPa geopolymer and OPC concretes (both of them steam cured at 60 °C) of 350 and 500 microstrains respectively. Wallah and Rangan (2006) reported drying shrinkage of 100 microstrain but for higher strength geopolymer concrete.

5.3.2.4 Creep performance

The creep behaviour of AAFA and fly ash–OPC blended cement concretes was studied on 150×300 mm cylinders. GP was cured at 60 °C for 24 hours in a dry oven. The creep test of first set of GP samples commenced immediately after elevated temperature curing under sustained stress of 40 % of the compressive strength on this day. A second set of GP samples after elevated temperature curing were placed in a room with constant temperature and humidity (25±2 °C and 55 %). On the 28th day samples were placed under sustained stress of 40 % of the 28-days compressive strength. NC samples were cured in water and also placed under sustained stress on the 28th day of curing.

Table 5.5 presents sustained stress and instantaneous (elastic) strain measured immediately after the application of sustained load. Instantaneous elastic modulus was calculated as sustained stress/instantaneous strain. The values of instantaneous elastic modulus are similar to those presented earlier in Table 5.4 suggesting good repeatability of the results.

Table 5.5: Instantaneous strain and elastic modulus of GP and NC concretes

	Cube compressive strength, MPa	Sustained stress, MPa	Instantaneous (elastic) strain, microstrain	Instantaneous elastic modulus, GPa
GP after heat curing (HC)	32.5	10.87	364	29.8
GP after 28 days	45.5	14.54	486	29.9
NC after 28 days	61.3	19.64	468	41.9

Creep performance of both GP and NC concretes are shown on Figure 5.10. Specific creep was calculated as creep strain per unit of applied stress. A basic creep coefficient was calculated as a creep strain divided by elastic strain. In general it can be seen that creep performance of GP concrete is better compared to NC concrete. After one year under load specific creep of NC concrete was 30 microstrain/MPa, while the value of GP concrete was only half of NC (less than 15 microstrain/MPa).

Sagoe-Crentsil et al. (2013) reported a basic creep coefficient for 40 MPa geopolymer concrete of 0.6, while for the OPC concrete creep coefficient was about 1.8, both concretes were steam cured. Wallah and Rangan (2006) obtained creep coefficients between 0.6 and 0.7 for heat cured geopolymer. Although, direct comparison of these results to that previously published is unfeasible due to difference in aggregate type and ratio, age of concrete and other factors, the results presented in this section have the similar trend to the results published previously by other researchers.

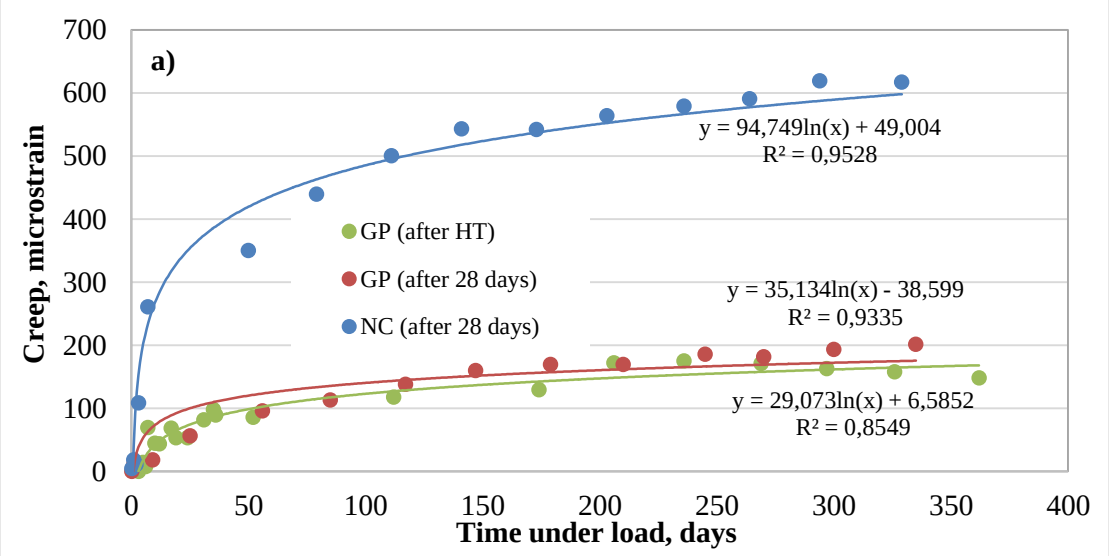

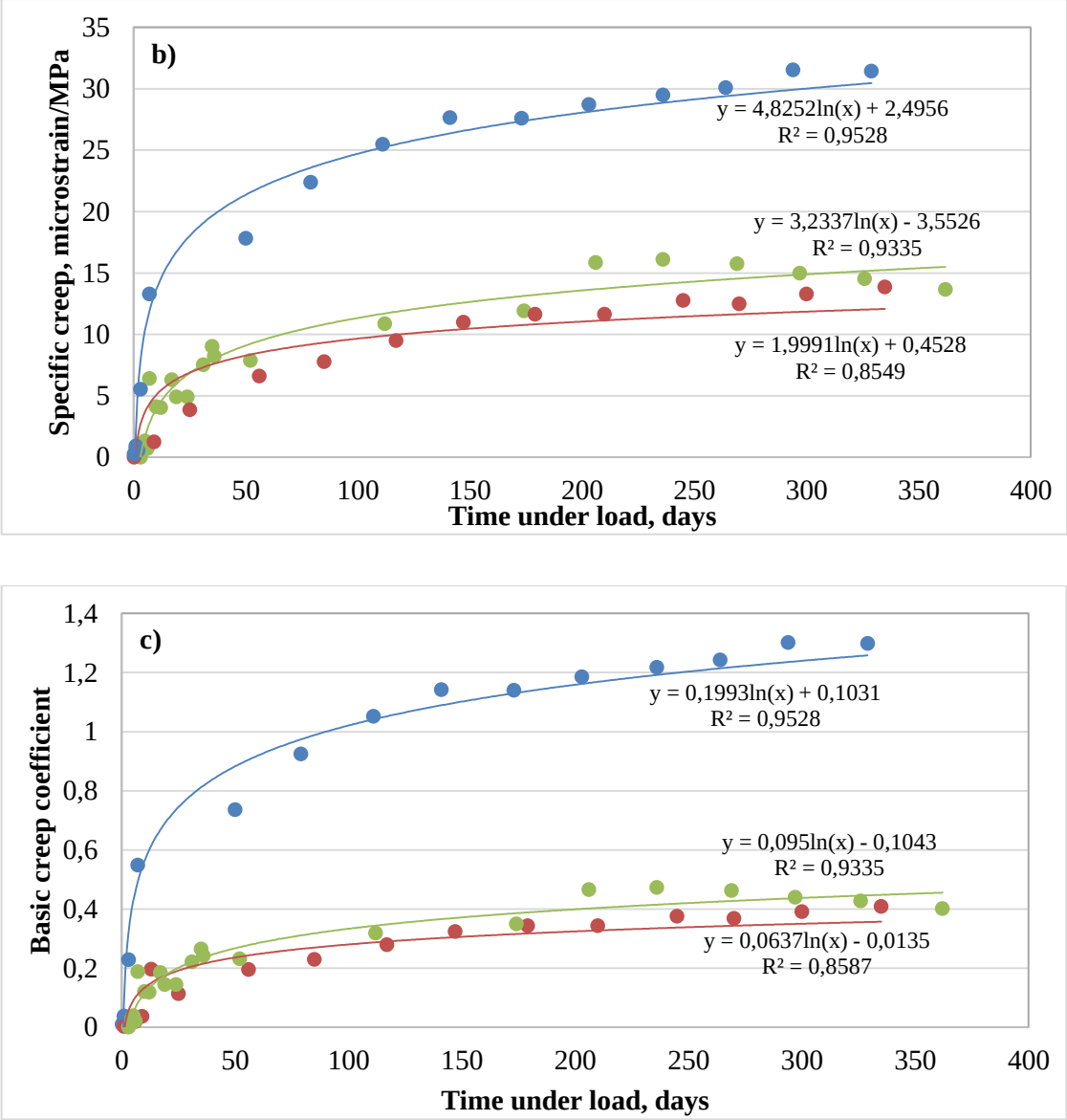

Figure 5.10: Creep performance of GP and NC concretes: a) creep; b) specific creep; c) basic creep coefficient

5.3.3 Durability of concrete

5.3.3.1 Basic acid immersion test

Basic acid immersion tests were conducted on three sets of samples. Samples of NC were placed into H_2SO_4 acid after 28 days of curing in water (tagged as NC (acid after 28 days)) and compared to samples cured in water (NC (water)). The first set of GP samples were placed into acid immediately after heat curing in oven, tagged as GP (acid after HC). The second set of GP samples was places into acid after curing in oven and following curing in the curing room (tagged as GP (acid after 28 days)). Both sets were compared to GP cured in curing room and in water. Strength development of GP and NC cured in H_2SO_4 acid is shown in Figure 5.11. Compressive strength and standard deviation values are presented in Table 5.3.

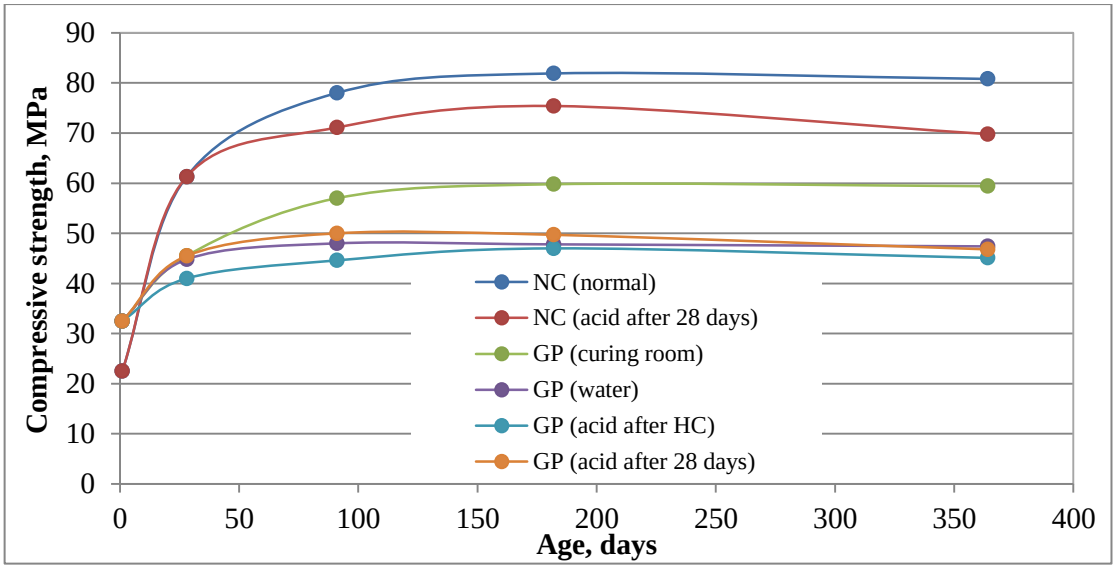

Figure 5.11: Strength development of AAFA concrete and fly ash – OPC blended concrete placed in H_2SO_4 acid (pH=2)

Table 5.6: Average compressive strength and standard deviation values of AAFA concrete and fly ash–OPC blended concrete exposed to H_2SO_4 acid (pH=2)

	Compressive strength and standard deviation (in brackets) at different age, MPa					
	1	**7**	**28**	**91**	**182**	**364**
NC (normal)	22.5 (0.4)	45.2 (1.6)	61.3 (2.1)	78.0 (2.5)	81.9 (3.2)	80.8 (1.4)
NC (acid after 28 days)				71.1 (1.8)	75.4 (2.0)	69.8 (4.9)
GP (curing room)	32.5 (2.1)	40.1 (3.9)	45.5 (2.8)	57.0 (3.6)	59.8 (2.8)	59.4 (0.8)
GP (water)		40.3 (3.6)	44.8 (1.8)	48.4 (0.3)	47.8 (2.0)	47.4 (1.6)
GP (acid after HC)			41.0 (2.4)	44.6 (3.0)	47.0 (2.8)	45.1 (4.5)
GP (acid after 28 days)				50.0 (1.9)	49.7 (2.1)	46.8 (3.1)

There is a clear trend of strength decreasing of NC samples immersed in acid compared to samples cured in water. At the age of 364 days, strength of NC (acid after 28 days) was 15 % lower than that of NC (water), showing there is a chemical process behind this strength decrease. Sulphuric acid reacts with calcium hydroxides of cement with formation of gypsum containing two water molecules and increased volume. The gypsum then reacts with tricalcium aluminate (C_3A) to form complex salts that have needle-like appearance and significantly increased volume. Volume changes related to the formation of new phases induce internal stress, resulting in cracking and scaling of concrete. Visual observation of NC samples immersed in sulphuric acid allows the detection of small needle-like white crystals together with a thick white deposit on the surface with a brownish coloured surface under it (see Figure 5.12). However, no visible crystals were found in the cross-sectional area of the sample, probably due to relatively low permeability of NC concrete to the aggressive solution. There were not any significant changes in dimensions of samples or signs of deterioration of concrete.

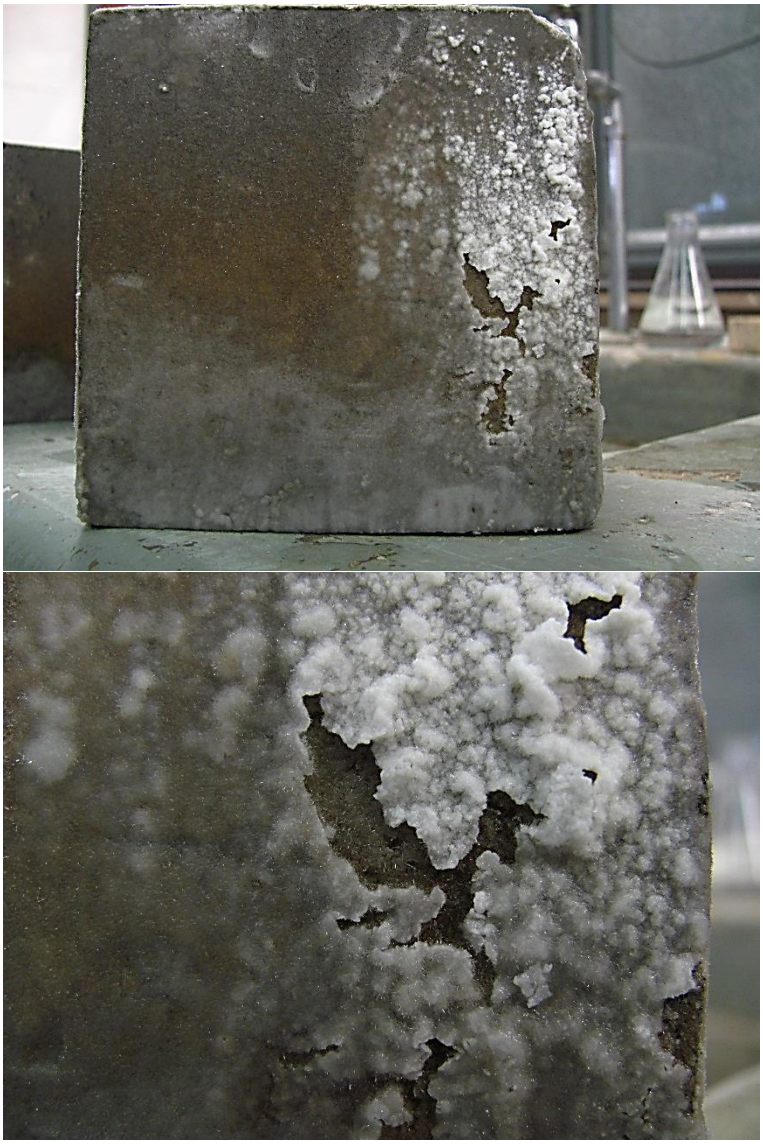

Figure 5.12: Appearance of fly ash–OPC blended concrete exposed to H_2SO_4 acid (pH=2) at 182 days

The attacking process of GP concrete with sulphuric acid should be completely different from the NC concrete as GP made out of fly ash and NaOH does not contain any $Ca(OH)_2$ at all. Moreover, it actually was different as the appearance of GP immersed in acid differs from NC under the same conditions. There were not many crystals on the surface of samples. The presence of crystals had a local character and they appeared to have "hedgehog" structure. Slight peeling of sample surfaces was observed after 91 days of curing in acid (See Figure 5.13). Strength of GP (acid after HC) was 25 % lower than that of GP (curing room) and only 5 % lower than that of GP (water) at the age of 364 days. It seems that the immersing environment (acid or water) is leaching out the activator and preventing on-going strength development.

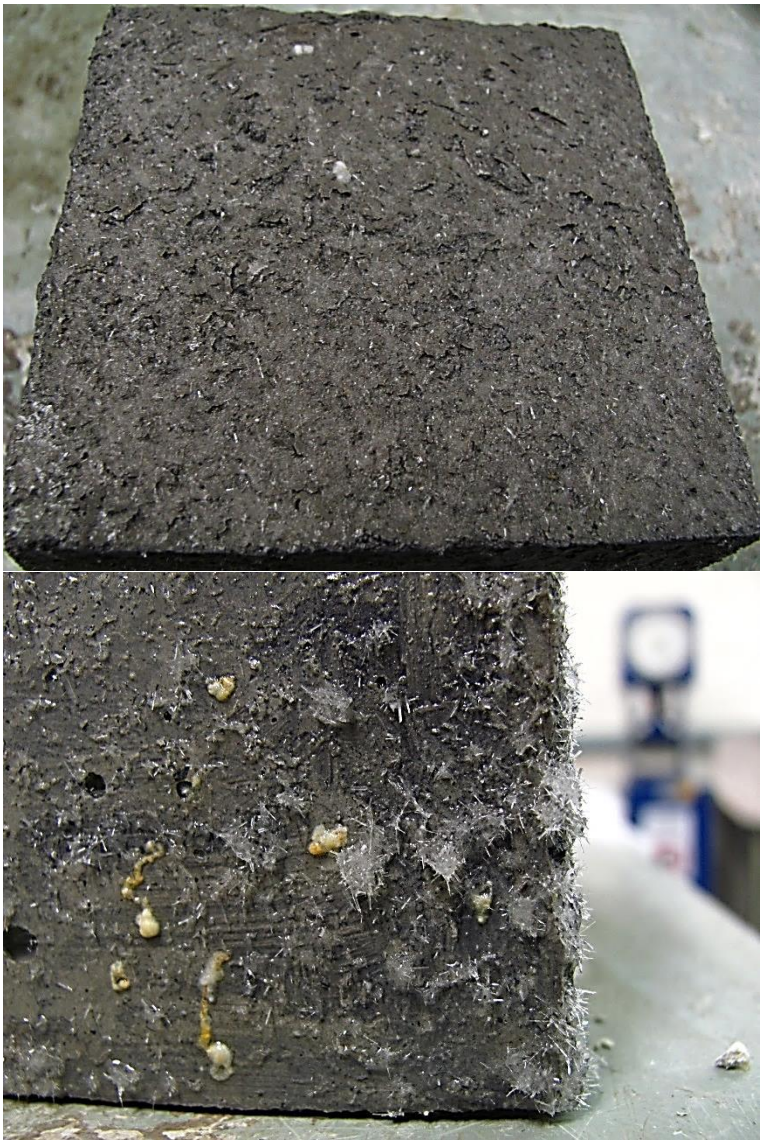

Figure 5.13: Appearance of AAFA concrete exposed to H_2SO_4 acid (pH=2) at 182 days

5.3.3.2 Oxygen permeability index, water sorptivity, chloride conductivity, porosity

Oxygen permeability, water sorptivity and chloride conductivity test methods, titled as durability indices, have been developed in South Africa by Alexander et al. (1999) to characterize the transport properties of concrete and its durability and results are presented in Table 5.7 for both, GP and NC concretes.

Table 5.7: Durability indices

	OPI	Water sorptivity, mm/h$^{1/2}$	Chloride conductivity, mS/cm	Porosity,%
GP (curing room)	10.06	12.6	1.44	13.0
GP (water)	10.21	12.6	1.32	11.1
NC (water)	10.56	8.1	1.14	9.1

Although the durability index approach is not widely used outside of South Africa, a comparison with internationally accepted methods for concrete durability characterization was performed by Beushausen and Alexander (2008). The results shows that oxygen permeability and chloride conductivity test methods can be successfully used in characterising concrete durability and have similar merit in establishing material properties as other internationally accepted methods. In general, the higher the OPI index, the more resistant the concrete to gas penetration (Alexander et al, 2008). The OPI indices of GP concrete are similar to those of NC concrete. The limits of durability index values for classification of concrete in terms of durability were reported elsewhere (Alexander and Magee, 1999; Olorunsogo and Padayachee, 2002) and shown in Table 5.8. According to these values the oxygen permeability index of both GP and NC concretes is excellent.

Table 5.8: Ranges of durability indices

Durability class	OPI, log scale	Sorptivity, mm/h$^{1/2}$	Conductivity, mS/cm
Excellent	>10	<6	<0.75
Good	9.5-10	6-10	0.75-1.5
Poor	9.0-9.5	10-15	1.50-2.50
Very poor	<9.0	>15	>2.5

Significantly better water sorptivity was found for NC concrete compare to GP concretes. Water sorptivity of GP concretes falls in the ‘poor’ category, while the sorptivity of NC is good. These results correlate well with the porosity test, showing that the porosity of GP concretes is higher compared to that of NC concrete. It seems that post-curing conditions do not affect the unidirectional absorption of samples.

The chloride conductivity test monitors the diffusion of chloride ions through the concrete sample saturated with a NaCl solution by means of using a voltage potential difference and measuring the electrical current. In general the lower the chloride conductivity value, the more resistant the concrete is. Both GP and NC concretes have similar values of chloride conductivity with slightly lower value for NC concrete. It means that both concretes have similar resistance to chloride ion penetration. The performance of both concretes is good, according to recommended values for durability classification (Olorunsogo and Padayachee,

2002). There is again a correlation between porosity and chloride conductivity value. Higher porosity makes it easier for chloride ions to penetrate the concrete matrix. Overall, durability indices values of AAFA concrete is similar to those for fly ash-OPC, suggesting that service life of structures made from the alkali-activated fly ash concrete should meet modern requirements.

5.4 QUANTIFICATION OF CO_2 EMISSION

Carbon dioxide emissions generated by typical normal strength concrete mixes using Portland cement as the only binder were found to be between 0.29 and 0.32 t CO_2-e per cubic meter of concrete (Flower and Sanjayan, 2007). Previous research showed that the production of geopolymer and alkali-activated concretes could reduce carbon dioxide emission by as much as 44-64 % (McLellan et al., 2011) to only 9 % (Turner and Collins, 2013) compare to Portland cement concrete.

Figure 5.14 presents a concrete CO_2 emissions system diagram in order to show which materials and processes during concrete manufacture contribute to overall carbon dioxide emission.

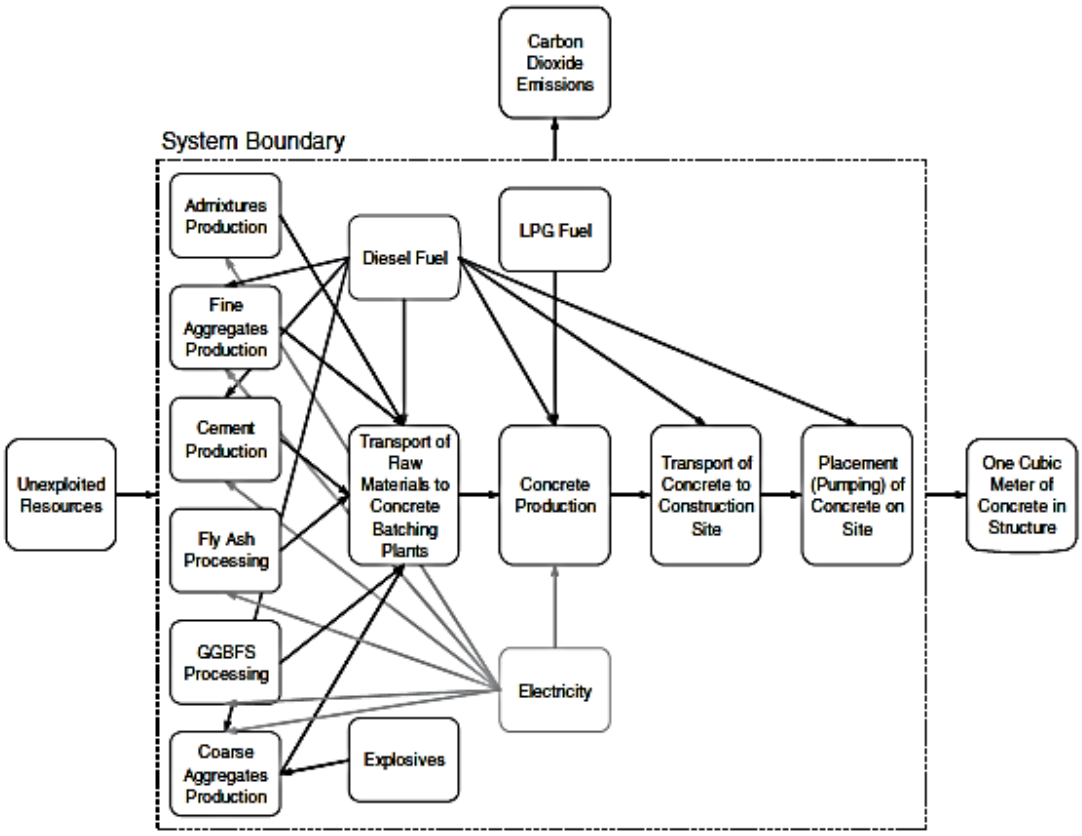

Figure 5.14: Concrete CO_2 emissions system diagram (Flower and Sanjayan, 2007)

In this section basic analysis of CO_2 emissions of alkali-activated fly ash concrete will be discussed. It was stated in previous chapters that alkali-activated fly ash concrete required heat curing in order to get adequate compressive strength in early age. Therefore a comparison of alkali-activated fly ash concrete and OPC concrete for precast technology is reasonable. Steam curing of OPC concrete at 60 °C and atmospheric pressure is usually exploited for precast concrete unit production, which is comparable with curing alkali-activated fly ash concrete at 60 °C. Thus, carbon dioxide emission related to curing of both concretes can be assumed equal and will be excluded from further calculations.

Heath et al. (2014) reported that global warming potential and CO_2-e of geopolymer binders are highly dependent on the mix design. Thus, CO_2-e emissions of raw materials for concrete manufacture will be discussed in details.

Alkali-activated and OPC concretes contain coarse and fine aggregates. CO_2-e emission of aggregates, associated with quarrying and crushing, was estimated in previous studies and are shown in Table 5.9.

Table 5.9: CO_2-e emission from different raw materials, kg/per kg produced material

OPC	Fly ash	Aggregates	NaOH
0.82 (Turner and Collins, 2013)	0.027 (Turner and Collins, 2013)	0.0408 coarse agg.; 0.0139 fine agg. (Turner and Collins, 2013)	1.915 (Turner and Collins, 2013)
0.892 (PPC integrated annual report, 2011)	0.027 (Flower and Sanjayan, 2007)	0.0357 coarse agg. (granite); 0.0459 coarse agg. (basalt); 0.0139 fine agg. (Flower and Sanjayan, 2007)	1.232 (Yang et al., 2013)
0.818 (Wright, 2011)	0.002 (Wright, 2011)	0.0012 (Wright, 2011)	
0.730 (Hasanbeigi et al., 2012)	no CO2 emissions are to be attributed to the ash fraction, since it is recovered from another industrial process (Papa et al., 2014)		

The major difference between both concretes is the binder. The process of cement manufacture consists of quarrying of limestone and clay, crushing and mixing those components, clinkering at 1400-1500 °C in a kiln, clinker grinding, batching of cement. During decomposition of limestone in a kiln 0.5 tonne of CO_2 is released for every tonne of CaO. High-energy consumption of the kiln contributes to overall emission of cement production resulting in emissions of greenhouse gases. There is no CO_2 emission attributed to the fly ash, as it is by-product of electricity production. However, classification, batching and transporting of fly ash require some energy efforts and thus insignificantly contribute to the

CO_2-e emission of concrete. The major contributor of carbon dioxide in alkali activation technology is the alkali itself. The process of making NaOH includes, transporting of brine to the plant, electrolysis and drying. There are three methods used for producing caustic soda, namely diaphragm cell, mercury cathode and membrane cells. Irrespective of the method used during electrolysis from salt water, chlorine and sodium hydroxide co-products are produced in near equivalent amounts (1.1 tonne of sodium hydroxide for every tonne of chlorine produced). Turner and Collins (2013) reported 1.915 tonne of CO_2-e for every tonne of produced NaOH, which is significantly greater than that for Portland cement. Using high alkali dosages in concrete can considerably affect the total CO_2-e emission of alkali-activated fly ash concrete.

Basic calculation of CO_2-e emissions associated with raw materials used for production of one cubic meter of alkali-activated fly ash concrete with mix proportions reported in Chapter 5 earlier, is conducted. An estimation of CO_2-e emissions of the fly ash-OPC blended concrete was not performed due to its different grade in comparison to the AAFA concrete. Compressive strength of the AAFA concrete at 28 days was 45.5 MPa, which corresponds to grade 30 MPa concrete, while the fly ash-OPC blended concrete was 45 MPa grade. New mix proportions of fly ash-OPC blended cement concrete were calculated (see Table 5.9) to produce concrete with grade similar to the AAFA concrete. The same type of aggregates, ratio between coarse and fine aggregate and the same workability as for AAFA concrete were used in the calculations. The new mix proportion of fly ash-OPC blended concrete was used for estimation of CO_2-e emissions associated with production of one cubic meter of concrete.

Table 5.10: Material consumption and an estimation of CO_2-e emission associated with raw materials for concrete production

	Mix proportion of AAFA concrete, kg/m^3	Mix proportion of fly ash-OPC concrete, kg/m^3	CO_2-e emission (from Table 5.9), kg/per kg produced material	CO_2-e emission of raw materials for 1m^3 of AAFA concrete, kg	CO_2-e emission of raw materials for 1m^3 of fly ash-OPC concrete, kg
Fly ash	500	130	0.0270	13.5	3.5
NaOH	58.1	-	1.9150	111.3	-
Coarse aggregate	1078.3	1135	0.0459	49.5	52.1
Fine aggregate	584.3	615	0.0139	8.1	8.5
Cement		310	0.8920	-	276.5
Total CO_2-e, kg/m^3				182.4	340.4

Total CO_2-e emission from raw materials of NaOH-activated fly ash concrete with 9 % Na_2O of fly ash mass is 182.4 kg per m^3 of concrete. Wright (2011) reported CO_2-e per cubic meter of 30 MPa fly ash blended cement concrete is about 270 kg. It can be seen that NaOH contributes more than 60 % of the overall CO_2-e emissions of alkali-activated fly ash

concrete. None the less AAFA concrete with sodium hydroxide activator (9 % Na_2O eq.) has a potential to reduce CO_2-e emissions by 30-40 % in comparison to fly ash-OPC blended concrete of the same grade in precast industry. At the same time it is also necessary to consider the positive effect of utilization high volumes of fly ashes.

5.5 CONCLUSIONS

From the results presented in this chapter the following conclusions can be drawn:

- The trends obtained for AAFA paste are relevant for AAFA concretes;
- With increase in sodium oxide content, the compressive strength of AAFA heat cured concrete increases;
- 12 % sodium oxide in AAFA heat cured concrete lead to higher standard deviation of compressive strength compared to the concrete with 9 % sodium oxide;
- Increasing water to binder solids ratio increases the consistency of AAFA concrete but decreases the compressive strength;
- Sodium oxide content of 9 % of fly ash mass provides sufficient repeatability of compressive strength of heat cured AAFA concrete at all ages;
- AAFA heat cured concrete is stable in water. However, its compressive strength is lower compared to samples cured in dry conditions. 28-day compressive strength of heat cured concrete with 9 % sodium oxide cured in water is 44.8 MPa;
- The compressive strength of heat cured AAFA concrete is affected by age and development of strength continue up to 91 days;
- Flexural strength AAFA heat cured concrete is about 4-5 MPa depending on post-curing environment, which is comparable to flexural strength of similar grade OPC concrete;
- Measured values of elasticity modulus of AAFA heat cured concrete are between 30 and 32 GPa which is lower than that of OPC concretes;
- The Poisson's ratio of AAFA heat cured concrete at 28 days is 0.11 – 0.12, which is similar to OPC and OPC blended cement concretes;

- Shrinkage of AAFA concrete during heat curing in the first 24 hours is about 1500 microstrains, which is significantly lower than the shrinkage of fly ash-OPC blended cement concrete of 2800 microstrains for the same period of time;

- Heat cured AAFA concrete undergo low drying shrinkage of about 350 microstrain after one year, which is significantly lower than that of fly ash-OPC blended cement concrete of 500 microstrains;

- Heat cured AAFA concrete has a low specific creep of 15 microstrain/MPa after one year, which is less than half that of fly-ash-OPC blended cement concrete;

- Exposure of AAFA concrete to sulphuric acid solution results in peeling of sample surfaces, but there was no significant degradation in compressive strength after one year. After one year of exposure in sulphuric acid, it was observed that fly ash-OPC blended cement concrete lost about 15 % of its strength compared to strength of samples cured in water. While AAFA concrete by the same time lost only 1.5 % of the strength compared to strength of samples cured in water. This observation suggests that the resistance of AAFA concrete to acid environments is better than that of fly ash-OPC blended cement concrete;

- Measured oxygen permeability and chloride conductivity suggest that AAFA concrete has excellent resistance to gas diffusion and chloride penetration. However, water sorptivity of AAFA is relatively high due to higher porosity;

- AAFA concrete can be recommended for producing precast concrete units;

- A basic estimation of CO_2-e emissions associated with raw materials used for concrete production show that AAFA with sodium hydroxide activator (9 % Na_2O eq.) has a potential to reduce CO_2-e emissions of precast concrete units by 30-40 % in comparison fly ash-OPC blended concrete of the same grade.

6 CONCLUSIONS AND RECOMMENDATIONS

6.1 INTRODUCTION

Production of electricity in South Africa relies on coal and huge amounts of by-product, such as fly ash, bottom ash, etc. is produced annually during coal combustion. Currently at thermal plants ash is collected and disposed in stockpiles and ash dumps causing environmental concern due to releasing toxic elements into soil and ground water as well as dust pollution. Fly ash is the residue of coal combustion captured by electrostatic precipitators from flue gases. Fly ash consists of fine particles and can be used as a cement extender, filler in a plastics, soil stabilizer, etc. However only about 5 % of all South African fly ash is beneficially used. This thesis provides the basis for developing an alternative application of fly ash, showing that fly ash is not only a waste, but rather underestimated resource. Utilization of fly ash in alkali-activated cements and concretes will help to reduce environmental problems related to ash disposal and conserve natural resources. The study was focused on utilization of fly ash as a raw source for the production of a value added sustainable construction material.

Particle size distribution, chemical and mineralogical composition of fly ashes was evaluated. The experimental study consists of two parts: a study of AAFA pastes and a study of AAFA concrete. In Chapter 4, different factors affecting the mechanical strength of AAFA pastes were investigated and linked to the microstructure and composition of those pastes as characterized by different techniques. The present study and previous research showed that high alkali content negatively affects the material performance and possible reasons for this phenomenon were investigated. Based on pastes experimental results AAFA concrete was cast. Short and long-term concrete performance was evaluated in Chapter 5 and compared, where it was possible to those of fly ash-OPC blended cement concrete and previously published results on AAFA concretes.

6.2 CONCLUSIONS

Different AAFA cement pastes were developed and investigated. The following relationships between investigated parameters and mechanical performance of AAFA pastes were established:

- An increase in Na_2O content results in an increase in compressive strength of alkali-activated fly ash cement. An excessive amount of Na_2O however leads to a decrease

in compressive strength, high standard deviation and efflorescence formation. The optimum alkali content in this research was 9 % Na_2O of fly ash mass.

- Curing of AAFA pastes at ambient temperature was found impractical due to delayed setting, slow strength development, relatively low strength, high strength deviation and efflorescence formation. Elevated temperature curing of AAFA pastes is recommended.

- Elevated temperature curing has a substantial effect on the early strength of AAFA pastes, but an increase in temperature over 60 °C did not noticeably affect 28- and 91-days compressive strength.

- The duration of elevated temperature curing has a more prominent effect on the early strength; however there is no significant increase in early age compressive strength when duration of the curing exceeds 16 hours.

- The compressive strength decreases significantly with an increase in water to binder solids ratio.

- Mineralogical composition of fly ash has a substantial effect on the compressive strength of AAFA pastes. The more amorphous phase in fly ash, the higher the compressive strength is.

- The use of potassium hydroxide as an activator results in the lowest compressive strength, while the presence of soluble silicates favors alkali activation and compressive strength development.

- Increasing amounts of soluble silicate in an activator solution at constant Na_2O leads to an increase in compressive strength only to a certain point, afterwards a strength decrease is observed. The optimal soluble silica oxide content for AAFA paste with respect to 6 and 9 % Na_2O is 3 % of fly ash mass.

XRD analysis of AAFA pastes indicated the major crystalline phases were quartz and mullite identified in initial fly ash. Apart from these phases, thermonatrite (sodium carbonate) and hydroxysodalite, not revealed in initial fly ash, were detected by XRD. The presence of carbonate species suggested that all the alkali was not consumed during the alkali activation process and the excess of alkali led to carbonization and, as a result, formation of efflorescence. The presence of hydroxysodalite was found to be a function of sodium oxide

content. There was no correlation between the presence of hydroxysodalite and the loss in the mechanical performance of AAFA pastes.

ATR-FTIR analysis showed a shift of the main peak in AAFA pastes compare to initial fly ash, assigned to transformation of amorphous phase. ATR-FTIR also confirmed the presence of sodium carbonate found during the XRD analysis.

The morphology of AAFA pastes, investigated by SEM, was found to be affected by concentration of alkaline activator. The microstructure of the pastes with low alkali content appeared friable with the presence of unreacted fly ash particles. AAFA pastes with high alkali content had a more solid and less porous microstructure. Microcracks were also observed in the pastes with high alkali content and solid microstructure. It was assumed that these microcracks might be the reason for the loss in mechanical performance of AAFA pastes as microstructure is known to be closely related to mechanical strength of material. The possible reasons of microcrack formation were investigated.

It was found that the temperature of the paste core increase significantly during elevated temperature curing when the paste to oven volume ratio was 0.0504 and different size moulds, made out of metal and plastic, were used together. Core temperature depended on different parameters and increased with increase in mould size and alkali content. Plastic moulds gave higher core temperature in comparison to metal moulds of the same size. Heat released during alkali activation of the pastes affected the temperature in the oven, increasing it significantly. A slight increase in pastes core temperatures was observed when paste to oven volume ratio was 0.0228 and only single sized moulds made out of plastic were used. However, the oven temperature was not influenced. The high core temperatures cause internal stresses in the pastes due to thermal gradient but also make free water boil. The boiling water produces vapor which build-up pressure inside the material structure inducing additional internal stresses, which could be the reason for the microcracks formation.

It was found that AAFA pastes experience relatively high shrinkage strains during elevated temperature curing and the shrinkage magnitude depends on alkali content. A high early shrinkage value of 4700 microstrains was recorded for 15 % Na_2O paste when a compressive strength was only 1.5 MPa. Tensile stresses due to the shrinkage were higher than the developed strength and microcracks were formed.

High sodium oxide content in AAFA pastes promote internal stresses caused by thermal gradient, internal vapor pressure due to boiling water and high early age shrinkage, which could be the reasons for the microcrack formation and strength decrease as a result.

Trends obtained for AAFA pastes are relevant for AAFA concretes: an increase in Na_2O leads not only to increase in the compressive strength but also to higher strength deviation. An increase of water to binder solids ratio leads to a decrease of compressive strength of AAFA concrete. Repeatable compressive strength of AAFA concrete can be achieved with 9 % Na_2O of fly ash mass.

Short- and long-term engineering properties of AAFA concrete were evaluated and compared to fly ash-OPC concrete (see Table 6.1).

Table 6.1: Comparison of properties of alkali-activated fly ash concrete (GP) and fly ash-Ordinary Portland cement blended concrete (NC)

	GP	NC
Compressive strength at 28 days, MPa	45.5	61.3
Flexural strength at 28 days, MPa	5.8	7.1
Split tensile strength at 28 days, MPa	3.7	4.1
E-value at 28 days, GPa	32.9	43.5
Poisson's ratio	0.11	0.12
Shrinkage at first 24 hours, microstrain	1400	2800
Drying shrinkage after one year, microstrain	360	500
Creep after one year, microstrain	180	600
Water sorptivity, $mm/h^{1/2}$	12.6	8.1
Oxygen permeability index	10.1	10.6
Chloride conductivity, mS/cm	1.44	1.14
Porosity, %	14.9	9.4

The comparison of concrete properties show that AAFA concrete with good mechanical and durability performance comparable to conventional concrete can be produced using fly ash and sodium hydroxide as a binder. Service life of structures made from the alkali-activated fly ash concrete should meet modern requirements.

A basic estimation of CO_2-e emissions associated with raw materials used for concrete production show that AAFA concrete with sodium hydroxide activator (9 % Na_2O eq.) has a potential to reduce CO_2-e emissions of precast concrete units by 30-40 % in comparison to fly ash-OPC blended concrete of the same grade.

6.3 RECOMMENDATIONS

More South African fly ashes need to be tested for use in the production of alkali-activated materials. A comparison of fly ashes from different sources is very important for wide application of alkali-activated materials.

The results of this research show that more attention should be paid to the conditions and process during elevated temperature curing of alkali-activated materials. Heat released during alkali activation increases core temperature of samples causing internal stresses and it might affect oven temperature.

Possible reasons of the flash setting of fly ash mixtures activated with the specific combinations of sodium hydroxide and sodium silicate (i.e. sodium silicates with the specific silica moduli) should be investigated.

More research is needed on the shrinkage behavior of AAFA materials with different activators during elevated temperature curing as extensive shrinkage can lead to early age cracking and result in loss of material performance. The mechanism of early shrinkage should be studied.

An accurate estimation of CO_2-e emissions of local materials used to produce of alkali-activated fly ash and OPC concretes is needed to evaluate ecological compatibility.

7 REFERENCES

Abdul Rahim, R.H. Rahmiati, T. Azizli, K. A. Man, Z. Nuruddin, M.F. Ismail, L., 2015. Comparison of using NaOH and KOH activated fly ash-based geopolymer on the mechanical properties. *Materials Science Forum*, Vol 803, pp 179-184.

Abrams D.A., 1919. *Design of Concrete Mixture*s. Bulletin 1. Structural Materials Research Laboratory. Lewis Institute, Chicago.

Addis, B.J., 1994. *Fulton's concrete technology*. 7th (revised) edition. Portland Cement Institute, Midrand, South Africa.

Akerlöf, G. Kegeles, G., 1939. The density of aqueous solutions of sodium hydroxide. *Journal of the American Chemical Society*, Vol 61, pp 1027-1032.

Al Bakri, M.M. Mohammed, H. Kamarudin, H. Niza, I.K. Zarina, Y., 2011. Review on fly ash-based geopolymer concrete without Portland cement. *Journal of Engineering and Technology Research*, Vol 3(1), pp 1-4.

Aldred, J. Day, J., 2012. Is geopolymer concrete a suitable alternative to traditional concrete? In *Our world in concrete and structures*. Singapore, 29-31 August 2012.

Alexander, M.G. Davis, D.E., 1992. The influence of aggregate on the compresiive strength and elastic modulus of concrete. *Die siviele ingenieur in Suid-Afrika*, May, pp 161-170.

Alexander, M.G., 1994. Deformation and volume change of hardened concrete. In B. J. Addis (ed). *Fulton's concrete technology*, pp 107-152. 7th ed. Portald Cement Institute.

Alexander, M.G. Ballim, Y. Mackechnie, J.R., 1999. *Concrete durability index testing manual*. Department of Civil Engineering, University of Cape Town, University of the Witwatersrand. Research monograph No 4.

Alexander, M.G. Ballim, Y. Stanish, K., 2008. A framework for use of durability indexes in performance-based design and specifications for reinforced concrete structures. *Materials and structures*, Vol 41, pp 921-936.

Alexander, M.G. Magee, B.J., 1999. Durability performance of concrete containing condensed silica fume. *Cement and Concrete Research*, Vol 29, pp 917-922.

Alkan, M. Hopa, Ç. Yilmaz, Z. Güler, H., 2005. The effect of alkali concentration and solid/liquid ratio on the hydrothermal synthesis of zeolite NaA from natural kaolinite. *Microporous and Masoporous Materials* , Vol 86, pp 176-184.

Alonso, S. Palomo, A., 2001a. Alkaline activation of metakaoline and calcium hydroxide mixtures: influence o temperature, activator concentration and solids ratio. *Material Letters*, Vol 47, pp 55-62.

Alonso, S. Palomo, A., 2001b. Calorimetric study of alkaline activation of calcium hydroxide metakaolin solid mixtures, Vol 31, pp 25-30.

Andini, S. Cioffi, R. Colangelo, F. Grieco, T. Montagnaro, F. Santoro, L., 2008. Coal fly ash as raw material for the manufacture of geopolymer-based products. *Waste Management*, Vol 28, pp 416-423.

Ariffin, M.A.M. Hussin, M.W. Bhutta, M.A.R., 2011. Mix design and compressive strength of geopolymer concrete containing blended ash from Agro-industrial wastes. *Advanced materials research*, Vol 339, pp 452-457.

Arioz, E. Arioz, O. Kockar, O.M., 2012. Leaching of F-type fly ash based geopolymers. In *20th International Congress of Chemical and Process Engineering CHISA 2012*. *Procedia Engineering*, Vol 42, pp 1114-1120.

Arjunan, P. Silsbee, M.R. Roy, D.M., 2001. Chemical activation of low calcium fly ash. Part II. Effect of mineralogical composition on alkali activation. In *International Ash Utilization Symposium*, 2001. Center of Applied Energy Research, University of Kentucky.

ASTM C469-02, 2002 Standard test method for static modulus of elasticity and Poisson's ratio of concrete in compression. ASTM International.

Atiş, C.D. Bilim, C. Çelik, Ö. Karahan, O., 2009. Influence of activator on the strength and drying shrinkage of alkali-activated slag mortar. *Construction and Building Materials*, Vol 23, pp 548-555.

Bada, S.O. Potgieter-Vermaak, S., 2008. Evaluation and treatment of coal fly ash for adsorption application. *Leonardo Electronic Journal of Practices and Technologies*, Vol 12, pp 37-48.

Bakharev, T. Sanjayan, J.G. Cheng, Y.-B., 1999. Alkali activation of Australian slag cements. *Cement and Concrete Research*, Vol 29, pp 113-120.

Bakharev, T. Sanjayan, J.G. Cheng, Y.-B., 2001a. Resistance of alkali-activated slag concrete to alkali-aggregate reaction. *Cement and Concrete Research*, Vol 31, pp 331-334.

Bakharev, T. Sanjayan, J.G. Cheng, Y.-B., 2001b. Resistance of alkali-activated slag concrete to carbonation. *Cement and Concrete Research*, Vol 31, pp 1277-1283.

Bakharev, T. Sanjayan, J.G. Cheng, Y.-B., 2003. Resistance of alkali-activated slag concrete to acid attack. *Cement and Concrete Research*, Vol 33, pp 1607-1611.

Bakharev, T., 2005a. Durability of geopolymer materials in sodium and magnesium sulfate solutions. *Cement and Concrete Research*, Vol 35, pp 1233-1246.

Bakharev, T., 2005b. Geopolymeric materials prepared using class F fly ash and elevated temperature curing. *Cement and concrete Research*, Vol 35, pp 1224-1232.

Bakharev, T., 2005c. Resistance of geopolymer materials to acid attack. *Cement and Concrete Research*, Vol 35, pp 658-670.

Bakharev, T., 2006. Thermal behaviour of geopolymers prepared using class F fly ash and elevated temperature curing. *Cement and Concrete Research*, Vol 36, pp 1134-1147.

Barbosa, V.F.F. MacKenzie, K.J.D. Thaumaturgo, C., 2000. Synthesis and characterisation of materials based on inorganic polymers of alumina and silica:sodium polysislate polymers. *International Journal of Inorganic Materials*, Vol 2, pp 309-317.

Bernal, S.A. Provis, J.L., 2014. Durability of alkali-activated materials: Progress and Perspectives. *Journal of the American Ceramic Society*, Vol 94(4), pp 997-1008.

Bernal, S.A. Provis, J.L. Rose, V. de Gutierrez, R.M., 2011. Evolution of binder structure in sodium silicate-activated slag-metakaolin blends. *Cement and concrete Composites*, Vol 33, pp 46-54.

Bernal, S.A. Provis, J.L. Brice, D.G. Kilcullen, A. Duxson, P. van Deventer, J.S.J., 2012. Accelerated carbonation testing of alkali-activated binders significantly underestimates servise life: The role of pore solution chemistry. *Cement and Concrete Research*, Vol 42, pp 1317-1326.

Bernal, S.A. Provis, J.L. Walkley, B. Nicolas, R.S. Gehman, J.D. Brice, D.G. Kilcullen, A.R. Duxson, P. van Deventer, J.S.J., 2013. Gel nanostructure in alkali-activated binders based on slag and fly ash, and effects of accelerated carbonation. *Cement and Concrte Research*, Vol 53, pp 127-144.

Bertolini, L. Elsener, B. Redaelli, E. Polder, R., 2004. Corrosion steel in concrete: Prevention, Diagnosis, Repair. Wiley-VCH Verlag GmbH Co. KGaA, Weinheim, Germany.

Beushausen, H. Alexander, M.G., 2008. The South African durability index tests in an international comparison. *Journal of South African Institution of Civil Engineering*, Vol 50 (1), pp 25-31.

Bosch, G.L. Willis, J.P., 1990. The chemical and mineral compositions, and particle size distribution, of fly ash from three south african stations. In *First national Symposium*, South African Coal Ash Association, May. CSIR, Pretoria, South Africa.

Brough, A.R. Atkinson, A., 2002. Sodium silicate-based, alkali-activated slag mortars Part I. Strength, hydration and microstructure. *Cement and Concrete Research*, Vol 32, pp 865-879.

Carlson, C. Adriano, D., 1993. Environmental impacts of coal combustion residues. *Journal of environmental Quality*, Vol 22(2), pp 227-247.

Chen, W. Brouwers, H.J.H., 2007. The hydration of slag. Part I: Reaction models for alkali-activated slag. *Journal of Material Science*, Vol 42, pp 428-443.

Chi, M., 2012. Effects of dosage of alkali-activated solution and curing conditions on the properties and durability of alkali-activated slag concrete. *Construction and building materials*, Vol 35, pp 240-245.

Chindaprasirt, P. Chareerat, T. Sirivivatnanon, V., 2007. Workability and strength of coarse high calcium fly ash geopolymer. *Cement and Concrete Composites*, Vol 29, pp 224-229.

Criado, M. Fernandez-Jimenez, A. de la Torre, A.G. Aranda, M.A.G. Palomo, A., 2007a. An XRD study of the effect of the SiO_2/Na_2O ratio on the alkali activation of fly ash. *Cement and Concrete Research*, Vol 37, pp 671-679.

Criado, M. Fernandez-Jimenez, A. Palomo, A., 2007b. Alkali activation of fly ash: Effect of the SiO_2/Na_2O ratio. Part I: FTIR study. *Microporous and Mesoporous Materials*, Vol 106 (1-3), pp 180-191.

Criado, M. Fernandez-Jimenez, A. Palomo, A. Sorbados, I. Sanz, J, 2008. Effect of the SiO_2/Na_2O ratio on the alkali activation of fly ash. Part II: ^{29}Si MAS-NMR Survey. *Microporous and Mesoporous materials*, Vol 109, pp 525-534.

Criado, M. Fernandez-Jimenez, A. Palomo, A., 2010. Alkali activation of fly ash. Part III: Effect of curing condition on reaction and its graphical description. *Fuel*, Vol 89, pp 3185-3192.

Davidovits, J., 1976. Process for the fabrication of sintered panels and panels resulting from the application of this process. US Patent 3940470.

Davidovits, J., 1982. Myneral polymers and methods of making them. US Patent 4349386.

Davidovits, J., 1985. Early high-strength mineral polymer. US Patent 4509985.

Davidovits, J., 1988. Geopolymer Chemistry and Properties. In *Geopolymer '88*. Universite de techlogie de compiegne.

Davidovits, J., 1994a. Geopolymers: Man-made rocks geosynthesis and the resulting development of very early high strength cement. Journal of *Materials Education*, Vol 16, pp 91-139.

Davidovits, J., 1994b. Properties of geopolymer cements. In *Proceedings First International Conference on Alkaline cements and concretes*, pp 131-149. Institute of binders and materials, Kiev State Thechnical University, Kiev, Ukraine.

Davidovits, J., 1999. Chemistry of geopolymer systems, terminology. In *Proceedings to Second Internatinal Conference Géopolymère '99*, pp 9-40. June 30 to July 2, 1999, Institut Géopolymère, Saint-Quentin, France.

Davidovits, J., 2005. Geopolymer chemistry and sustainable development. The Poly(sialate) terminology: a very useful and simple model for the promotion and understanding of green chemistry. In *World Congress Geopolymer 2005: Geopolymer, Green Chemistry and Sustainable Development Solutions*, pp 9-15. Institut Géopolymère, Saint-Quentin, France.

Davidovits, J., 2008. Scientific tools, X-rays, FTIR, NMR. In J. Davidovits(ed) *Geopolymer. Chemistry and applications*, pp 61-76. Institut Géopolymère, Saint-Quentin, France.

Deir, E. Gebregziabiher, B.S. Peethamparan, S., 2014. Influence of starting material on the early hydration kinetics, microstructure and composition of binding gel in alkali activated binder systems. *Cement and Concrete Composites*, Vol 48, pp 108-117.

De Silva, P. Sagoe-Crensil, K., 2009. The role of Al_2O_3, SiO_2 and Na_2O on the amorphous to crystalline phase transformation in geopolymer systems. *Journal of the Australian Ceramic Society* , Vol 45(1), pp 63-71.

De Vargas, A.S. Dal Molin, D.C.C. Vilela, A.C.F. da Silva, F.J. Pavão, B. Veit, H., 2011. The effects of Na_2O/SiO_2 molar ratio, curing temperature and age on compressive strength, morphology and microstructure of alkali-activated fly ash-based geopolymers. *Cement and Concrete Composites*, Vol 33, pp 653-660.

Dhir, R.K. Hubbard, F.H. Munday, J.G.L. Jones, M.R. Duerden, S.L., 1988. Contribution of PFA to concrete workability and strength development. *Cement and Concrete Research*, Vol 18(2), pp 277-289.

Diamond, S., 1975. A review of alkali-silica reaction and expansion mechanisms. 1 Alkalies in cements and in concrete pore solutions. *Cement and Concrete Research*, Vol 5, pp 329-346.

Diaz, E.I. Allouche, E.N. Ekhuld, S., 2003. Factors affecting the suitability of fly ash as source material for geopolymers. *Fuel*, Vol 89, pp 992-996.

Diaz-Loya, E.I. Allouche, E.N. Vaidya, S., 2011. Mechanical properties of fly-ash-based geopolymer concrete. *ACI Materials Journal*, Vol 108(3), pp 300-306.

Douglas, E. Bilodeau, A. Brandstetr, J. Malhotra, V.M., 1991. Alkali activated ground granulated blast-furnace slag concrete: preliminary investigation. *Cement and Concrete Research*, Vol 21, pp 101-108.

Duxson, P., Provis, J.L. Lukey, G. Separovic, F. van Deventer, J.S.J., 2005. ^{29}Si NMR Study of structural ordering in aluminosilicate geopolymer gels. *Langmuir*, Vol 21, pp 3028-3036.

Duxson, P., Provis, J.L. Lukey, G Mallicoat, S.W. Kriven, W.M. van Deventer, J.S.J., 2005. Understanding the relationship between geopolymer composition, microstructure and mechanical properties. *Colloids and Surfaces A: Physicochem. Eng. Aspects*, Vol 269, pp 47-58.

Duxson, P., 2006. *The structure and thermal evolution of metakaolin geopolymers*. PhD thesis. Department of Chemical and Biomolecular Engineering, The University of Melbourne.

Duxson, P. Lukey, G.C. van Deventer, J.S.J., 2007a. The thermal evolution of metakaolin geopolymers: Part 2 – Phase stability and structural development. *Journal of Non-crystalline solids*, Vol 353, pp 2186-2200.

Duxson, P. Fernandez-Jimenez, A. Provis, J.L. Lukey, G.C. Palomo, A. van Deventer, J.S.J., 2007b. Geopolymer technology: the current state of the art. *Journal Materials Science*, Vol 42, pp 2917-2933.

Duxson, P. van Deventer, J.S.J., 2009. Commercialization of geopolymers for construction - opportunities and obstacles. In J.L. Provis, J.S.J. van Deventer (eds) *Geopolymers. Structure, processing, properties and industrial application*. *Part III. Applications of geopolymers*, pp 379-400. Woodhead Publishing Limited.

Duxson, P., 2009. Geopolymer precursor design. In J.L. Provis, J.S.J. van Deventer (eds) *Geopolymers. Structure, processing, properties and industrial application*. *Part I. Geopolymer synthesis and characterization*, pp 37-46. Woodhead Publishing Limited.

Eppers, S Müller, C., 2010. The shrinkagee cone method for measuring the autogenous shrinkage - an alternative to the corrugated tube method. In *International RILEM Conference on Use of Superabsorbent Polymers and Other New Additives in Concrete*. Lyngby, Denmark.

EN 197-1, 2000. Cement - Part 1: Composition, specification and conformity criteria for common cements.

Eskom Holdings Ltd, 2011. Key facts about Eskom. *Integrated Report 2011*. Accessed 1 October 2012 <http://financialresults.co.za/2011/eskom_ar2011/profile_key_facts.php>.

Eskom Holding Ltd, n.d. Ash Management in Eskom. Accessed 8 August 2014. <http://www.eskom.co.za/AboutElectricity/FactsFigures/Documents/CO0004AshManagementRev10.pdf>

Eskom Holdings Ltd, 2012. Appendices: Statistical overview. *Integrated Report 2012*. Accessed 4 November 2013 <http://financialresults.co.za/2012/eskom_ar2012/divisional-report/statistical-overview.php>.

Farmer, V.C., 1974. *The infrared spectra of minerals.* Mineralogical Society.

Fernandez-Jimenez, A. Puertas, F., 1997. Alkali-activated slag cements: kinetic studies. *Cement and Concrete Research*, Vol 27(3), pp 359-368.

Fernandez-Jimenez, A. Palomo, J.G. Puertas, F., 1999. Alkali-activated slag mortars: mechanical strength behaviour. *Cement and Concrete Research*, Vol 29, pp 1313-1321.

Fernandez-Jimenez, A. Palomo, A., 2003. Characterization of fly ashes. Potential reactivity as alkaline cements. *Fuel*, Vol 82, pp 2259-2265.

Fernandez-Jimenez, A. Palomo, A., 2005a. Composition and microstructure of alkali activated fly ash binder. Effect of the activator. *Cement and Concrete Research*, Vol 35, pp 1984-1992.

Fernandez-Jimenez, A. Palomo, A., 2005b. Mid-infrared spectroscopic studies of alkali-activated fly ash structure. *Microporous and Mesoporous Materials*, Vol 86, pp 207-214.

Fernandez-Jimenez, A. Palomo, A. Criado, M., 2005c. Microstructure development of alkali-activated fly ash cement: a descriptive model. *Cement and Concrete Research*, Vol 35, pp 1204-1209.

Fernandez-Jimenez, A. de la Torre A.G. Palomo, A. Lopez-Olmo, G. Alonso, M.M. Aranda, M.A.G., 2006a. Quantitative determination of phases in the alkaline activation of fly ash. Part II: Degree of reaction. *Fuel*, Vol 85, pp 1960-1969.

Fernandez-Jimenez, A. Palomo, A. Sorbados, I. Sanz, J., 2006b. The role played by the reactive alumina content in the alkaline activation of fly ashes. *Microporous and Mesoporous Materials*, Vol 91, pp 111-119.

Fernandez-Jimenez, A. Garcia-Lodeiro, I. Palomo, A., 2007. Durability of alkali-activated fly ash cementitious materials. *Journal Material Science*, Vol 42, pp 3055-3065.

Fernandez-Jimenez, A. Garcia-Lodeiro, I. Blanco, M. Palomo, A., 2008. FTIR study of the sol-gel synthesis of cementitious gel: C-S-H and N-A-S-H. *Journal of Sol-Gel Science Thechology*, Vol 45, pp 63-72.

Fernandez-Jimenez, A. Palomo, A., 2009. Chemical durability of geopolymers. In J.L. Provis, J.S.J. van Deventer (eds). *Geopolymers. Structure, processing, properties and industrial application. Part II. Manufacture and properties of geopolymers*, pp 167-190. Woodhead Publishing Limited.

Fraay, A.L.A. Bijen, J.M. de Haan, Y.M., 1989. The reaction of fly ash in concrete. A critical examination. *Cement and Concrete Research*, Vol 19, pp 235-246.

Flower, D.J.M. Sanjayan, J.G., 2007. Green house gas emissions due to concrete manufacture. *The International Journal of Life Cycle Assessment*, Vol 12(5), pp 282-288.

Gervais, F. Blin, A. Massiot, D. Coutures, J.P., 1987. Infrared reflectivity spectroscopy of silicate glasses. *Journal of Non-Crystalline Solids*, Vol 89, pp 384-401.

Ghosh, S.N., 1978. Infra-red spectra of some selected minerals, rocks and products. *Journal of Materials Science*, Vol 13, pp 1877-1886.

Glukhovsky, V.D., 1959. *Soil Silicates (in Russian)*. The state publishing house of literature on construction and architecture, Kiev.

Glukhovsky, V.D. Pakhomov, V.A., 1978. *Alkali-slag cement and concretes (in Russian)*. Budivelnik, Kiev.

Gokhale, C., 2001. *The immobilisation of organic waste by geopolymerisation*. MSc(Ing) Thesis. University of Stellenbosch, Stellenbosch.

Görhan, G. Kürklü, G, 2014. The influence of the NaOH solution on the properties of the fly ash-based geopolymer mortar cured at different temperatures. *Composites: Part B*, Vol 58, pp 371-377.

Gourley, J.T. Johnson, G.B., 2005. Developments in geopolymer precast concrete. In *World Congress Geopolymer. Geopolymer, Green Chemistry and Sustainable Development Solutions*, 2005. Institut Géopolymère, Saint-Quentin, France.

Guo, X. Shi, H. Dick, W.A., 2010a. Compressive strength and microstructural characteristics of class C fly ash geopolymer. *Cement and Concrete Composites*, Vol 32, pp 142-147.

Guo, X. Shi, H. Cheng, L. Dick, W.A., 2010b. Alkali-activated complex binders from class C fly ash and Ca-containing admixtures. *Journal of Hazardous Materials*, Vol 173(1-3), pp 480-486.

Hardjito, D. Rangan, B.V., 2005. *Development and properties of low-calcium fly ash-based geopolymer concrete*. Research Report GC 1. Faculty of Engineering, Curtin University of Technology, Perth, Australia.

Hasanbeigi, A. Price, L. Lin, E., 2012. Emerging energy-efficiency and CO_2 emission-reduction technologies for cement and concrete production: A technical review. *Renewable and Sustainable Energy Reviews*, Vol 16, pp 6220-6238.

Heah, C.Y. Kamarudin, H. Mustafa Al Bakri, A.M. Bnhussain, M. Lugman, M. Nizar, K. Ruzaidi, C.M. Liew, Y.M., 2013. Kaolin-based geopolymers with various NaOH concentration. *International Journal of Minerals, Metallurgy and Materials*, Vol 20(3), pp 313-322.

Heath, A. Paine, K. McManus, M., 2014. Minimising the global warming potential of clay based geopolymers. *Journal of Cleaner Production*, Vol 78, pp 75-83.

Henmi, T., 1987. Synthesis of hydroxy-sodalite (‘zeolite’) from waste coal ash. *Soil Science and Plant Nutrition*, Vol 33(3), pp 517-521.

Hole, D., 2009. *The mix design development of geopolymer concrete under ambient curing conditions*. Civil Engineering Project 461 and 462. Department of Civil Engineering Curtin University of Technology, Perth.

Ilia, I.K. Stamatakis, M.G. Perraki, T.S., 2009. Mineralogy and tecnical properties of clayey diatomites from north and central Greece. *Central European Journal of Geosciences,* Vol 1(4), pp 393-403.

Jonker, A., 2006. *Insulating refractory materials from inorganic waste resourses.* PhD Thesis. Department of Chemistry, Tshwane University of Technology, Pretoria.

Kani, E.N. Allahverdi, A. Provis, J.L., 2011. Efflorescence control in geopolymer binder based on natural pozzolan. *Cement and Concrete Composites*, Vol 34(1), pp 25-33.

Katz, A., 1998. Microscopic study of alkali-activation fly ash. *Cement and Concrete Research*, Vol 28(2), pp 197-208.

Kearsley, E.P. Wainwright, P.J., 2003. The effect of fly ash properties on concrete strength. *Journal of the South African Institution of Civil Engineering*, Vol 45(1), pp 19-24.

Khale, D. Chaudhary, R., 2007. Mechanism of geopolymerization and factors influencing its development: a review. *Journal Materials Science*, Vol 42, pp 729-746.

Komljenović, M. Baščarević, Z. Bradić, V., 2010. Mechanical and microstructural properties of alkali-activated fly ash geopolymers. *Journal of Hazardous Materials*, Vol 181, pp 35-42.

Kong, D.L.Y. Sanjayan, J.G. Sagoe-Crentsil, K., 2007. Comparative performance of geopolymers made with metakaolin and fly ash after exposure to elevated temperatures. *Cement and Concrete Research*, Vol 37, pp 1583-1589.

Kong, D.L.Y. Sanjayan, J.G., 2008. Damage behavior of geopolymer composites exposed to elevated temperatures. *Cement and Concrete Composites*, Vol 30, pp 986-991.

Kong, D.L.Y. Sanjayan, J.G., 2010. Effect of elevated temperatures on geopolymer paste, mortar and concrete. *Cement and Concrete Research*, Vol 40, pp 334-339.

Korneev, V.I. Danilov, V.V., 1996. *Liquid and soluble glass (in Russian)*. Stroizdat SPb, Saint Petersburg.

Kovalchuk, G. Fernandez-Jimenez, A. Palomo, A., 2007. Alkali-activated fly ash: Effect of thermal curing conditions on mechanical and microstructural development - Part II. *Fuel*, Vol 86(3), pp 315-322.

Krizan, D. Zivanovic, B., 2002. Effects of dosage and modulus of water glass on early hydration of alkali-slag cements. *Cement and Concrete Research*, Vol 32, pp 1181-1188.

Krüger, J., 2003. *South African fly ash: a cement extender*. The South African Coal Ash Association.

Kruger, R. A. Krueger, J. E., 2005. Historical development of coal ash utilization in South Africa. In *Proceedings to World of Coal Ash (WOCA) Conference*. Lexington, Kentucky, USA.

Kumar, S. Kumar R., 2011. Mechanical activation of fly ash: Effect on reaction, structure and properties of resulting geopolymer. *Ceramics International*, Vol 37, pp 533-541.

Lancellotti, I. Catauro, M. Ponzoni, C. Bollino, F. Leonelli, C., 2013. Inorganic polymers from alkali activation of metakaoline: Effect of setting and curing on structure. *Journal of Solid State Chemistry*, 200, Vol 200, pp 341-348.

Langan, B.W. Weng, K. Ward, M.A., 2002. Effect of silica fume and fly ash on heat of hydration of Portland cement. *Cement and Concrete Research*, Vol 32, pp 1045-1051.

Lazarev, A.I. Kharlamov, I.I. Yakovlev, P.Y. Yakovleva, E.F., 1976. *Spravochnik khimika analitika (Hadbook of chemist-analyst)* (In Russian). Metallurgiya.

Lee, W.K.W. van Deventer, J.S.J., 2002. The effect of ionic contaminants on the early-age properties of alkali-activated fly ash-based cements. *Cement and Concrete Research*, Vol 32, pp 577-584.

Lee, W.K.W van Deventer, J.S.J., 2003. Use of infrared spectroscopy to study geopolymerization of heterogeneous amourphous aluminosilicates. *Langmuir*, Vol 19, pp 8726-8734.

Lemougna, P.N. MacKenzie, K.J.D. Chinje Melo, U.F., 2011. Synthesis and thermal properties of inorganic polymers (geopolymers) for structural and refractory applications from volcanic ash. *Ceramics International*, Vol 37, pp 3011-3018.

Li, K.-L. Huang, G.-H. Chen, J. Wang, D. Tang, X.-S., 2005. Early mechanical property and durability of geopolymer. In *World Congrees Geopolymer. Geopolymer, green chemistry and sustainable development solutions*, pp 117-21. Institut Géopolymère, Saint-Quentin, France.

Li, X. Ma, X. Zhang, S. Zheng, E., 2013. Mechanical properties and microstructure of class C fly ash-based geopolymer paste and mortar. *Materials*, Vol 6, pp 1485-1495.

Li C. Sun, H. Li, L., 2010. A review: The comparison between alkali-activated slag (Si+Ca) and metakaolin (Si+Al) cements. *Cement and Concrete Research*, Vol 40, pp 1341-1349.

Lloyd, R.R., 2009. Accelerated ageing of geopolymers. In J.L. Provis, J.S.J. van Deventer, (eds). *Geopolymers. Structure, processing, properties and industrial application*. *Part II. Manufacture and properties of geopolymers*, pp 139-164. Woodhead Publishung Limited.

Lloyd, R.R. Provis, J.L. van Deventer, J.S.J., 2012. Acid resistance of inorganic polymer binders. 1. Corrosion rate. *Materials and structures*, Vol 45(1-2), pp 1-14.

Ma, Y. Hu, J. Ye, G., 2012. The effect of activating solution on the mechanical strength, reaction rate, mineralogy, and microstructure of alkali-activated fly ash. *Journal of Material Science*, Vol 47, pp 4568-4578.

Mahasenan, N. Smith, S. Humphreys, K., 2003. The cement industry and global climate change: current and potential future cement industry CO2 emissions. In J. Gale, Y. Kaya (eds). *Greenhouse Gas Control Technologies*, Volume II, pp 995-1000. Published by Elsevier Science Ltd.

Mandal, S. Pal, S., 2012. Thermal activation effect on fly ash based geopolymer concrete. In *Concrete in the low carbon era. Proceedings of the international conference*. University of Dundee, Scotland, UK, 9-11 July 2012.

Matjie, R.H., Ginster, M. van Alphen, C. Sobiecki, A., 2005. Detailed characterisation of Sasol ashes. In *World of Coal Ash (WOCA)*. Lexington, Kentucky, USA, April 11-15, 2005.

McLellan, B.C. Williams, R.P. Lay, J. Riessen, A. Corder, G.D., 2011. Costs and carbon emissions for geopolymer pastes in comparnison to ordinary portland cement. *Journal of Cleaner Production*. Vol 19, pp 1080-1090.

Miller, F.A. Wilkins, C.H., 1952. Infrared spectra and characteristic frequencies of inorganic ions. Their use in qualitative analysis. *Analytical chemistry*, Vol 24(8), pp 1253-1294.

Miranda, J.M. Fernandez-Jimenez, A. Gonzalez, J.A. Palomo, A., 2005. Corrosion resistance in activated fly ash mortars. *Cement and Concrete Research*, Vol 35, pp 1210-1217.

Morris, J. Hodges, S., 2005. Corrosion of metals in fly ash-based geopolymers. In *World Congress Geopolymer. Geopolymer, green chemistry and sustainable development solutions*, pp 51-57. Institut Géopolymère, Saint-Quentin, France.

Muñiz-Villarreal, M.S. Manzano-Ramirez, A. Sampieri-Bulbarela, S. Gasca-Tirado, J. Reyes-Araiza, J.L. Rubio-Avalos, J.C. Perez-Bueno, J.J. Apatiga, L.M. Zaldivar-Cadena, A. Amigo-Borras, V., 2011. The effect of temperature on the geopolymerization process of a metakaolin-based geopolymer. *Materials Letters*, Vol 65, pp 995-998.

Muntingh, Y., 2006. *Durability and diffusive behaviour evaluation of geopolymeric material*. M.Sc.Eng. (Chem) thesis. Department of Process Engineering, University of Stellenbosch, Stellenbosch.

Nuruddin, M.F. Samuel, D. Shafig, N., 2012. An experimental study of curing temperatures on workability characteristics and compressive strength of self-compacting geopolymer concretes. In *Concrete in the low carbon era. Proceedings of the international conference.* University of Dundee, Scotland, UK, 9-11 July 2012.

Oh, J.E. Moon, J. Oh, S.-G. Clark, S.M. Monteiro, P.J.M., 2012. Microstructural and compositional change of NaOH-activated high calcium fly ash by incorporating Na-aluminate and co-existence of geopolymeric gel and C-S-H (I). *Cement and Concrete Research*, Vol 42, pp 673-685.

Olorunsogo, F.T. Padayachee, N., 2002. Performance of recycled aggregate concrete monitored by durability indexes. *Cement and concrete Research*, Vol 32, pp 179-185.

Pacheco-Torgal, F. Moura, D. Ding, Y. Jalali, S., 2011. Composition, strength and workability of alkali-activated metakaolin based mortars. *Construction and Building Materials*, Vol 25, pp 3732-3745.

Pacheco-Torgal, F. Abdollahnejad, Z. Camoes, A.F. Jamshidi, M. Ding, Y., 2012. Durability of alkali-activated binders: A clear advantage over Portland cement or an unproven issue? *Conctruction and Building Materials*, Vol 30, pp 400-405.

Pachego-Torgal, F. Castro-Gomes, J. Jalali, S., 2008a. Alkali-activated binders: A review. Part 1. Historical background, terminology, reaction mechanisms and hydration products. *Construction and Building Materials*, Vol 22, pp 1305-1314.

Pachego-Torgal, F. Castro-Gomes, J. Jalali, S., 2008b. Alkali-activated binders: A review. Part 2. About materials and binders manufacture. *Construction and Building Materials*, Vol 22, pp 1315-1322.

Palomo, A. Grutzeck, Blanko, M.T., 1999a. Alkali activated fly ashes: A cement for the future. *Cement and Concrete Research*, Vol 29, pp 1323-1329.

Palomo, A. Blanco-Varela, M.T. Granizo, M.L. Puertas, F. Vazquez, T. Grutzeck, M.W., 1999b. Chemical stability of cementitious materials based on metakaolin. *Cement and Concrete Research*, Vol 29, pp 997-1004.

Panias, D. Giannopoulou, I.P., 2006. Development of inorganic polymeric materials based on fired coal fly ash. *Acta Metallurgica Slovaca*, Vol 12, pp 321-327.

Panias, D. Giannopoulou, I.P. Perraki, T., 2007. Effect of synthesis parameters on the mechanical properties of fly ash-based geopolymers. *Colloids and Surfaces A: Physicochem. Eng. Aspects*, Vol 301, pp 246-254.

'PPC Integrated Annual report, 2011' Accessed 3 June 2013 <http//www.ppc.co.za>.

Provis, J.L. Lukey, G.C. van Deventer, J.S.J., 2005. Do geopolymers actually contain nanocrystalline zeolites? A reexamination of existing results. *Chemistry of Materials*, Vol 17, pp 3075-3085.

Provis, J.L. van Deventer, J.S.J., 2007. Geopolymerisation kinetics. 2. Reaction kinetic modelling. *Chemical Engineering Science*, Vol 62, pp 2318-2329.

Provis, J.L., 2009. Activating solution chemistry for geopolymers. In J.L. Provis, J.S.J. van Deventer (eds) *Geopolymers. Structure, processing, properties and industrial application. Part I. Geopolymer synthesis and characterization*, pp 50-71. Woodhead publishing limited.

Puertas, F. Palomo, A. Fernandez-Jimenez, A. Izquierdo, J.D. Granizo, M.L., 2003. Effect of superplasticisers on the behavior and properties of alkaline cements. *Advances in Cement Research*, Vol 15(1), pp 23-28.

Puertas, F. Torres-Carrasco, M., 2014. Use of glass waste as an activator in the preparation of alkali-activated slag. Mechanical strength and paste characterization. *Cement and Concrete Research*, Vol 57, pp 95-104.

Purdon, A.O., 1940. The action of alkalis on blast furnace slag. *Journul of the Society of chemical Industry*, pp 191-202.

Rahier, H. van Mele, B., 1996. Low-temperature synthesized aluminosilicate glasses. Part I. Low-temperature reaction stoichiometry and structure of a model compound. *Journal of Material Sciences*, Vol 31, pp 71-79.

Rahier, H. Simons, W. van Mele, B. Biesemans, M., 1997. Low-temperature synthesized aluminosilicate glasses. Part III Influence of the composition of the silicate solution on production, stucture and properties. *Journal of Materials Science*, Vol 32, pp 2237-2247.

Rahier, H. Denayer, J.F. van Mele, B., 2003. Low-temperature synthezed aluminosilicate glasses. Part IV Modulated DSC study on the effect of particle size of metakaolinite on the production of inorganic polymer glasses. *Journal of Materials Science*, Vol 38, pp 3131-3136.

Ramachandran, V.S., 2002. Supplementary cementing materials and other additions. In V.S. Ramachandran, R.M. Paroli, J.J. Beaudoin, A.H. Delgado (eds). *Handbook of thermal analysis of construction materials*, pp 293-353. William Andrew Publishing.

Rangan, B.V. Hardjito, D. Wallah, S.E. Sumajouw, D.M.J., 2005. Studies on fly ash-based geopolymer concrete. In *World Congress Geopolymer. Geopolyemr, green chemistry and sustainable development solutions*, pp 133-139. Institut Géopolymère, Saint-Quentin, France.

Rangan, B.V., 2008. Fly ash-based geopolymer concrete. Research Report GC 4. Faculty of Engineering, Curtin University of Technogy, Perth, Australia.

Rangan, B.V., 2009. Engineering properties of geopolymer concrete. In J.L. Provis, J.S.J. van Deventer (eds) *Geopolymers. Structure, processing, propertis and industrial application. Part II. Manufacture and properties of geopolymers*, pp 139-167. Woodhead Publishing Limited.

Rashad, A.M. Zeedan, S.R., 2011. The effect of activator concentration on the residual strength of alkali-activated fly ash pastes subjected to thermal load. *Construction and Building Materials*, Vol 25, pp 3098-3107.

Rattanasak, U. Chindaprasit, P., 2009. Influence of NaOH solution on the synthesis of fly ash geopolymer. *Minerals Engineering*, Vol 22, pp 1073-1078.

Ravikumar, D. Peethamparan, S. Neithalath, N., 2010. Structure and strength of NaOH activated concretes containing fly ash of GGBFS as the sole binder. *Cement and Concrete Composites*, Vol 30, pp 399-410.

Rickard, W.D.A. Williams, R. Temuujin, J. van Riessen, A., 2011. Assessing the suitability of three Australian fly ashes as an aluminosilicates source for geopolymers in high temperature applications. *Materials Science and Engineering*, Vol 528, pp 3390-3397.

Rocla Pty Ltd, 2011. Greener Graves: Rocla's Latest Innovation Aims Six Feet Under. Accessed 11 January 2013 < http://www.rocla.com.au/News.php?page=3>.

Rovnaník, P., 2010. Effect of curing temperature on the development of hard structure of metakaolin-based geopolymer. *Construction and Building Materials*, Vol 24, pp 1176-1183.

Rowles, M.R., 2004. *The structural nature of aluminosilicate inorganic polymers: a macro to nanoscale study*. PhD thesis. Faculty of Science, Department of Applied Physics, Curtin University of Technology.

Roy, D.M. Jiang, W. Silsbee, M.R., 2000. Chloride diffusion in ordinary, blended, and alkali-activated cement pastes ans its relation to other properties. *Cement and Concrete Research*, Vol 30, pp 1879-1884.

Sagoe-Crentsil, K. Brown, T. Taylor, A., 2013. Drying shrinkage and creep performance of geopolymer concrete. *Journal of sustainable cement-based materials*, Vol 2(1), pp 35-42.

Saikia, B.J. Parthasarathy, G. Sarmah, N.C., 2008. Fourier transform infrared spectroscopic estimation of crystallinity in SiO_2 based rocks. *Bulletin of Mateials Science*,Vol 31(5), pp 775-779.

SANS 50196-1:2006. Methods of testing cement. Part 1: Determination of strength. SABS, Pretoria.

SANS 50197-1:2000. Cement. Part 1: Composition, specifications and conformity criteria for common cements. SABS, Pretoria.

SANS 50450-1:2014. Fly ash for concrete. Part 1: Definition, specifications and conformity criteria. SABS, Pretoria.

SANS 5863:2006. Concrete tests – Compressive strength of hardened concrete. SABS, Pretoria.

SANS 5864:2006. Concrete tests – Flexural strength of hardened concrete. SABS, Pretoria.

SANS 6253:2006. Concrete tests – Tensile splitting strength of concrete. SABS, Pretoria.

SANS 516-2:2009. Concrete durability index testing. Part 2: Oxygen permeability test. Draft. SABS, Pretoria.

SANS 516-3:2009. Concrete durability index testing. Part 3: Water sorptivity test. Draft. SABS, Pretoria.

SANS 516-4:2009. Concrete durability index testing. Part 4: Chloride conductivity and porosity tests. Draft. SABS, Pretoria.

Schroeder, R.A. Lyons, L.L., 1966. Infra-red spectra of the crystalline inorganic aluminates. *Journal of Inorganic and Nuclear Chemistry*, Vol 28, pp 1155-1163.

Shuttleworth, L.S., 1995. *Factors influencing the reactivity of fly ash in the synthesis of mineral polymers*. Ms. Scien.(Geol) thesis. Faculty of Science, University of Witwatersrand, Johannesburg.

Škvára, F. Šlosar, J. Bohunek, J. Markova, A., 2003. Alkali-activated fly ash geopolymeric materials. In *11 th International Congress on the Chemistry of Cement*. Durban, South Africa.

Škvára, F. Kopecky, L. Šmilauer, V. Bittnar, Z., 2009. Material and structural characterization of alkali activated low-calcium brown coal fly ash. *Journal of Hazardous Materials*, Vol 168, pp 711-720.

Somna, K. Jaturapitakkul, C. Kajitvichyanukul, P. Chindaprasirt, P., 2011. NaOH-activated ground fly ash geopolymer cured at ambient temperature. *Fuel*, Vol 90, pp 2118-2124.

Song, X., 2007. Development and performance of class F fly ash based geopolymer concretes against sulphuric acid attack. PhD thesis. The University of New South Wales, Sydney.

Steveson, M. Sagoe-Crentsil, K., 2005a. Relationships between composition, structure and strength of inorganic polymers. Part I. Metakaolin-derived inorganic polymers. *Journal of Materials Science*, Vol 40, pp 2023-2036.

Steveson, M. Sagoe-Crentsil, K., 2005b. Relationships between composition, structure and strength of inorganic polymers. Part 2: Fly ash-derived inorganic polymers. *Journal Materials Science*, Vol 40, pp 4247-4259.

Swanepoel, J.S., 2001. *Utilisation of fly ash and brine in a geopolymeric material*. M. Sc. thesis. Faculty of Natural and Agricultural Sciences, University of Pretoria, Pretoria.

Swanepoel, J.C. Strydom, C.A., 2002. Utilisation of fly ash in a geopolymeric material. *Applied Geochemistry*, Vol 17, pp 1143-1148.

Talling, B. Krivenko, P., 1996. Blast furnace slag-the ultimate binder. In S. Chandra (ed.) *Waste materials used in concrete manufacturing*, pp 235-283. Noyes Publications, Technology & Engineering.

Temuujin, J. van Riessen, A., 2009. Effect of fly ash preliminary calcination on the properties of geopolymer. *Journal of Hazardous Materials*, Vol 164, pp 634-639.

Turner, L.K. Collins, F.G., 2013. Carbon dioxide equivalen (CO_2-e) emissions: A comparison between geopolymer and OPC cement concrete. *Construction and Building Materials*, Vol 43, pp 125-130.

Uchino, T. Sakka, T. Hotta, K. Iwasaki, M., 1989. Attenuated total reflectrance Fourier-Transform infrared spectra of a hydrated sodium silicate glass. *Journal of American Ceramic Society*, Vol 72(11), pp 2173-2175.

Unated States Environmental Protection Agency, 2009. *TVA Kingston Fly ash Release*. Pollution Report #7. Acsessed 21 November 2014 <http://www.epaosc.org/site/polrep_profile.aspx?site_id=4642>.

Van Deventer, J.S.J. Provis, J.L. Duxson, P., 2012. Technical and commercial progress in the adoption of geopolymer cement. *Minerals Engineering*, Vol 29, pp 89-104.

Van Deventer, J.S.J. Provis, J.L. Duxson, P. Brice, D.G., 2010. Chemical Research and Climate Change as Drivers in the Commercial Adoption of Alkali-Activated Materials. *Waste Biomass Valorisation*, Vol 1, pp 145-155.

Van Jaarsveld, J.G.S. van Deventer, J.S.J. Lorenzen, L., 1996. The potential use of geopolymeric material to immobilise toxic metals: Part I. Theory and applications. *Minerals Engineering*, Vol 10(7), pp 659-669.

Van Jaarsveld, J.G.S. van Deventer, J.S.J., 1999a. Effect of the alkali metal activator on the properties of fly ash-based geopolymers. *Industrial and Engineering Chemistry Research*, Vol 38, pp 3932-3941.

Van Jaarsveld, J.G.S. van Deventer, J.S.J. Schwartzman, A., 1999b. The potential use of geopolymeric materials to immobilise toxic metals: Part II. Material and leaching characteristics. *Minerals Engineering*, Vol 12(1), pp 75-91.

Van Jaarsveld, J.G.S. van Deventer, J.S.J. Lukey, G.C., 2003. The characterisation of source materials in fly ash-based geopolymers. *Materials Letters*, Vol 57, pp 1272-1280.

Van Jaarsveld, J.G.S. van Deventer, J.S.J. Lukey, G.C., 2002. The effect of composition and temperature on the properties of fly ash- and kaolinite-based geopolymers. *Chemical Engineering Journal*, Vol 89, pp 63-73.

Verdolotti, L. Iannace, S. Lavorgna, M. Lamanna, R., 2008. Geopolymerization reaction to consolidate incoherent pozzolanic soil. *Journal of Materials Science*, Vol 43, pp 865-873.

Voll, D. Angerer, P. Schneider, H., 2002. A new assignment of IR vibrational modes in mullite. *Vibrational Spectroscopy*, Vol 30, pp 237-343.

Wagners Concrete Pty Ltd, 2012. Wagners EFC set new standard: The Global Change Institute Building, from 22 of May 2012. Accessed 29 April 2013 <http://www.wagner.com.au/news>.

Wallah, S.E. Hardjito, D. Sumajouw, D.M.J. Rangan, B.V., 2005. Performance of fly ash-based geopolymer concrete under sulphate and acid exposure. In *World Congress Geopolymer. Geopolymer, green chemistry and sustainable development solutions*, pp 153-157. Institut Géopolymère, Saint-Quentin, France.

Wallah, S.E. Rangan B.V., 2006. *Low-calcium fly ash-based geopolymer concrete: long-term properties*. Research Report GC 2. Faculty of Engineering, Curtin University of Technogy, Perth, Australia.

Wang, S.D. Scrivener, K.L. Pratt, P.L., 1994. Factors affecting the strength of alkali-activated slag. *Cement and Concrete Research*, Vol 24(6), pp 1033-1043.

Wang, S.D. Scrivener, K.L., 1995. Hydration products of alkali activated slag cement. *Cement and Concrete Research*, Vol 25(3), pp 561-571.

Wang, M.-R. Jia, D.-C. He, P.-G. Zhou, Y., 2011. Microstructural and mechanical characterization of fly ash cenosphere/metakaolin-based geopolymeric composites. *Ceramics International*, Vol 37, pp 1661-1666.

Wang, J. Wu, X.-I. Wang, J.-X. Liu, C.-Z. Lai, Y.-M. Hong, Z.-K. Zheng, J.-P., 2012. Hydrothermal synthesis and characterization of alkali-activated slag - fly ash - metakaolin cementitious materials. *Microporous and Mesoporous Materials*, Vol 155, pp 186-191.

Winnenfeld, F. Leemann, A. Lucuk, M. Svoboda, P. Neuroth, M., 2010. Assessment of phase formation in alkali activated low and high calcium fly ashes in building materials. *Construction and Building Materials*, Vol 24, pp 1086-1093.

www.afrisam.co.za, 2014. 'The Afrisam Technical Reference Guide' Accessed 31 August 2014. http://www.afrisam.co.za/for-professionals/technical-reference-guide/.

www.dow.com, 2014. 'Densities of pure (salt free) caustic soda solutions at various temperatures and concentrations' Accessed 2 May 2014. <http://www.dow.com/causticsoda/offer/physical.htm>.

www.perkinelmer.com, 2014. 'FT-IR Spectroscopy Attenuated Total Reflectance (ATR)' Accessed 4 February 2014.<http://www.utsc.utoronto.ca/~traceslab/ATR_FTIR.pdf>.

Xu, A., 1996. Fly ash in concrete. In S. Chandra (ed) *Waste materials used in concrete manufacture*, pp.142-75. . Noyes Publications, Technology & Engineering.

Xu, H. van Deventer, J.S.J., 2000. The geopolymerisation of alumino-silicate minerals. *International Journal of Mineral Processing*, Vol 59, pp 247-266.

Xu, H. Provis, J.L.van Deventer, J.S.J. Krivenko, P.V., 2008. Characterization of aged slag concretes. *ACI Materials journal*, Vol 105(2), pp 131-139.

Yang, K.-H. Song, J.-K. Song, K.-I., 2013. Assessment of CO_2 reduction of alkali-activated concrete. *Journal of Cleaner Production*, Vol 39, pp 265-272.

Yip, C.K. Provis, J.L. Lukey, G.C. van Deventer, J.S.J., 2008. Carbonate mineral addition to metakaolin-based geopolymers. *Cement and Concrete Composites*, Vol 30, pp 979-985.

Zaharaki, D. Komnitas, K. Perdikatsis, V., 2010. Use of analytical techniques for identification of inorganic polymer gel composition. *Journal of Materials Sciences*, Vol 45, pp 2715-2724.

Zeobond Pty Ltd, n.d. R&D E-Crete™ Plant. Accessed 3 December 2012 <http://www.zeobond.com/projects-rd-e-crete.html>

Zhang M. El-Korchi, T. Zhabg, G. Liang, J. Tao, M., 2014. Synthesis factors affecting mechanical properties, microstructure and chemical composition of red mud-fly ash based geopolymers. *Fuel*, Vol 134, pp 315-325.

Zhang, Y.-S. Sun, W. Li, Z.-J., 2009. Preparation and microstructure characterization of poly-sialate-disiloxo type of geopolymeric cement. *Journal of Central South University of Technology*, Vol 16, pp 906-913.

Zhang, Z. Wang, H. Provis, J.L., 2012a. Quantitative study of the reactivity of fly ash in geopolymerization by FTIR. *Journal of sustainable cement-based material*, Vol 1(4), pp 154-166.

Zhang, Z. Wang, H. Provis, J.L. Bullen, F. Reid, A. Zhu, Y., 2012b. Quantitative kinetic and structural analysis of geopolymers. Part 1. The activation of metakaolin with sodium hydroxide. *Thermochimica Acta*, Vol 539, pp 23-33.

Zhang, Z. Provis, J.L. Wang, H. Bullen, F. Reid, A., 2013. Quantitative kinetic and structural analysis of geopolymers. Part 2. Thermodynamics of sodium silicate activation of metakaolin. *Thermochimica Acta*, Vol 565, pp 163-171.

Zhang, Z. Wang, H. Zhu, Y. Reid, A. Provis, J.L., 2014. Using fly ash to pertially substitute metakaolin in geopolymer synthesis. *Applied Clay Science*, Vol 88-89, pp 194-201.

Zhao, F.-Q. Ni, W. Wang, H.-J. Liu, H.J., 2007. Activated fly ash/slag blended cement. *Resources, Conservation and Recycling*, Vol 52, pp 303-313.

Zhihua, P. Donqxu, L. Jian, Y. Nanru, Y., 2003. Properties and microstructure of the hardened alkali activated red mud-slag cementitious material. *Cement and Concrete Research*, Vol 33, pp 1437-1441.

Zibouche, F. Kerdjoudj, H. de Lacaillerie, J.-B. van Damme, H., 2009. Geopolymers from Algerian metakaolin. Influence of secondary minerals. *Applied Clay Science*, Vol 43, pp 453-458.

Zuhua, Z. Xiao, Y. Huajun, Z. Yue, C., 2009. Role of water in the synthesis of calcined kaolin-based geopolymer. *Applied Clay Science*, Vol 43, pp 218-223.

APPENDIX A: EXAMPLE OF MIX DESIGN OF ALKALI-ACTIVATED FLY ASH CEMENT PASTE

Assume that amount of fly ash is 1000.0 g. Sodium hydroxide was used as an activator solution and sodium oxide content (in percentage of fly ash mass) is a variable parameter. To make a paste with a 9 % of sodium oxide it is necessary to take 1000.0×9/100=90.0 g of sodium oxide which is 90×80.0/62.0=116.1 g in terms of sodium hydroxide, where 80.0 is the molecular weight of two molecules of sodium hydroxide, and 62.0 molecular weight of sodium oxide.

$$\underset{90.0}{Na_2O} + \underset{}{H_2O} = \underset{x}{2NaOH}$$

The amount of water was controlled by water to binder solids parameter. The amount of water was calculated as total mass of water used for making the sodium hydroxide solution and the amount of water from sodium hydroxide flakes. Mass of binder solids is the sum of the mass of fly ash and mass of Na_2O from NaOH flakes. Thus 116.1 g of NaOH contains 90.0 g of Na_2O and 26.1 g of H_2O (116.1×18/80, where 18 is the molecular weight of H_2O). Water to binder solids ratio was kept constant of 0.2, thus amount of water (y) was calculated as (y+26.1)/(1000.0+90.0)=0.2, y=0.2×1090.0-26.1=191.9 g. Consumption of material for mixture with 9 % of sodium oxide of fly ash mass and water to binder solids ration of 0.2 is: fly ash 1000 g, NaOH 116.1g, water 191.9 g.

Activator solution was prepared by mixing 116.1g of NaOH with 191.9 g of water. The solution concentration is 116.1/(116.1+191.9)×100=37.7 %. By interpolation the density of the NaOH solution can be calculated as indicated in Table C 3 Appendix C. The density is 1.4071 g/cm^3.

Find the volume of ready paste:

$$\frac{1000}{2.23} + \frac{(116.1 + 191.9)}{1.4071} = 667.3\ cm^3$$

Consumption of materials per 1 liter of paste: fly ash 1499 g, NaOH 174 g, water 288 g.

At mix design of paste with a sodium silicate as activator mass of binder solids is the sum of fly ash, mass of solids in sodium silicate solution (i.e. the mass of Na_2O and SiO_2). Mass of water from sodium silicate solution was also added to mass of total water in numerator.

APPENDIX B: SUITABILITY OF USING 'WATER TO BINDER SOLIDS' RATIO AS A VARIABLE PARAMETER INSTEAD OF SOLUTION TO FLY ASH MASS RATIO, WATER TO FLY ASH MASS RATIO AND ETC.

The suitability of 'water / binder solids mass ratio' as a variable parameter was evaluated in this appendix. The amount of sodium oxide to fly ash was kept constant of 9 % for all mixes, while the water was varied for each mix, affecting the final volume of AAFA paste. The final volume of AAFA paste increased with increasing water content. Different independent variables reflecting the amount of water were recalculated from the same mixtures and plotted against compressive strength. Linear trend line was found to be the best fit for all variables with an insignificant difference in R-squared value above at least 0.93. Such a high R-squared value for all variables suggests a high goodness of fit and shows that all variables mentioned in Figure B.1 – B.6 can be used to design AAFA pastes.

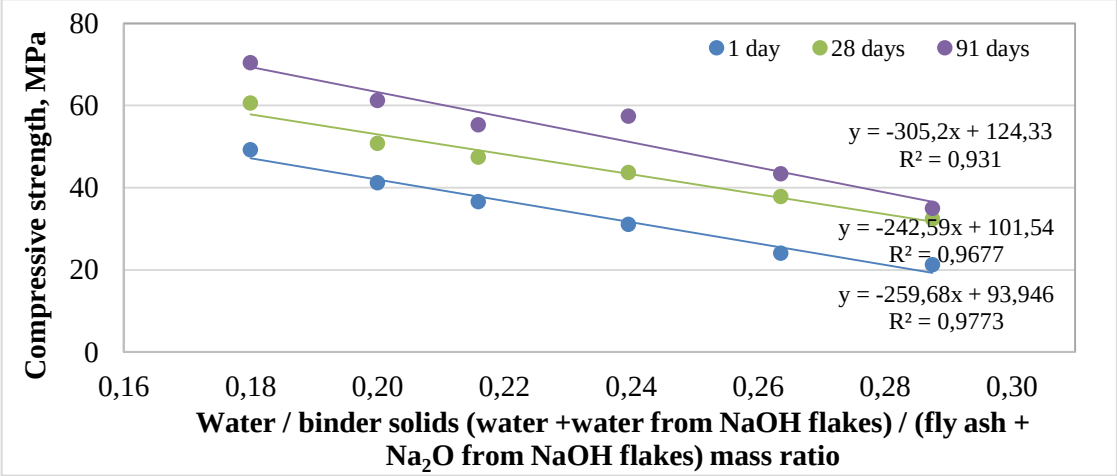

Figure B.1: Relationship between water / binder solids mass ratio and compressive strength of AAFA paste with 9 % sodium oxide

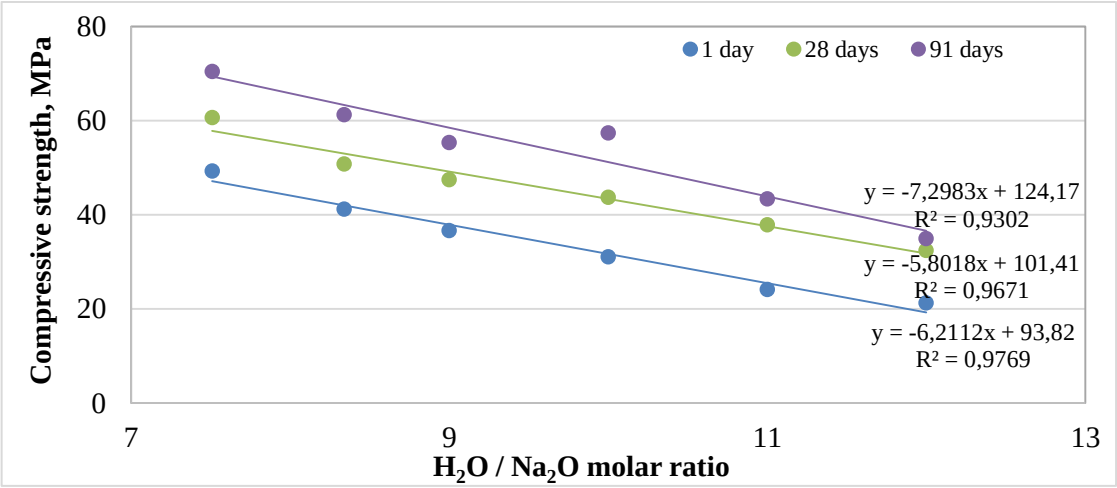

Figure B.2: Relationship between H_2O/ Na_2O molar ratio and compressive strength of AAFA paste with 9 % sodium oxide

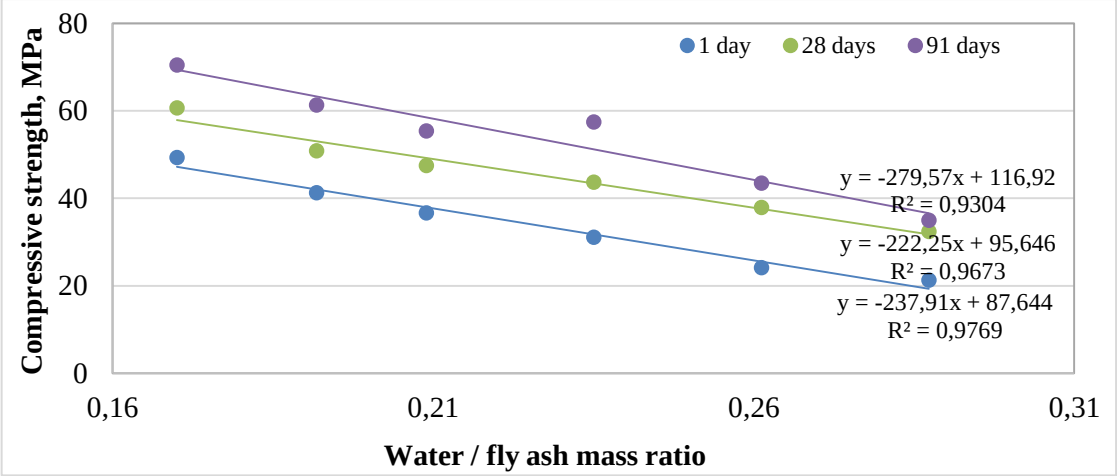

Figure B.3: Relationship between water / fly ash mass ratio and compressive strength of AAFA paste with 9 % sodium oxide

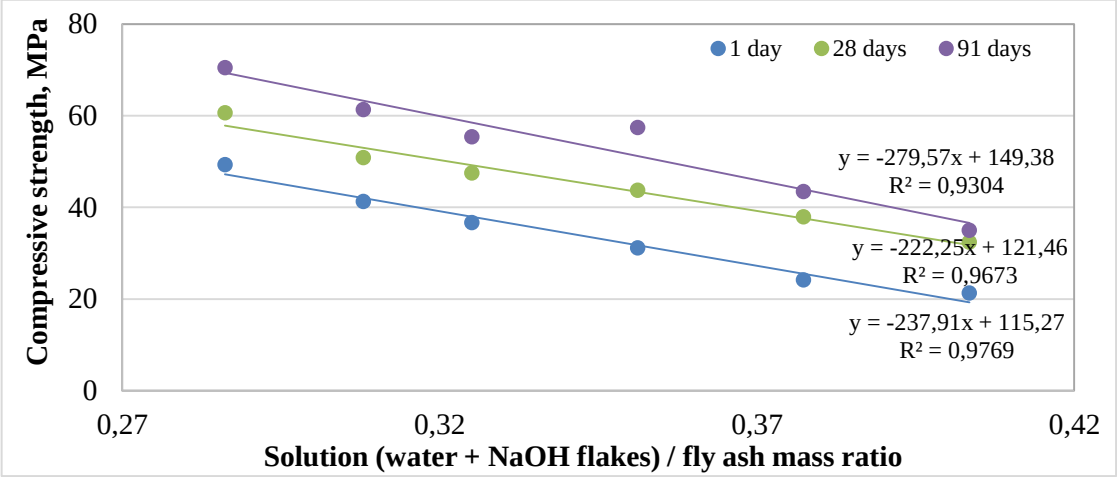

Figure B.4: Relationship between solution / fly ash mass ratio and compressive strength of AAFA paste with 9 % sodium oxide

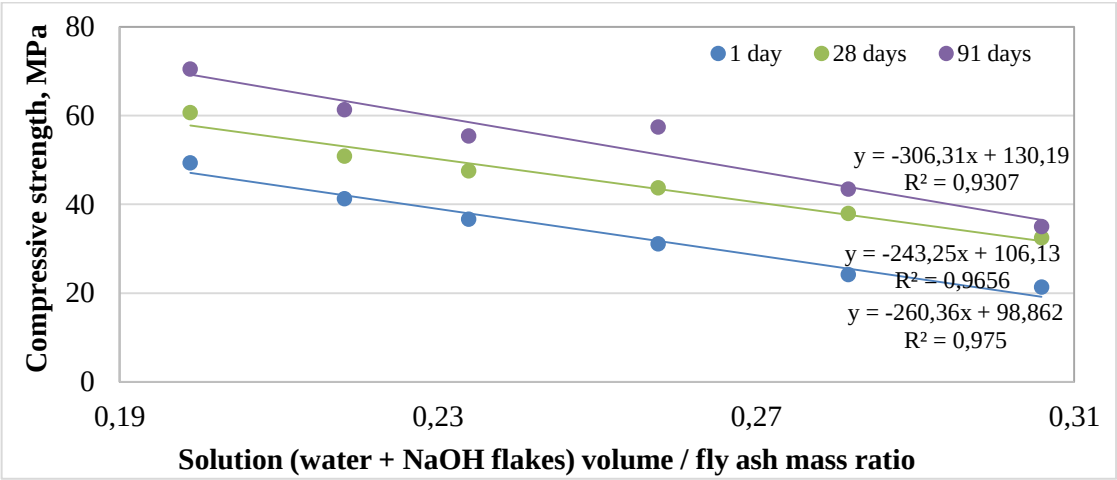

Figure B.5: Relationship between solution volume / fly ash mass ratio and compressive strength of AAFA paste with 9 % sodium oxide

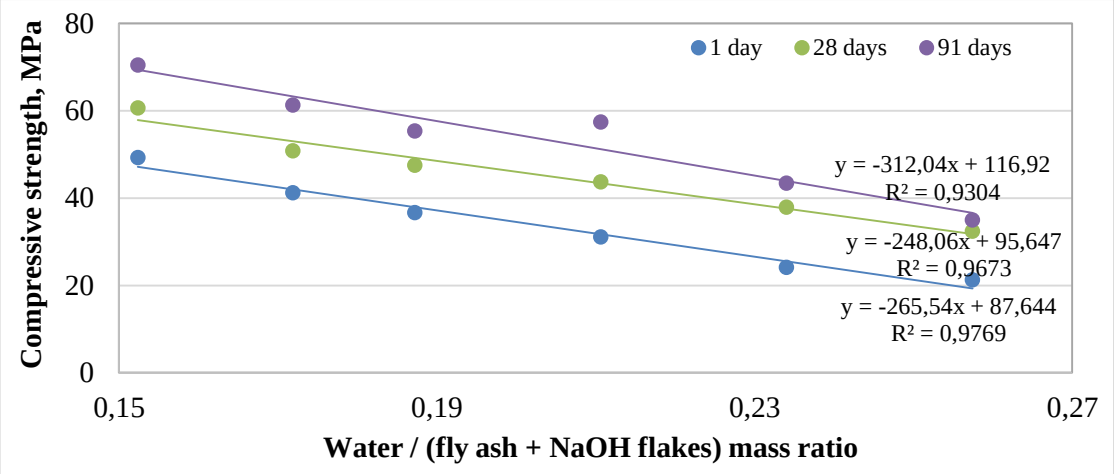

Figure B.6: Relationship between water / (fly ash + NaOH flakes) mass ratio and compressive strength of AAFA paste with 9 % sodium oxide

APPENDIX C: TABLE OF DENSITIES OF AQUEOUS SODIUM HYDROXIDE SOLUTIONS

Table C.1: Density of sodium hydroxide solutions (Lazarev, 1976)

Density at 20 °C	NaOH			Density at 20 °C	NaOH		
	%	g/l	mol/l		%	g/l	mol/l
1.0095	1	10.10	0.2525	1.2848	26	334.0	8.351
1.0207	2	20.41	0.5103	1.2956	27	349.8	8.746
1.0318	3	30.95	0.7738	1.3064	28	365.8	9.146
1.0428	4	41.71	1.043	1.3172	29	382.0	9.551
1.0538	5	52.69	1.317	1.3279	30	398.4	9.960
1.0648	6	63.89	1.597	1.3385	31	414.9	10.37
1.0758	7	75.31	1.883	1.3490	32	431.7	10.79
1.0869	8	86.95	2.174	1.3593	33	448.6	11.22
1.0979	9	98.81	2.470	1.3696	34	465.7	11.64
1.1089	10	110.9	2.773	1.3798	35	482.9	12.07
1.1199	11	123.2	3.080	1.3900	36	500.4	12.51
1.1309	12	135.7	3.393	1.4001	37	518.0	12.95
1.1420	13	148.5	3.713	1.4101	38	535.8	13.40
1.1530	14	161.4	4.035	1.4201	39	553.8	13.85
1.1641	15	174.6	4.365	1.4300	40	572.0	14.30
1.1751	16	188.0	4.701	1.4397	41	590.3	14.76
1.1862	17	201.7	5.040	1.4494	42	608.7	15.22
1.1972	18	215.5	5.388	1.4590	43	627.4	15.69
1.2082	19	229.6	5.740	1.4685	44	646.1	16.15
1.2191	20	243.8	6.095	1.4779	45	665.1	16.63
1.2301	21	258.3	6.458	1.4873	46	684.2	17.11
1.2411	22	273.0	6.825	1.4969	47	703.5	17.59
1.2520	23	288.0	7.201	1.5065	48	723.1	18.08
1.2629	24	303.1	7.578	1.5159	49	742.8	18.57
1.2739	25	318.5	7.963	1.5253	50	762.7	19.07

APPENDIX D: RECOMMENDED FACTORS FOR K_0' AND α SUITABLE FOR ESTIMATING E FOR DESIGN PURPOSES FOR DOLOMITE

Table D.1: Factors for K_0' and α for design purposes (www.afrisam.co.za/, 2014)

Aggregate sourse and type	Design value, 3 to 28 days		Design value, 6 month or older	
	K_0'	α	K_0'	α
Olifantsfontain dolomite	24	0.45	41	0.25

APPENDIX E: SHRINKAGE CONE METHOD. CORRELATION BETWEEN HEIGHT AND VOLUME CHANGES

Cone formed specimen container is using to ensure that the measured distance correlates with the relative length change of the material. So the height changes always correlates with the volume change (http://www.schleibinger.com)

So, why the cone shape works?

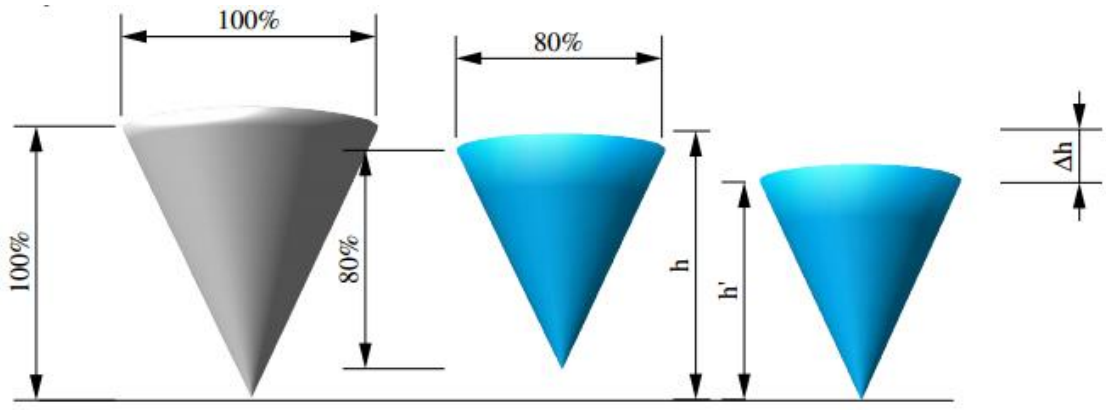

$$General: V=\frac{1}{3}\pi r^2 h;\ V'=\frac{1}{3}\pi r'^2 h'$$

$$r=h\tan(\alpha)\rightarrow V=\frac{1}{3}(h\tan(\alpha))^2 h$$

$$\alpha=const\rightarrow V=c\,h^3;\ V'=c\,h'^3$$

$$\frac{V'}{V}=\frac{h'^3}{h^3}\rightarrow\frac{h'}{h}=\sqrt[3]{\frac{V'}{V}}$$

$$Example: k=0{,}8;\ \alpha=30°;\ h=10\,cm$$

$$h'=0{,}8\,h=8\,cm\rightarrow\Delta h=2\,cm$$

$$V=\frac{1}{3}(h\tan(\alpha))^2\pi h=349\,cm^3$$

$$V'=\frac{1}{3}(h'\tan(\alpha))^2\pi h'=178{,}7\,cm^3$$

$$\frac{h'}{h}=\frac{8}{10}=\sqrt[3]{\frac{V'}{V}}=\sqrt[3]{\frac{178{,}7}{349}}=0{,}8$$

And cylinder doesn't

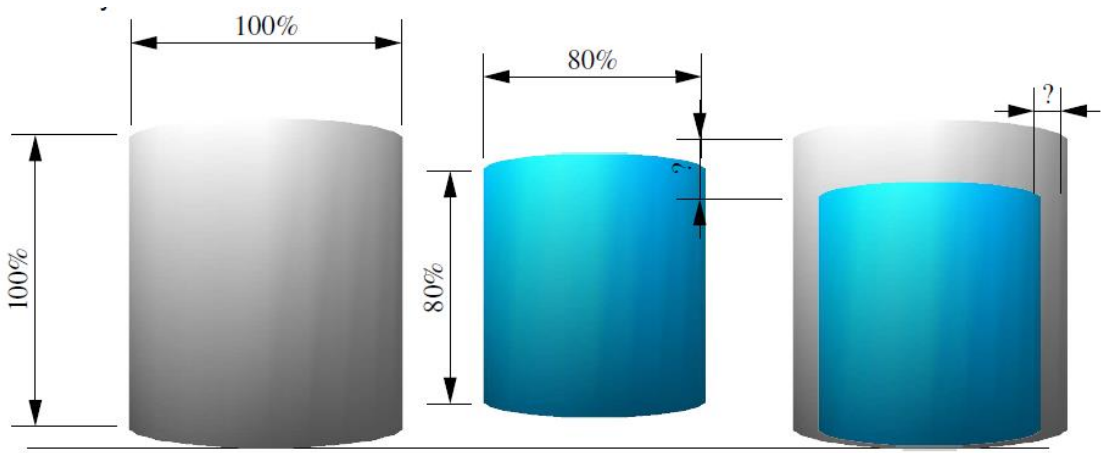

APPENDIX F: TABLES FORM CHAPTER 4

Table F.1: Compressive strength and standard deviation of alkali-activated unclassified Lethabo fly ash pastes with different levels of sodium oxide

Mixture	Na_2O, % fly ash weight	Average compressive strength and standard deviation (in brackets) at different testing ages, MPa			
		after heat curing	7 days	28 days	56 days
Na3	3	12.2(0.8)	18.3(1.2)	22.4(1.8)	23.2(1.3)
Na6	6	23.9(1.4)	25.9(1.6)	30.6(1.8)	35.5(2.1)
Na9	9	40.4(1.7)	43.1(1.3)	57.0(1.8)	57.4(1.0)
Na12	12	42.3(1.1)	49.9(2.1)	56.3(3.1)	59.5(2.8)
Na15	15	44.9(2.1)	50.4(2.3)	52.6(3.5)	55.4(3.1)

Table F.2: Flexural strength and standard deviation of alkali-activated classified Lethabo fly ash pastes with different levels of sodium oxide

Mixture	Na_2O, % fly ash mass	Average flexural strength and standard deviation (in brackets) at different testing ages, MPa					
		after heat curing	7 days	28 days	91 days	182 days	364 days
Na3	3	2.3 (0.5)	3.3 (0.4)	3.9 (0.5)	4.3 (0.4)	3.4 (0.7)	3.5 (0.9)
Na6	6	5.5 (0.3)	6.0 (0.4)	5.2 (1.5)	7.7 (0.6)	7.7 (1.4)	8.1 (0.5)
Na9	9	4.7 (0.6)	6.2 (0.7)	5.8 (2.1)	9.0 (1.4)	8.7 (0.6)	7.8 (1.4)
Na12	12	4.8 (0.8)	6.2 (1.1)	7.0 (0.7)	10.0 (0.7)	11.3 (0.9)	12.7 (0.4)
Na15	15	4.5 (0.6)	7.0 (1.2)	6.3 (0.8)	8.2 (1.2)	8.6 (0.3)	8.8 (1.1)

Table F.3: Compressive strength and standard deviation of alkali-activated classified Lethabo fly ash pastes with different levels of sodium oxide

Mixture	Na_2O, % fly ash mass	Average compressive strength and standard deviation (in brackets) at different testing ages, MPa					
		after heat curing	7 days	28 days	91 days	182 days	364 days
Na3	3	17.7 (1.2)	19.8 (0.9)	26.1 (1.0)	25.4 (1.5)	23.7 (1.4)	25.7 (2.1)
Na6	6	36.0 (1.2)	36.6 (1.4)	43.7 (2.0)	49.1 (2.4)	44.4 (1.9)	51.7 (2.9)
Na9	9	43.1 (1.2)	41.6 (2.8)	50.8 (2.0)	60.0 (2.9)	63.6 (1.5)	67.9 (5.2)
Na12	12	36.1 (1.1)	39.8 (2.0)	48.6 (1.8)	62.8 (4.0)	68.9 (3.9)	64.9 (1.4)
Na15	15	36.6 (2.8)	38.8 (3.9)	49.8 (2.4)	55.4 (6.1)*	60.8 (8.7)*	62.7 (4.5)

* These values include more than one statistical outlier which was varied by more than ± 10 % from the mean and would normally be excluded as in SANS 50196-1:2006

Table F.4: Compressive strength and standard deviation of pastes cured at different temperatures and periods of time

Mixtures ID (T for temperature in °C; D for duration in hours)	Average compressive strength and standard deviation (in brackets) at different testing ages, MPa		
	after heat curing	28 days	91 days
T65D4	3.1 (0.2)	44.7 (2.4)	61.0 (3.9)
T70D4	15.5 (0.9)	44.8 (1.6)	59.3 (3.6)
T75D4	31.4 (1.6)	46.6 (2.8)	54.2 (8.9)*
T25D24	-	10.9 (0.7)	34.7 (10.0)*
T40D24	1.6 (0.1)	25.5 (1.6)	49.4 (3.1)
T60D4	2.1 (0.1)	40.5 (1.8)	55.8 (3.3)
T60D8	15.2 (1.4)	47.9 (1.9)	62.0 (2.7)
T60D12	28.5 (0.9)	48.9 (1.8)	56.1 (4.6)
T60D16	43.3 (1.5)	59.0 (3.8)	61.5 (5.5)
T60D20	49.8 (2.5)	59.9 (1.2)	68.4 (4.2)
T60D24	49.4 (1.5)	59.1 (2.6)	66.3 (1.3)
T80D4	36.0 (1.2)	50.8 (2.2)	56.1 (3.2)
T80D8	40.2 (2.6)	52.1 (1.8)	58.3 (3.6)
T80D12	42.9 (2.0)	53.5 (3.7)	58.9 (2.6)
T80D16	51.0 (3.3)	64.3 (3.3)	63.6 (2.2)
T80D20	50.9 (3.7)	61.2 (2.6)	58.1 (2.1)
T80D24	53.0 (3.7)	63.5 (1.8)	58.1 (2.8)

* These values include more than one statistical outlier which varied by more than ± 10 % from the mean and would normally be excluded as in SANS 50196-1:2006

Table F.5: Compressive strength and flexural strength of pastes with different water to binder solid ratios

Mixtures ID (WS for water to binder solids ratio)	Average compressive strength (standard deviation) - flexural strength (standard deviation) at different testing ages, MPa		
	after heat curing	28 days	91 days
WS0.18	49.3 (2.1) - 6.6 (0.4)	60.6 (5.7) - 7.6 (1.7)	68.3 (4.3) - 9.3 (3.1)
WS0.20	43.1 (1.2) - 4.7 (0.6)	50.8 (2.0) - 5.8 (2.2)	60.0 (2.9) - 9.0 (3.1)
WS0.22	36.6 (2.5) - 4.0 (0.8)	47.5 (2.2) - 7.7 (1.0)	53.5 (3.6) - 6.6 (1.1)
WS0.24	31.1 (1.9) - 3.8 (0.2)	44.7 (2.4) - 7.0 (0.5)	56.2 (3.2) - 6.3 (1.4)
WS0.26	24.1 (0.8) - 3.4 (0.3)	37.9 (1.9) - 5.6 (1.4)	43.4 (6.6)* - 4.9 (1.8)
WS0.29	21.3 (1.3) - 4.2 (0.4)	32.4 (2.0) - 6.4 (0.5)	34.0 (2.5) - 5.6 (2.8)

* These values include more than one statistical outlier which varied by more than ± 10 % from the mean and would normally be excluded as in SANS 50196-1:2006

Table F.6: Compressive strength, standard deviation of alkali-activated classified Matla and Lethabo fly ash pastes

Mixture	Average compressive strength and standard deviation (in brackets) at different testing ages, MPa		
	after heat curing	28 days	91 days
Matla	32.4 (2.7)	45.0 (4.2)	44.9 (6.1)*
Lethabo	31.1 (1.9)	44.7 (2.4)	56.2 (3.8)

* These values include more than one statistical outlier which varied by more than ± 10 % from the mean and would normally be excluded as in SANS 50196-1:2006

Table F.7: Compressive strength and standard deviation of fly ash cement pastes activated by different alkaline solutions

Mixture ID	Average compressive strength and standard deviation (in brackets) at different testing ages, MPa					
	after heat curing	7 days	28 days	91 days	182 days	364 days
K3	1.0(0.2)*	2.0 (0.3)*	3.9 (0.2)	4.1 (0.6)	4.6 (0.6)*	4.3 (0.6)*
K6	6.4 (0.0)*	8.1 (0.5)	14.8 (0.7)	17.1 (0.6)	17.0 (2.5)*	16.9 (1.3)
K8	3.8 (0.4)	7.7 (0.6)	17.3 (0.7)	25.4 (1.3)	24.5 (1.7)	28.0 (1.6)
K11	2.3 (0.3)*	3.8 (0.2)	8.5 (0.4)	26.2 (1.0)	33.8 (3.6)*	27.4 (3.4)*
Na3	17.7 (1.2)	19.8 (0.9)	26.1 (1.0)	25.4 (1.5)	23.7 (1.4)	25.7 (2.1)
Na6	36.0 (1.2)	36.6 (1.4)	43.7 (2.0)	49.1 (2.4)	44.4 (1.9)	51.7 (2.9)
Na9	43.1 (1.2)	41.6 (2.8)	50.8 (2.0)	60.0 (2.9)	63.6 (1.5)	67.9 (5.2)
Na5.7Si6.5	76.7 (3.9)	81.6 (4.1)	79.2 (12.3) *	88.4 (14.6) *	93.3 (5.1)	93.2 (4.0)

* These values include more than one statistical outlier which varied by more than ± 10 % from the mean and would normally be excluded as in SANS 50196-1:2006

Table F.8: Compressive strength and standard deviation of Na-Si series of AAFA cement pastes

Mixture ID	Average compressive strength and standard deviation (in brackets) at different testing ages, MPa					
	after heat curing	7 days	28 days	91 days	182 days	364 days
Na3Si0	17.7 (1.2)	19.8 (0.9)	26.1 (1.0)	25.4 (1.5)	23.7 (1.4)	25.7 (2.1)
Na3Si3	17.5 (0.5)	19.4 (1.0)	22.1 (1.7)	23.4 (1.0)	26.9 (1.4)	24.0 (1.3)
Na3Si6	15.8 (0.7)	19.5 (0.7)	30.8 (1.9)	36.4 (2.3)	41.6 (2.5)	39.9 (3.7)
Na6Si0	36.0 (1.2)	36.6 (1.4)	43.7 (2.0)	49.1 (2.4)	44.4 (1.5)	51.7 (2.9)
Na6Si3	50.2 (2.8)	53.8 (3.6)	60.4 (4.1)	61.1 (4.9)	62.7 (7.6)*	75.2 (4.1)
Na6Si6	Flash setting					
Na6Si9	64.3 (3.8)	67.4 (10.0)*	73.8 (7.8)*	71.2 (18.4)*	64.1 (10.0)*	88.8 (3.9)
Na6Si12	22.4 (1.3)	32.1 (1.1)	52.8 (0.9)	37.2 (5.9)*	57.3 (17.6)*	38.9 (11.9)*
Na9Si0	43.1 (1.2)	41.6 (2.8)	50.8 (2.0)	60.0 (2.9)	63.6 (1.5)	67.9 (5.2)
Na9Si3	60.6 (4.6)	65.0 (3.1)	65.6 (3.8)	77.9 (4.8)	86.1 (4.8)	86.2 (6.2)
Na9Si6	Flash setting					
Na9Si9	74.9 (5.6)	72.9 (12.0)*	86.4 (10.7)*	94.0 (10.1)*	86.0 (5.0)	71.6 (4.9)
Na9Si12	72.4 (4.9)	80.2 (4.0)	80.6 (4.4)	86.1 (5.6)	72.0 (6.6)	48.3 (15.4)*

* These values include more than one statistical outlier which varied by more than ± 10 % from the mean and would normally be excluded as in SANS 50196-1:2006

APPENDIX G: DESIGN OF CONCRETE MIXTURES FROM CHAPTER 5

Table G.1: Mixture compositions of AAFA concretes

Na_2O, % of fly ash mass	W/S	Fly ash, kg/m^3	Dolomite stone 9,5 mm, kg/m^3	Dolomite sand, kg/m^3	NaOH, kg/m^3	Water, kg/m^3
6	0.3	400	1261,6	683,6	31.0	120,2
9	0.3	400	1253,7	679,3	46,5	120,3
12	0.3	400	1243,9	673,9	61,9	120,5
9	0.3	500	1113,2	603,1	58,1	150,4
9	0.35	400	1216,1	659,0	46,5	142,1
9	0.35	500	1066,2	577,6	58,1	177,7
9	0.25	500	1159,3	628,1	58,1	123,2
12	0.3	500	1100,7	596,6	77,4	150,6